SILICON CARBIDE AT NANOSCALE: FINITE SINGLE-WALLED TO "INFINITE" MULTI-WALLED TUBES

by

KAPIL ADHIKARI

Presented to the Faculty of the Graduate School of

The University of Texas at Arlington in Partial Fulfillment

of the Requirements

for the Degree of

DOCTOR OF PHILOSOPHY

THE UNIVERSITY OF TEXAS AT ARLINGTON

August 2012

ACKNOWLEDGEMENTS

I would like to express my gratitude to my advisor, Prof. Dr. A. K. Ray for his guidance through the course of my study and research. I wish to thank my committee mummers, Dr. I also would like to extend my thanks to my committee members, Dr. Nail Fazleev, Dr. Muhammad N. Huda, Dr. Ali R. Koymen, and Dr. Qiming Zhang, for the their interest in my research work.

I would also like to thank members of our research groups for being very helpful throughout my research work. Their valuable suggestions during our regular research meetings have enriched my research experience. I am very greatful to Dr. Raymond Atta-Fynn for being helpful in the very beginning of my research work.

I am very greatful to my parents and siblings for providing me an encouraging environment for my academic career. Special thanks go to my wife Manju for her continuous support and care.

Finally I would like to acknowledge the support from the Welch Foundation, Houston, Texas.

July 9th, 2012

ABSTRACT

SILICON CARBIDE AT NANOSCALE: FINITE SINGLE-WALLED TO "INFINITE" MULTI-WALLED TUBES.

Kapil Adhikari, PhD

The University of Texas at Arlington, 2012

Supervising Professor: Asok K. Ray

A systematic *ab initio* study of silicon carbide (SiC) nanostructures, especially finite single-walled, infinite double- and multi-walled nanotubes and nanocones is presented. Electronic and structural properties of all these nanostructures have been calculated using hybrid density functionals (B3LYP and PBE0) as implemented in the *GAUSSIAN 03/09* suite of software. The unusual dependence of band gap of silicon carbide nanotubes (SiCNT) has been explained as a direct consequence of curvature effect on the ionicity of the bonds. The study of fullerene hemisphere capped, finite SiC nanotubes indicates that the carbon-capped SiC nanotubes are energetically more preferred than silicon-capped finite or hydrogen terminated infinite nanotubes. Capping a nanotube by fullerene hemisphere reduces its band gap. SiC nanocones have also been investigated as possible cap structures of nanotubes. Electronic properties of the nanocones are found to be strongly dependent upon their tip and edge structures, with possible interesting applications in surface science.

Three types of double-walled SiCNTs (n, n)@(m, m) ($3 \leq n \leq 6$; $7 \leq m \leq 12$) have been studied using the finite cluster approximation. The stabilities of these nanotubes are of the same order as those of the single-walled SiC nanotubes and it should be experimentally possible to

synthesize both single-walled and double-walled SiC nanotubes. The binding energy per atom or the cohesive energy of the double-walled nanotubes depends not only on the number of atoms but also on the coupling of the constituent single-walled nanotubes and their types. A study of binding energies, Mulliken charges, density of states and HOMO-LUMO gaps has been performed for all nanotubes from (n, n)@(n+3,n+3) to (n, n)@(n+6, n+6) (n=3-6). Evolution of band gaps of the SiCNTs with increase in the number of walls has also been investigated. The nature of interaction between transition metal atoms and silicon carbide nanotubes with different curvature has also been investigated. The curvature of the nanotubes affects the nature of the interaction between the nanotubes and the transition teal atoms. Our study of functionalized SiCNTs by *3d* transition metal atoms indicates that these nanostructures can have possible applications in spintronics and nano-magnetic storage

.

TABLE OF CONTENTS

LIST OF ILLUSTRATIONS

LIST OF TABLES

CHAPTER 1

INTRODUCTION

Discovery of multi-walled carbon nanotubes (CNT) in 1991[1], has led to an explosive growth of interest in these kinds of quasi-one-dimensional structures. Carbon nanotubes have interesting physical and electronic properties which make them very useful in electronics industry [2-8]. Depending on their chirality, carbon nanotubes are either metallic or semiconductor which makes them useful for a wide range of applications. However, this property of carbon nanotubes also limits some of their applications, in gas sensors for instance [9]. Also the strong dependence of electrical properties on chirality limits the application of carbon nanotubes in many nanoelectronic applications because the semiconducting and metallic nanotubes are mixed in the sample of nanotubes grown in the lab. This involves an extra work for manufacturing electronic devices of carbon nanotubes because to obtain carbon nanotubes with similar electronic properties one has to do post synthesis separation of metallic and semiconducting nanotubes or control the synthesis of the nanotubes very precisely [10-12]. The strong need of materials which can be used even in harsh conditions has prompted a search for “better” alternatives to CNT. In search for “better” alternatives to CNT, a significant number of experimental and theoretical research works on nanostructures of other elements have been done. A typical example is a nanotube formed by group-III nitrides. Group-III nitride nanotubes, such as BN, AlN, and GaN, have been synthesized through different techniques [13-15]. Synthesis of several other nanotubes has been reported, for example, $NiCl_2$, $H_2Ti_3O_3$, TiO_2, and Si [16-20]. Dai *et al*. [21] reported the synthesis of nanostructures by converting carbon nanotubes to carbide rods from reaction with volatile oxide and/or halide species. One of the nanorods produced was SiC, among others such as TiC, NbC, Fe_3C, and BC_x. These rods had diameters between 2 and 30 nm and lengths up to 20 μm. An interesting candidate here is

silicon carbide (SiC) which, in bulk form, is one of the hardest materials and is very suitable for electronic devices designed for operations in extreme environments. Bulk silicon carbide has a wide band gap from 2.2 eV for 3C-SiC to 3.0 eV for 6H-SiC, and to 3.3 eV for 4H-SiC [22]. It has high thermal conductivity up to about 500 W/(mK) at room temperature [23] and thermal expansion coefficient smaller than 6 μ/K [24]. It has very high decomposition temperature of about 2545℃ [25]. 3C-SiC has very high Young's modulus 360-600 GPa depending upon its orientations [26].

In addition to the properties due to quantum size effect, silicon carbide nanostructures have some of these unique properties of bulk silicon carbide. Studies, in fact, have shown that silicon carbide nanostructures have additional unique properties compared to the bulk. Wong *et al.* [27] have measured the strength of SiC nanowires by using atomic force microscopy and lithography technique and reported that SiC nanowires of 23 nm in diameter have maximum bending strength of 53.4 GPa, much higher than similar size carbon nanotubes. SiC nanowires of diameter 3-40 nm show better photoluminescence properties than SiC bulk [28]. Thus, the silicon carbide nanostructures carry unique properties of their bulk form with some additional properties due to quantum size effects. Like silicon carbide nanowires, silicon carbide nanotubes (SiCNT's) might also have some advantages over carbon nanotubes. Due to its partially ionic nature, SiCNTs have higher reactivity of the exterior surface than that of carbon nanotubes. This might be helpful to facilitate sidewall decoration.

Motivated by these extraordinary characteristics of bulk silicon carbide as well as silicon carbide nanowires, there has been numerous attempts, both theoretical and experimental, to study the possible graphitic phases of silicon carbide and possible applications in various fields. Most of the experimental attempts of fabricating SiCNTs showed the formation of β-SiC nanorods. Comparing total energy of graphitic form with that of β-SiC according to calculation based on density functional theory, Miyamoto and Yu [29] have noted that SiC has a large difference between sp^2 and sp^3 bond structures with a value of 1.25 eV per Si-C pair. This

energy difference makes the realization of graphitic phase of SiC very difficult. However, in the same study, Miyamoto and Yu have demonstrated the possibility of forming SiC nanotubes. They have reported that the strain energies of SiCNTs are lower than those of carbon nanotubes. They have also proposed the synthesis pathways by using an electronic technique of an extreme hole injection which would cause the graphitic sheet of SiC exfoliate from SiC (111) surface. Different groups have synthesized the SiCNTs using different techniques. First report on synthesis of SiCNTs by C. Pham-Huu *et al*. [30] used a technique called shape memory synthesis (SMS). This technique has yielded SiCNTs with the wall morphology of β-SiC. Similarly, Borowiak-Palen *et al*. [31] produced SiC nanotubes based on high-temperature reactions between silicon powders and multi-walled carbon nanotubes. Hu *et al.* [32] formed SiC nanotubes by reacting CH_4 with SiO. Most of the attempts of fabricating SiCNTs have yielded either β-SiC nanotubes or the nanotubes with the wall morphologies which are not quite clear [30-37]. Sun *et al.* [38] have reported the synthesis of multi-walled SiC nanotubes through a substitutional reaction with Si atoms replacing half of the C atoms from a multi-walled carbon nanotube. The observed SiC nanotubes were multi-walled but with higher inter-planar spacing than those of multi-walled carbon nanotubes. Also the interlayer separation between the layers of nanotubes was found to be greater than 2.5 Å, which is typical for β-SiC. This indicated that the wall morphology of the observed nanotubes might correspond to graphitic phase rather than the cubic phase of the silicon carbide. The graphitic multi-walled SiCNTs stabilize in experimental environment, and the fact that 200 kV electron beam annealing for 5 minutes was needed to collapse the nanotubes indicates an energy barrier between collapsed nanotubes and the multi-walled nanotubes. Electron-energy-loss-spectroscopy (EELS) of the multi-walled SiCNTs has indicated possible π bonding between Si and C atom. The interlayer separations of the multi-walled nanotubes were observed to be 3.5-4.5 Å. This indicated weak coupling between inner and outer tubes and possibility of separating them with ease.

Although the experimental results of SiCNT synthesis have suggested the possibility of multi-walled SiCNTs, single-walled SiCNTs are not yet observed experimentally. In a study by Pokropivnyi *et al.* [39], three kinds of SiCNTs have been proposed. Based on the wall structures, SiCNTs have been classified into CNT-like SiCNT, polynanocrystalline nanotubes and monocrystalline synthetic nanotubes. The authors have claimed that the SiCNTs with wall structures similar to "traditional" CNTs are unstable with the exception of one or two layer nanotubes. CNT-like multi-layered SiCNTs would eventually be transformed into polycrystalline or monocrystalline structures as the tendency of Si atoms to form sp^3 bonding may overcome the existing sp^2 bonding. The collapse of CNT-like SiCNTs may be triggered by a buckling of the individual layers, charge transfer between the layers or by defect formation on the walls of nanotubes. However, the experimental results by Sun *et al.* [38], as mentioned above, have suggested the possibility of multi-walled graphitic phase SiCNT. Therefore, the question of the stability of multi-walled SiCNTs is still unsettled in general.

In a theoretical study, Huda *et al.* [40] have justified the π-bonding feature shown by electron-energy-loss spectroscopy (EELS) as observed by Sun *et al.* [38] in multi-walled SiCNTs and suggested that graphene-like SiC layers can exist. The study has claimed that Si=C double bond has been found in periodic SiC graphene-like multi-layer systems. By using density functional theory, they observed that initially buckled silicon carbide monolayer relaxes into flat layer without buckling indicating that the silicon carbide monolayer favors sp^2 bonding. Also, in a recent study by Yu *et al.* [41], authors have reported that the unbuckled silicon carbide is more favorable than the buckled one. The authors have shown that a transition from the dominant sp^3 bonding in buckled silicon carbide monolayer to the sp^2 type of bonding in the unbuckled flat monolayer structure is energetically feasible. This indicates that different types of bondings are possible between silicon and carbon atoms. The density functional calculation has shown that the B.E./atom of the optimized silicon carbide graphitic sheet is 0.49 eV higher

than that of bulk β-SiC. Similar results have been observed in graphitic-like structures of group-III nitrides [42, 43]. This suggests the possibility of graphitic phase of silicon carbide.

Most of the theoretical studies on SiCNTs are based on the graphene-like structure of silicon carbide. Although SiC graphitic monolayers have not yet been observed experimentally, some theoretical studies have predicted their possibilities. Also, the experimental observation by Sun *et al.* [38] has provided some evidences of graphitic phase of silicon carbide. The major driving force behind all the studies on SiCNTs is mainly their potential applications. Some *ab initio* methods [44] have shown that the most stable SiC nanotube has the ratio of Si to C of 1 to 1. These studies claim that the nanotubes other ratios will eventually collapse the tube into nanowires or clusters with solid interiors. Similar to carbon nanotube, a SiCNT can be considered as a roll of silicon carbide graphene-like sheet. This rolling up can be described in terms of the chiral vector $\mathbf{C_h}$, which connects two sites of the two-dimensional graphene-like sheet that are crystallographically equivalent. This chiral vector maps an atom from the left hand border onto an atom on the right border line and is an integer multiple of the two basis vectors $\mathbf{a_1}$ and $\mathbf{a_2}$, i.e., $\mathbf{C_h}=n\mathbf{a_1}+m\mathbf{a_2}$. So the geometry of any nanotube can be described by the integer pair (n,m) which determines the chiral vector. An armchair nanotube corresponds to the case of n=m, and a zigzag nanotube corresponds to the case of m=0. All other (n,m) chiral vectors correspond to chiral nanotubes. The strain energy of such SiCNTs with respect to their bulk material is calculated by Zhao *et al.* [45] in their computational work. The strain energy of SiCNT decreases with increasing tube diameter. The strain energy involved in (5, 5) SiCNT relative to cubic SiC (β-SiC) material is about 0.686 eV/atom which decrease to 0.6134 eV/atom for (11, 11) SiCNT. Since these strain energies are relatively high, the authors claim that SiCNTs are a meta-stable phase and likely to transform to cubic structures, such as β-SiC nanowires, under certain conditions. Menon *et al.* [46] have shown that the armchair SiCNT is slightly more stable than the zigzag SiCNT, whereas the studies by Kazi and Ray [47, 48] suggest the opposite. Another *ab initio* study by Baierle *et al.* [49] does not show any significant

energy difference between zigzag and armchair SiCNT. Therefore the chirality preference of SiCNTs is still not clear and needs some closer look.

In one of the first attempts to study mechanical properties of SiCNTs, Moon *et al.* [50] have reported that the SiCNTs have lower strain energy than carbon and boron nitride nanotubes. They simulated the SiCNTs using classical molecular dynamics method based on the Tersoff empirical potential. The strain energies obtained by this classical molecular dynamics methods are little lower than the results obtained by Miyamoto and Yu [29] using density functional theory. The Young's modulus of SiCNTs are reported to be 0.591- 0.626 GPa which is smaller than that of carbon nanotubes and boron nitride nanotubes [51]. However the Young modulus of SiCNTs is larger than that of β-SiC [26] and is almost equal to that of silicon carbide nanorods [27] and whiskers [52]. In another similar *ab initio* study by Baumeier *et al.* [53], authors have reported that Young's modulus of SiCNT increase with its diameter and very quickly reaches a saturation of about 0.17 TPa nm in the unit independent of shell thickness [51]. The Young's modulus of SiCNTs is found to be independent of chirality. Similar results are reported by Zhang and Huang [54] using classical molecular dynamics and also by Setoodeh, Jahanshahi, and Attariani [55]. Recently, X. Wang *et al.* [56] have shown that ultra thin SiCNTs can transform from zigzag to armchair under uniaxial compression. They have used density functional theory to study the transformation of zigzag nanotube into armchair. This indicates that the electronic properties of SiCNTs can be altered by applying uniaxial compression. The similar observation is reported by Z. Wang *et al.* [57] also. In their first principles study they have shown that the indirect band gap of armchair SiCNTs tends to be almost like direct when the nanotube is stretched by 10%, whereas the direct band gap of zigzag nanotubes remains direct. This indicates that the electronic properties of stretched SiCNTs tend to be like those of zigzag whereas the electronic properties of compressed nanotubes tend to be like those of armchair.

The melting point of silicon carbide nanotubes is reported to be up to 5600 K [58]. Molecular dynamics simulation studies of silicon carbide nanotubes with an empirical potential has shown that the melting of silicon carbide nanotubes start from the thermally activated Stone-Wales defects and large area Stones-Wales defects facilitates the three dimensional stacking of atoms [54]. At temperature of 1100 K or higher, SiC nanotubes with free ends reconstruct by forming a closed cap containing non-hexagonal defects at the free end. The cap is stable up to 1600 K and the serves as the nucleation site of heterogeneous melting at 1620 K [54]. Recently, Wang *et al.* [59] carried out a density functional molecular dynamics simulation of silicon carbide nanotubes and showed that the melting of the nanotubes starts from the thermally activated Stone-Wales defects. The melting point they have reported for SiC (7,0) nanotube is 3630 K and that for (6,6) is 4065 K. The melting temperature of the SiC nanotubes increases with the increasing diameter. The melting temperature of SiC nanotubes varies from 2910 to 4265 K as the diameter of the nanotubes increases from 0.5 to 1.5 nm [59].

As mentioned before, all silicon carbide nanotubes are semiconducting, independent of chirality. The band gap of silicon carbide nanotubes depend on diameter of the nanotubes. This is due to polar nature of silicon carbide nanotubes. Miyamoto and Yu [29] have predicted that the band gaps of SiCNTs can be direct or indirect depending on chirality. The armchair and chiral SiCNTs have indirect gap and zigzag SiCNTs have direct gap. And this gap increases with increase in diameter of the nanotubes. This has been consistently predicted by all the *ab initio* studies on SiCNTs. The armchair tube has a larger band gap than the zigzag tube while the band gap or chiral SiCNT is in the middle. These results imply that the curvature-induced sp-hybridization has the most pronounced effect on zigzag SiCNT's, resulting in a strong downshift of the conduction bands, whereas the electronic band structure of armchair and chiral tubes is less affected [45]. It is worth noting that the bulk silicon carbide (3C-SiC) has only direct band gap whereas the zigzag SiCNTs have indirect band gap. This suggests that zigzag SiCNTs may find application in optical and optoelectronic devices such as SiC lasers. Using

LDA within density functional theory, Wu and Guo [60] have shown that the ultrasmall diameter zigzag (3,0) and (4,0) tubes are metallic. However, this prediction of metallic (3,0) and (4,0) zigzag SiC nanotubes should be treated with caution because the LDA tends to underestimate the band gap. The authors have reported that the band gap of the small SiCNTs increases with diameter and approaches the band gap of the isolated SiC sheet (2.58 eV) as the diameter becomes larger than 20 Å.

Various theoretical studies have shown that SiCNT can be a very efficient hydrogen storage material. Hydrogen storage in carbon nanotubes is an increasingly important area of research because of the need of clean alternate source of energy. Dillon *et al.* [61, 62] have reported that carbon nanotubes can be used for hydrogen storage and measured the H_2 adsorption capacity of SWCNT and the gravimetric storage capacity ranging between 5-10 wt%. However some experimental studies suggest that the hydrogen-storage capability of carbon nanotubes is less than 1 wt% and binding energy of hydrogen molecule with the carbon nanotube is about 0.030 eV [63-65]. These values are too small for any practical purpose. There have been attempts to dope carbon nanotubes to enhance its hydrogen-storage capability and binding energy with hydrogen molecule. Unlike pristine carbon nanotubes, pristine SiCNTs have shown superior characteristics in terms of hydrogen storage capability. Theoretical calculations by Mpourmpakis *et al.* [66] have shown that there is a 20% increase in binding energy of H_2 with SiCNTs compared with pure carbon nanotubes. Mpourmpakis *et al.* [66] have found the binding energies of about -0.07ev/H2 for H_2 molecule on (9,9) and (11,11) SiCNTs. Baierle and Miwa [67] have found the binding energies within -0.06 to -0.10 eV/H_2 for H_2 molecules on SiCNTs, depending on the nanotube chirality and the adsorption site. The hydrogen capacity of the SiCNTs is, however, a function of the pressure and temperature. Mukharjee and Ray [68-70] have studied the adsorption of hydrogen molecule in pristine SiCNTs using hybrid density functional theory and found that the SiCNT can be a very good candidate for the hydrogen storage medium. Recently, Malek and Sahimi [71] have studied

diffusion and adsorption of several gases in the SiCNTs using molecular dynamics and reported that the adsorption capacity of SiCNTs for hydrogen is higher than the carbon nanotubes. They have studied the effect of nanotubes' size, curvature, and chirality on the adsorption of hydrogen and other gases. The study has found that the chirality of SiCNT plays a significant role for the storage of hydrogen in the nanotubes. For example, the chiral nanotube (20, 10) exhibits a noticeable capacity for hydrogen adsorption at 300 K over a wide range of pressures. Compared with the armchair nanotube (10, 10) the chiral nanotube (20, 10) adsorbs about three times more H_2 at a pressure of 1000 bars. The adsorption capacity of a bigger armchair nanotube (20,20) is slightly more than that of (10,10) but still less than that of (20,10). Some experimental and theoretical studies have shown that the functionalization of carbon nanotubes by transition metals enhances the hydrogen storage capacity of the nanotubes. In their first-principles studies, Meng *et al.* [72] and recently Banerjee *et al.* [73] have reported that the Ti-decorated SiCNTs can adsorb up to four molecules of hydrogen per Ti atom. The storage of hydrogen in functionalized SiCNT has a promising future. There are very few works done on that area. One of these very few studies using density functional theory by Wang and Liew [74] has shown that the hydrogen adsorption on SiCNT is greatly enhanced by lithium doping. The study has predicted that the physisorption binding energies of hydrogen molecule with Li-adsorbed SiCNT are about 2.5 times larger than those with a pure SiCNT. Functionalization of SiCNTs by a wide range of metals and investigating the hydrogen storage capability of the functionalized nanotubes could be one of potential research in hydrogen storage problem. However in practical case, some of the air components, oxygen in particular, might suppress the hydrogen storage capability of SiCNT. So to understand how oxygen might compete with hydrogen for adsorption in pristine and functionalized SiCNTs is very important for any practical prediction of hydrogen storage in SiCNTs.

To fully understand the behavior of nanotubes implemented in actual nano-scale electronic circuits, one has to first understand the transport properties of the nanotubes in

various conditions. Computational and theoretical studies on carbon nanotube and other molecular wires junctions implemented in various nanoelectronic circuits [75-78] have predicted some very important transport characteristics of such nanostructures. There are relatively few works on transport properties of silicon carbide nanotube available in literature [9, 79-84]. Song *et al.* [81] investigated electronic transport properties of (4,4) armchair SiCNT and found the negative differential resistance (NDR) in the I-V curve of the SiCNT in the bias from +1.6 to +2.2 V. This comes from the variation in density of states (DOS) and the fluctuation of the transmission coefficient caused by the applied bias voltage. In another similar study on (7,0) zigzag SiCNT [79], it is reported that the current decreases when the bias is between +1.4 V and +1.7 V indicating that NDR appears in this bias range. NDR is an important property of the nanotubes for application in molecular switches and other electronic devices. The bias range for NDR changes when the nanotube is doped by boron [82]. A recent study [84] has shown that co-doping BN impurities in the silicon carbide nanotube suppress this important NDR property due to introduction of new electronic states near the Fermi level followed by weak orbital localization. The transport properties of SiCNT can be altered by attaching a molecule on the wall of the nanotube. Ding *et al.* [9] have shown that under a bias of +1.5 V, the current through a gas molecule NO_2 adsorbed (8, 0) zigzag SiCNT is about 1.5 times that with no gas molecule adsorbed. This effect is large enough for the detection of the gas. This can help to design nanoelectronic circuits for the detection of toxic gases.

Menon *et al.* [46] have shown that there are two different arrangements (type 1 and type 2) for the most stable SiC nanotubes. They have studied certain nanotubes in armchair and zigzag configuration. Type 1 consists of alternating Si and C atoms with each Si atoms having three C neighbors and vice versa. In type 2 configuration, each Si atom has two C neighbors and one Si neighbor and vice versa. Kazi and Ray [47, 48] have proposed a new type 3 SiC tube which has the same number of Si and C atoms, but differs in the relative spatial positions of Si and C atoms. In this type, each Si has two C and one Si neighbors, has the same

constraint as type 2, but Si and C atoms are arranged alternatively in each layer unlike in type 2 where each layer contains either Si or C atoms. Thus, type 3 has one similarity with type 1 in alternating Si and C atoms along one layer perpendicular to the tube axis, though it differs in overall atomic arrangement. SiC nanotubes of type 1 configuration are found to be more stable than those of type 2 and type 3. This is in contrast to other silicon carbide nano-clusters which prefer segregation of silicon and carbon atoms [85, 86]. The SiCNTs prefer uniform distribution of silicon and carbon atom. Kazi and Ray [47,48] have shown that since type-1 SiCNTs have only Si-C bonds which are partially ionic, these nanotubes have greater band gaps that the type-2 and type-3. Also, due to the ionic nature of Si-C bonds, band gap of the type-1 SiCNTs show anomalous dependence on diameter.

CHAPTER 2

THEORY

2.1 Introduction

To understand behavior of any electronic system such as an atom, molecule, nano-cluster, or solid, we have to first know the fundamental properties of the system. The ground state properties like total energy, atomization energy, vibrational frequency, equilibrium geometry etc. of the system can be calculated by solving the N-electron Schrodinger equation for the N-electron ground state wavefunctions. This method of solving Schrodinger equations is exact in principle but not useful for any practical purpose, especially for large N. Density functional theory (DFT) methods are efficient and practical methods to solve any electronic system with large N. DFT methods are most widely used methods in computational material sciences. DFT takes the electron density as the basic variable for the description of the energies of an electronic system. DFT is in principle an exact formulation for the ground state of many-electron systems and it expresses ground state properties– such as equilibrium positions, total energies, and magnetic moments as functional of the electron density $\rho(\vec{r})$. DFT maps an N electron-system to a single variable, the electron-density. This reduces the computational cost significantly. DFT provides an elegant way to solve a many-electron problem with improvable compromise between accuracy and efficiency.

The orbital-free formulation of n-electron problem started with Thomas-Fermi theory [87, 88] in 1920s. In Thomas-Fermi model of an electronic system, the total energy is expressed as the functional of the electron density and the energy functional is minimized keeping fixed electron number. This model gives the total energy of electronic systems with an error of about 10%. However, this model is not good enough to estimate most properties of interest. Because of the crude formulation and absence of exchange-correlation energy, atoms do not bind

together to form molecules and solids in Thomas-Fermi theory [89]. The electron exchange energy was included into the Thomas-Fermi functional by Dirac in 1930 [90]. The use of electron-density as the basic variable in many electron systems was re-established by two Hohenberg-Kohn theorems published in 1964 [91] and Kohn-Sham theorems published in 1965 [92].These theorems, often regarded as twin pillars of modern density functional theory (DFT), are exact in principle. There has been a significant amount of theoretical and computational research works based on this theory in past forty years [93-100].

2.2 Density Functional Theory

The Hamiltonian for an N-electron and N'-nuclei system is given by

$$H = -\sum_{i=1}^{N}\frac{\hbar^2}{2m}\nabla_i^2 - \sum_{I=1}^{N'}\frac{\hbar^2}{2M_I}\nabla_I^2 - \frac{1}{4\pi\epsilon_0}\sum_{I=1}^{N'}\sum_{i=1}^{N}\frac{Ze^2}{r_{iI}} + \frac{1}{4\pi\epsilon_0}\sum_{i<j}^{N}\frac{e^2}{r_{ij}} + \frac{1}{4\pi\epsilon_0}\sum_{I<J}^{N'}\frac{Z_I Z_J e^2}{R_{IJ}} \quad (2.1)$$

Where the first and second terms give the kinetic energies of electrons, and nuclei respectively, the third term gives electrons-nuclei interaction energy, the fourth term gives the electron-electron interaction energy and the last term gives the nuclei-nuclei interaction energy.

In Born-Oppenheimer approximation, the electrons in a molecule are considered to be moving in the field of fixed nuclei. The second term of the equation (2.1) is therefore can be neglected and the last term can be taken as a constant. Since the last term is taken as a constant the equation (2.1) can be written as

$$H = -\sum_{i=1}^{N}\frac{\hbar^2}{2m}\nabla_i^2 - \frac{1}{4\pi\epsilon_0}\sum_{I=1}^{N'}\sum_{i=1}^{N}\frac{Ze^2}{r_{iI}} + \frac{1}{4\pi\epsilon_0}\sum_{i<j}^{N}\frac{e^2}{r_{ij}} \quad (2.2)$$

since a constant added to the operator does not have effect on eigenfunction of the operator. In atomic unit equation (2.2) has the form

$$H = \sum_{i=1}^{N}\left(-\frac{1}{2}\nabla_i^2\right) + \sum_{i=1}^{N} v(r_i) + \sum_{i<j}^{N}\frac{1}{r_{ij}} \quad (2.3)$$

In many cases the problems related to electronic structures can be studied by the time-independent Schrödinger equation

$$H\Psi = E\Psi \quad (2.4)$$

where H is the Hamiltonian given by equation (2.3), E is the electronic energy and $\Psi = \Psi(x_1, x_2, x_3, \ldots, x_N)$ is the many-electron wave function where x_i's are the electron coordinates and spins. One of the methods to solve the many electron problems is to solve equation (2.4) to find this many-electron wave function and then calculate the properties of the system by taking this many-electron wave function a basic variable. In Hartree approximation [101], this many electron wavefunction is taken as the product of single electron wavefunctions,

$$\Psi(x_1, x_2, x_3, \ldots \ldots x_N) = \Psi_1(x_1)\Psi_2(x_2)\Psi_3(x_3) \ldots \ldots \Psi_N(x_N) \quad (2.5)$$

The single-electron wave functions $\Psi_i(x_i)$ satisfy one-electron Schrodinger equation

$$\left[-\frac{1}{2}\nabla^2 + v(r_i) + \varphi_i\right]\Psi_i(r) = \varepsilon_i\Psi_i(r) \quad (2.6)$$

Where $v(r_i)$ is the potential due to nuclei and the Coulomb potential φ_i is determined by the equation

$$\nabla^2\varphi_i = -4\pi\sum_{j=1,i\neq j}^{N}\left|\Psi_j\right|^2 \quad (2.7)$$

The equation (2.5) takes no account of indistinguishability of electrons since it assigns a specific state to a specific electrons. Therefore, even if we consider the electrons to be independent particles (which is not the case) the equation (2.5) has a fundamental problem. Accroding to Pauli's exclusion principle a many-electron wave function must be antisymmetric with respect to the interchange of space and spin coordinates of any two electrons. A correct antisymmetrized wave function can be represented by a single determinantal functions called Slater determinant. Hartree-Fock approximation [101-102] makes the use of this antisymmetrized wave function. Use of the Slater determinant introduces a nonlocal exchage effect in the schrodinger equation and this improves the total energy calculation but the single particle picture, with the wave function described in terms of orbital with particular spins and occupation numbers is unchanged. It has been noted that a single Slater determinant wave function must inevitably lead to a poor energy since the lowest-lying configuration is generally only one of very many with comparable energies, and a better approximation would result from taking a linear combination [103]. This approach known as "configuration interaction" (CI) includes the

correlation effects beyond Hartree-Fock approximation by improving the many-particle wave functions. In principle, CI provides an exact solution of the many-electron problems. In practice, however, the explosive increase in the number of configurations with increasing electron number limits its application to only small systems with relatively few electrons. Furthermore, the complexity of the resulting solutions means that a simple interpretation of the results is often difficult.

Thomas-Fermi model [87, 88] represented the total energy of a many-electron system as the functional of electron-density,

$$\rho(r) = N \int \Psi^*(r, r_2, r_3, \dots\ r_N)\Psi(r, r_2, r_3, \dots\ r_N)dr_2 dr_3 \dots dr_N \tag{2.8}$$

The total energy is given by,

$$E_{TF}[\rho] = E_{TF}[\rho] + E_{ne}[\rho] + J[\rho] \tag{2.9}$$

Where the first term is the kinetic energy, second term is the nuclei-electron interaction energy and the third term is the Coulombic electron-electron interaction energy. The kinetic energy is calculated by assuming that the motions of the electrons are uncorrelated. The Thomas-Fermi model is entirely a local approximation in which the kinetic energy is calculated based on the results for uniform electron-gas. Also, the Thomas-Fermi model does not require the antisymmetrized wave function with respect to permutation of any pair of electrons. Therefore the exchange effect is not taken into account. Dirac [90] added an exchange term to the Thomas-Fermi model by incorporating a term derived from the exchange energy density in a homogenous system. As discussed in introduction the Thomas-Fermi model is too crude to estimate general characteristics of an electronic system. The most important deficiency of this model is that it fails to explain the formation of bonds between atoms in a molecule [89].

2.1.1. Hohenberg-Kohn Theorems

The Hohenberg-Kohn theorems establish that one can use electron-density as the basic variable and get rigorously accurate results for any many-electron system. It states that

the external potential can be determined, within a trivial additive constant, by the electron-density.

If $\rho(r)$ is the electron density for the non-degenerate ground state of some N-electron system, then,

$$\int \rho(r)dr = N \tag{2.10}$$

The external potential $v(r)$ can be determined from $\rho(r)$. Hence the ground-state wave function Ψ can be determined from $\rho(r)$. Similarly, other electronic properties can also be determined from $\rho(r)$.

If there were two external potentials v and v' each giving the same electron density $\rho(r)$ for its ground state, we would have two Hamiltonians H and H' whose ground state densities were the same although the normalized wave functions Ψ and Ψ' would be different

$$H\Psi = E\Psi \tag{2.11}$$

$$H'\Psi' = E'\Psi' \tag{2.12}$$

H and H' have the ground-state energies E and E_1 respectively.

Now taking Ψ' as the trial function for H problem,

$$E < \langle\Psi'|H|\Psi'\rangle$$

$$=\langle\Psi'|H'|\Psi'\rangle + \langle\Psi'|H - H'|\Psi'\rangle$$

$$=E' + \langle\Psi'|v(r) - v'(r)|\Psi'\rangle$$

$$=E' + \int\big(v(r) - v'(r)\big)\rho(r)dr \tag{2.13}$$

Similarly, taking Ψ as the trial function for H' problem,

$$E' < \langle\Psi|H'|\Psi\rangle$$

$$=\langle\Psi|H|\Psi\rangle + \langle\Psi|H' - H|\Psi\rangle$$

$$=E + \langle\Psi|v'(r) - v(r)|\Psi\rangle$$

$$=E - \int\big(v(r) - v'(r)\big)\rho(r)dr \tag{2.14}$$

Adding inequalities (2.13) and (2.14) we get,

$$E + E' < E' + E \tag{2.15}$$

This is a contradiction. Therefore the initial assumption that there are two different potential for the same electron-density is wrong. Thus, the density must uniquely determine the external potential, and hence the Hamiltonian and the ground state energy of the system. The ground state total energy can be written as a functional of the electron density,

$$E[\rho] = T[\rho] + V_{ne}[\rho] + V_{ee}[\rho] = \int \rho(r) v(r) dr + F_{HK}[\rho] \tag{2.16}$$

where $T[\rho]$ is the kinetic energy, $V_{ne}[\rho]$ is the nuclei-electron interaction energy and $V_{ee}[\rho]$ is the electron-electron Coulomb interaction energy and $F_{HK}[\rho] = T[\rho] + V_{ee}[\rho]$ is a universal functional of $\rho(r)$ in a sense that $F_{HK}[\rho]$ is defined independently of the external potential $v(r)$.

The second Hohenberg-Kohn theorem states: *For a trial density* $\rho_1(r)$, *such that* $\rho_1(r) \geq 0$ *and* $\int \rho_1(r) dr = N$,

$$E_0 \leq E[\rho_1] \tag{2.17}$$

where E_0 *is the ground state energy and* $E[\rho_1]$ *is the energy functional of (2.16).*

The energy variational principle can be obtained from this theorem. It means that the ground-state electron density is the density that minimizes $E[\rho]$. The first theorem assures that $\rho_1(r)$ determines its own v_1, Hamiltonian H_1, and wave function Ψ_1. Let us take Ψ_1 as a trial function for the Hamiltonian H of interest with external potential v. The variational principle asserts that,

$$\left\langle \Psi_1 \middle| \hat{H} \middle| \Psi_1 \right\rangle \geq \left\langle \Psi_0 \middle| \hat{H} \middle| \Psi_0 \right\rangle \tag{2.18}$$

where Ψ_0 is the ground state wavefunction.

$$\left\langle \Psi_1 \middle| \hat{F}_{HK} \middle| \Psi_1 \right\rangle + \left\langle \Psi_1 \middle| \hat{v} \middle| \Psi_1 \right\rangle \geq \left\langle \Psi_0 \middle| \hat{F}_{HK} \middle| \Psi_0 \right\rangle + \left\langle \Psi_0 \middle| \hat{v} \middle| \Psi_0 \right\rangle$$

$$F_{HK}[\rho_1(r)] + \int \rho_1(r)v(r)dr \geq F_{HK}[\rho_0(r)] + \int \rho_0(r)v(r)dr$$

$$E[\rho_1(r)] \geq E[\rho_0(r)] \tag{2.19}$$

Assuming differentiability of $E[\rho]$ the variational principle requires that the ground state density satisfies the stationary principle-

$$\delta\left\{E[\rho] - \mu\left(\int \rho(r)dr - N\right)\right\} = 0 \tag{2.20}$$

which gives the Euler-Lagrange equation

$$\mu = \frac{\delta \mathrm{E}[\rho]}{\delta\rho(r)} = v(r) + \frac{\delta F_{HK}[\rho]}{\delta\rho(r)} \tag{2.21}$$

where μ is the Lagrange multiplier associated with the constraint $\int \rho(r)dr = N$.

The functional $F_{HK}[\rho]$ known as Hohenberg-Kohn functional or the universal functional is very important in the formulation of density functional theory. Once the functional $F_{HK}[\rho] = T[\rho] + V_{ee}[\rho]$ is known exactly we would have exact solution of any many-electron problem. Therefore it is regarded as the 'holy grail of density functional theory' [98]. The functional $F_{HK}[\rho]$ contains the functional for kinetic energy and that for electron-electron interaction energy. The exact form for both of these is not known. The classical part of the electron-electron interaction is known exactly, but the explicit and exact forms for non-classical effects are still unknown. The non-classical contribution the electron-electron interaction contains all the effects of self-interaction correction, and exchange –correlation. Although the Hohenberg-Kohn theorems do not give insights of actual methods of calculation, and it is usually $v(r)$ rather than $\rho(r)$ that is known, they provide confidence that it is sensible to seek solutions of many-body problems based on the density rather than the wave functions.

2.1.2. Kohn-Sham Method

The second major work on density functional theory appeared in 1965. In this work the Kohn and Sham proposed a systematic way of approaching the unknown universal functional. It was in fact very important step towards implementing density functional theory in practical computational calculations. Early attempts to approximate the universal functional $F_{HK}[\rho]$ used the Thomas-Fermi approximation for the kinetic component $T[\rho]$. It was soon realized that only very crude answers can be obtained with this local functional for the kinetic energy, no matter how sophisticated the approximation for the $V_{ee}[\rho]$ component is. Kohn and Sham therefore proposed a functional giving the major part of the kinetic energy and the scheme makes the density functional theory practical. Kohn and Sham assumed that the kinetic energy term has a component that is independent of the electron-electron interaction and that the electron-electron potential term has a component that is described as a classical Coulomb potential. Therefore the universal functional is given by,

$$F_{HK}[\rho]=T[\rho]+V_{ee}[\rho]=T_s[\rho]+J[\rho]+E_{xc}[\rho] \tag{2.22}$$

where the first term is the kinetic energy term which is independent of electron-electron interaction, the second term is the classical Coulomb potential and the third term is the exchange-correlation energy defined by the equation-

$$E_{xc}[\rho]\equiv T[\rho]-T_s[\rho]+V_{ee}[\rho]-J[\rho] \tag{2.23}$$

Kohn-Sham method invokes a noninteracting reference system, with the Hamiltonian,

$$H_s=\sum_i^N(-\frac{1}{2}\nabla_i^2)+\sum_i^N v_{eff}(r_i) \tag{2.24}$$

for which the ground-state electron density is exactly $\rho(r)$. For a non-interacting system, the many electron wavefunction is a single Slater determinant

$$\Psi_s=\frac{1}{\sqrt{N!}}\det\left[\Psi_1\Psi_2...\Psi_n\right] \tag{2.25}$$

where the Ψ_i are the N lowest eigenstates of the one-electron Hamiltonian h_s:

$$h_s \Psi_i = \left[-\tfrac{1}{2} \nabla^2 + v_{eff}(r) \right] \Psi_i = \varepsilon_i \Psi_i$$

(2.26)

$$\rho(r) = \sum_i^N \sum_s \left| \Psi_i(r,s) \right|^2 \tag{2.27}$$

The kinetic energy is then given by,

$$T_s[\rho] = \sum_{i=1}^N \left\langle \Psi_i \left| -\frac{1}{2} \nabla^2 \right| \Psi_i \right\rangle \tag{2.28}$$

It is to be noted that $T_s[\rho]$ here is not the true kinetic energy of the interacting system whose ground state density is $\rho(r)$, but is in fact much closer to the kinetic energy $T[\rho]$, in the final optimized description, than it is to the Thomas-Fermi kinetic energy. There are two parts of contributions to the exchange correlation energy $E_{xc}[\rho]$: one is from the non-classical effects of the electron-electron interactions and the other is from the kinetic energy. The Euler equation now becomes

$$\mu = v_{eff}(r) + \frac{\delta T_s[\rho]}{\delta \rho(r)} \tag{2.29}$$

where the Kohn-Sham effective potential is defined by

$$v_{eff}(r) = v(r) + \frac{\delta J[\rho]}{\delta \rho(r)} + \frac{\delta E_{xc}[\rho]}{\delta \rho(r)} \tag{2.30}$$

$$= v(r) + \int \frac{\rho(r')}{|r - r'|} dr' + v_{xc}(r)$$

which the exchange-correlation potential

$$v_{xc}(r) = \frac{\delta E_{xc}[\rho]}{\delta \rho(r)} \tag{2.31}$$

Equations 2.26, 2.27, 2.30, and 2.31 are the four essential Kohn-Sham equations. The effective potential v_{eff} as we see from equation (2.30) is also a functional of the electron density. Therefore, the Kohn-Sham equations have to be solved self-consistently. Figure 2.1 shows the flowchart for the standard DFT calculations.

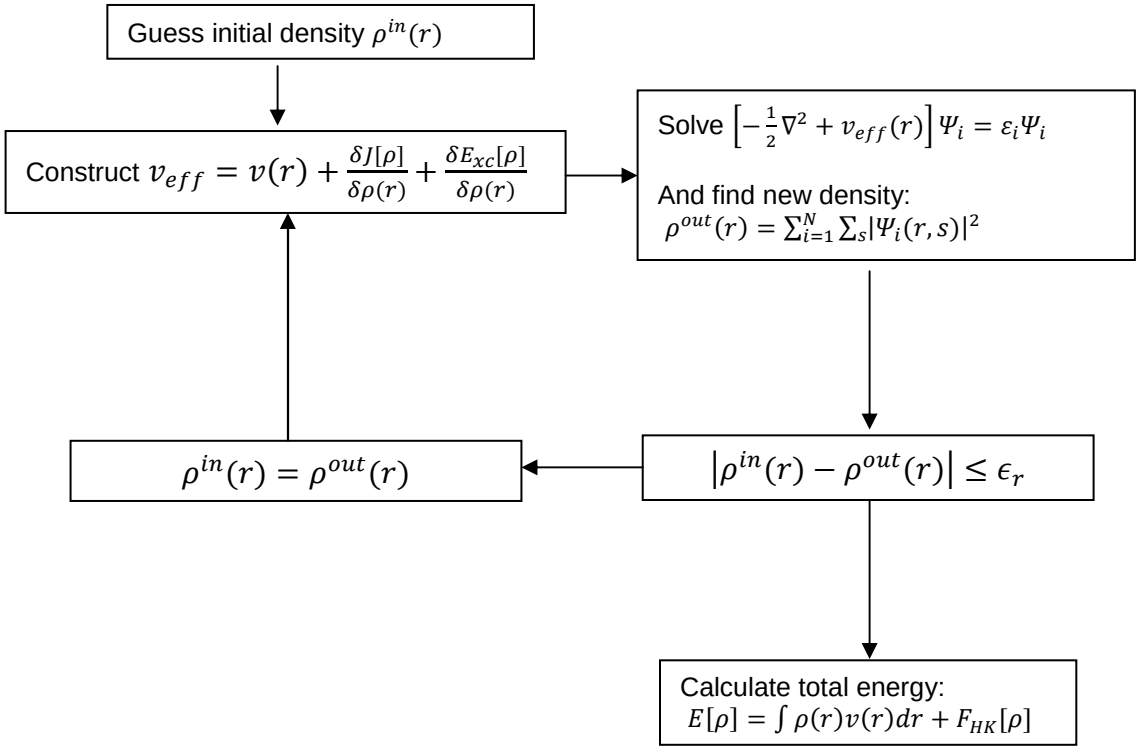

Figure 2.1 Flowchart for DFT calculations

The Kohn-Sham scheme provides a simple but rigorous way to compute the electronic properties within density functional theory. In principle, the Kohn-Sham equations will yield exact ground state properties if an exact exchange correlation potential is given. However, the Kohn-Sham scheme does not provide methods to obtain the explicit exchange and correlation functionals and therefore, approximations have to be considered.

2.3 Exchange and Correlation Functionals

Kohn-Sham formalism exactly incorporates most of the contributions to the electronic energy of an atomic or molecular system. All the unknown quantities are collectively put in the term called exchange-correlation functional. As discussed above, this functional contains non-classical contribution of the electron-electron interactions and the kinetic energy not covered by the non-interacting reference system. An explicit form for this exchange-correlation functional is needed to specify Kohn-Sham equations. Finding the explicit form for this functional the greatest challenge in density functional theory. In fact, the accuracy of the approximate exchange-correlation functional determines the quality of any DFT calculation. In the following section we discuss three major approximations to the exchange-correlation functional, namely, local density approximation (LDA), generalized gradient approximation (GGA), and the hybrid functional approximations.

2.3.1. Local Density Approximation

Local density approximation (LDA) is the simplest approximation based on uniform electron gas. This was first proposed by Kohn and Sham [92]. LDA is a fairly good model for simple metals like sodium. For any system with very slowly varying densities this approximation is reasonably good but for the systems characterized by rapidly varying densities it is not good enough. However, LDA has a prominent role in DFT because uniform electron gas is the only system for which we know the form of exchange and correlation energy functionals exactly or at least to vary high accuracy and this represents the bedrock of almost all current functionals [98].

The total exchange-correlation energy of a system with very slowly varying density can be given by,

$$E_{xc}^{LDA}[\rho] = \int \rho(r)\varepsilon_{xc}(\rho)dr \qquad (2.32)$$

where $\varepsilon_{xc}(\rho)$ is the exchange and correlation energy per particle of a uniform electron gas of density $\rho(r)$. The functional derivative of $E_{xc}^{LDA}[\rho]$ gives the local approximation to the Kohn-Sham exchange-correlation potential

$$v_{xc}^{LDA}(r)=\frac{\delta E_{xc}^{LDA}}{\delta\rho(r)}=\varepsilon_{xc}(\rho(r))=\rho(r)\frac{\delta\varepsilon_{xc}(\rho)}{\delta\rho} \tag{2.33}$$

The Kohn-Sham equation becomes

$$\left[-\frac{1}{2}\nabla^2+v(r)+\int\frac{\rho(r')}{|r-r'|}dr'+v_{xc}^{LDA}(r)\right]\Psi_i=\varepsilon_i\Psi_i \tag{2.34}$$

The local exchange-correlation energy is the sum of correlation and exchange effects,

$$\varepsilon_{xc}(\rho)=\varepsilon_x(\rho)+\varepsilon_c(\rho) \tag{2.35}$$

where $\varepsilon_x(\rho)$ is the exchange energy per particle of a homogenous electron gas. The analytical expression of this term for homogeneous electron gas is known exactly and is given by,

$$\varepsilon_x(\rho)=-\frac{3}{4}\left(\frac{3}{\pi}\right)^{1/3}\rho(r)^{1/3}=-\frac{0.4582}{r_s} \tag{2.36}$$

Here r_s is the Wigner-Seitz radius,

$$\frac{4}{3}\pi r_s^3=\frac{1}{\rho} \tag{2.37}$$

There is no simple analytical formula for the correlation energy $\varepsilon_c(\rho)$. Only some limiting cases are found to have analytic form. For example, in high-density limit the correlation energy is given by [104, 105],

$$\varepsilon_c=0.0311\ln r_s-0.048+r_s(A\ln r_s+C),\qquad r_s\ll 1 \tag{2.38}$$

And in low-density limit the correlation energy is given by [106, 107],

$$\varepsilon_c=\frac{1}{2}\left(\frac{g_0}{r_s}+\frac{g_1}{r_s^{3/2}}+\frac{g_2}{r_s^2}+\cdots\right),\qquad r_s\gg 1 \tag{2.39}$$

The Kohn-Sham-LDA is further extended to the spin dependent case by replacing the scalar external potential $v(r)$ by a spin dependent potential $v_{\alpha\beta}(r)$ and replacing the charge density $\rho(r)$ by the density matrix $\rho_{\alpha\beta}(r)$ [108-110]. The electron densities with spin projection up $\rho_{\alpha}(r)$ and down $\rho_{\beta}(r)$ are treated separately. Similarly, one can deal with $\rho(r)=\rho_{\alpha}(r)+\rho_{\beta}(r)$, along with the polarization $\zeta(r)=[\rho_{\alpha}(r)-\rho_{\beta}(r)]/\rho(r)$. ζ takes values between -1 (fully polarized downwards) and +1 (fully polarized upwards). The spin-up and spin-down densities are generated from the spin-up and spin-down Kohn-Sham wave functions. This so-called local spin density (LSD) approximation improved LDA for atomic and molecular systems with unpaired spins. Most of the modern LDA functional are very similar having the difference only in how the correlation energy is fitted into the functional. Vosko-Wilk-Nusair (VWN) [110], Cole-Perdew (CP) [111], Perdew-Zunger(PZ81) [112] and Perdew-Wang (PW92) [113] functionals are commonly used in modern LDA.

LDA and its spin generalization LSD allow one to use the knowledge of the uniform electron gas to predict properties of the in homogenous electron gases occurring in atoms, molecules and solids. Specifically, LSD usually has moderate accuracy for most systems of interest, making errors of order 5-10%. Its most remarkable feature is its reliability, making the same kinds of errors on every system it's applied to. The success of LDA is due to the systematic error cancellation in its formulation. In general, LDA underestimate correlation but overestimates exchange in inhomogeneous systems. This error cancellation is due to the fact that the exchange-correlation hole $\rho_{xc}^{LDA}(r_1,r_2)$ is spherically symmetric and it obeys the sum rule [109, 114-116] which corresponds to the fact that, if an electron has been found at r_1 , then there is one less electron left to find elsewhere (i.e. , by integral over all r_2),

$$\int n_{xc}^{LDA}(r_1,r_2)dr_2=-1 \qquad (2.40)$$

where the exchange-correlation hole $\rho_{xc}^{LDA}(r_1, r_2)$ is defined by

$$V_{ee} = \iint \frac{1}{r_{12}} \rho_2(r_1, r_2) dr_1 dr_2 = J[\rho] + \frac{1}{2} \iint \frac{1}{r_{12}} \rho(r_1) \rho_{xc}^{LDA}(r_1, r_2) dr_1 dr_2 \quad (2.41)$$

with $J[\rho]$ being the classical Coulomb interaction. This is true because for every r_1, $\rho_{xc}^{LDA}(r_1, r_2)$ is the exact exchange-correlation hole of a homogenous electron gas with density $\rho(r_1)$. Hence, the LDA and LSD describe the total charge of $\rho_{xc}^{LDA}(r_1, r_2)$ correctly.

2.3.2. Generalized Gradient Approximation

Since the LDA formula for E_{xc} is formally justified for systems with slow varying densities, the logical first step ahead is the suggestion of using not only the information about $\rho(r)$ but to supplement this with information about the gradient of charge density $\nabla\rho(r)$ in order to account for the non homogeneity of the true electron density[54]. The exchange correlation functional is expanded in a Taylor series in the gradient of density. .

$$E_{XC}^{GEA} = \int \rho(r) \varepsilon_{XC}(\rho) dr + \int C_{XC}(\rho) \frac{\nabla \rho}{\rho^{2/3}} dr + ... \quad (2.42)$$

This approximation is called gradient expansion approximation (GEA). As we can see in the above equation, the first term of this expansion is LDA. It is expected that this gradient expansion should be a better approximation. However, GEA does not make significant correction to the LDA. The GEA was even worse than LDA. This is because the LDA has much more 'first-principles character' than GEA. LDA preserves the properties of exchange correlation holes [109] but GEA does not. GEA exchange-correlation hole improves the LDA hole only at short separations, but is poorly damped and oscillatory at large separations, and GEA violates the sum rule of the exchange-correlation hole [117,118].

Perdew and others introduced the so-called generalized gradient approximation [95, 113, 119-124] such that the exchange correlation energy can be written as a functional of both the density and its gradient:

$$E_{xc}^{GGA}[\rho_\alpha, \rho_\beta] = \int d^3 r f(\rho_\alpha(r), \rho_\beta(r), \nabla\rho_\alpha(r), \nabla\rho_\beta(r)) \qquad (2.43)$$

The first modern GGA was that of Langreth and Mehl [87], who proposed the idea of truncating the gradient expansion for the exchange-correlation hole. Considering the problems encountered by GEA, Perdew *et al.* [95, 119] proposed several versions of GGA functional by introducing the real-space cutoff procedure on the hole, which restores the sum rule or the normalization and negativity conditions on the GGA hole and generates a short-ranged hole whose angular and system average was much closer to the true hole. The Perdew-Wang 1991 (PW91) GGA functional [113] incorporates no free parameters and is entirely determined from uniform electron gas properties and extract constraints. The Perdew-Burke-Ernzerhof [125] functional is a simplified and refined version of the PW91 functional. Becke [120, 121] derived an exchange functional known as B88 incorporating the known behavior of the exchange hole at large distances outside a finite system. Lee, Yang and Parr [122] obtained the correlation energy as an explicit functional of the density and its gradient and Laplacian, now generally known as the “LYP” functional.

The well-known GGA functionals systematically improve the LDA and, in some calculations, approach the accuracy of traditional quantum chemical (e.g. Configuration Interaction) methods, at much less computational cost. However, according to the quasilocal nature of GGA, the dispersion or long-ranged van der Waals interaction arising from long-ranged correlated electronic density fluctuations in the weak bonding systems such as noble gas dimmers could not be accurately described by either LDA or GGA. On the other hand, similar to LDA, GGA has the difficulty to describe the hole centered far from the electron causing the hole.

2.3.3. Hybrid Density Functional Method

Considering the local or semi local nature of LDA and GGA, Becke proposed the so-called Hybrid Density Functional method which incorporates the exact treatment of exchange by Hartree-Fock theory with DFT approximations for dynamical correlation. This idea was motivated by re-examination of the adiabatic connection,

$$H_{\lambda} = T + \lambda V_{ee} + \sum_{i} v_{\lambda}(r_i) \tag{2.44}$$

where $\lambda$is an inter-electronic coupling-strength parameter that "switches on" the $1/r_{12}$ Coulomb repulsion between electrons. $\lambda = 0$ corresponds to the non-interacting Kohn-Sham reference system, while $\lambda = 1$ corresponds to the fully interacting real system, with $\rho(r)$ being fixed as the exact ground state density of H_{λ} . The $E_{xc}[\rho]$can be written as

$$E_{xc}[\rho] = \int_0^1 d\lambda U_{xc}^{\lambda}[\rho] \tag{2.45}$$

where,

$$U_{xc}^{\lambda}[\rho] = \left\langle \Psi_n^{\lambda} \mid V_{ee} \mid \Psi_n^{\lambda} \right\rangle - J[\rho] \tag{2.46}$$

The obvious first approximation for the λdependence of the integrated in equation (2.45) is a linear interpolation, resulting in the Becke's half-and-half functional:

$$E_{xc}^{h\&h}[\rho] = \frac{1}{2}\left(U_{xc}^{0} + U_{xc}^{1}\right) \tag{2.47}$$

where U_{xc}^{o} is the exact exchange energy of the KS determinant and U_{xc}^{1} is the potential energy contribution to the exchange-correlation energy of the fully interacting system. This half and half functional has the merit of having a finite slope as $\lambda \to 0$, and becomes exact if $E_{xc,\lambda=1}^{DFT}$ is exact and the system has high density. However, it does not provide a good quality of the total energy

and the uniform gas limit is not obtained. Due to this Becke proposed the semi-empirical generalization of 3-parameter hybrid exchange-correlation functional

$$E_{xc}^{B3} = E_{xc}^{LSDA} + a_o(E_x^{exact} - E_x^{LSDA}) + a_x \Delta E_x^{GGA} + a_c \Delta E_c^{GGA} \quad (2.48)$$

Where a_o, a_x and a_c are semiempirical coefficients to be determined by an appropriate fit to experimental data. E_x^{exact} is the exchange energy of the Slater determinant of the Kohn-Sham orbitals. ΔE_x^{GGA} is the gradient correction for the exchange and ΔE_c^{GGA} is the gradient correction for the correlation.

Both methods based on Hartree-Fock (HF) theory and density functional theory (DFT) have their advantages and disadvantages. For example, DFT within the local spin density approximation (LSDA) calculations underestimate the band gaps of semiconductors. The discontinuity of exchange-correlation Kohn-Sham potential results in this discrepancy between theoretical and experimental band gaps. On the other hand, hybrid density functional theory incorporating HF exchange with DFT exchange-correlation has proved to be an efficient method for many systems. It has been verified that hybrid functionals can reproduce the band gaps of semiconductors and insulators quite well.

Though different DFT functionals may produce slightly different quantitatively but not qualitatively different results, studies on semi-conducting materials have shown that, hybrid functionals, in particular B3LYP, is one of the most efficient and computationally inexpensive among all the DFT functionals available for calculation of electronic and structural properties of the semiconducting materials. Hybrid functionals are in general found to be efficient in reproducing the band gaps of semiconductors and insulators [126,127] by treating the exchange part of the interactions better. Muscat *et al.* [126] have shown that the hybrid functional B3LYP reproduces the observed band gaps reliably in a wide variety of materials including semiconductors, ionic and semi-ionic oxides, sulphides and the transition metal oxides.

Bauschlicher [128] has studied the geometries, zero-point energies, and atomization energies of molecules containing first and second row atoms for several levels of theory, including Hartree-Fock theory, second order Moller-Plesset perturbation theory, and density functional theory with five different functionals, including two hybrid functionals and found that B3LYP yielded the best results. Studies by Tomic *et al.* [129,130] have shown that that the B3LYP functional provides better agreements with experimentally derived band gaps compared with results obtained with PBE0, correlated calculations, perturbation theories, and screened exchange functionals for a wide class of zinc-blend and wurtzite structured III-V materials. Similarly, calculations of properties such as ionization energies, electron affinities, electronegativities, hardnesses, fundamental frequencies, and zero-point energies of a wide range of molecules have shown that the hybrid functionals such as B3LYP represent a significant improvement over local and non-local density functional [131,132].

However, the performance of B3LYP functional is very poor in metals [133]. This functional cannot describe periodic systems with homogeneous electron gas (i.e. metals) properly. Also, the semiempirical construction of B3LYP is also regarded as a major drawback of this functional. PBE0 is another hybrid functional which is parameter free and can explain the homogeneous electron gas in an extended system. The PBE0 exchange correlation functional is given by [134]

$$E_{XC}^{PBE0} = E_{XC}^{PBE} + \frac{1}{4}(E_X^{HF} - E_X^{PBE}) \qquad (2.49)$$

Two major advantages of this functionals are its parameter-free construction and its ability to attain exact homogeneous electron gas limit. Therefore PBE0 is a better choice whenever metals are involved in the calculation.

2.4 Basis Set

Whatever be the approximation for the exchange correlation functional we have to solve for a set of one-electron equation of type

$$\left[-\frac{1}{2}\nabla^2 + v_{eff}(r)\right]\Psi_i = \varepsilon_i \Psi_i \tag{2.50}$$

To solve this equation we need to find the coefficients c_i required to express Ψ_i in a given basis set φ_i^b:

$$\Psi_i = \sum_{i=1}^{N} c_i \varphi_i^b \tag{2.51}$$

N is in principle infinite but is practice one works with a limited set of basis functions. The types of basis functions are chosen according to the system under study. Generally, plane-wave basis sets are used in periodic calculations and Gaussian basis sets are used in cluster calculations.

A general expression for a basis function is given by,

$$f = N \times e^{-\alpha r} \tag{2.52}$$

Where N is the normalization constant, α is the orbital exponent and r is the radius. In 1950, S. F. Boys [135] suggested to use Gaussian type of function in molecular calculation. The Gaussian type functions contain the exponential $e^{-\beta r^2}$ rather than $e^{-\alpha r}$. The use of Gaussian type functions, being very easy to evaluate, significantly reduces the computational cost of molecular calculations. There are a significant number of basis sets which use such Gaussian-type orbitals (GTOs) [136-138]. Most commonly used basis sets are minimal basis sets, double-, triple- quadruple- zeta basis sets, split-valence basis sets, polarized basis sets and diffuse basis sets. The minimal basis set has a single basis function for each orbital. In double triple or quadruple zeta basis set there are multiple basis functions corresponding to each valence atomic orbitals. The split-valence basis set often denoted in the form X-YZg have X number of primitive Gaussians comprising each core atomic orbitals. The valence orbitals are composed of two basis functions, one composed of a linear combination of Y primitive Gaussian and the other composed of a linear combination of Z primitive Gaussians. For example the basis set 3-21G splits each valence orbital into two parts, an inner shell and an outer shell. The basis function of the inner shell is represented by two Gaussians, and that of the outer shell by one Gaussian; the core orbitals are each represented by one basis function, each composed of

three Gaussians. The 3-21G basis set supplemented with d-functions called polarization functions is designated 3-21G*.

CHAPTER 3

ANOMALOUS DEPENDENCE OF BAND GAPS OF SILICON CARBIDE NANOTUBES ON DIAMETER

3.1 Introduction

Nanotubes consisting of binary elements, such as BN, are important due to their fascinating chemical and physical properties and huge potential applications in the electronics and opto-electronics industries. Often, such applications are very sensitive to the tube dimensions and band gaps. To have similar structures as those of CNTs, these other hetero-atomic structures are usually isovalent to the carbon based structures. For example, a Si-C or B-N binary complexes in their corresponding nanotubes are isovalent to a C-C pair in CNT. However, while it is well known that the electronic properties of CNTs depend largely on the chirality and diameter of the tubes, the all group-III nitrides and some other similar nanotubes, such as SiC and GeC, do not show such strong dependence on chirality. In addition, the binary nanotubes bring the additional feature of ionicity in the bonding, compared to the only covalent bonding observed in CNT. In this chapter we demonstrate that, the electronic properties of these nanotubes tend to depend strongly on the dimension, namely on the diameter of the nanotubes. This can influence the ionic feature of the bonding and hence the band gap. This general understanding for a set of binary nanotubes also explains several studies indicating the anomalous dependence of band gap on the tube diameter. The main objective of this chapter is to recognize that the silicon carbide nanotube falls under a broad category of binary nanotubes which apparently defy quantum confinement effect.

The band gap in single-walled carbon nanotubes (SWCNTs) decreases as the diameter of nanotube increases [139]. This dependence of band gap on dimension can be explained by theories of quantum size effects. Such dependence has also been observed in other different types of nano-structures, for example, in metal clusters [140]. However, band gaps in group-III nitride, and some group IV binary nanotubes show the opposite trend. Recently, Bekaroglu *et al.* [141] have also studied silicon carbide honeycomb structure and have shown that there is a significant difference between band gap trends in graphene and silicon carbide in term of the variation of the gap with respect to the width of the nanoribbon. Band gap of the bare armchair graphene nanoribbon decreases with increasing the ribbon width and eventually vanish at the limit of infinite-width graphene. Whereas, band gap of the silicon carbide nanoribbon increases with increasing ribbon width and gets saturated after ribbon width of 15 atoms. In fact the band gap shows an oscillatory dependence on ribbon width below 15 atoms. This is in contrast with quantum confinement effects. This anomalous behavior is also shown by SiCNTs. The band gap of silicon carbide nanotubes increases with increase in diameter. The band gap of group-III nitride nanotubes also increases as the diameter increases. In a study by Garcia and Cohen [142], it is predicted that the bulk SiC has the ionicity similar to many group III-V materials. Therefore, it is expected that the band gap of SiC nanostructures follow characteristics similar to group-III nitride nanostructures. However, this phenomenon cannot be explained by only quantum size effects, as it is well known that in standard quantum systems, the separations of the energy levels increase with the decrease of the system's spatial dimension. This unusual band gap dependence on the tube's diameter has been reported earlier. In a recent study of GaN nanotubes by Ismail-Beigi [143], this was attributed to the chemical environment. Some other earlier studies on these nanotubes have attributed this behavior to the increment of strain energy as nanotube diameter becomes smaller [43]. It has also been reported that such band gap dependence can be explained qualitatively by the fact that in the hexagonal phase of AlN [144] and BN [145], band gap decreases as external pressure increases. Similar explanation

has been reported for such kind of band gap dependence on tube diameter in GaSe nanotubes [146]. However, the nanotubes under consideration here are not under any incremental pressure change. Also this does not explain why CNTs show the reverse trend. So far, to the best of our knowledge, *no detailed study and a general explanation which can connect this anomalous behavior of band gaps for all the diverse binary nanotubes have been reported*. In this chapter, from an *ab initio* electronic structure study of group-III nitride, silicon carbide, germanium carbide and silicon germanium nanotubes, we show that the increase of band gap with diameter is a general phenomenon exhibited by all binary nanotubes having an ionic contribution to the bonding between the two constituent atoms in the tube. This ionic contribution, arising from several chemical features of the nanotubes, decreases as the curvature of the tube increases and that the decrease in ionicity causes the HOMO-LUMO gap to decrease. Group-III nitrides, such as BN, AlN and GaN have been synthesized through different techniques [13-15]. There have been several first-principles studies on electronic and structural properties of these group-III nitride nanotubes at various levels of theories [43, 53, 143-145, 147-157]. Density functional theory (DFT) based calculation of InN nanotubes has shown their stability between those of GaNNTs and AlNNTs [158]. Nanostructures of group IV – IV combinations like Si-Ge, Ge-C, and Si-C have been interesting areas of research, both at various experimental and computational levels. Silicon carbide nanotubes are being synthesized by different techniques [31, 32, 38]. Also, some significant amounts of theoretical research have been reported in the literature on SiC nanotubes. Successful synthesis of silicon germanium (SiGe) nanotubes has also been reported [159, 160], and has been studied theoretically. In the following these various nanotubes are studied *on an equal level* by first-principles density functional theory, the focus being on an understanding of the dependency of the band gaps on the dimensions, specifically the diameters of the tubes. Our study demonstrates a very general trend of the band gaps of hetero-atomic CNT-like nanotubes where the bonding has a partial ionic contribution.

3.2 Construction of Nanotubes

The approach used to construct nanotubes in this study comprises of rolling a graphenelike sheet to form a nanotube. As discussed briefly in the first chapter, there are three different arrangements of atoms in silicon carbide nanotubes. The first two, type 1 and type 2, were proposed by Menon *et al.* [46] and the third , type 3, was proposed by Alam and Ray [47,48]. Type 1 consists of alternating Si and C atoms with each Si atoms having three C neighbors and vice versa. In type 2 configuration, each Si atom has two C neighbors and one Si neighbor and vice versa. Type 3 the same constraint as type 2, but Si and C atoms are arranged alternatively in each layer unlike in type 2 where each layer contains either Si or C atoms. It has been reported that type 1 is more stable than other two types (types 2 and 3) of the nanotubes [47, 48]. For example, B.E./atom of an armchair type 1 (11, 11) SiC nanotube is 4.638 eV whereas the corresponding values for types 2 and 3 configurations are 4.452 eV and 4.445 eV, respectively. For this reason we have chosen the type-1 configuration for all the nanotubes discussed in this chapter. The type-2 and type-3 nanotubes do not show the anomalous dependence of band gap on diameter this is another reason of choosing only type-1 configuration for this study. Figure 3.1 shows the atomic arrangement in type-1 binary nanotubes.

We have used the finite cluster approximation, using six unit cells of each nanotube with the dangling bonds at both ends of the tube saturated by hydrogen atoms to simulate the effect of infinite nanotubes. The presence of the hydrogen energy levels will not affect the band gaps of the nanotubes. The finite cluster approach for a single wall nanotube comprises of rolling a graphene like sheet of respective atoms (Si and C, B and N, Ga and N, Al and N, Ge and C, Si and Ge) to form a nanotube. Figure 3.2 shows the optimized structure of silicon carbide nanotube (5, 5) and (10, 10) in type-1 configuration. It has been shown that, this type of CNT-like structure is usually the stable structure for an infinite tube with possible sp^2 double

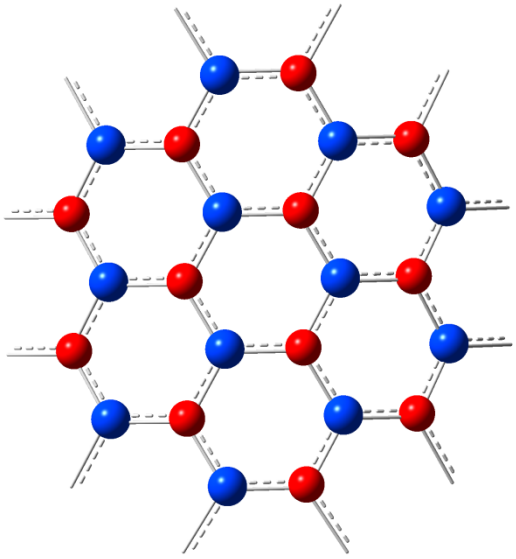

Figure 3.1 Atomic arrangements in type-1 binary nanotubes. The red and blue spheres represent two difference species of atoms.

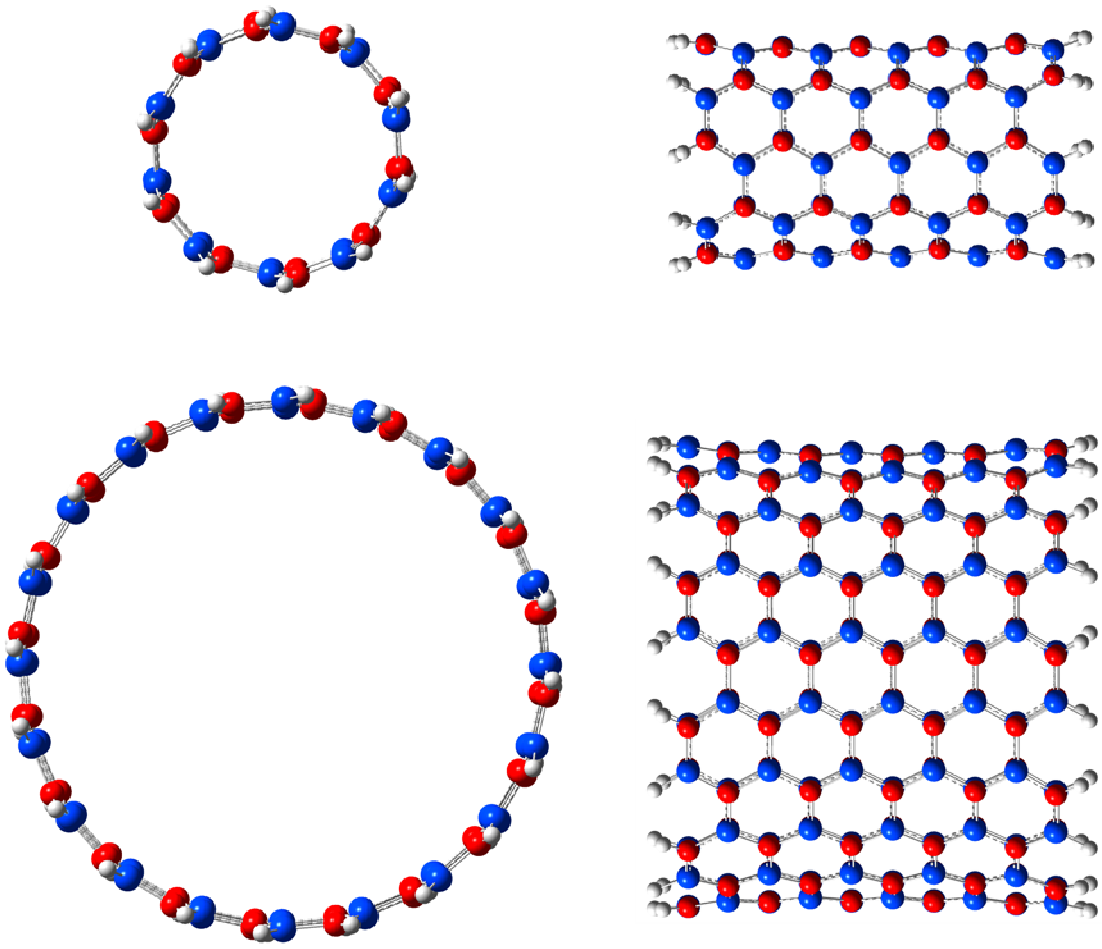

Figure 3.2 Top and side views of binary nanotubes (5, 5) and (10, 10). The red and blue spheres represent two different species of atoms and the grey spheres represent hydrogen atoms used to saturate dangling bonds.

bonding between the atomic species [40]; and also these are lower in energy compared to the atomically segregated ones which may be suitable for finite and closed structures [161]. As the purpose of this chapter is to present the general band gap nature and their trend with the diameter of the tubes, we consider only the CNT-like hexagonal nanotubes [162].

3.3 Computational Method and Discussions of Results

Hybrid density functional theory incorporating Hartree-Fock (HF) exchange [101,102, 136] with density functional theory (DFT) exchange-correlation [163] is used to study the electronic properties of the nanotubes. In particular, we have used the B3LYP hybrid functional [110, 120, 122, 164] and the Los Alamos National Laboratory double ζ basis set [165-167] as implemented in the *GAUSSIAN 03* suite of programs [168] for full geometry optimizations without any symmetry constraints of the nanotube structures. Hybrid functionals are in general found to be efficient in reproducing the band gaps of semiconductors and insulators [126, 127] by treating the exchange part of the interactions better. The reason behind choosing the hybrid functional for this kind of calculation is described in the Chapter 2. Also, the accuracy of this method was tested by calculating the bond lengths of the various dimers, ionization potentials, and the electron affinities of the atoms under consideration. The calculated values were found to be in good agreement with the corresponding experimental values. To give a few examples, the calculated bond length of the SiC dimer is 1.87 Å corresponding to the experimental value of 1.89 Å. The calculated ionization potential and electron affinity of silicon are 8.46 eV and 0.89 eV corresponding to experimental values 8.15 eV and 1.39 eV, respectively. It is well known that a rather large basis set is necessary for a theoretical electron affinity to be in excellent agreement with the experimental value and this was not computationally feasible for the very large systems considered here. However, this should have *no effect* on the results of this study. Similarly, calculated bond length of the BN dimer is 1.35 Å corresponding to an experimental

value 1.28 Å. All computations were performed at the supercomputing facilities of the University of Texas at Arlington.

Before we discuss the results for the band gaps of the nanotubes, we first make some points regarding the stability of the nanotubes and the binding energy. The stability of the nanotubes was estimated by calculating the B.E./atom for each of the nanotubes under consideration. The binding energy was calculated with respect to the infinitely separated atomic limit. Thus the B.E./atom for the binary XY nanotubes with ends saturated by hydrogen atoms was calculated from:

$$E_b = [a\,E(X) + b\,E(Y) + c\,E(H) - E(X_aY_bH_c)]/(a+b+c) \qquad (3.1)$$

where a, b and c are the numbers of X, Y and H atoms, respectively. Depending on the particular XY nanotube studied here, the X and Y represents B, Ga, Al, Si, Ge, N, and/or C atoms. $E(X)$, $E(Y)$ and $E(H)$ are the ground state total energies of X, Y and H atoms respectively; and $E(X_aY_bH_c)$ is the total energy of the optimized clusters representing the nanotubes. Thus a positive binding energy represents a bound and stable nanotube.

The variation of B.E./atom with respect to the number of atoms is shown in Table 3.1 and Figure 3.3. In general, B.E./atom for each nanotube increases as the number of atoms in the nanotube (and consequently the diameter) increases and tends to saturate. Clearly, the saturated binding energy would be equal to that of the graphene-like sheet for each of the corresponding nanotube. The lower binding energy at smaller diameter is caused by the increased strain due to bending of the tube wall. At the limit of graphene-like sheet, i.e. at a very large diameter, the strain on the tube becomes negligible. In the following we will show that this strain on the bonds also changes the nature of the bonding. As we can see from Table 3.1 and Figure 3.3, the most stable nanotube is BN followed by SiC, AlN, GeC, GaN and SiGe. Interestingly, the difference in binding energy from the smallest to the largest diameter tube is also higher in BN nanotubes, followed by SiC. For BN nanotube, this difference is 0.263 eV per atom and for SiC is 0.239eV per atom, which are relatively large differences. Given the fact that

Table 3.1: Binding Energies per Atom (in eV) for Type 1 Armchair Nanotubes

Nanotubes (n,n)	Number of Atoms	BN	GaN	AlN	SiC	GeC	SiGe
(3,3)	72	5.416	3.598	4.020	4.399	3.882	2.733
(4,4)	96	5.537	3.664	4.084	4.507	3.977	2.783
(5,5)	120	5.595	3.696	4.115	4.560	4.019	2.804
(6,6)	144	5.627	3.713	4.132	4.590	4.050	2.822
(7,7)	168	5.647	3.724	4.143	4.608	4.066	2.830
(8,8)	192	5.660	3.731	4.150	4.620	4.077	2.836
(9,9)	216	5.668	3.736	4.155	4.628	4.084	2.840
(10,10)	240	5.675	3.740	4.159	4.634	4.089	2.843
(11,11)	264	5.679	3.743	4.162	4.638	4.092	2.843

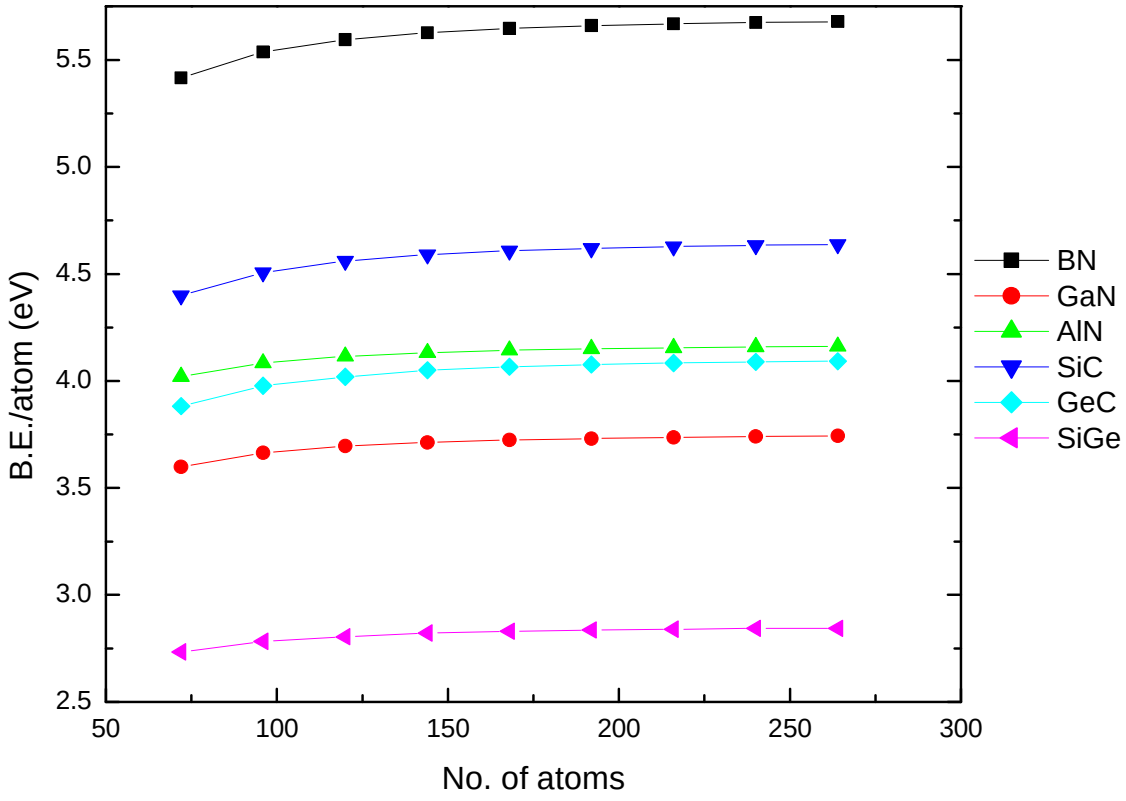

Figure 3.3: B.E./atom (eV) *versus* the number of atoms in the nanotubes.

each atom is three-fold coordinated, the bonding energy changes by approximately 2/3 of the B.E./atom per B-N (or Si-C or other tubes) bond. So the estimates of the changes in bonding energy in B-N or Si-C would be 0.175eV per bond or 0.159eV per bond, respectively, as one proceeds from the smallest to the largest nanotubes considered here. This considerable change in bonding energy clearly indicates the change in the nature of bonding between the smaller and larger nanotubes.

The energy differences between the highest occupied molecular orbital (HOMO) and the lowest unoccupied molecular orbital (LUMO) give a measure of the “band gap” for the infinite nanotubes. This is approximate because the tubes studied here are “finite” in length, apart from the fact that hybrid density functional B3LYP tends to slightly over estimate energy gap [126]. This measure is at least qualitatively correct to compare within a given type of nanotubes with different diameters, and this is sufficient for our present discussions. Table 3.2 and Figure 3.4 show the variation of HOMO-LUMO gaps with respect to the diameter of group III-nitride and group IV-IV nanotubes. It is clear that all tubes under consideration are semiconductors or insulators having band gaps varying from 1.006 eV for the (11, 11) SiGe nanotube to 6.1577 eV for (11, 11) BN nanotube. As the diameter increases, the curvature of the surface decreases and hence the electronic behaviors like that of graphene-like sheet are expected. Therefore, the HOMO-LUMO gaps tend to saturate as its value reaches the band gap for the corresponding graphene-like sheet. In the present set of nanotubes, all the nanotubes, except SiGe, have partial ionic contribution in their bonds. Since SiGe bond is almost perfectly covalent as compared to SiC, GeC and group-III nitride bonds, the band gap saturation limit for the SiGe nanotubes is smaller compared to the other nanotubes. In addition to the quantitative difference in limiting band gaps, there is a qualitative difference in the trend followed by the band gap of the other nanotubes. The interesting and noteworthy feature for the present set of nanotubes is that, except for SiGe, the band gaps of the tubes increases with the increase in diameters. This is in apparent contradiction with the general expected quantum size effect

Table 3.2: Diameter (D in Å) and HOMO-LUMO Gaps (E_g in eV) of Type 1 Armchair Nanotubes

Nanotube		**(3,3)**	**(4,4)**	**(5,5)**	**(6,6)**	**(7,7)**	**(8,8)**	**(9,9)**	**(10,10)**	**(11,11)**
BN	**D**	4.3	5.7	7.0	8.4	9.8	11.2	12.6	14.0	15.4
	E_g	6.0	6.0	6.1	6.1	6.1	6.2	6.2	6.2	6.2
GaN	**D**	5.4	7.1	8.9	10.6	12.4	14.2	15.9	17.7	19.4
	E_g	4.0	4.4	4.6	4.7	4.7	4.7	4.7	4.7	4.7
AlN	**D**	5.3	7.1	8.8	10.5	11.9	14.0	15.8	17.5	19.3
	E_g	4.3	4.5	4.7	4.8	4.9	4.9	5.0	5.0	5.0
SiC	**D**	5.3	7.0	8.7	10.5	12.2	13.9	15.6	17.4	19.1
	E_g	2.8	2.8	2.9	2.9	2.9	2.9	2.9	2.9	2.9
GeC	**D**	4.6	6.1	7.6	9.1	10.6	12.1	13.6	15.1	16.6
	E_g	2.7	2.8	3.0	3.0	3.0	3.0	3.0	3.0	3.0
SiGe	**D**	5.7	7.5	9.3	11.1	13.2	14.8	16.6	18.4	20.3
	E_g	1.6	1.4	1.3	1.2	1.2	1.1	1.1	1.0	1.0

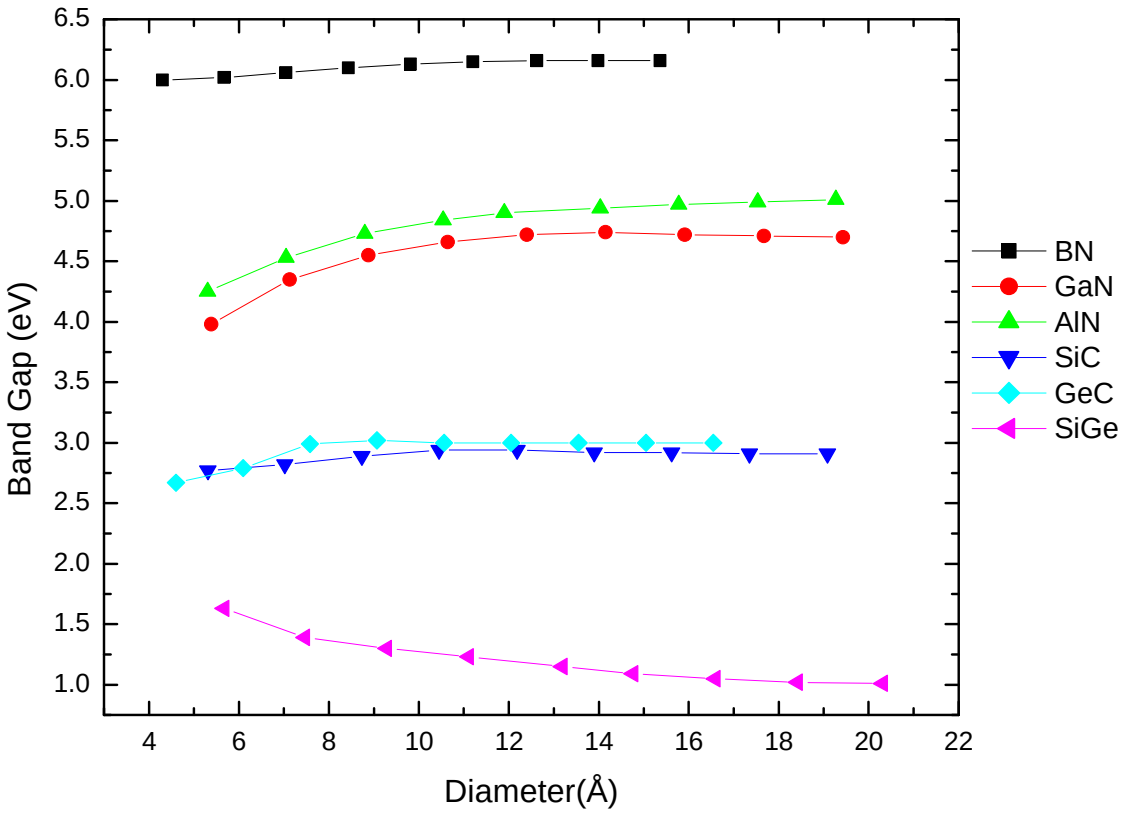

Figure 3.4: Band gap (eV) *versus* the diameter (Å) of the nanotubes.

behavior. At the atomic level, it can be shown easily that the energy difference between the levels increases as the dimension of the system gets smaller. For example, band gaps of carbon nanotubes decrease as the diameter of the tubes get larger, and saturates at the value of that of graphene which is almost zero. This apparent contradiction in the behavior of the band gaps with diameter needs proper explanations. This type of behavior is in agreement with previously published studies of different nanotubes [43, 47, 48, 53,145, 169] where the tubes were considered individually. However, these previous studies did not explain this anomalous feature as a general feature of a class of nanotubes and most of the studies relate this phenomenon to strain energy or chemical environment which does not completely explain the opposite feature of other class of nanotubes like carbon nanotubes and SiGe nanotubes. A fundamental explanation unifying this apparently diverse set of nanotubes is needed to explain this opposing kind of dependence of band gap on diameter.

We propose here that this anomalous dependence of HOMO-LUMO gap on diameter of the tube can be explained by the change in the ionic nature of the bonds between the atoms of the nanotube as the diameter of the tube increases. Table 3.3 and Figure 3.5 show charge transfer, in electronic charge units, between two adjacent atoms in the middle of the nanotubes as a function of the diameter of the tubes. Two atoms in the middle of the nanotubes were taken because they are far from the ends of the tubes, and so would be much less affected by the "ends" of the tubes. Here the "charge transfer" is basically defined by the difference between the Mulliken charges between these two atoms. As is well known, Mulliken charges give only qualitative descriptions of charges on the atoms, so the charge differences given in table 3.3 or Figure 3.5 should be viewed as only qualitative for a given set of nanotubes, not as precise numerical numbers. For our present purpose this should be considered as more than sufficient.

The nanotubes considered here are hetero-atomic structures composed of two types of atoms, one acting as an anion and the other as a cation. The difference between the electronegativity would determine the extent of ionic bonding between the atoms. In general,

Table 3.3: Charge transfer between two adjacent atoms in the middle of nanotubes

	(3,3)	(4,4)	(5,5)	(6,6)	(7,7)	(8,8)	(9,9)	(10,10)	(11,11)
N	-1.52	-1.52	-1.52	-1.53	-1.53	-1.53	-1.53	-1.54	-1.54
Al	1.49	1.48	1.48	1.48	1.48	1.48	1.49	1.49	1.49
N	-1.26	-1.29	-1.30	-1.31	-1.31	-1.32	-1.32	-1.32	-1.32
Ga	1.29	1.30	1.31	1.32	1.32	1.33	1.33	1.33	1.34
C	-1.47	-1.58	-1.63	-1.67	-1.69	-1.71	-1.72	-1.73	-1.73
Si	1.48	1.58	1.64	1.67	1.70	1.72	1.73	1.74	1.74
N	-0.40	-0.60	-0.67	-0.71	-0.74	-0.76	-0.77	-0.77	-0.79
B	0.39	0.60	0.70	0.78	0.80	0.81	0.80	0.79	0.80
C	-1.14	-1.19	-1.22	-1.24	-1.25	-1.26	-1.27	-1.28	-1.29
Ge	1.16	1.20	1.24	1.25	1.27	1.28	1.29	1.29	1.30
Si	0.08	0.04	0.02	0.01	0.00	0.00	-0.01	-0.01	-0.01
Ge	-0.08	-0.04	-0.02	-0.01	0.00	0.00	0.00	0.01	0.01

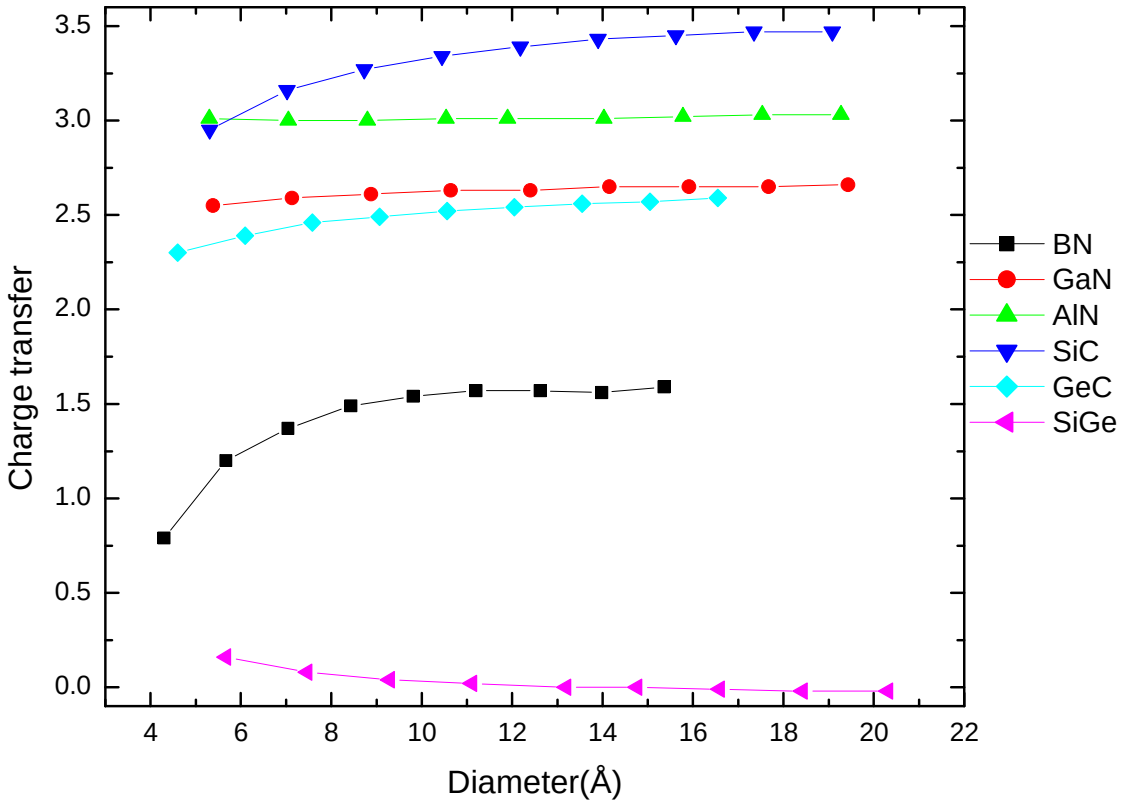

Figure 3.5: Charge transfer between two adjacent atoms in the middle of nanotubes *versus* the diameter of the nanotubes.

higher ionicity may result in higher band gap. The nanotubes presented here have contributions from both ionic and covalent bondings. However, the ionic nature of the bonding in the tubes comes not only from their inherent electronegativity, but also from the curvature of the tubes. Figure 3.5 shows clearly that the ionicity in bonding for a given nanotube increases as the diameter of the tube increases. So, at smaller diameter, ionic contribution is the lowest, and is suppressed by some extra hybridization. This implies that the nature of the hybridization also contributes to the charge transfer between the atoms. For example, at one extreme when the diameter is maximum the local structure of the tubes are almost flat, and the dominant hybridization is sp^2. As the diameter gets smaller, the orientations of the out of plane p_z orbitals are distorted and start hybridizing with other s and p orbitals. The increased curvature causes triangular distribution of hybrid orbital to distort into slightly tetrahedron distribution of the orbitals. This may bring in some sp^3 contribution. So at smaller diameters, the sp^3 hybridization is relatively higher, as can be seen from the buckling of smaller nanotubes [47]. In general, sp^3 hybridization results in slightly lower bond length, and the charge distributions become more covalent-like. So the ionicity at this level could be rather low. As the diameter of a nanotubes increases ionicity of the bonds takes over the sp^3 hybridization until sp^2 hybridization becomes dominant. Once sp^2 hybridization becomes dominant, the ionicity no more increases with increase in diameter. This explains the saturation of band gap in large diameter tube. For the SiGe nanotubes, the electronegativity difference is almost zero; hence the ionic part of the bonding is not prominent even at the large diameter tube.

To visualize the nature of hybridization, we have plotted the HOMO and LUMO for different diameter tubes. For example, Figure 3.6 shows the HOMO and LUMO orbitals of two extreme end tubes, namely, the (3, 3) and (10,10) SiC nanotubes. The important feature of these orbitals is that at the smaller diameter the overlapping of the orbitals due to hybridizations is prominent, and the tube also showed relatively higher buckling [47]. On the other hand, for the bigger diameter tube, the orbitals are distinctly separated, and are clearly p_z in nature. The

(a)

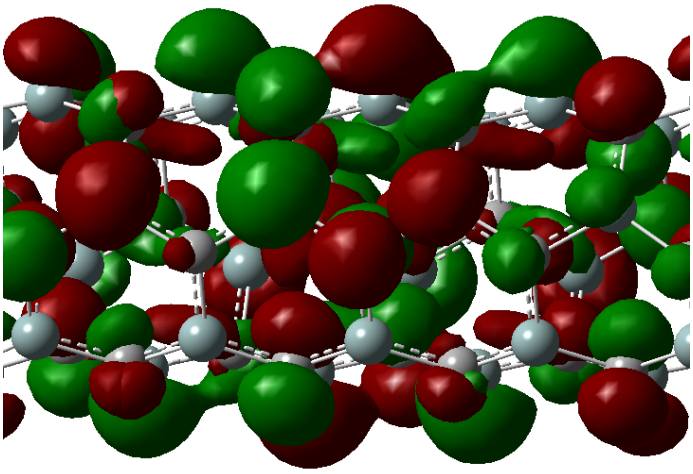

(b)

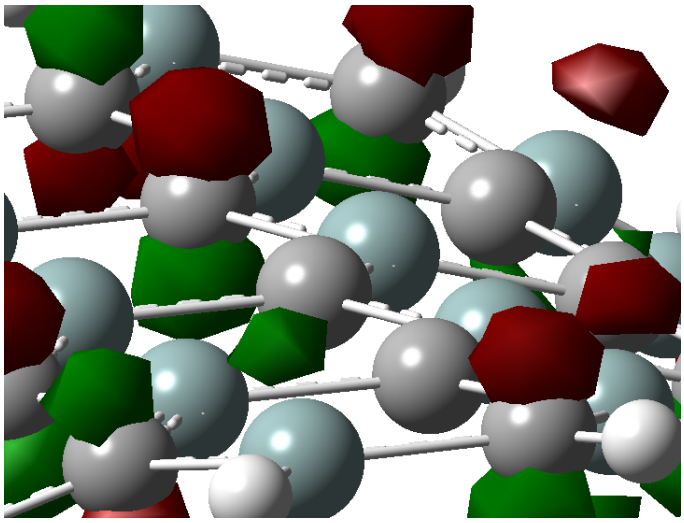

Figure 3.6 HOMO-LUMO plot for (a) (3, 3) and (b) (10, 10) SiC nanotubes. In the smaller diameter tube in (a), the orbital overlap among the neighboring atoms are seen which indicate higher level of sp-hybridization. On the other hand, in (b) at higher diameter, overlap among the neighboring atoms is not sufficient and also the majority of the orbital tend to localize on individual atoms, a sign for higher ionic contribution in the bonding.

localized orbitals in atoms in Figure 3.6(b) demonstrate the higher ionic contribution. As a consequence, the buckling also is reduced significantly. This reduced sp^3 covalency in bonding is compensated by increased ionic contribution as is seen from Figure 3.5.

If we compare Figure 3.5 with Figure 3.4, we see the same trend of increment of the HOMO-LUMO gap and ionicity with respect to the diameter for a given nanotube. This is a clear indication of the dependence of HOMO-LUMO gap on the ionicity of the bonding in a tube. As the ionicity of the bond increases, the band gap of the tube increases. Since C-C bond is perfectly covalent without any ionicity, the band gap does not increase as the diameter increases. Therefore the general trend of the quantum size effect is dominant in carbon nanotube and in silicon germanium nanotubes as seen in the figures. The B-N, Al-N, Ga-N, Si-C and Ge-C bonds have ionic contribution in them, and therefore the effect of ionicity is dominant in these nanotubes as the curvature of the nanotubes increases. The nanotubes with similar kinds of bonds are expected to show the same trend. For example, first principles study on indium nitride (InN) nanotube [158] has shown that the gap increases with diameter of the tube. The reverse trend is observed in types 2 and 3 structures of SiC nanotubes [47]. This can be attributed to presence of the Si-Si, and C-C bonds which are perfectly covalent, in such structure.

3.4 Conclusions

In summary, we have explained and established a general trend for the anomalous band gap behavior with respect to the diameter of the tubes in hetero-atomic CNT-like nanotubes where partial ionic bonding between the constituent atoms plays a major role. Unlike CNT or other finite nanostructures, band gaps of these hetero-atomic nanotubes increase with the tube diameter. This anomaly is explained by the increase in ionic contribution to the bonds with decreasing curvature in these nanotubes which comes from two sources: from the electronegativity differences of the constituent atoms, and from the change in the covalent

nature of the bonding with the curvature of the tubes. Our discussions showed that, with higher hybridization at lower tube diameters, ionic nature of the bonding is suppressed. We also showed that the ionicity in the bonding of nanotubes with type-1 hetero-atomic structure increases with diameter. This increment of ionicity increases the HOMO-LUMO gap of the tubes. Turning off the ionicity of the bonding, such as in SiGe nanotubes, restores the normal band gap behavior consistent with quantum size effect. With the addition of some like pairs of atoms in the nanotube, it might be possible to construct nanotubes in which quantum confinement effect is balanced by the effect of ionicity, resulting in a constant band gap with respect to the diameter.

CHAPTER 4

CARBON – AND SILICON – CAPPED SILICON CARBIDE NANOTUBES

4.1 Introduction

Depending upon the method and environment of synthesis nanotubes terminate in various ways. Most of the experimental studies have shown that the single-walled carbon nanotubes (SWCNT) terminate with hemispherical or conical cap. Molecular dynamics simulation of the formation process of SWNTs has suggested that an appropriate nanotube cap structure is formed before the growth of a SWNT on top of the cap [170]. The study shows that in the catalytic chemical vapor deposition (CCVD) method to fabricate nanotubes, the hexagonal networks are formed both inside and on the surface of the transition metal catalyst cluster when the cluster reaches saturation with carbon atoms. Then an appropriate nanotube cap is formed and nanotube grows on top of the cap [170]. Experimental studies on SWNTs have also shown that nanotubes are grown by attaching carbon atoms to the hemispherical base formed on the surface of catalyst [171-173]. Also, the techniques of growing nanotubes on hemispherical cap produce the nanotubes with controlled structure or controlled chirality. Since the properties of nanotubes, especially carbon nanotubes, are strongly dependent on chirality, the controlled growth of the nanotubes is highly desirable for their application in nanoelectronic devices [174].

Therefore the initial cap structure is crucial in determining the dimension and chirality of the SWNT. The structure of a cap formed during nucleation stage uniquely determines the chirality of the nanotube that can be attached to it [175]. Therefore it is possible to control the chirality of the nanotubes by controlling the cap formation process [176]. For example, two different hemispheres of the fullerene C_{20} as shown in Figure 4.1 (a) lead us to two entirely

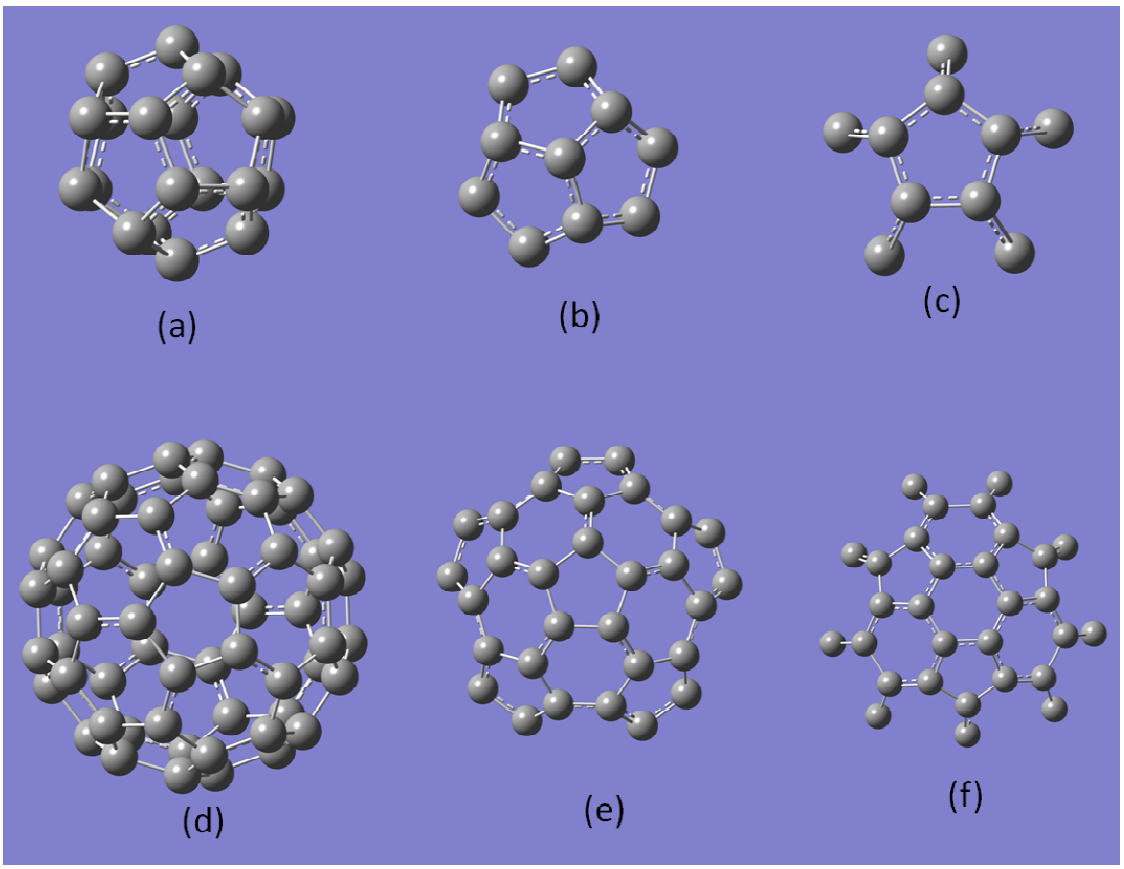

Figure 4.1 Structure of (a) C_{20} fullerene (b) fullerene hemisphere C_{10} to cap nanotube (3,3) (c) fullerene hemisphere C_{10} to cap nanotube (5,0), (d) C_{60} fullerene, (e) fullerene hemisphere C_{30} to cap nanotube (5,5), and (f) fullerene hemisphere C_{30} to cap nanotube (9,0).

different nanotubes. Although the diameter of the nanotubes grown on both of these hemisphere would be same, the chirality and hence the properties of these nanotubes would differ greatly. If a nanotube is grown on top of the cap as shown in Figure 4.1 (b) the nanotube becomes (3,3) and if the nanotube is grown on the top of the cap as shown in Figure 4.1 (c) the nanotube becomes (5,0). Although both the caps are hemisphere of C_{20} fullerene, the orientation of the cap does make a significant difference in the chirality of the nanotube grown upon it. Similarly, two different hemispheres of the fullerene C_{60} as shown in Figure 4.1 (d) can cap nanotubes (5, 5) and (9, 0). Various possible structures of caps can be generated using detailed numerical techniques [177-179]. For a single-walled nanotube (n, m) there are a finite number of possible caps. Typical carbon nanotubes with diameters on the order of 1 nm have 10^3-10^4 different cap structures that fit on them [178]. However a given cap fits only onto one nanotube [176]. Number of possible caps of a nanotube determines the abundance and stability of the nanotubes [180]. C_{60} is the most abundant fullerene structure. The fullerene hemisphere C_{30} can be oriented in two different ways to cap SWNTs (5, 5) and (9, 0). Similarly, the C_{20} is the smallest fullerene structure. C_{20} fullerene does not have hexagonal rings but just 12 pentagons. As mentioned earlier, the fullerene hemisphere C_{10} can cap SWNTs (3, 3) and (5, 0) which are therefore among the smallest nanotubes synthesized so far. Recently, Guan *et al.* [181] have synthesized one of the smallest nanotubes (3, 3) and identified its cap as the fullerene hemisphere C_{10}. All these studies are related to carbon SWNTs. This indicates that understanding the effect of capping a nanotube is very important for determining the synthesis pathways to carbon nanotubes and possibly for other carbon-based nanotubes like silicon carbide nanotubes. Understanding the capping of a nanotube might be helpful for the optimal use of capped nanotube as chemical couriers [182]. Also, understanding structural and electronic properties of capped nanotubes can give insight to their potential applications as liquid crystals [183] and in field emission display (FED) [184]. These applications of capped carbon nanotubes (CNTs) have already been demonstrated. Given the stability of SiC at high

temperature and harsh environment, capped SiC nanotubes can give an alternative towards such application in harsh environment in which carbon nanotubes cannot be used. Also, capped nanotubes can be used as nanocapsules for the delivery of chemicals

In this chapter, we present a detailed *ab initio* systematic study of fullerene capped SiC nanotubes and compare with silicon-capped SiC nanotubes. The nanotubes under study are of two kinds- (i) nanotubes which can be capped by hemisphere of fullerene C_{20}, (3,3) and (5,0); and (ii) nanotubes which can be capped by hemisphere of fullerene C_{60}, (5,5) and (9,0). In the following section, we first discuss our computational details followed by results and discussions.

4.2 Discussions of Results

In this work, we have used the B3LYP hybrid functional [110, 120, 122, 164] and the all electron 3-21G* basis set [136] as implemented in the *GAUSSIAN 03* suite of programs [168] for *full* geometry optimizations without any symmetry constraints of the nanotube structures.

In Chapter 3 we have discussed about the construction of nanotubes based on the rolling of graphene like sheet. The same approach is used to construct the nanotubes discussed in this chapter. The nanotubes studied in Chapter 3 were open and the dangling bonds were saturated with hydrogen to simulate the effect of infinite tube. We can consider those nanotubes “infinite”, whereas, the nanotubes that are discussed in this chapter are closed and finite. Both end of the nanotubes are closed either carbon-fullerene hemisphere or by silicon-fullerene hemisphere. Here we present electronic and geometrical properties of those finite SiC nanotubes. As mentioned in introduction, we have considered two sets of nanotubes in this study: one that can be capped by C_{10} (hemisphere of C_{20} fullerene) and the other that can be capped by C_{30} (hemisphere of C_{60}). Figures 4.2 and 4.3 show the top view of the caps used to terminate SiC nanotubes and the respective capped nanotubes (3,3), (5,0), (5,5) and (9,0). As mentioned before, nanotubes (3, 3) and (5, 0) can be capped by the fullerene hemisphere C_{10} in two different orientations. Similarly, nanotubes (5, 5) and (9, 0) can be capped by the fullerene

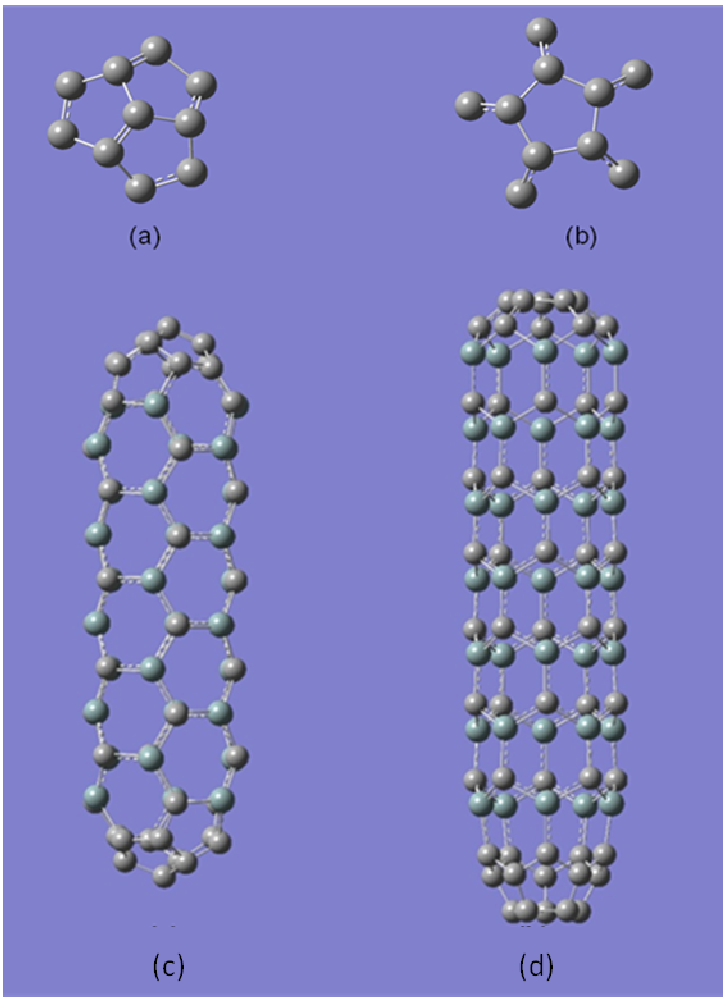

Figure 4.2 [a] Top view of fullerene hemisphere cap of (3, 3), [b] top view of fullerene hemisphere cap of (5, 0), [c] fullerene capped (3, 3), and [d] fullerene capped (5, 0).

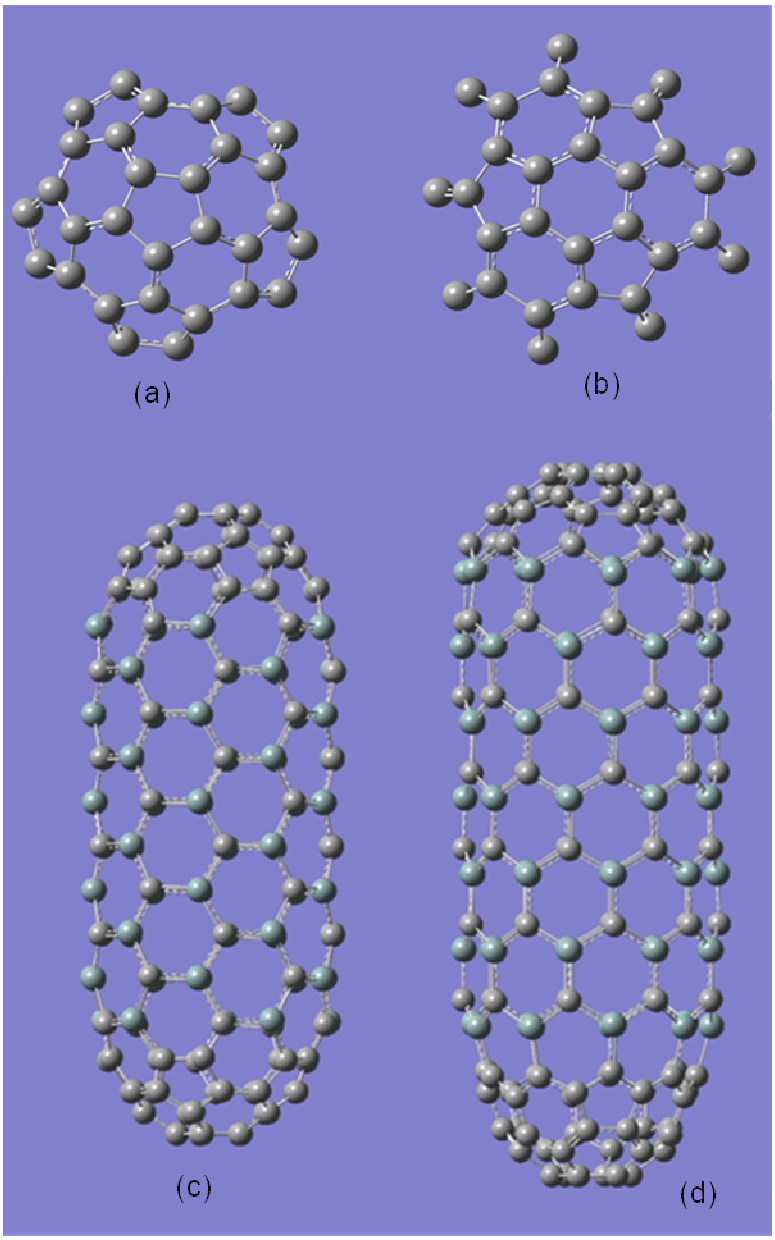

Figure 4.3 [a] Top view of fullerene hemisphere cap of (5, 5), [b] top view of fullerene hemisphere cap of (9, 0), [c] fullerene capped (5, 5), and [d] fullerene capped (9, 0).

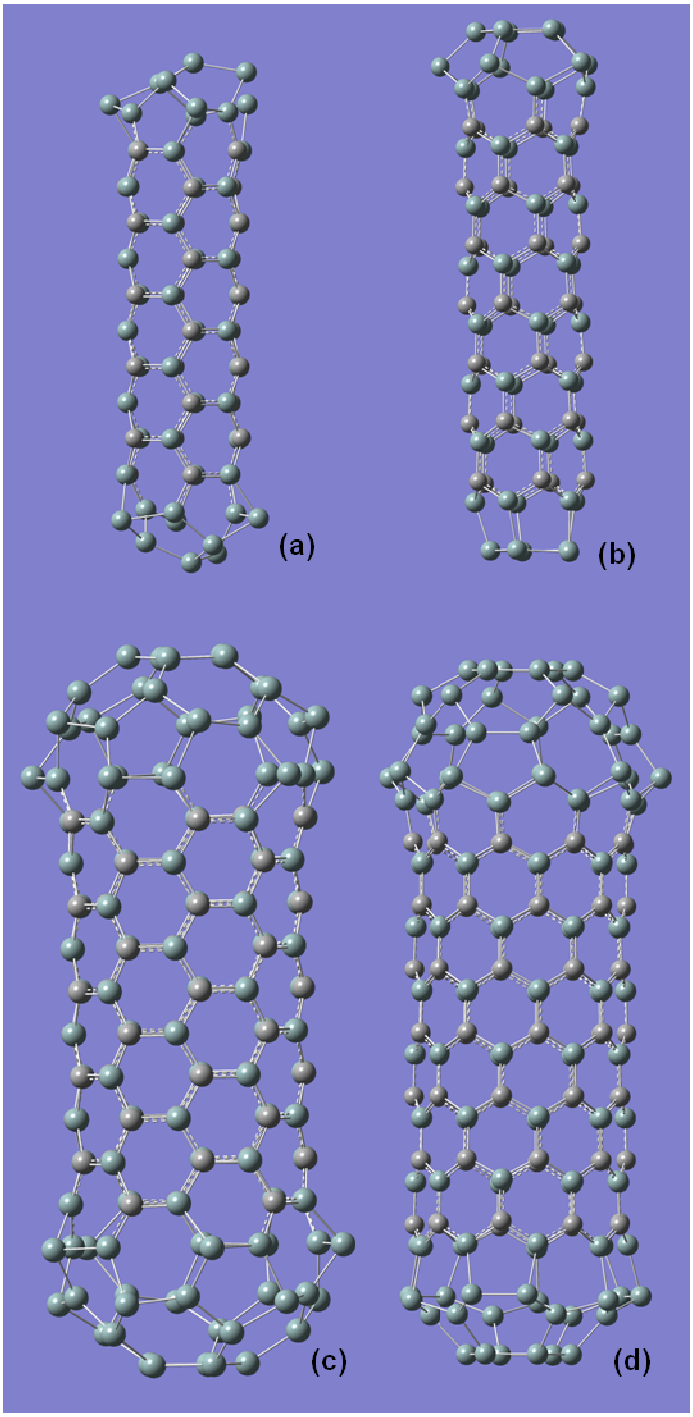

Figure 4.4 Silicon-capped SiC nanotubes- (a) (3, 3), (b) (5, 0), (c) (5, 5), and (d) (9, 0).

hemisphere C_{30}. For purposes of comparison, we have capped the nanotubes with silicon hemispheres and calculated the properties of some of those silicon capped nanotubes. The results below indicate that these tubes are significantly less stable compared to carbon capping. Figure 4.4 shows the optimized structure of silicon-capped SiC nanotubes. Multi-walled SiC nanotubes have been synthesized by using carbon nanotubes as template and partially substituting carbon atoms by silicon atoms and thus therefore there is a finite possibility of silicon capping although silicon does not favor fullerene structure.

To check the stability of the capped nanotubes, the cohesive energy or the B.E./atom of each nanotube is calculated from:

$$E_b=[aE(Si)+bE(C)-E(Si_aC_b)]/(a+b) \qquad (4.1)$$

where a and b are the numbers of Si of C atoms respectively; E(Si) and E(C) are the ground state total energies of Si and C atoms respectively; $E(Si_a C_b)$ is the total energy of the optimized capped nanotubes. The default energy convergence criterion was set to 10^{-6} a. u. Tables 4.1 and 4.2 and Figures 4.5 and 4.6 show the variation of the cohesive energies per atom with respect to the unit cells for all capped nanotubes. From the figures it is evident that binding energies per atom decrease as the length of the nanotube increases when it is capped with carbon whereas it increases with the length when it is capped with silicon. As we can see from the stoichiometry, the ratio of the number of carbon atoms to the number of silicon atoms decreases (increases) with length in carbon-capped (silicon-capped) nanotube. Therefore the binding energies decrease (increase) with increase in length as expected since C-C bond strength is greater than Si-Si and Si-C bond strengths. The binding energies per atom as a function of the number of atoms for armchair and zigzag nanotubes having same diameter do not show any significant difference. Therefore the stability of capped nanotube does not have any preference over chirality as long as they have same diameter and capped with same fullerene hemisphere in different orientations. A comparison between open *versus* capped nanotube shows a significant difference in the B.E./atom. For example, the B.E./atom for SiC

Table 4.1 Variation of binding energy (E_b, eV) per atom, HOMO-LUMO gap(E_g, eV) and dipole moment (D, Debye) of capped (3,3) and (5,0) SiC nanotubes with number of unit cells (NC) and number of atoms (n).

NC	n	**C-capped (3,3)**				**Si-capped (3,3)**			
		Stoichiometry	E_b	E_g	D	Stoichiometry	E_b	E_g	D
1	32	$C_{26}Si_6$	5.767	1.424	0.001	C_6Si_{26}	4.184	1.890	0.005
2	44	$C_{32}Si_{12}$	5.641	1.342	0.887	$C_{12}Si_{32}$	4.485	1.706	3.510
3	56	$C_{38}Si_{18}$	5.584	1.435	0.735	$C_{18}Si_{38}$	4.708	2.130	0.007
4	68	$C_{44}Si_{24}$	5.550	1.491	0.733	$C_{24}Si_{44}$	4.815	1.860	0.985
5	80	$C_{50}Si_{30}$	5.527	1.496	0.740	$C_{30}Si_{50}$	4.894	1.762	3.579
6	92	$C_{56}Si_{36}$	5.510	1.500	0.792	$C_{36}Si_{56}$	4.960	1.736	3.584
7	104	$C_{62}Si_{42}$	5.497	1.497	0.005	$C_{42}Si_{62}$	5.010	1.786	0.227
8	116	$C_{68}Si_{48}$	5.486	1.474	0.109	$C_{48}Si_{68}$	5.055	1.860	1.019
9	128	$C_{74}Si_{54}$	5.478	1.502	0.764	$C_{54}Si_{74}$	5.088	1.718	2.355
		C-capped (5,0)				**Si-capped (5,0)**			
1	30	$C_{25}Si_5$	5.768	1.158	2.072	C_5Si_{25}	4.044	0.972	4.212
2	50	$C_{35}Si_{15}$	5.607	0.835	6.278	$C_{15}Si_{35}$	4.562	0.801	3.064
3	70	$C_{45}Si_{25}$	5.538	0.736	11.174	$C_{25}Si_{45}$	4.786	0.624	5.281
4	90	$C_{55}Si_{35}$	5.494	0.565	14.480				
5	110	$C_{65}Si_{45}$	5.468	0.424	17.097				
6	130	$C_{75}Si_{55}$	5.447	0.270	18.601				
7	150	$C_{85}Si_{65}$	5.435	0.182	20.450				
8	170	$C_{95}Si_{75}$	5.425	0.131	22.114				
9	190	$C_{105}Si_{85}$	5.417	0.101	24.088				

Table 4.2 Variation of binding energy (E_b, eV) per atom, HOMO-LUMO gap(E_g, eV) and dipole moment (D, Debye) of capped (5,5) and (9,0) SiC nanotubes with number of unit cells (NC) and number of atoms (n).

NC	n	**C-capped (5,5)**				**Si-capped (5,5)**			
		Stoichiometry	E_b	E_g	D	Stoichiometry	E_b	E_g	D
1	80	$C_{70}Si_{10}$	6.414	1.212	0.007	$Si_{70}C_{10}$	4.066	1.663	0.011
2	100	$C_{80}Si_{20}$	6.249	2.011	0.008	$Si_{80}C_{20}$	4.369	1.645	0.013
3	120	$C_{90}Si_{30}$	6.132	2.130	0.009	$Si_{90}C_{30}$	4.568	1.621	0.729
4	140	$C_{100}Si_{40}$	6.050	2.125	0.010	$Si_{100}C_{40}$	4.705	1.670	0.005
5	160	$C_{110}Si_{50}$	5.989	2.180	0.000	$Si_{110}C_{50}$	4.812	1.664	0.057
6	180	$C_{120}Si_{60}$	5.941	2.192	0.156	$Si_{120}C_{60}$	4.899	1.637	1.410
7	200	$C_{130}Si_{70}$	5.903	2.208	0.111	$Si_{130}C_{70}$	4.963	1.687	1.371
8	220	$C_{140}Si_{80}$	5.872	2.210	0.091	$Si_{140}C_{80}$	5.018	1.659	1.383
9	240	$C_{150}Si_{90}$	5.847	2.215	0.000				
10	260	$C_{160}Si_{100}$	5.825	2.214	0.031				
		C-capped (9,0)				**Si-capped (9,0)**			
1	78	$C_{69}Si_{9}$	6.386	1.952	1.983	$C_{9}Si_{69}$	4.021	1.354	4.008
2	114	$C_{87}Si_{27}$	6.150	2.022	0.687	$C_{27}Si_{87}$	4.514	1.157	7.592
3	150	$C_{105}Si_{45}$	6.009	2.027	1.100	$C_{45}Si_{105}$	4.763	0.869	8.282
4	186	$C_{123}Si_{63}$	5.924	2.038	1.360	$C_{63}Si_{123}$	4.918	0.894	8.866
5	222	$C_{141}Si_{81}$	5.866	2.048	1.401	$C_{81}Si_{141}$	5.026	1.221	9.609
6	258	$C_{159}Si_{99}$	5.824	2.058	1.560	$C_{99}Si_{159}$	5.099	0.919	9.703
7	294	$C_{177}Si_{117}$	5.792	2.059	1.507	$C_{117}Si_{177}$	5.156	0.928	10.008
8	330	$C_{195}Si_{135}$	5.768	2.065	1.646				
9	366	$C_{213}Si_{153}$	5.748	2.070	1.606				
10	402	$C_{231}Si_{171}$	5.732	2.073	1.534				

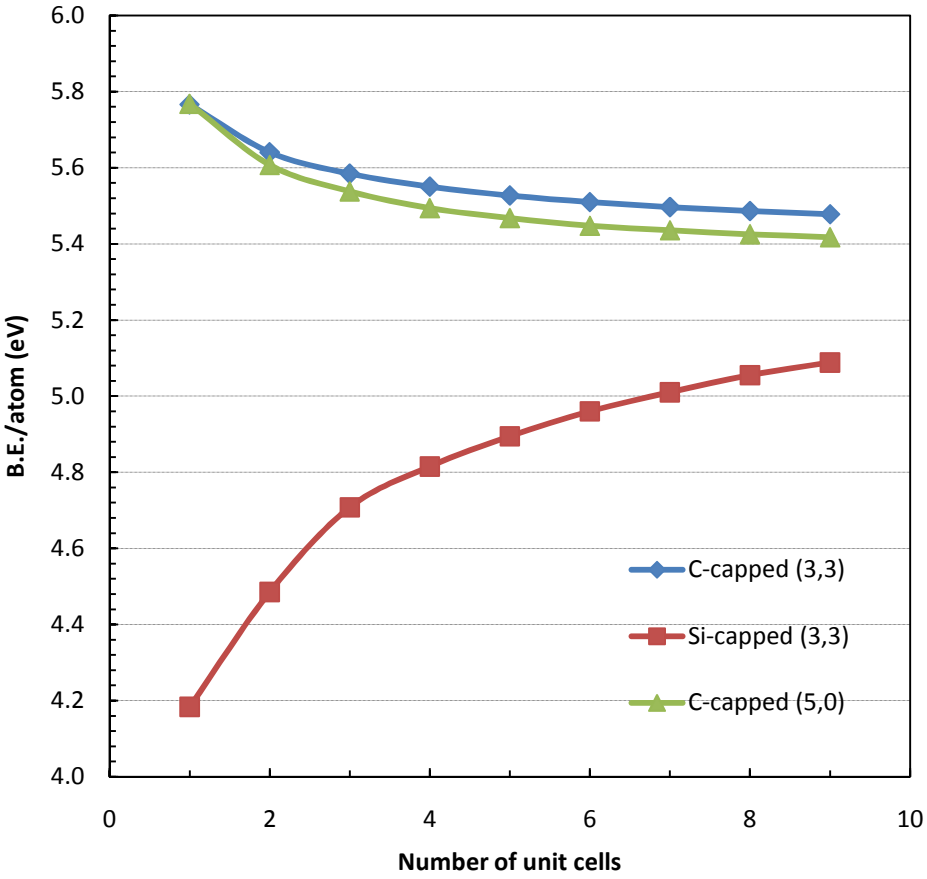

Figure 4.5 B.E./atom (eV) *versus* number of unit cells

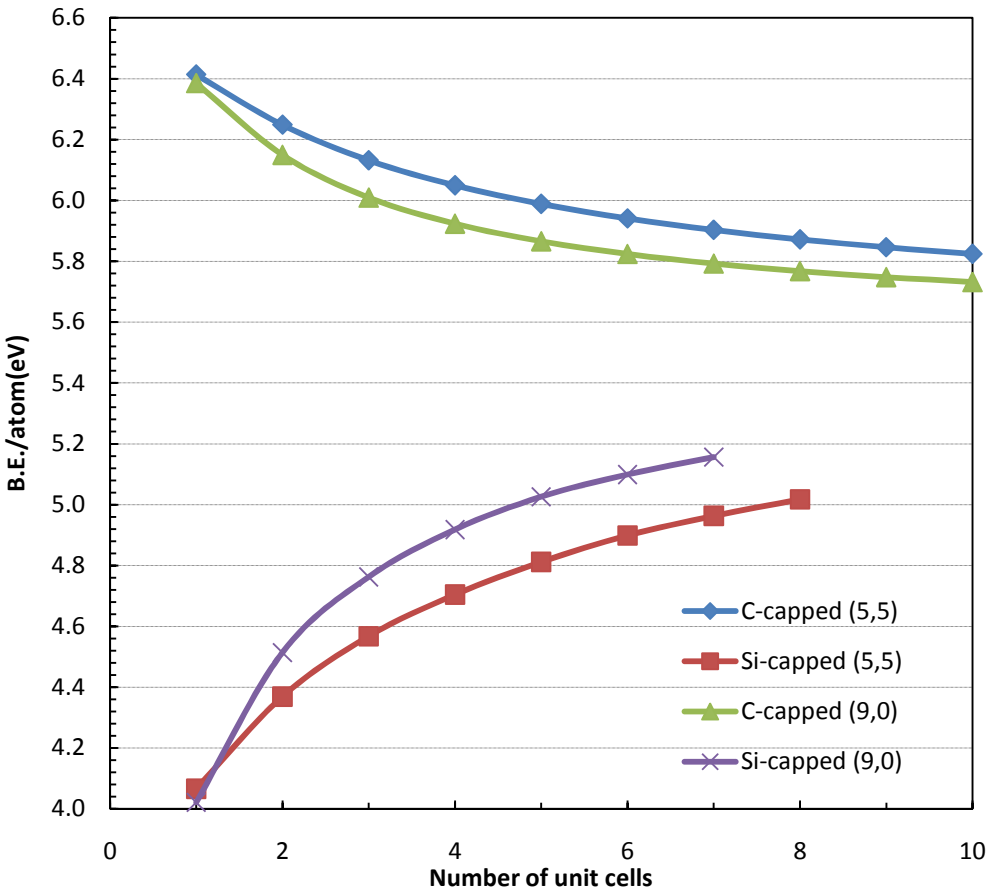

Figure 4.6 B.E./atom (eV) *versus* number of unit cells

nanotube (5,5) having five unit cells and hydrogen saturating the dangling bond is found to be 4.993 eV whereas the same nanotube with C-cap has the B.E./atom 5.989 eV and with Si-cap has the B.E./atom 4.812 eV. This trend is seen in all the nanotubes we studied. This suggests that the stability of SiC nanotubes can be improved significantly by capping the ends with carbon fullerene hemispheres.

Tables 4.1 and 4.2 and Figures 4.7 and 4.8 show the variation of the energy differences between the highest occupied molecular orbital (HOMO) and the lowest unoccupied molecular orbital (LUMO) with respect to the number of unit cells. It is clear from the figures that HOMO-LUMO gap of C-capped armchair SiC nanotube increases with length of the tube and reaches a saturation value. For example, HOMO-LUMO gap of C-capped (5, 5) increases from 1.2 eV (for one unit cell) to fairly saturated 2.2 eV (for five or more unit cells). Whereas, the HOMO-LUMO gap of C-capped (3,3) SiC nanotubes shows small oscillation for relatively shorter length and remains steady at about 1.5 eV for longer tubes having number of unit cells greater than 3. In case of C-capped zigzag SiC nanotubes, we see an opposing trend in (5, 0) and (9, 0). HOMO-LUMO gap of (5, 0) decreases monotonically with increasing length of the tube whereas HOMO-LUMO gap of (9, 0) increases with length. This opposing trend is due to the hybridization of orbitals and decrease in ionicity of the bonds in very small diameter tubes. As the length of the tube increases, number of Si-C bonds increases whereas number of C-C bonds is unchanged since the C-C bonds are only on the cap of the tube. C-C bond is perfectly covalent whereas Si-C bond is partially ionic. As the number of partially ionic bond increases, the HOMO-LUMO gap increases. Therefore the HOMO-LUMO gap of C-capped (9, 0) increases with length. However the ionicity in bonding for a given nanotube decreases as the diameter of the tube decreases. So, at smaller diameter, ionic contribution is the lowest, and is suppressed by some extra hybridization. The increased curvature causes triangular distribution of hybrid orbital to distort into slightly tetrahedron distribution of the orbitals. This may bring in some sp^3 contribution. So at smaller diameters, the sp^3 hybridization is relatively higher. Also,

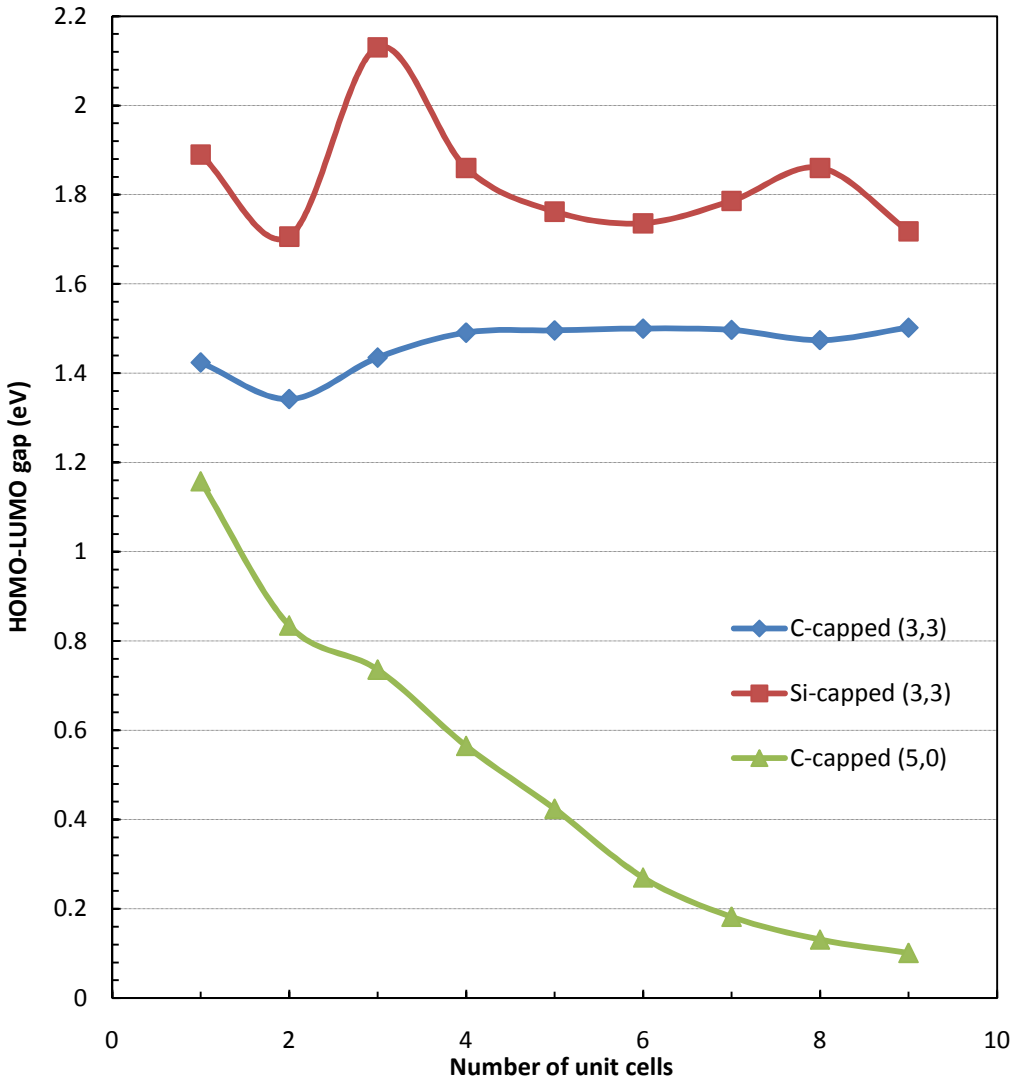

Figure 4.7 HOMO-LUMO gaps *versus* number of unit cells

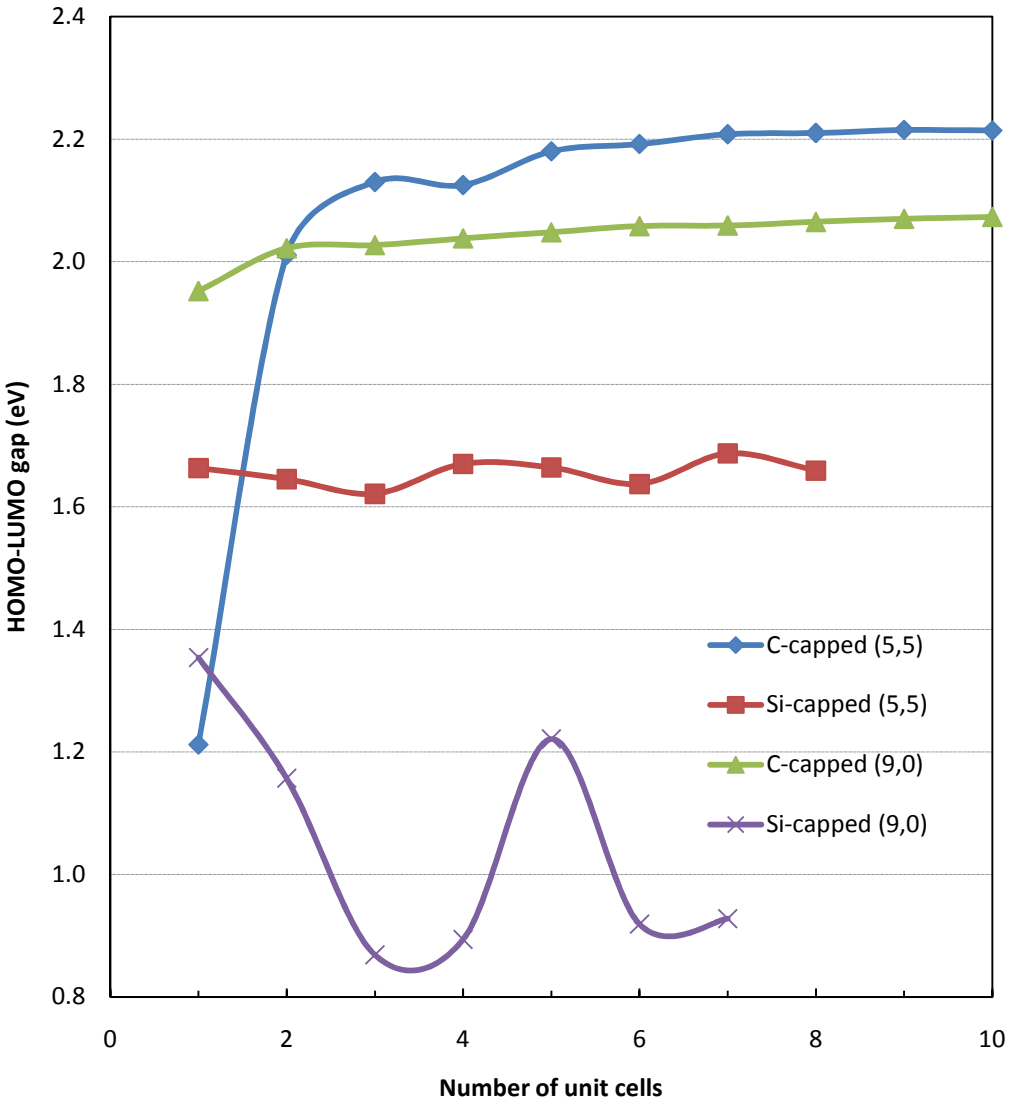

Figure 4.8 HOMO-LUMO gaps *versus* number of unit cells

the curvature induced sp-hybridization has the most pronounced effect in zigzag nanotubes as discussed in Chapter 1. Therefore the all the bonds in (5, 0) nanotubes are almost covalent due to its curvature. Hence as the size of the tube increases, its HOMO-LUMO gap decreases according to quantum confinement effect. Figure 4.9 shows the HOMO-LUMO plots of carbon-capped SiC nanotubes (3, 3), (5, 5), (5, 0), and (9, 0). The HOMO-LUMO of (3, 3), (5, 5), and (9, 0) are localized at the cap of the tubes whereas the HOMO-LUMO of (5, 0) is distributed uniformly over the nanotube. This clearly shows the hybridization of orbitals is more pronounced in (5, 0) than in all the other nanotubes. HOMO-LUMO gap of all Si-capped nanotubes oscillates with length. Similar kind of oscillation of HOMO-LUMO gap has been reported for capped carbon nanotubes [185-188]. HOMO-LUMO gaps of the capped SiC nanotubes are found to be always less than that of open nanotubes with dangling bonds saturated with hydrogen. For example, an open SiC nanotube (3, 3) having length equal to five unit cells and with hydrogen atoms at the end, the HOMO-LUMO gap is found to be 3.3 eV whereas the same nanotubes with C-cap has the gap of 1.5 eV and with Si-cap has the gap of 1.8 eV. Figure 4.10 shows density of states of open and capped SiC nanotube (5, 5) having same number of unit cells. The figure clearly shows that capping decreases the HOMO-LUMO gap of SiC nanotube.

We also studied the effect of capping on the buckling of the SiC nanotubes. The buckling measures the rippling of the surface of a nanotube. It is observed that the buckling of a SiC nanotube is lowered as a result of capping. For an open SiC nanotube (3, 3) having length equal to five unit cells and with hydrogen atoms saturating the dangling bond has a radial buckling of 0.09 Å whereas the same nanotube with C-cap has the buckling of 0.07 Å and with Si-cap has the buckling of 0.06 Å. Similarly the open SiC nanotube (5, 5) has radial buckling of 0.05 Å whereas C-capped and Si-capped (5, 5) has the buckling of 0.02 Å and 0.03 Å respectively.

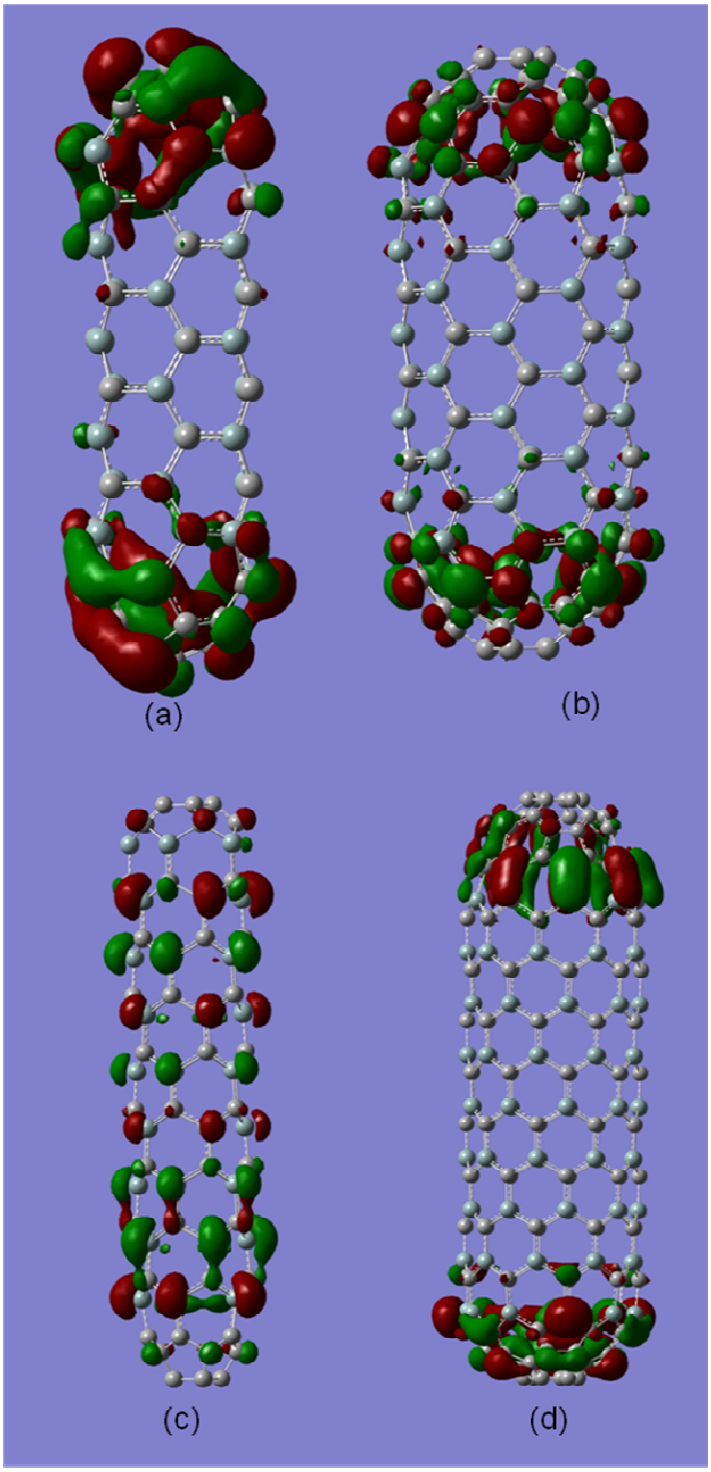

Figure 4.9 HOMO-LUMO plots of carbon-capped (a) (3,3), (b) (5,5), (c) (5,0), and (9,0).

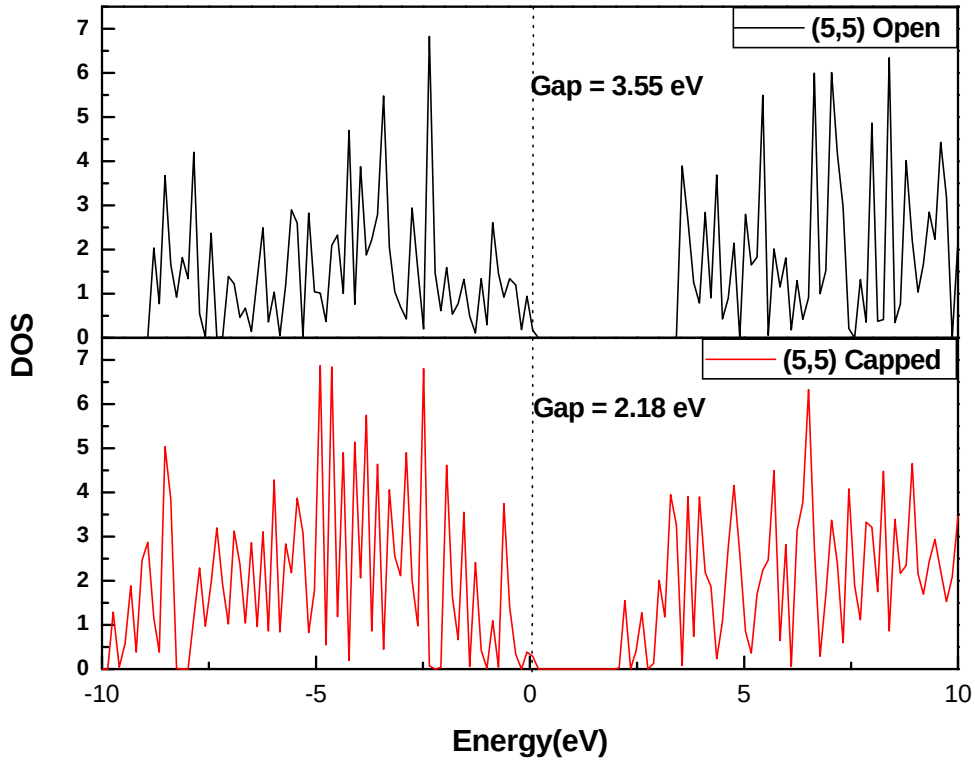

Figure 4.10 Density of states (DOS) of open and capped SiC nanotube (5, 5).

4.3 Conclusions

In summary, we have studied fullerene hemisphere capped silicon carbide nanotube with chirality (3, 3), (5, 0), (5, 5) and (9, 0). The evolution of electronic properties with the size of nanotubes has been performed. The study shows that the stability of a SiC nanotube is significantly improved by capping with carbon fullerene hemisphere. We also studied the possibility of capping a SiC nanotube with silicon fullerene hemisphere. The results show that the relative stability of the tubes when capped with silicon is significantly low. The study shows that capping significantly decreases the HOMO-LUMO gap of nanotubes.

CHAPTER 5

SILICON CARBIDE NANOCONES: CONICAL CAPS OF SILICON CARBIDE NANOTUBES

5.1 Introduction

As discussed in the previous chapter, a nanotube can terminate in various ways depending on the method of synthesis. One of the possible terminations is the formation of hemispherical cap and the other possible termination is the formation of conical cap. The hemispherical cap structures are very important at the beginning stage of the nanotube growth since the nanotubes grow on top of the hemispherical cap structure formed on the catalysts. However, the conical termination of the nanotubes is equally possible at the final stage of the nanotube growth. Near the end of the nanotubes, very interesting geometrical and electronic structural features are observed due to the closure of the tube by the incorporation of topological defect such as pentagons in the hexagonal carbon lattice [189, 190]. Carbon nanocones are observed as caps on the ends of nanotubes, and also as free standing nanostructures [1, 2, 191]. Conical ends of the nanotube can be very useful in applications as atomic force microscopy and scanning tunneling microscopy probes [192]. Nanocones arrays have exhibited enhanced absorption due to superior antireflection properties over a large range of wavelengths and angles of incidence. This also suggests application of nanocones as promising nanostructures to enhance the solar cell energy conversion efficiency [193]. SiC nanocones may have potential application as field emitters. It has been demonstrated that the nanometer-size SiC caps on silicon nanotips have excellent field emission property [194]. Also, study of interactions of various gases like NO_2, H_2S, HCN, among others, with silicon carbide nanocone tips might help develop detection and removal techniques for these toxic gases up to the precision of a single molecule. Therefore study of SiC nanocones is useful not only for the

possible capping of nanotubes but also for their standalone applications. Despite all these facts, there are very few theoretical attempts [195, 196] to study SiC nanocones. Mavrandonakis *et al.* [195] have studied some SiC nanotubes with conical tip and suggested their possible applications in atomic force microscopy and scanning tunneling microscopy probes. More recently, using the software SIESTA, a theoretical study by Alfieri and Kimoto [196] have indicated that only nanocones with disclination angle 60°, 120° and 300° are stable. They constructed nanocones by rolling a single layer SiC layer with a SiC bond length of 1.78 Å and studied their properties as a function of the disclination angle defined as the angle of the sector removed from a flat SiC sheet and of an electric field parallel or perpendicular to the cone axis. However, nanocones with different topological defects at the tip were not considered. Here, in addition to nanocones with disclination angle 60^0, 120^0 and 300^0, we construct also optimized nanocones with disclination angles of 240^0 and 300^0 by introducing pentagonal defects at the tips to avoid dangling bonds. In the work to follow, we present a detailed *ab initio* study of the evolution of electronic properties with the size of SiC nanocones of all possible disclination angles.

5.2 Discussions of Results

In this work, we have used the B3LYP hybrid functional [110, 120, 122, 164] and the all electron 3-21G* basis set [136] as implemented in the GAUSSIAN 03 suite of programs [168] for full geometry optimizations without any symmetry constraints of the nanocone structures.

The open nanocone can be modeled as a wrapped graphene-like sheet. In order to have strain-free, seamless wrapping, a sector has to be cut out of the sheet. That sector should have an angle of n × 60°, where n = 1- 5 and thus, the resulting cone angle has only certain discrete values $\theta = 2 \sin^{-1}(1 - n/6) = 19°, 39°, 60°, 84°, 113°$. A nanotube is a nanocone with a cone angle of 0°. Figure 5.1 shows the modeling of a SiC nanocone of disclination angle 60° where a section of 60° is cut out and the cone sheet is wrapped to form a nanocone of cone

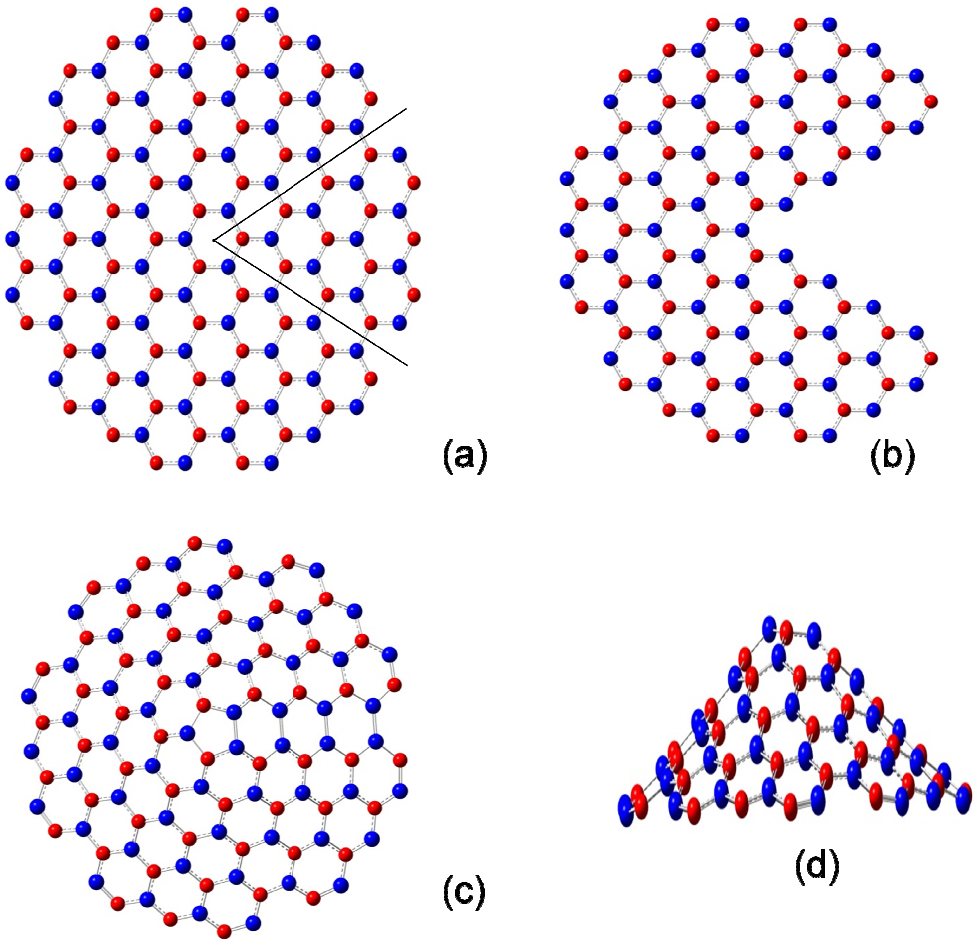

Figure 5.1: a) Modeling of a SiC nanocone by cutting a section of a two dimensional graphene like sheet and wrapping the cone sheet; (b) forming a nanocone; (c) top view, and (d) side view. Red and blue atoms represent carbon and silicon atoms, respectively.

angle 113°. If a cut-out sector is of 60°, the cone has one pentagon at its apex. The pentagonal defect in the structure leads to the construction of either carbon-rich or silicon-rich nanocones. Figures 5.1 (c) and 5.1(d) show top and side views of a silicon-rich nanocone of disclination angle 60°. In cases of nanocones of disclination angles 180° and 300° also, we have either carbon-rich or silicon-rich structures. Similarly, if the cut-out sector is 120°, the nanocone has a rhombic defect at its apex, and because of this even-numbered ring at the apex, the numbers of silicon atoms and carbon atoms are equal. This scheme of constructing nanocones leads to a problem in the cases of nanocones of disclination angle of 240° and 300°. The defects at the apices of nanocones of disclination angles 240° and 300° are a dimer and a single atom, respectively. Such apices might not be energetically favorable due to unavoidable dangling bonds at the apices of the nanocones.

To elaborate further, we therefore modeled these nanocones (nanocones of disclination angles 240° and 300°) in such a way that they have only pentagonal defects at their apices. The disclination of nanocone structure corresponds to the presence of a given number of pentagonal defects at or around nanocone apex. When a pentagonal defect is introduced in a two dimensional graphitic sheet, a disclination of 60° is produced. In general, if n (n=1-5) pentagons replace the hexagonal rings in a graphitic sheet; a nanocone of disclination angle n×60° is formed. If n=6 the structure becomes hemispherical cap structure of nanotubes (5, 0) or (3, 3). A detailed explanation of these tubes can be found in previous chapter where we have explored the electronic properties of silicon carbide nanotubes capped with fullerene hemisphere. Therefore there are two approaches of modeling a nanocone. One is cutting out a sector of different angles from the graphitic sheet and then wrapping it seamlessly and the other approach is introducing a number of pentagonal defects in the hexagonal graphitic sheet. In case of disclination angle of 120° and 180° we have used both approaches of constructing the nanocones. In the case of disclination angles of 240° and 300°, we constructed nanocones with pentagonal defects only, because of the problem with unavoidable dangling bonds at the apices

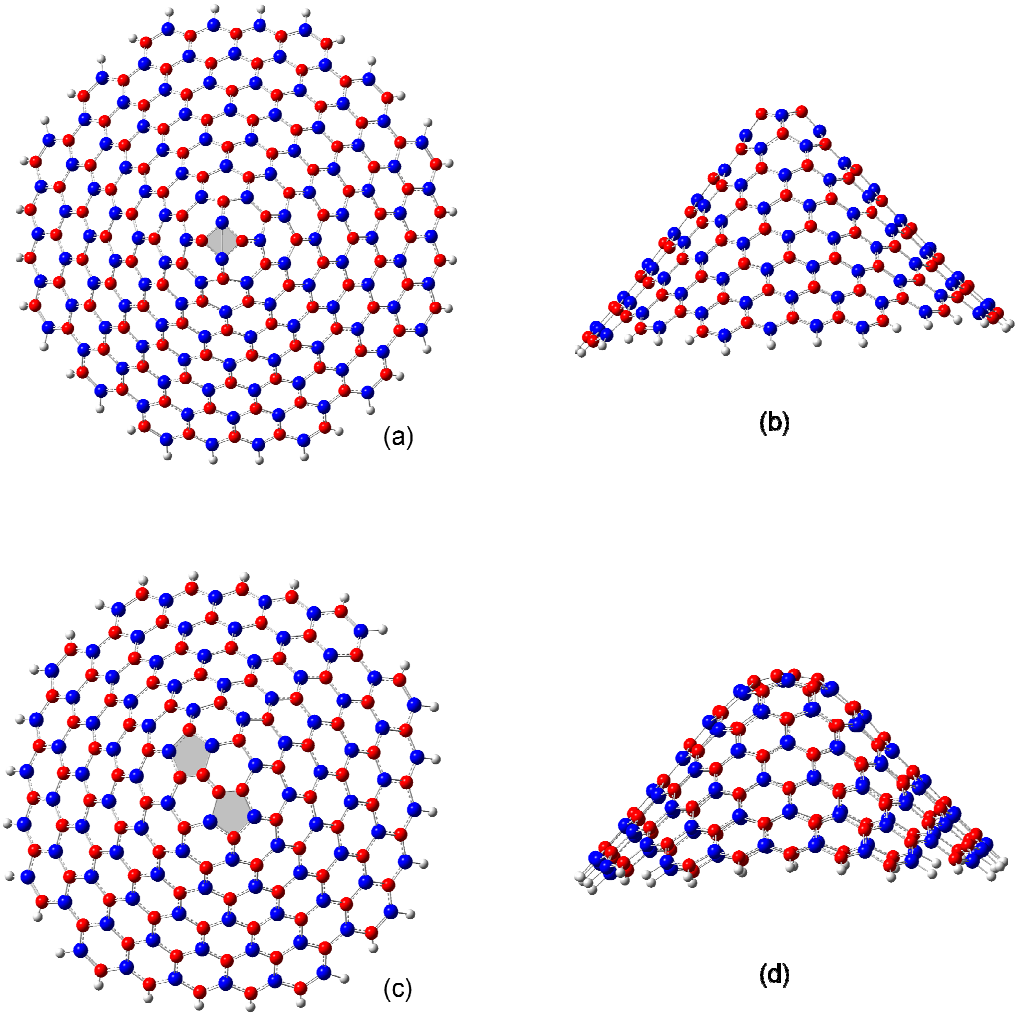

Figure 5.2: (a) top view of a nanocone with disclination angle 120^0 and a rhombohedral tip; (b) side view of the nanocone; (c) top view of a nanocone with disclination angle 120^0 with two pentagonal defects at the tip; (d) side view of the nanocone. The shaded regions show rhombohedral and pentagonal rings.

of these nanocones. In the case of carbon nanocones it is well established that the most common defects at the apices of the nanocones are pentagonal defects [192]. However in the cases of heteronuclear nanocones like silicon carbide nanocones, introduction of pentagonal defect introduces homonuclear bond in the pentagonal ring. This affects the overall symmetry of the nanocone at its tip. As the previous studies on boron nitride nanocones [197-200] have suggested, detailed theoretical and experimental studies are required to establish the most favorable defects at the apices of such binary nanocones. To construct nanocones, first the smallest nanocones of different disclination angles are constructed and the nanocones are gradually grown by attaching silicon and/or carbon atoms at the open end of the nanocones. The dangling bonds at the open ends of all the nanocones are passivated by hydrogen atoms to avoid instability of the edges of the nanocones due to unsaturated bonds. Figure 5.2 shows nanocones of disclination angle 120° with different topological defects i.e. rhombohedral and pentagonal defects. Figure 5.3 shows top views of nanocones of disclination angle 180°, 240° and 300° in different configurations.

To examine the stability of the nanocones, the cohesive energy or the B.E./atom of each nanotube is calculated from:

$$E_b = [a\,E(Si) + b\,E(C) + c\,E(H) - E(Si_a\,C_b H_c)] / (a + b + c) \qquad (5.1)$$

where a. b, and c are the numbers of Si, C, and H atoms respectively; E(Si), E(C), E(H) are the ground state total energies of Si, C, and H atoms respectively; $E(Si_a\,C_b\,H_c)$ is the total energy of the optimized nanocones. The default energy convergence criterion was set to 10^{-6} a. u.

Tables 5.1 and 5.2 and Figures 5.4 and 5.5 show the variation of the B.E./atom (E_b) with respect to the size of the nanocones. It is evident from the data that the B.E./atom increases with the size of the nanocones with eventual saturation. For relatively smaller clusters, the B.E./atom oscillates in all cases except in nanocones of disclination angle 300° where the binding energy increases monotonically. This indicates greater stability of nanocones

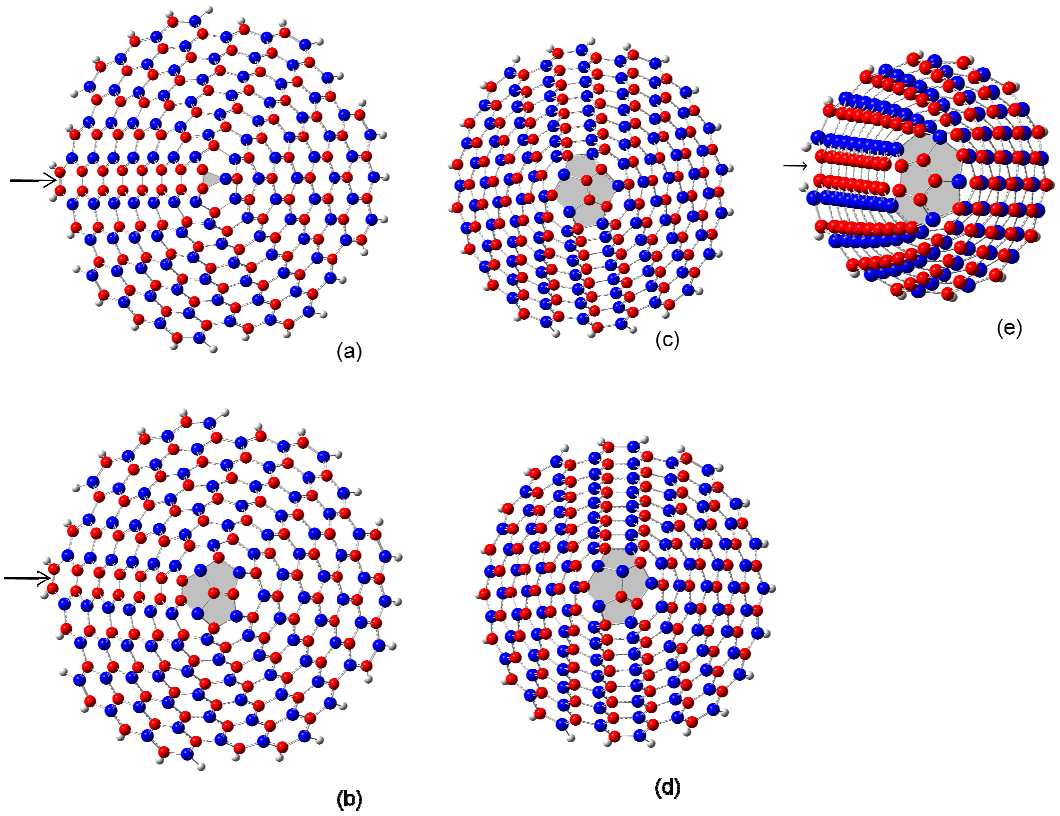

Figure 5.3: Top views of nanocones (a) of disclination angle 180^0 with triangular tip, (b) of disclination angle 180^0 with pentagonal defects, (c) of disclination angle 240^0 with pentagonal defect and C-C tip, (d) of disclination angle 240^0 with pentagonal defects and Si-C tip, (e) of disclination angle 300^0. The shaded regions show defects. Arrows in (a), (b), and (e) show the homo-nuclear bonds.

of some particular size as compared with its neighboring sizes. For example, in the case of nanocones with disclination angle 60°, nanocones $Si_{21}C_{24}H_{15}$, $Si_{38}C_{42}H_{20}$, $Si_{60}C_{65}H_{25}$ have relatively greater binding energies per atom as compared with nanocones with neighboring sizes. The oscillatory pattern vanishes for bigger nanocones. As expected, the carbon-rich nanocones have greater binding energies as compared to their respective silicon-rich counterparts. We have plotted the graphs only for carbon-rich nanocones in Figure 5.4, but if we closely look values of binding energies for silicon-rich nanocones in Table 5.1, we can see the same pattern for silicon-rich nanocones with slightly smaller values. Nanocones with same disclination angle but different tip topology have almost same B.E./atom. For example, $Si_{109}C_{116}H_{27}$, a nanocone of disclination angle 180° with triangular tip has a B.E./atom 5.23 eV and $Si_{108}C_{115}H_{27}$, the same nanocone with pentagonal defects at the tip, has a B.E./atom 5.24eV. This slightly greater value can be attributed to slightly greater ratio of the number of carbon atoms to silicon atoms in the second nanocone. Figure 5.6 shows a closer look into the binding energies per atom for nanocones of all disclination angles with large numbers of constituent atoms. It is evident that the binding energies per atom increases as the disclination angle increases. A nanocone of disclination angle 60° is closer to the two dimensional graphene-like geometry whereas that of disclination angle 300° is closer to the nanotube geometry. Therefore, Figure 5.6 suggests that, given the similar cluster size, silicon carbide favors conic structures more than two dimensional graphene-like structures. This is because of the huge difference between sp^2 and sp^3 bond structure with a value of 1.25 eV per Si-C pair [29]. As the curvature of the nanocone structure increases, geometry of the bond structures at the tip becomes more sp^3-like. This increases the overall stability of the structure.

Tables 5.1 and 5.2, and Figures 5.7 and 5.8 show the variation in HOMO-LUMO gap with respect to the size of nanocone clusters. HOMO-LUMO gaps of all nanocones show oscillatory pattern with respect to the size of the cluster. This kind of oscillatory pattern has been observed in finite length carbon nanotubes [188].The oscillation in the HOMO-LUMO gap is due

Table 5.1 Binding energies per atom (E_b) and HOMO-LUMO gaps (E_g) of carbon-rich nanocones. Numbers in parentheses give the value for E_b and/or E_g for corresponding silicon-rich nanocones. Stoichiometries $Si_xC_yH_z$ given in the table are those of carbon-rich. For silicon-rich nanocones the corresponding stoichiometries are $Si_yC_xH_z$.

D_θ	Stoichiometry	N	E_b	E_g
60^0	$Si_9C_{11}H_{10}$	30	4.49 (4.27)	2.66 (2.16)
	$Si_{17}C_{18}H_{15}$	50	4.54 (4.49)	2.14 (1.69)
	$Si_{21}C_{24}H_{15}$	60	4.77 (4.60)	1.78 (1.52)
	$Si_{34}C_{36}H_{20}$	90	4.84 (4.78)	1.72 (1.34)
	$Si_{38}C_{42}H_{20}$	100	4.95 (4.81)	1.50 (1.21)
	$Si_{56}C_{59}H_{25}$	140	5.01 (4.94)	1.32 (1.16)
	$Si_{60}C_{65}H_{25}$	150	5.06 (4.95)	1.19 (1.10)
	$Si_{73}C_{77}H_{30}$	180	5.07 (5.00)	1.44 (1.18)
	$Si_{83}C_{87}H_{30}$	200	5.11 (5.05)	1.10 (0.81)
	$Si_{105}C_{110}H_{35}$	250	5.16 (5.10)	1.20 (1.00)
	$Si_{115}C_{120}H_{35}$	270	5.18 (5.13)	0.80 (0.48)
	$Si_{142}C_{148}H_{40}$	330	5.23 (5.17)	1.00 (0.62)
	$Si_{152}C_{158}H_{40}$	350	5.24 (5.19)	0.34 (0.22)
180^0	$Si_5C_7H_6$	18	4.18 (3.90)	0.80 (1.75)
(With triangular	$Si_{10}C_{11}H_9$	30	4.26 (4.25)	0.98 (0.64)
tip)	$Si_{12}C_{15}H_9$	36	4.56 (4.35)	0.78 (1.11)
	$Si_{20}C_{22}H_{12}$	54	4.67 (4.60)	1.52 (0.73)
	$Si_{22}C_{26}H_{12}$	60	4.80 (4.62)	1.66 (0.69)
	$Si_{33}C_{36}H_{15}$	84	4.89 (4.81)	1.01 (0.94)
	$Si_{35}C_{40}H_{15}$	90	4.97 (4.81)	0.95 (0.91)
	$Si_{43}C_{47}H_{18}$	108	4.97 (4.88)	1.61 (0.70)
	$Si_{49}C_{53}H_{18}$	120	5.02 (4.94)	0.59 (0.55)
	$Si_{62}C_{67}H_{21}$	150	5.10 (5.00)	0.95 (0.84)
	$Si_{68}C_{73}H_{21}$	162	5.12 (5.04)	0.81 (0.68)
	$Si_{84}C_{90}H_{24}$	198	5.17 (5.08)	1.05 (0.53)
	$Si_{90}C_{96}H_{24}$	210	5.19 (5.11)	0.56 (0.39)
	$Si_{103}C_{110}H_{27}$	240	5.22 (5.13)	0.87 (0.98)

Table 5.1 – *Continued*

	$Si_{109}C_{116}H_{27}$	252	5.23 (5.15)	0.50 (0.34)
	$Si_{131}C_{139}H_{30}$	300	5.27 (5.19)	0.58 (0.57)
	$Si_{137}C_{145}H_{30}$	312	5.28 (5.21)	0.17 (0.15)
180^0	$Si_4C_6H_6$	16	4.28 (3.86)	2.37 (1.23)
(With pentagonal	$Si_9C_{10}H_9$	28	4.34 (4.27)	1.50 (2.28)
defects)	$Si_{11}C_{14}H_9$	34	4.61 (4.34)	1.32 (1.54)
	$Si_{19}C_{21}H_{12}$	52	4.70 (4.62)	1.49 (1.60)
	$Si_{21}C_{25}H_{12}$	58	4.84 (4.63)	1.42 (1.39)
	$Si_{32}C_{35}H_{15}$	82	4.91 (4.81)	1.03 (1.21)
	$Si_{34}C_{39}H_{15}$	88	4.99 (4.81)	0.83 (1.10)
	$Si_{42}C_{46}H_{18}$	106	5.00 (4.89)	1.37 (1.40)
	$Si_{48}C_{52}H_{18}$	118	5.04 (4.95)	1.04 (0.98)
	$Si_{61}C_{66}H_{21}$	148	5.11 (5.01)	1.11 (1.10)
	$Si_{67}C_{72}H_{21}$	160	5.13 (5.04)	0.87 (0.74)
	$Si_{83}C_{89}H_{24}$	196	5.18 (5.09)	0.93 (0.84)
	$Si_{89}C_{95}H_{24}$	208	5.20 (5.11)	0.53 (0.44)
	$Si_{102}C_{109}H_{27}$	238	5.23 (5.14)	0.97 (0.94)
	$Si_{108}C_{115}H_{27}$	250	5.24 (5.16)	0.46 (0.32)
	$Si_{130}C_{138}H_{30}$	298	5.28 (5.19)	0.62 (0.51)
	$Si_{136}C_{144}H_{30}$	310	5.28 (5.20)	0.17 (0.16)
300^0	$Si_5C_9H_6$	20	4.55 (3.95)	3.05 (2.15)
(With pentagonal	$Si_{11}C_{16}H_7$	34	4.77 (4.36)	1.43 (0.63)
defect)	$Si_{18}C_{24}H_8$	50	4.94 (4.60)	1.24 (0.76)
	$Si_{26}C_{33}H_9$	68	5.05 (4.76)	0.74 (1.09)
	$Si_{35}C_{43}H_{10}$	88	5.13 (4.87)	0.59 (1.15)
	$Si_{45}C_{54}H_{11}$	110	5.19 (4.96)	0.84 (0.84)
	$Si_{56}C_{66}H_{12}$	134	5.24 (5.02)	0.42 (0.35)
	$Si_{68}C_{79}H_{13}$	160	5.28 (5.08)	0.73 (0.68)
	$Si_{81}C_{93}H_{14}$	188	5.31 (5.12)	0.41 (0.50)
	$Si_{95}C_{108}H_{15}$	218	5.34 (5.16)	0.68 (0.66)
	$Si_{110}C_{124}H_{16}$	250	5.36 (5.20)	0.36 (0.29)
	$Si_{124}C_{139}H_{17}$	280	5.38 (5.23)	0.43 (0.69)
	$Si_{139}C_{153}H_{18}$	310	5.39 (5.26)	0.34 (0.17)

Table 5.2 Binding energies per atom (E_b) and HOMO-LUMO gaps (E_g) of nanocones having equal number of carbon and silicon atoms and having Si-C bond at the tip in case of 120^0 and 240^0 with pentagonal defects. Numbers in parentheses give the value for E_b and/or E_g for corresponding nanocones having C-C bond at the tip. Stoichiometries $Si_xC_yH_z$ given in the table are those of nanocones with Si-C bond at the tip. For nanocones with C-C tip, the corresponding stoichiometries are $Si_{x-1}C_{y+1}H_z$.

D_θ	Stoichiometry	N	E_b	E_g
120^0 (With rhombic tip)	$Si_8C_8H_8$	24	4.30	3.64
	$Si_{14}C_{14}H_{12}$	40	4.47	3.01
	$Si_{18}C_{18}H_{12}$	48	4.65	2.82
	$Si_{28}C_{28}H_{16}$	72	4.79	3.24
	$Si_{32}C_{32}H_{16}$	80	4.86	2.47
	$Si_{46}C_{46}H_{20}$	112	4.97	2.62
	$Si_{50}C_{50}H_{20}$	120	5.00	1.81
	$Si_{60}C_{60}H_{24}$	144	5.02	3.20
	$Si_{68}C_{68}H_{24}$	160	5.08	1.75
	$Si_{86}C_{86}H_{28}$	200	5.13	2.33
	$Si_{94}C_{94}H_{28}$	216	5.16	0.95
	$Si_{116}C_{116}H_{32}$	264	5.20	1.26
	$Si_{124}C_{124}H_{32}$	280	5.22	0.35
	$Si_{142}C_{142}H_{36}$	320	5.24	1.68
	$Si_{150}C_{150}H_{36}$	336	5.25	0.38
120^0 (With pentagonal defects)	$Si_7C_7H_8$	22	4.23 (4.41)	2.45 (3.00)
	$Si_{13}C_{13}H_{12}$	38	4.43 (4.55)	2.12 (2.32)
	$Si_{17}C_{17}H_{12}$	46	4.61 (4.68)	2.42 (2.66)
	$Si_{27}C_{27}H_{16}$	70	4.76 (4.81)	2.34 (2.54)
	$Si_{31}C_{31}H_{16}$	78	4.84 (4.88)	2.34 (2.43)
	$Si_{45}C_{45}H_{20}$	110	4.95 (4.98)	2.34 (2.48)
	$Si_{49}C_{59}H_{20}$	118	4.99 (5.01)	1.82 (1.84)
	$Si_{59}C_{59}H_{24}$	142	5.01 (5.04)	2.34 (2.53)
	$Si_{67}C_{67}H_{24}$	158	5.07 (5.09)	1.75 (1.77)

Table 5.2 – *Continued*

	$Si_{85}C_{85}H_{28}$	198	5.12 (5.14)	2.27 (2.33)
	$Si_{93}C_{93}H_{28}$	214	5.15 (5.17)	0.95 (0.96)
	$Si_{115}C_{115}H_{32}$	262	5.19 (5.21)	1.26 (1.27)
	$Si_{123}C_{123}H_{32}$	278	5.21 (5.22)	0.35 (0.35)
	$Si_{141}C_{141}H_{36}$	318	5.23 (5.24)	1.67 (1.68)
	$Si_{149}C_{149}H_{36}$	334	5.25 (5.26)	0.38 (0.38)
240^0 (With pentagonal defects)	$Si_6C_6H_6$	18	4.17 (4.38)	3.06 (2.59)
	$Si_{11}C_{11}H_8$	30	4.46 (4.56)	2.38 (2.59)
	$Si_{13}C_{13}H_8$	34	4.55 (4.63)	2.27 (2.57)
	$Si_{20}C_{20}H_{10}$	50	4.74 (4.80)	2.23 (2.41)
	$Si_{22}C_{22}H_{10}$	54	4.79 (4.84)	1.86 (2.14)
	$Si_{27}C_{27}H_{12}$	66	4.85 (4.89)	2.24 (2.39)
	$Si_{31}C_{31}H_{12}$	74	4.92 (4.95)	1.87 (2.04)
	$Si_{40}C_{40}H_{14}$	94	5.00 (5.03)	2.14 (2.37)
	$Si_{44}C_{44}H_{14}$	102	5.03 (5.06)	1.19 (1.20)
	$Si_{55}C_{55}H_{16}$	126	5.10 (5.12)	1.47 (1.47)
	$Si_{59}C_{59}H_{16}$	134	5.12 (5.14)	0.52 (0.52)
	$Si_{68}C_{68}H_{18}$	154	5.15 (5.17)	1.76 (1.83)
	$Si_{72}C_{72}H_{18}$	162	5.17 (5.18)	0.56 (0.56)
	$Si_{87}C_{87}H_{20}$	194	5.21 (5.22)	0.76 (0.76)
	$Si_{91}C_{91}H_{20}$	202	5.22 (5.24)	0.23 (0.23)
	$Si_{106}C_{106}H_{22}$	234	5.25 (5.26)	0.21 (0.21)
	$Si_{112}C_{112}H_{22}$	246	5.27 (5.28)	0.18 (0.18)

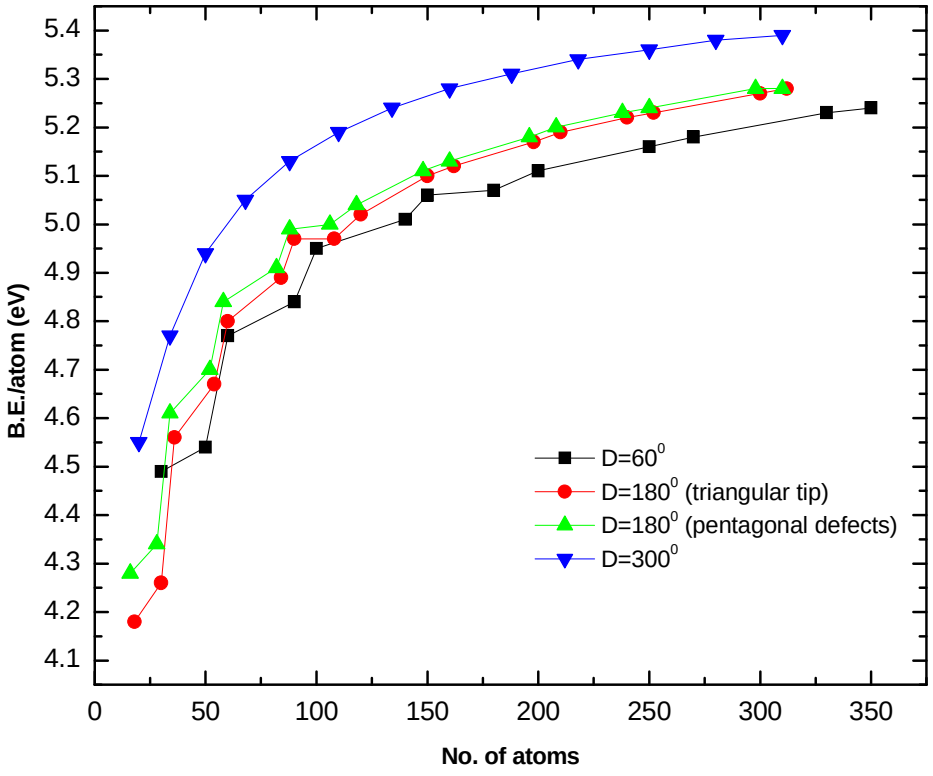

Figure 5.4: B.E./atom *versus* number of atoms in carbon-rich nanocones with disclination angle 60^0, 180^0 and 300^0.

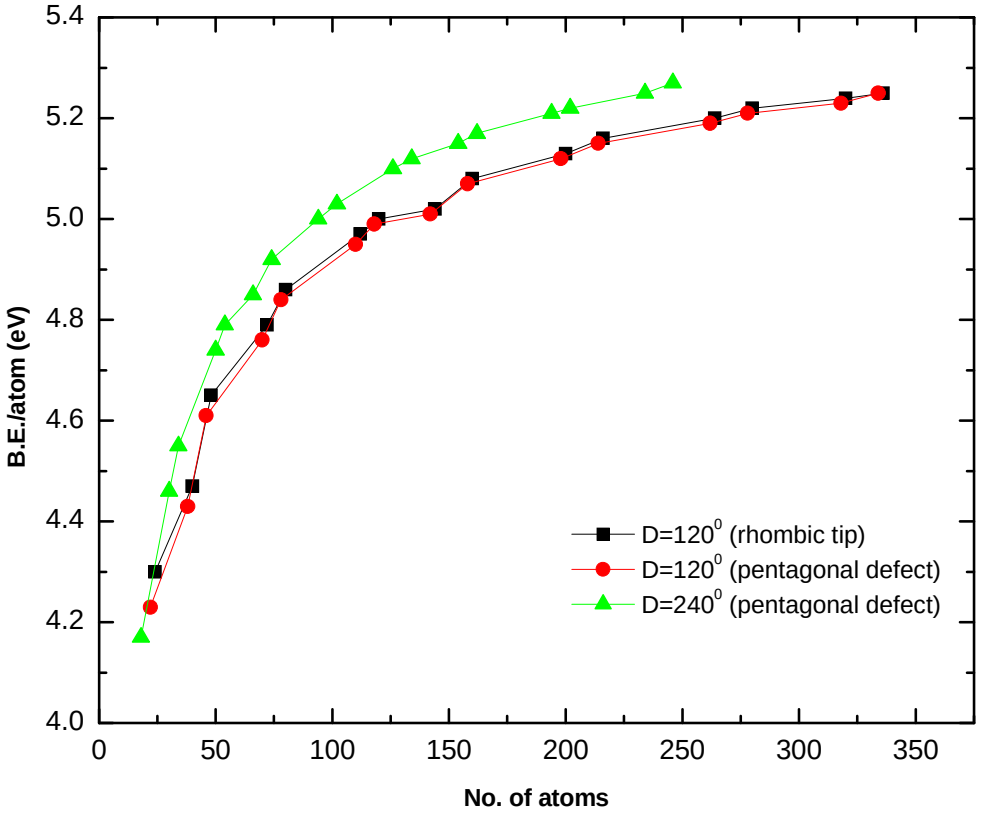

Figure 5.5: B.E./atom *versus* number of atoms in nanocones with disclination angle 120^0 and 240^0.

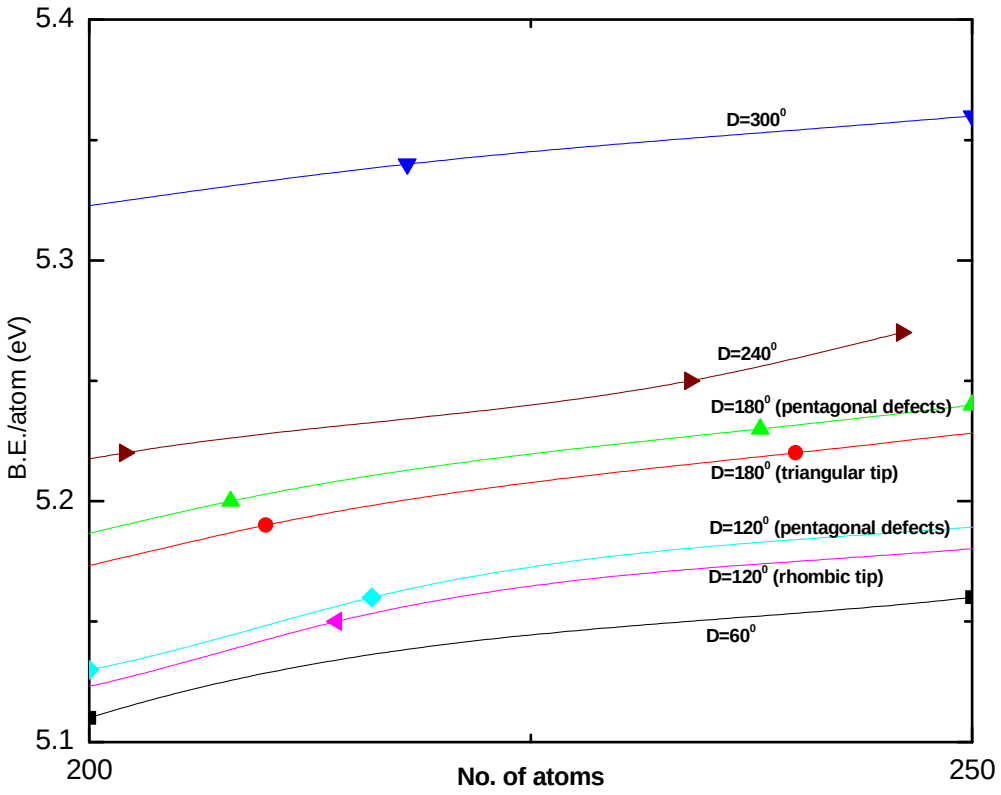

Figure 5.6: B.E./atom *versus* number of atoms for nanocones of disclination angle D=60^0-300^0.

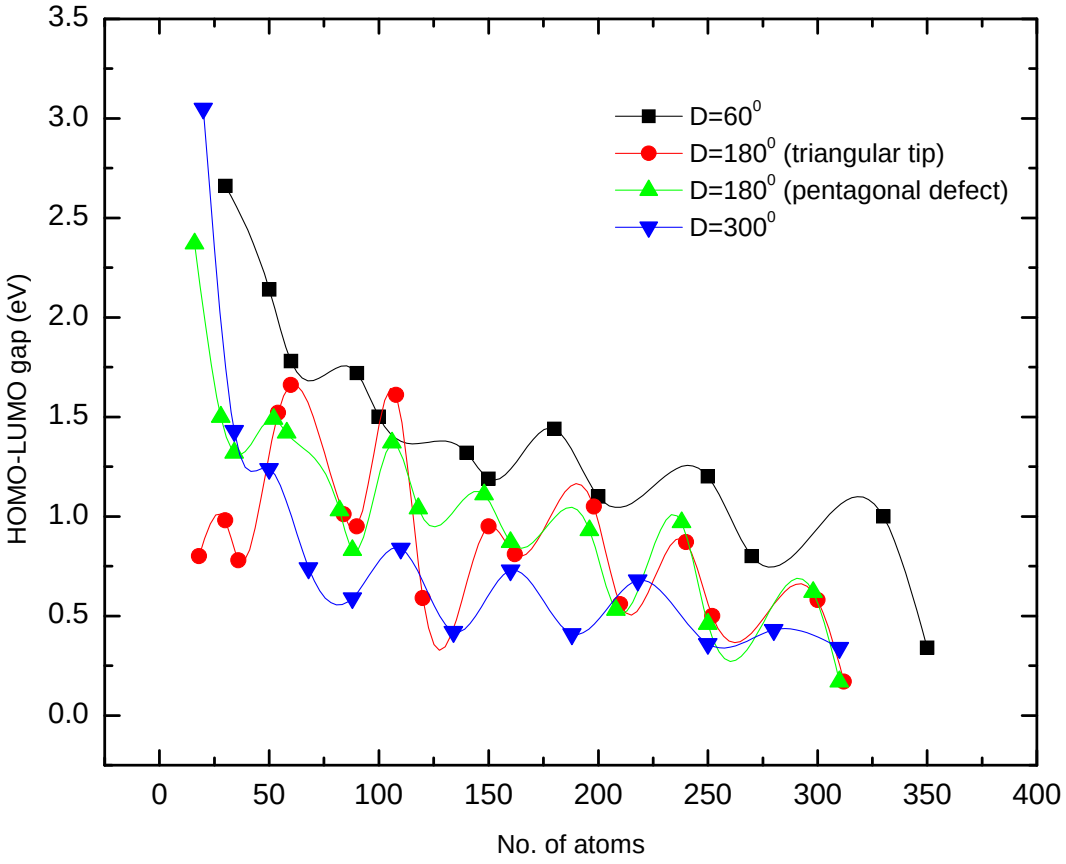

Figure 5.7: HOMO-LUMO gap *versus* number of atoms in carbon-rich nanocones with disclination angle 60^0, 180^0 and 300^0.

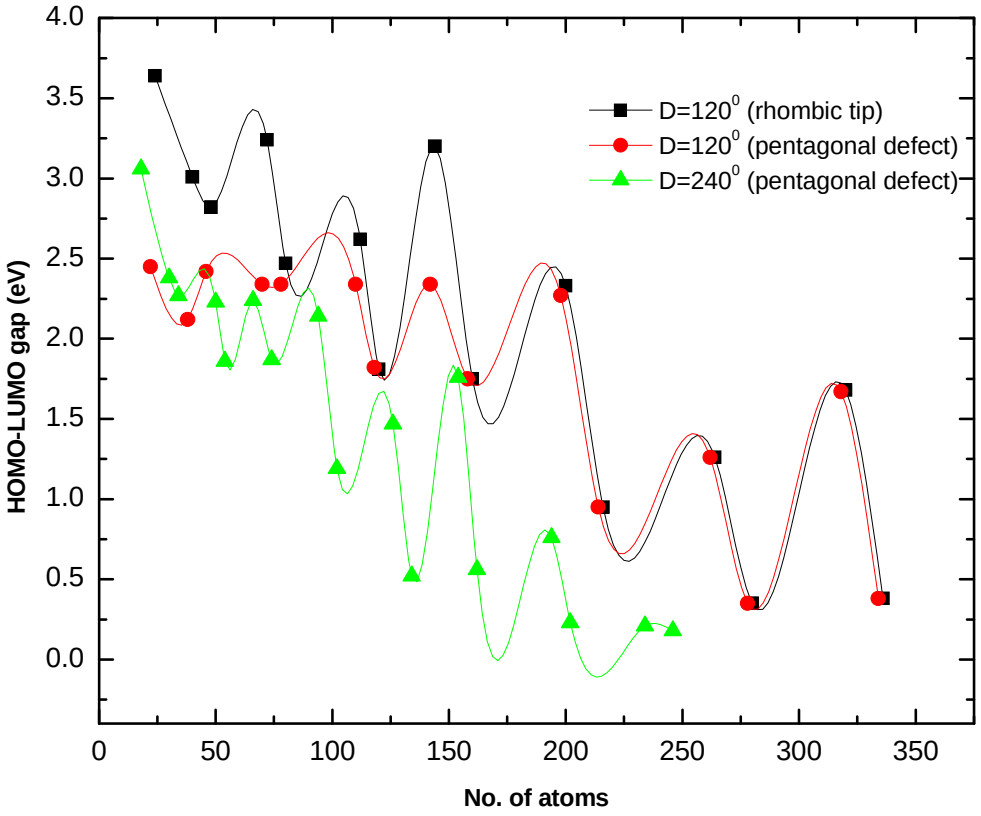

Figure 5.8: HOMO-LUMO gap *versus* number of atoms in nanocones with disclination angle 120^0 and 240^0.

to the difference in edge structures of the nanocones when we gradually increase the size of the nanocones. For example, Figure 5.9 shows the structure of nanocones with disclination angle 60° of three different sizes- $Si_{60}C_{65}H_{25}$, $Si_{73}C_{77}H_{30}$, and $Si_{83}C_{87}H_{30}$. They have HOMO-LUMO gaps of 1.19 eV, 1.44 eV, and 1.10 eV, respectively. As indicated before, this points to an oscillatory pattern in the HOMO-LUMO gaps. But also, as we can clearly see in the figure that the edge of the first nanocone in this example does not have any armchair-like configuration, whereas in the second there are 10 armchair-like configurations at the edge and there are only 5 armchair-like configurations at the edge of the third nanocone. Equal number of hydrogen in the second and the third nanocones suggest that they have similar opening sizes. The major difference between them is the edge structures – one has more armchair regions than the other one. This suggests that larger the number of armchair-like edges, larger is the HOMO-LUMO gap. This holds for all nanocones under study. This has been also confirmed by the HOMO-LUMO gaps of armchair and zigzag silicon carbide nanotubes in our previous studies [47, 48] it is shown that the band gaps of zigzag nanotubes are significantly lower than those of armchair nanotubes. Figure 5.10 shows difference among density-of-states plots of the three nanocones discussed in the example. In all of the nanocones we studied here, the HOMO and LUMO are localized around the open ends and around C-rich or Si-rich regions of the nanocones except in some of the nanocones with disclination angle 120°. In the case of some nanocones with disclination angle 120° we observed that the HOMO is distributed over the wall of the nanocone and LUMO is localized around the tip of the nanocone if the nanocone tip is rhombic. Also, the localization of HOMO and LUMO are affected by the structure of the tip. If the tip has pentagonal defects, both HOMO and LUMO are localized around the tip. Figure 5.11 shows the HOMO and LUMO surface plots of nanocone of disclination angle 120° of identical cone-opening but with different tip structure. It is evident from the figure that the localization of HOMO and LUMO is greatly affected by the structure of the tip.

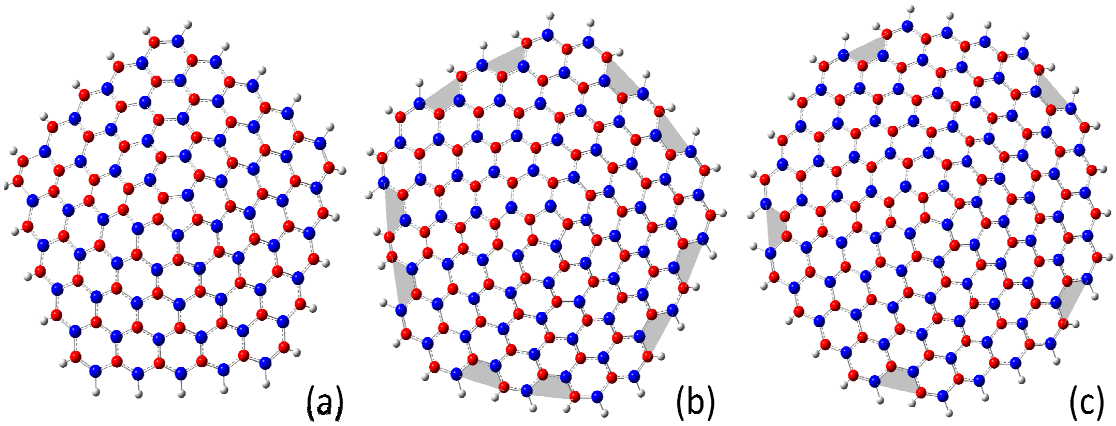

Figure 5.9: Three different sizes of nanocones with disclination angle 60^0. (a) $Si_{60}C_{65}H_{25}$, (b) $Si_{73}C_{77}H_{30}$, and (c) $Si_{83}C_{87}H_{30}$. Armchair region at the edges of nanocones are shaded.

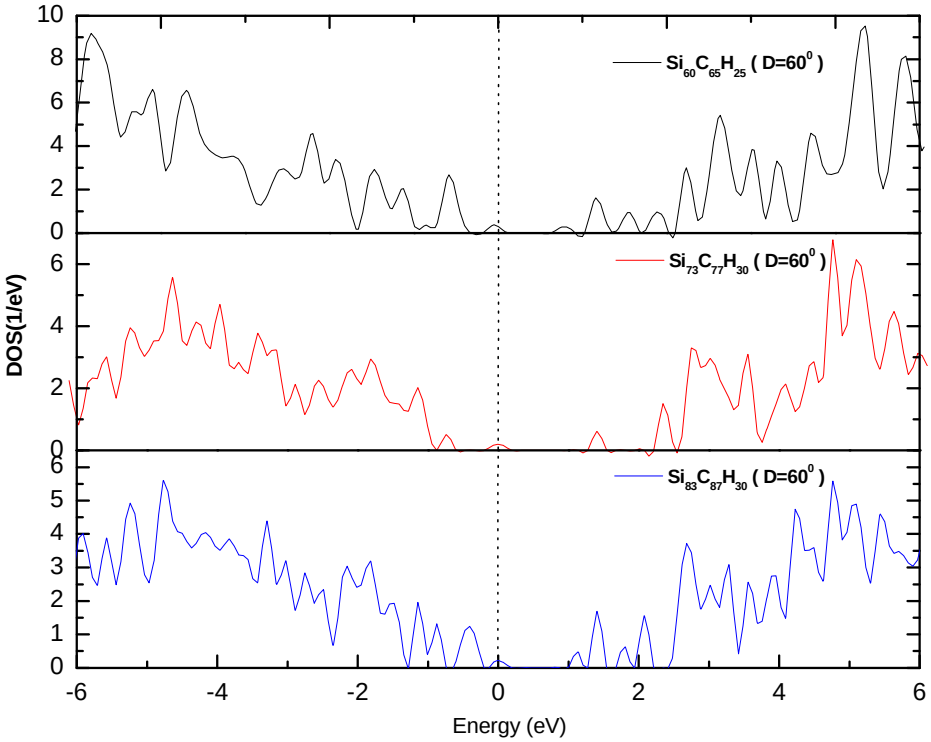

Figure 5.10: Density of states of three different sizes of nanocones with disclination angle 60^0.

(a) $Si_{60}C_{65}H_{25}$, (b) $Si_{73}C_{77}H_{30}$, and (c) $Si_{83}C_{87}H_{30}$.

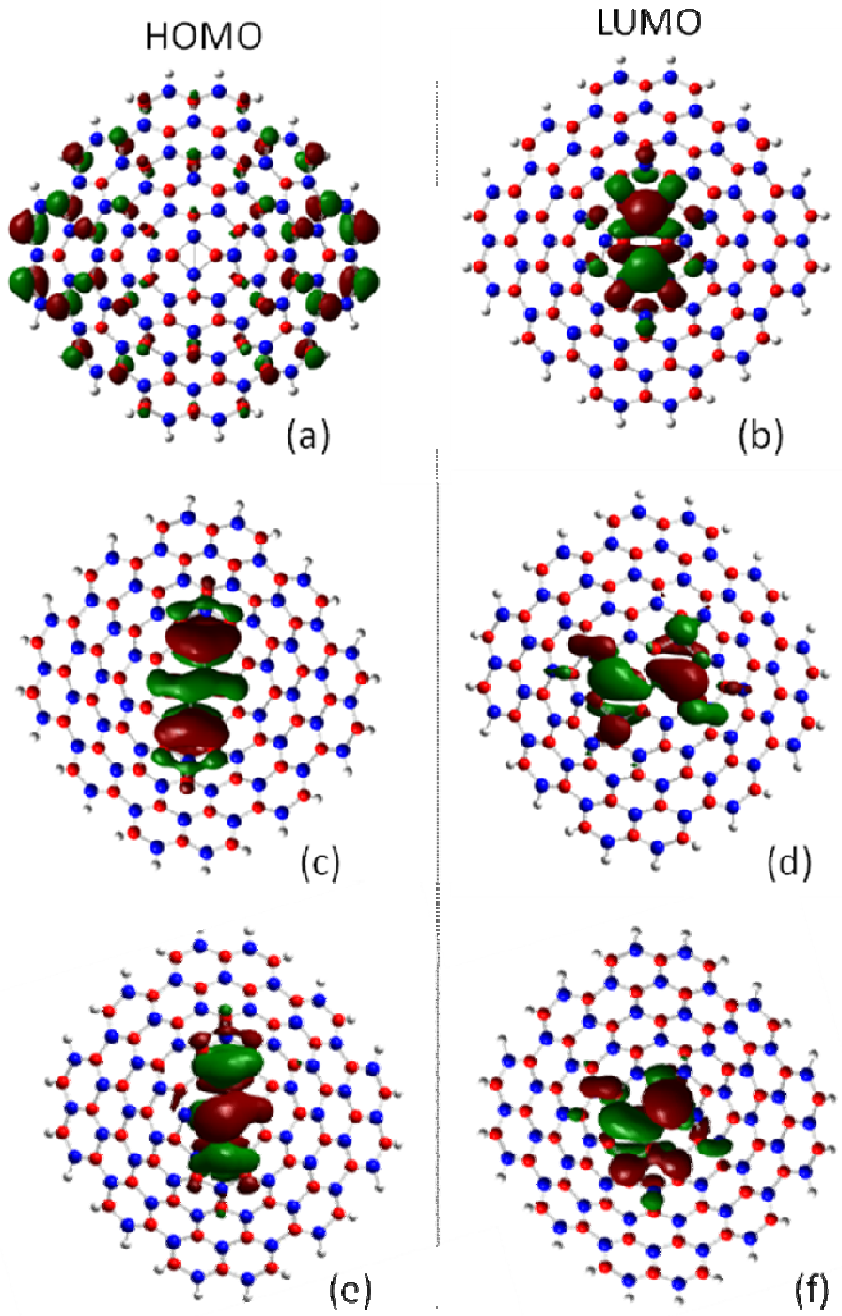

Figure 5.11: HOMO plots [(a),(c),(e)] and LUMO plots [(b),(d),(f)] of nanocone of disclination angle 120^0 with rhombic tip [(a),(b)]; with pentagonal defects and C-C bond at the tip[(c),(d)]; and with pentagonal defects and Si-C bond at the tip[(e), (f)].

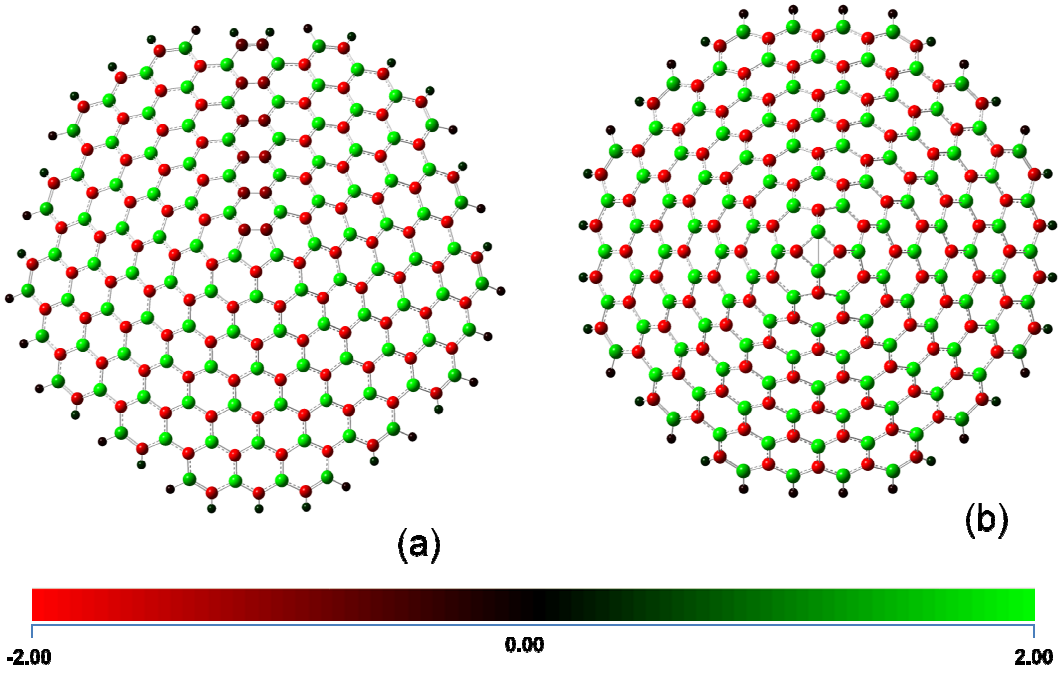

Figure 5.12: Natural bond orbital (NBO) charge distributions for nanocones (a) D=60^0 and (b) 120^0. Carbon gained and silicon atoms lost charge. Hydrogen atoms at dangling bonds remain almost neutral.

We also performed NBO charge analysis [201] for the nanocones studied here. All the structures show significant electron transfer from Si to C atoms. Figure 5.12 implies that carbon-rich nanocone structures are less ionic than the nanocones with equal number of silicon and carbon atoms, as they have some homo-nuclear bonds (C-C). In fact, the Si-C bonds in nanocones with disclination angle 120° and 240° are all partially ionic, whereas in case of 60°, 180°, and 300°, bonds Si-C, C-C (or Si-Si), are a m ixture of partially ionic and covalent bonds. The asymmetry in charge distribution in SiC nanocones can further be exploited to achieve different electronic properties by exterior-wall decoration at different adsorption sites.

5.3 Conclusions

In summary, we have studied silicon carbide nanocones of different disclination angles and different tip structures. Evolution of electronic properties with the size of the nanocones within each category is also studied. The study suggests the possibilities of experimental synthesis of free standing silicon carbide nanocones. The B.E./atom or the cohesive energy of the nanocones depends not only on the number of atoms but also on the disclination angle of the nanocone. Cohesive energies of nanocones with greater disclination angle are greater as compared to the nanocones of smaller disclination angle. This suggests that the tubular structure of silicon carbide is more favored than two dimensional graphene-like sheets. Also, the study shows that the electronic properties of nanocones strongly depend on the edge structure of the nanocones.

CHAPTER 6

DOUBLE-WALLED SILICON CARBIDE NANOTUBES

6.1 Introduction

Although multi-walled nanotubes (MWNTs) have been synthesized and investigated first, there are very few *ab initio* studies on MWNTs compared to single-walled nanotubes (SWNTs), partly because of the complexity of MWNTs compared to SWNTs. The first logical step towards the study of MWNTs would obviously be double-walled nanotubes (DWNTs) constructed inserting one nanotube inside another. DWNTs were first observed by Iijima in 1991, along with MWNTs [1]. The selective synthesis of DWNTs is reported by Hutchison *et al.* in 2001[202]. Two coaxial SWNTs (n_1, m_1) and (n_2, m_2) make a DWNT (n_1, m_1) @ (n_2, m_2) where (n_1, m_1) and (n_2, m_2) represent the inner and outer tubes, respectively. Double walled nanotubes are the simplest multi-walled nanotubes. Study of double walled nanotubes might elucidate the nature of inter-wall interaction in multi-walled nanotubes. Double walled carbon nanotubes possess higher thermal and chemical stability than single walled nanotubes [203-211]. Kim *et al.* [209] have studied the sequential structural changes of double walled nanotubes as a function of temperature and found that the double walled nanotubes with inner wall diameter greater than 9 nm are structurally stable up to 2000 ^{0}C. The single walled nanotubes have thermal stability up to about 1800° C [212]. Liu *et al.* [210] performed thermogravimetric analysis (TGA) of double-walled carbon nanotubes in air and reported that the double-walled nanotubes have oxidation resistance up to about 800℃, whereas single-walled nanotube have oxidation resistance up to about 750℃ [213]. The Young's modulus and tensile strength of double walled nanotubes are found to be 0.73-1.33 TPa and 13-46 GPa respectively [211]. Double walled nanotubes are superior to the single walled and multi-walled

nanotubes in many respects, for example, they have shown better performance as field emitters [214] and in field-effect transistors [215, 216]. In an experimental study, Shimada *et al.* [215] have compared subthreshold swing factor of DWNTs with that of SWNTs and shown that DWNTs are better FET channels than SWNTs. The authors used double walled nanotubes as channels of field-effect transistors (FET) and reported that DWNTs-FETs show metallic or semiconducting behavior depending on the tube diameters. The semiconducting double walled nanotubes exhibit both p- and n-type characteristics which is absent in normal single-walled-nanotubes-FETs. Kuwahara *et al.* [217] have successfully used double-walled nanotubes as AFM tips and found that the double-walled nanotubes as AFM tip possess higher resolution, high aspect ratio imaging and a longer lifetime of the tip as compared to multi-walled or single-walled nanotube tips. These novel characteristics of DWNT–AFM tips are attributed to mechanical robustness, and the bending rigidity of DWNTs. Double-walled carbon nanotubes are found to have interlayer separation greater than that observed in multiwalled carbon nanotubes. Cumings *et al.* [218] have reported the synthesis of DWCNTs with interlayer seperation of 7 Å. Double walled nanotubes provide ideal structure for the functionalization of the tubes since one can find a way to functionalize the outer tube while preserving the electrical properties of inner tubes [219-221]. Therefore the study of double-walled nanotubes is important not only to understand the interlayer interaction in multi-walled nanotubes but also to explore their stand alone applications. A detailed discussion of double-walled carbon nanotubes is provided in a recent review article by Shen *et al.* [222].

6.2 Construction of Double-Walled Nanotubes

As discussed before, a DWNT is represented by $(n_1, m_1)@(n_2, m_2)$. If (n_1, m_1) be the chiral indices of the inner wall and the chiral indices of the outer wall (n_2, m_2) of a DWNT can be given by the solution of equation, $m_2^{\,2} + m_2 n_2 + (n_2^{\,2} - k) = 0$ for a given value of n_2. The

factor k is given by $k=[2\pi(r_{t1}+\Delta r)/a]^2$ where r_{t1}, Δr, and a represent radius of inner tube, interlayer spacing and lattice constant respectively. The radius of inner tube is given by $r_{t1}=a\sqrt{n_1^{\,2}+m_1^{\,2}+n_1m_1}/2\pi$ [223]. These equations are particularly important when one has to model polychiral nanotubes with certain interlayer separation. The study of polychiral nanotubes is quite interesting in carbon nanotubes [224] since a slight change in chirality changes the electronic properties of the nanotubes, whereas, all the single-walled SiCNTs are semiconducting irrespective of their chirality. Therefore, for the symmetry consideration and for computational convenience all the double-walled SiCNTs we studied are armchair@armchair nanotubes. An armchair@armchair nanotube can be represented by (m, m) @(n, n). The radius of the nanotube (m, m) is given by $r_m = a\sqrt{3}m/2\pi = 3ma_{Si-C}/2\pi$, where a_{Si-C} is the SiC bond length in the nanotube. If we take $a_{Si-C} \approx 1.79\text{Å}$ then the radius of nanotube (m, m) is approximately $0.85m$. Therefore the theoretical interlayer separation of armchair@armchair double-walled SiCNT (m, m) @ (n, n) is given by $\Delta r \approx 0.85\Delta n$ Å where $\Delta n = n - m$. In our study we have considered double-walled nanotube with various interlayer separations. In particular, we have investigated the structural and electronic properties of nanotubes form (3,3)@(6,6) to (6,6)@(12,12). We have used cluster approximation to represent double-walled silicon carbide nanotubes. As explained before, this approach simulates effect of the infinite nanotubes by saturating the dangling bond at both ends of the nanotubes by hydrogen atoms. As discussed in the Chapters 1 and 2, there are three types of SiC nanotubes depending upon the arrangement of atoms in the tube. Figure 6.1 shows the arrangement of atoms in three types of nanotubes. All three types of nanotubes are used to model double-walled nanotubes. Figure 6.2 shows the side and top views of (4,4)@(10,10) double-walled SiC nanotube in type 1, 2, and 3 configurations. From the previous studies on single walled SiCNTs it is clear that the type 1 nanotubes are more stable than type 2 and type 3. The band gaps of the type 2 and type 3

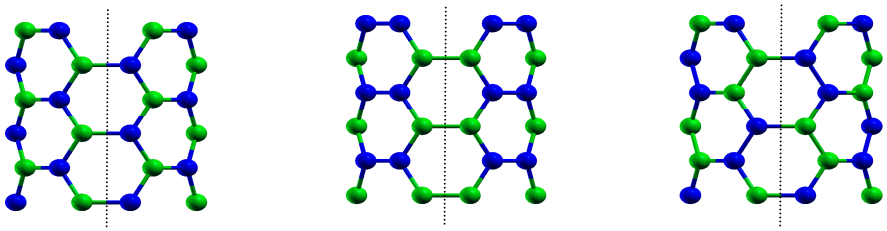

Figure 6.1: Atomic arrangements for (a) type 1, (b) type 2, and (c) type 3 nanotubes, with carbon atoms as green and silicon atoms blue. The dashed lines represent the orientation of tube axis.

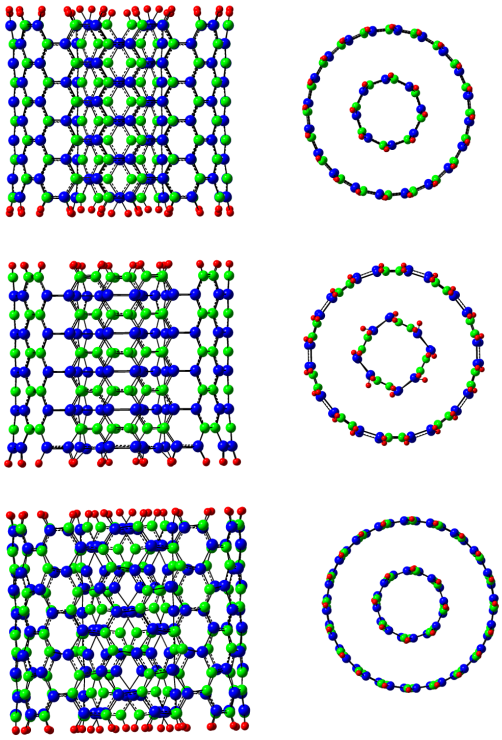

Figure 6.2: Side and top views of (4,4)@(10,10) double-walled SiC nanotube in (a) type 1, (b) type 2, and (c) type 3 configuration. Green atoms are carbon, blue atoms are silicon and red atoms are hydrogen attached to the dangling bonds.

nanotubes are smaller as compared to type 1. It is interesting to see how these properties change from single-walled to double-walled nanotubes.

6.3 Discussions of Results

In this work, we have used the B3LYP hybrid functional [110, 120, 122, 164] and the all electron 3-21G* basis set [136] as implemented in the GAUSSIAN 03 suite of programs [168] for full geometry optimizations without any symmetry constraints of the nanotube structures.

The stability of a double-walled nanotube is calculated using two different approaches. The B.E./atom was calculated from

$$E_b=[aE(Si)+bE(C)+cE(H)-E(Si_aC_bH_c)]/(a+b+c) \quad (6.1)$$

where a, b and c are the numbers of Si, C, and H atoms respectively and $E(Si_aC_bH_c)$ is the total energy of the clusters representing the nanotubes. The formation energy for each DWNT is given by:

$$\Delta E = E\,(m, m) + E\,(n, n) – E\,[(m.\ m)\ @\ (n, n)] \quad (6.2)$$

where E(m, m) and E (n, n) are the optimized ground state total energies of SWNTs (m, m) and (n, n), respectively and E[(m, m)@(n, n)] is the optimized ground state total energy of a DWNT (m, m)@(n, n) with the energy convergence criterion being set to 10^{-6} a.u. Obviously, according to our definitions, both the B.E./atom and the formation energy have to be positive for a DWNT to be stable. For the sake of comparison with DWNTs, Table 6.1 shows the results of (3, 3) to (12, 12) SiC SWNTs of all three types, including the tube diameter, radial bucking, B.E./atom, and the highest-occupied-molecular-orbital to lowest-unoccupied-molecular-orbital (HOMO-LUMO) gap using the all-electron 3-21G* basis set. Figures 6.3, 6.4, and 6.5 show the plot of B.E./atom, HOMO-LUMO gap, and radial buckling respectively as the function of diameter of the single-walled silicon carbide nanotubes. It is worth noting that the B.E./atom of a SiC SWNT increases monotonically with the size/diameter of the tube, the value of the binding energy being 5.060 eV for (12,12) type 1. Type 2 and type 3 nanotubes have relatively lower binding

Table 6.1: Tube diameter (in Å), radial buckling (in Å), binding energy per atom (in eV), and HOMO-LUMO gap (in eV) for single-walled SiC nanotubes.

Nanotube	Number of atoms	Diameter (Å)			Buckling (Å)			B.E./atom (eV)			HOMO-LUMO gap (eV)		
		Type 1	Type 2	Type 3	Type 1	Type 2	Type 3	Type 1	Type 2	Type 3	Type 1	Type 2	Type 3
(3,3)	72	5.206	5.222	5.242	0.091	0.298	0.175	4.869	4.686	4.588	3.335	1.439	1.281
(4,4)	96	6.926	6.989	7.023	0.062	0.267	0.003	4.952	4.681	4.678	3.306	1.422	1.080
(5,5)	120	8.636	8.879	8.738	0.050	0.155	0.001	4.994	4.707	4.725	3.547	0.913	1.039
(6,6)	144	10.344	10.645	10.463	0.042	0.136	0.002	5.017	4.730	4.751	3.535	0.958	1.017
(7,7)	168	12.060	12.418	12.191	0.033	0.113	0.004	5.032	4.745	4.768	3.493	0.961	1.008
(8,8)	192	13.772	14.187	13.913	0.028	0.102	0.004	5.041	4.754	4.779	3.471	0.978	1.005
(9,9)	216	15.484	15.955	15.640	0.024	0.096	0.005	5.048	4.761	4.786	3.459	0.994	1.004
(10,10)	240	17.197	17.725	17.367	0.021	0.092	0.006	5.053	4.766	4.791	3.449	0.988	1.003
(11,11)	264	18.906	19.494	19.094	0.018	0.084	0.005	5.057	4.769	4.795	3.441	0.982	1.003
(12,12)	288	20.623	21.264	20.822	0.018	0.081	0.005	5.060	4.772	4.798	3.438	0.980	1.003

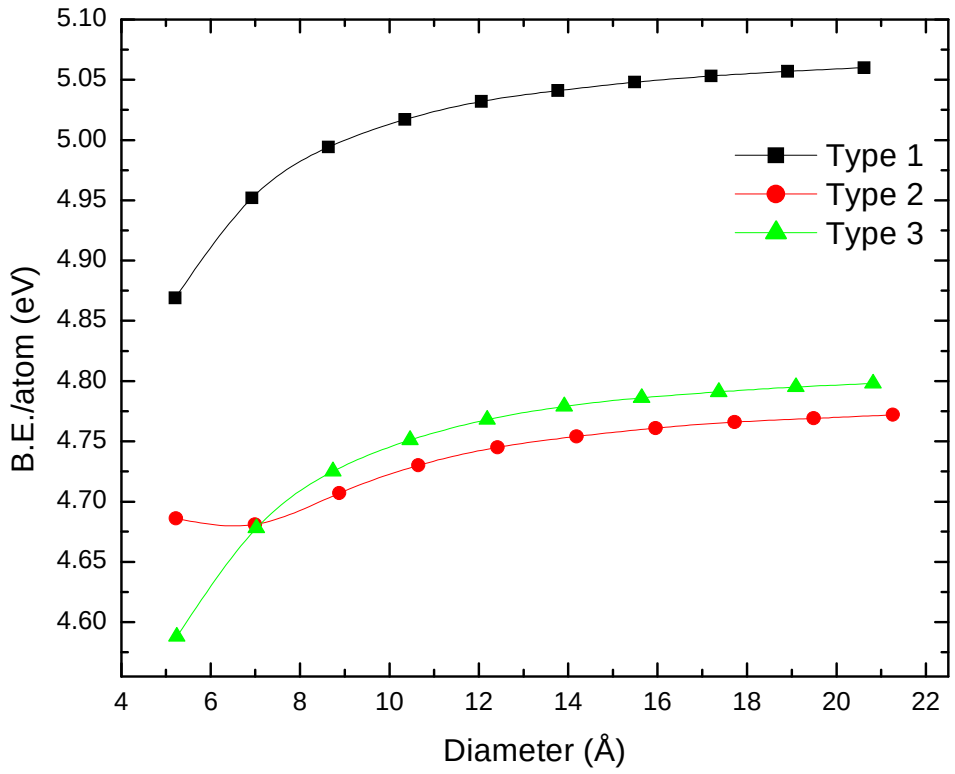

Figure 6.3: B.E./atom (eV) *versus* diameter of single-walled silicon carbide nanotubes.

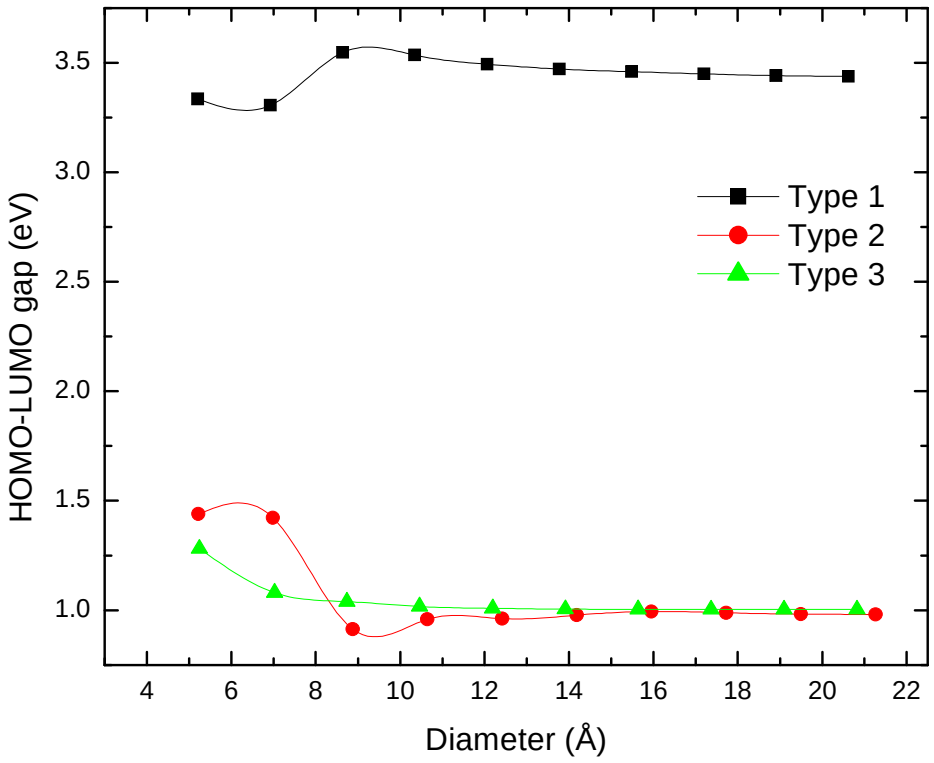

Figure 6.4: HOMO-LUMO gap (eV) *versus* diameter of single-walled silicon carbide nanotubes.

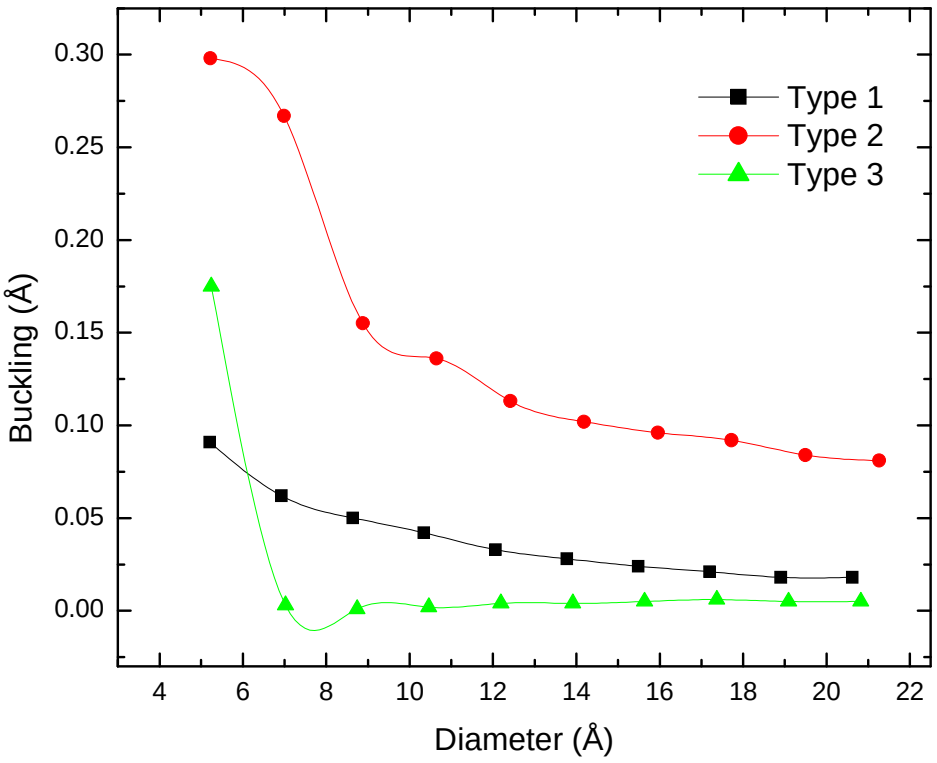

Figure 6.5: Buckling *versus* diameter of single-walled silicon carbide nanotubes.

energies and HOMO-LUMO gap than those of type 1. The radial buckling all the nanotubes decrease with increase in diameter. For a given nanotube, radial buckling is significantly greater in type-2 configuration than in type 1 and type 3. As we will see later, the amount of radial buckling in individual single-walled nanotube plays an important role in determining whether a double-walled nanotubes preserves a co-axial geometry or not.

Table 6.2 and Figure 6.6 show the variations of binding energies per atom with respect to the total number of atoms. As in the case of single-walled nanotubes, type 1 DWNTs have relatively higher binding energies compared to those of types 2 and 3. This can be attributed to the overall symmetry of type 1 nanotubes since clusters tend to prefer symmetric structures with higher binding energies. Also, type 1 tubes have only Si-C bonds which are stronger than Si-Si bonds and this makes types 2 and 3 nanotubes slightly less stable. Types 2 and 3 DWNTs have nearly equal binding energies per atom. Since SiC prefers sp^3 bonding more than sp^2, the collapsed nanotubes (indicated by "C" in Figure 6.6) have relatively higher binding energies than those with co-axial tubular geometry in all three configurations. However, the difference between the B.E./atom of collapsed and co-axial tubular nanotubes is very small. For example, the collapsed nanotube (4,4)@(8,8) type 2 has a B.E./atom of 4.9150 eV and (4,4)@(10,10) type 2 which has co-axial tubular geometry has a B.E./atom of 4.7432 eV. In type 1 configuration it is evident that there is an opposing trend in B.E./atom as the inner tube increases in diameter. For (3, 3) @ (n, n) (n =7-12), the binding energy first decreases and then shows a monotonically increasing pattern. For the other tubes, the B.E./atom tends to show an oscillatory pattern, with some DWNT structures such as (4,4)@(9,9), (5,5)@(9,9), and (6,6)@(10,10) indicating increased stabilities. In type 2, binding energy first decreases going from collapsed to co-axial tubular nanotubes and then increases with size for all co-axial tubular nanotubes. However the increase in B.E./atom is not significant. In type 3, B.E./atom shows similar trends as in type 1. For co-axial tubular DWNTs there is an opposing trend in B.E./atom as the inner tube increases in size. For DWNTs having inner tube (3,3) and (4,4), i.e.

Table 6.2: Interlayer separation (in (Å), B.E./atom (in eV), and formation energy (eV) for SiC DWNTs ("collapsed" indicates nanotubes without co-axial tubular geometry.)

Nanotube	Inter Layer Seperation			B.E./atom (eV)			Formation energy (eV)		
	Type 1	Type 2	Type 3	Type 1	Type 2	Type 3	Type 1	Type 2	Type 3
(3,3)@(6,6)	Collapsed	Collapsed	Collapsed	5.0731	4.8675	4.8242	22.7479	32.8540	27.5162
(3,3)@(7,7)	3.3756	Collapsed	Collapsed	5.0162	4.8802	4.8385	7.9662	36.7652	29.9382
(3,3)@(8,8)	4.2578	Collapsed	4.2971	5.0063	4.8448	4.7366	3.1099	28.8432	2.6665
(3,3)@(9,9)	5.1339	5.2907	5.1659	5.0058	4.7357	4.7376	0.6374	1.8342	0.3445
(3,3)@(10,10)	6.0429	6.2325	6.0562	5.0101	4.7470	4.7436	−0.2321	-0.0925	-0.2408
(3,3)@(11,11)	6.8553	7.1381	6.9072	5.0167	4.7512	4.7503	0.0007	0.0386	0.1768
(3,3)@(12,12)	7.7133	8.0173	7.7602	5.0216	4.7546	4.7558	0.0039	0.0310	0.1713
(4,4)@(7,7)	Collapsed	Collapsed	Collapsed	5.0749	4.8770	4.8495	19.0937	41.0162	30.2179
(4,4)@(8,8)	3.4525	Collapsed	Collapsed	5.0307	4.9150	4.8226	5.5516	53.3098	22.3629
(4,4)@(9,9)	4.2985	Collapsed	4.2566	5.0317	4.8596	4.7627	4.1219	38.4673	3.1206
(4,4)@(10,10)	5.1555	5.3494	5.1804	5.0262	4.7432	4.7601	0.6730	0.5346	0.4119
(4,4)@(11,11)	5.9742	6.2492	6.0284	5.0289	4.7462	4.7638	0.0704	0.1552	-0.0659
(4,4)@(12,12)	6.8525	7.1381	6.8897	5.0325	4.7492	4.7680	−0.0268	-0.0278	-0.0860
(5,5)@(10,10)	4.2635	Collapsed	4.2207	5.0458	4.8901	4.7794	4.4682	51.8035	3.6557
(5,5)@(11,11)	5.1592	5.3176	5.1687	5.0459	4.7485	4.7748	4.2310	0.5233	0.5407
(5,5)@(12,12)	6.0223	6.1885	6.0360	5.0382	4.7527	4.7766	−0.0059	0.0970	-0.0984
(6,6)@(9,9)	2.9931	Collapsed	Collapsed	5.0152	4.9344	4.8707	−0.7022	66.9246	35.4919
(6,6)@(11,11)	4.1838	Collapsed	4.2114	5.0564	4.9224	4.7902	5.5508	68.1388	4.2352

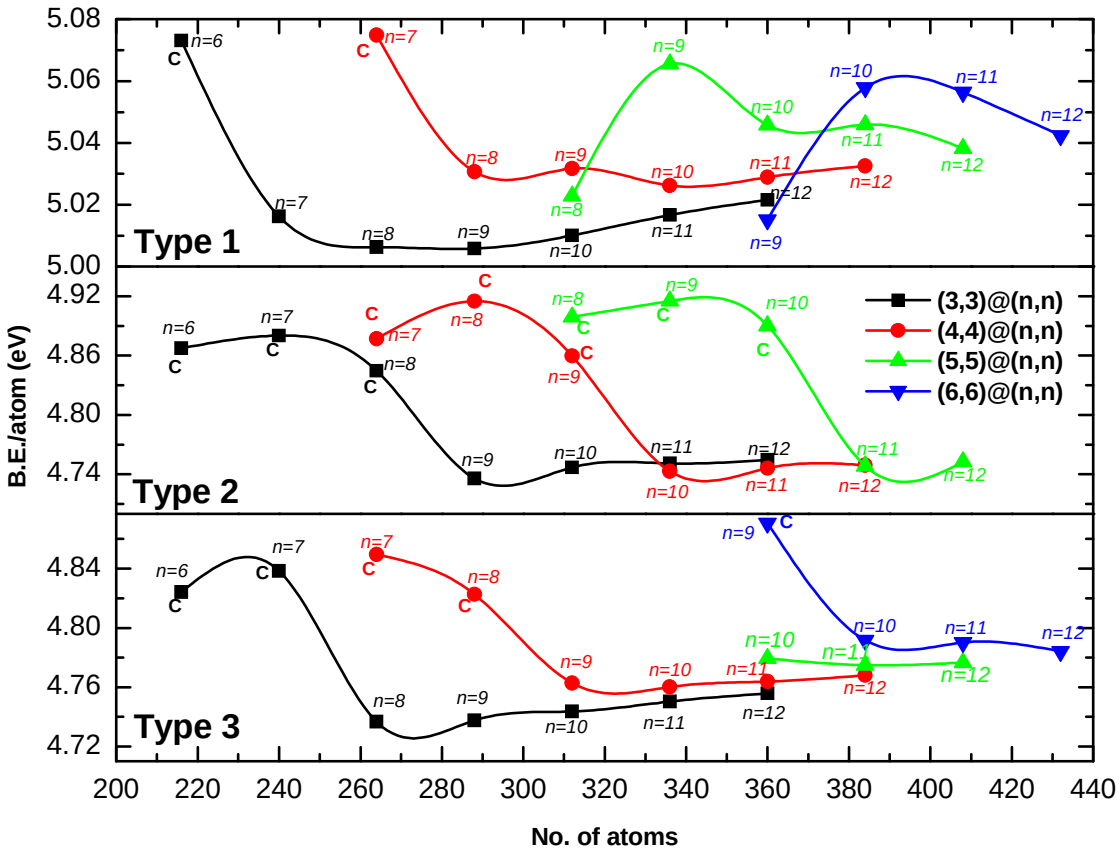

Figure 6.6 : Variation of B.E./atom (eV) *versus* the number of atoms.

(3,3)@(n,n) and (4,4)@(n,n) B.E./atom increases as the size of the tube increases whereas the B.E./atom of (5,5)@(n,n) shows small oscillations and that of (6,6)@(n,n) shows slightly decreasing trend. The collapsed nanotubes have greater binding energies per atom than those of co-axial tubular DWNTs as in types 1 and 2 tubes. The oscillatory pattern of B.E./atom in type 1 and type 3 DWNTs is similar to the patterns observed in nanoclusters and reminiscent of the concept of "magic numbers" in clusters. A closer examination of the values of the binding energies per atom for all the DWNTs studied here, however, show that the binding energies per atom do not vary significantly, from about 4.7 eV to about 5.0 eV, a difference of about 6%. We also note from Tables 1 and 2 that the stabilities of SiC DWNTs are of the same order as those of SiC SWNTs. It should therefore be, in principle, possible to synthesize both SiC DWNTs and SWNTs under experimental conditions. As mentioned before, the largest value of the binding energy of a SWNT obtained in this study is 5.06 eV/atom for the (12, 12) tube whereas the largest value of a non-collapsed DWNT is 5.07 eV/atom for the (5,5)@(9,9) tube.

Table 6.2 and Figure 6.7 show the variation of the formation energy with respect to the interlayer separation of DWNTs. The formation energy gives a measure of the stability of a DWNT with respect to the individual SWNTs. The variation of the formation energy with respect to interlayer separation, as studied in some earlier computational works on DWNTs, has shown that there is a most favorable interlayer separation of a DWNT depending on the constituent atoms of the nanotubes. The most favorable interlayer separation of binary nanotubes like boron nitride [225] and silicon carbide [41] depends on atomic arrangements in the inner and outer nanotubes. Yu *et al.* [41] have shown that the interlayer separation of graphene-like layers of silicon carbide is about 3.7 Å for Si on top of C sequence of bi-layer arrangement and about 4.8 Å for Si on top of Si or C on top of C sequence of bi-layer arrangement. A similar study on multilayered graphene-like SiC sheets by Huda *et al.* [40] has shown that the interlayer separation is 2.1 Å for Si on top of C sequence and 4.1 Å for Si on top of Si sequence. However, DWNTs having such definite sequence of bi-layer arrangement can be realized in

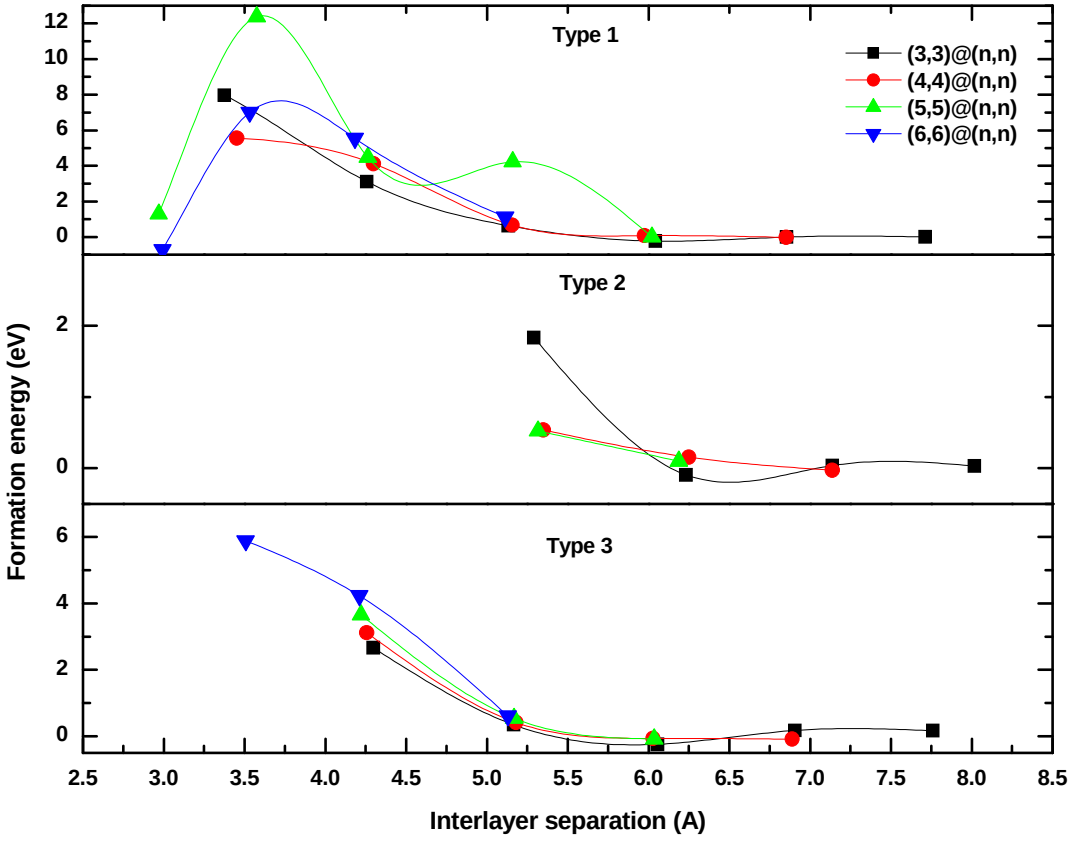

Figure 6.7: Variation of formation energy (eV) *versus* the interlayer seperation (Å)

relatively big DWNTs having nearly equal number of Si (and/or C) atoms in outer and inner nanotubes. Since the nanotubes considered in this study are relatively small, numbers of Si and C atoms in inner and outer nanotubes are significantly different. Therefore in the cases of types 1 and 3 tubes, it is not possible to get a definite sequence of the atoms in the inner and outer nanotubes like in two graphene-like layers of SiC. However, in case of type 2 DWNTs there is a definite sequence of the atoms (Si on top of Si, C on top of C) because of its construction. Therefore, in case of type 2 DWNTs we expect greater interlayer separation than in type 1 and type 3 DWNTs. It is found that all type 2 nanotubes which have interlayer separation of about 4.2 Å collapse and lose the geometry of DWNTs, at least in the sense that they are no longer co-axial tubes. In the case of type 3, DWNTs with interlayer separation of about 3.5 Å collapse except (6,6)@(10,10) which has interlayer separation of 3.5 Å. Type1 DWNTs preserve their geometry for relatively smaller interlayer separation. The type 1 configuration favors interlayer separation of about 3.5 Å. It is found that the smaller DWNTs having interlayer separation of about 2.5 Å, in particular (3,3)@(6,6), (4,4)@(7,7) collapse (see Figure 6.8). The greater buckling of smaller nanotube brings atoms in the outer and inner tubes closer which causes bonding of atoms in the inner and outer nanotubes collapsing the DWNT. However the bigger nanotubes (5,5)@(8,8) and (6,6)@(9,9) do not collapse like smaller nanotubes because they have comparatively small buckling. Although (5,5) @(8,8) and (6,6)@(9,9), both with interlayer separation of about 3 Å, seem to preserve their co-axial geometry, their very low formation energy suggests that they are either unstable or less stable. In terms of chiral indices of DWNTs, (n,n)@(m,m), type 1 configuration collapse or becomes unstable when (m-n)≤3, type 2 configuration collapse when (m-n) ≤ 5, and type 3 configuration collapse when (m-n) ≤ 4 except (6,6)@(10,10) and probably bigger DWNTs. Figure 6.9 shows the double-walled nanotube (4,4)@(8,8) of three types. It is clear from the figure that type 1 is preserving co-axial geometry of the double-walled nanotubes whereas type 2 and type 3 configuration of this double-walled nanotube are collapsed and no longer double-walled in the sense that the outer and inner walls

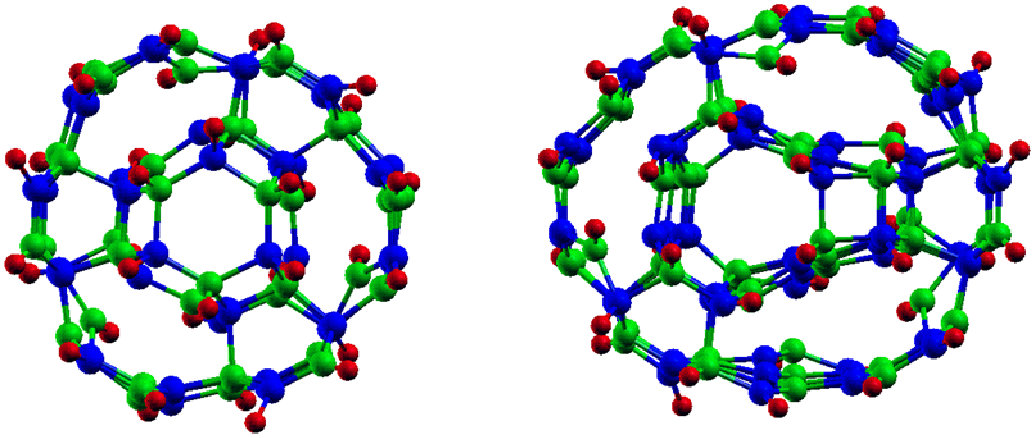

Figure 6.8 Top views of (a) (3,3)@(6,6) and (b) (4,4)@(7,7) of “collapsed” double-walled SiC nanotubes in type 1 configuration. Green atoms are carbon, blue atoms are silicon and red atoms are hdrogen attached to the dangling bonds.

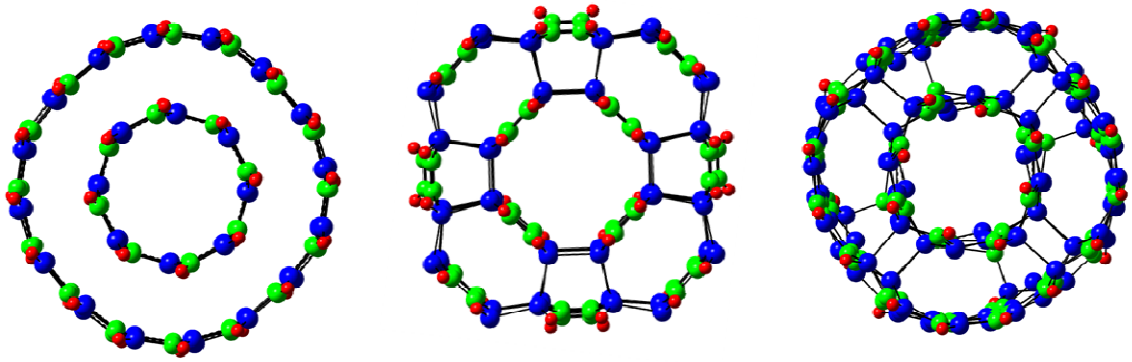

Figure 6.9 Top views of (4,4)@(8,8) SiC nanotube in (a) type 1, (b) type 2, and (c) type3 configuration. Green atoms are carbon, blue atoms are silicon and red atoms are hydrogen attached to dangling bonds.

are meshed. In fact, in the experiment of Sun *et al.* [38], multi-walled SiC nanotubes, with interlayer spacing ranging from 3.5-4.5 Å was observed, resulting from the reaction of silicon (via disproportionation of SiO) and multi-walled carbon nanotubes (as templates). We note that (5,5)@(9,9) type 1 tube with an interlayer separation 3.57 Å is a particularly stable SiC DWNT, with the highest formation energy among all the tubes studied here. In type 2 configuration, (3,3)@(9,9), with an interlayer separation of 5.3 Å, has the maximum formation energy of 1.83 eV, and in type 3 configuration, (6,6)@(10,10) with an interlayer separation of 3.5 Å, has the maximum formation energy of 5.89 eV. Therefore type 3 DWNTs are more stable than type 2. From these results, it is clear that the interlayer separation of multi-walled silicon carbide nanotubes is greater than that of multi-walled carbon nanotubes. Most of the attempts to synthesize silicon carbide are done by taking multi-walled carbon nanotubes as templates and reacting the carbon nanotubes with SiO. However this approach has yielded very few cases of success in synthesizing silicon carbide nanotubes. In most of the cases β-SiC nanowires are formed. This is because interlayer separation of the template itself is very small compared to what might be suitable for multi-walled silicon carbide nanotubes. So it collapses to form nanowires when reacted with SiO. From our theoretical calculation, we expect that if the templates chosen for the fabrication have interlayer separation of the order of 4 Å, the method would yield high percentage of hollow silicon carbide nanotubes.

Table 6.3 and figure 6.10 show the variation of the band gaps of the DWNTs with respect to the number of atoms. All the ground state structures we have studied here are in singlet state i.e. no magnetic structure has been found. It is evident that band gaps of all type 1 DWNTs are greater than those of type 2 and type 3 DWNTs as expected. We note here that type 1 nanotubes have only Si-C bonds which is partially ionic as compared to types 2 and 3 tubes which have some covalent C-C and Si-Si bonds in addition to Si-C bonds. Figure 6.11 shows the density of states (DOS) of (4,4)@(10,10) double-walled SiC nanotube of all three types.The band gap of the DWNTs which preserve the co-axial tubular geometry varies from

Table 6.3: HOMO-LUMO gap (in eV) of SiC DWNT

Nanotube	Number of Atoms	HOMO-LUMO gap (eV)		
		Type 1	Type 2	Type 3
(3,3)@(6,6)	216	2.1366	0.4814	0.6090
(3,3)@(7,7)	240	2.0060	0.4087	0.7429
(3,3)@(8,8)	264	3.0624	0.3380	0.8054
(3,3)@(9,9)	288	3.1182	0.7717	0.7886
(3,3)@(10,10)	312	3.1527	0.9782	0.7869
(3,3)@(11,11)	336	3.1647	0.9755	0.7831
(3,3)@(12,12)	360	3.1927	0.9782	0.7918
(4,4)@(7,7)	264	1.8305	0.4073	0.6139
(4,4)@(8,8)	288	2.6482	0.6027	0.8246
(4,4)@(9,9)	312	3.1152	0.4367	0.6278
(4,4)@(10,10)	336	3.1682	0.9475	0.7826
(4,4)@(11,11)	360	3.1758	0.9771	0.7981
(4,4)@(12,12)	384	3.1941	0.9782	0.7940
(5,5)@(10,10)	360	3.2787	0.6688	0.6152
(5,5)@(11,11)	384	3.2335	0.5211	0.7927
(5,5)@(12,12)	408	3.3099	0.6158	0.8114
(6,6)@(9,9)	360	2.5472	0.5948	0.5758
(6,6)@(11,11)	408	3.2860	0.7423	0.6155

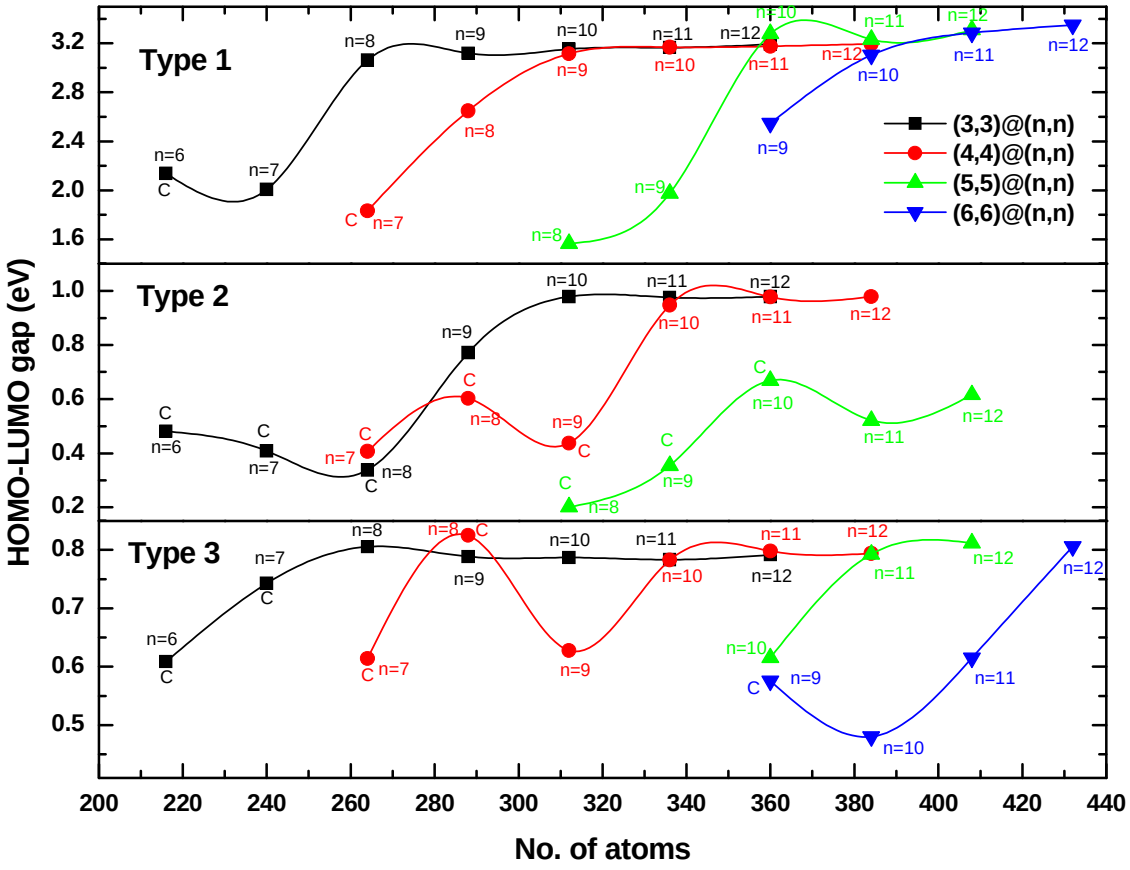

Figure 6.10 : HOMO-LUMO gap *versus* the number of atoms.

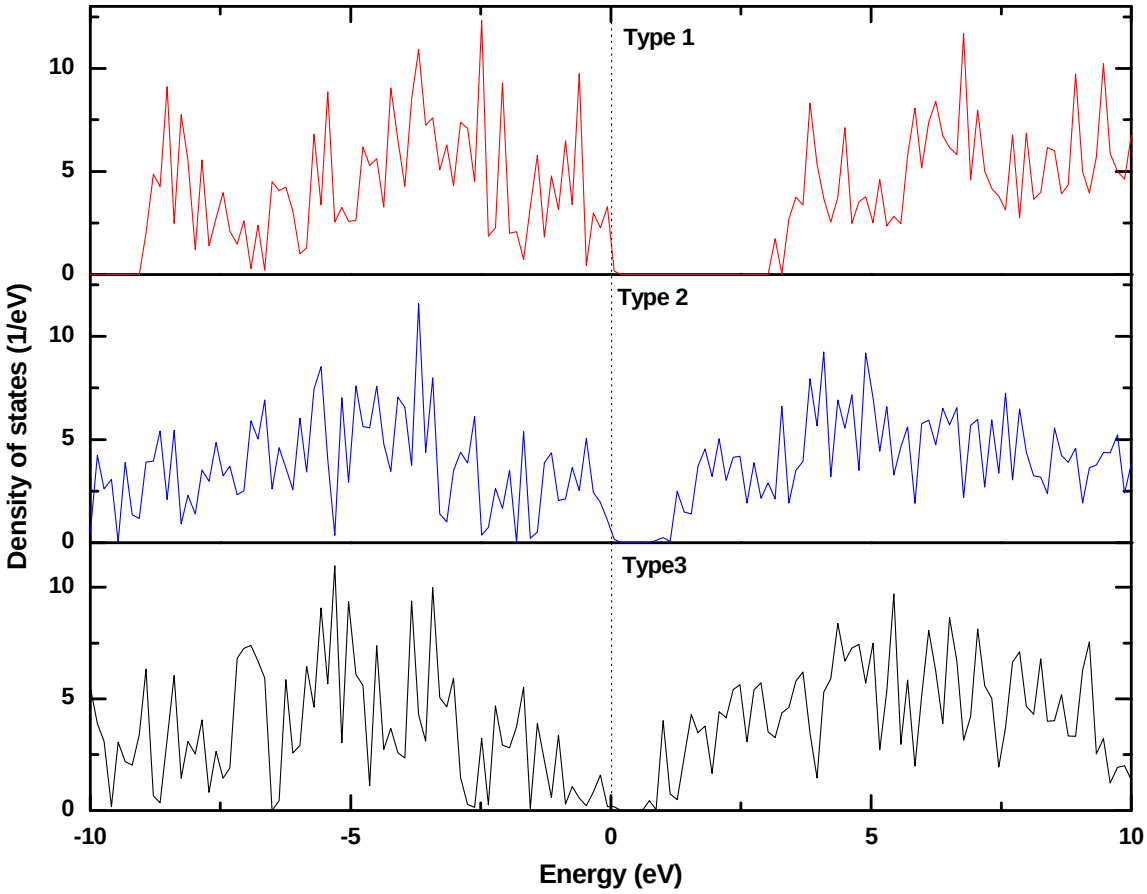

Figure 6.11 Density of states (DOS) of (4,4)@(10,10) double-walled SiC nanotube in (a) type 1, (b) type 2, and (c) type 3 configurations.

0.48 eV to 3.35 eV. The collapsed tubes have significantly smaller band gaps as compared to the co-axial tubular DWNTs. For example, the collapsed nanotube (5,5)@(8,8) type 2 has a band gap of 0.20 eV and gaps of all DWNTs are found to be less than their individual constituent SWNTs. As an example, band gap of type 1 SWNTs (5,5) and (9,9) are 3.55 eV and 3.46 eV, respectively whereas the band gap of type 1 DWNT (5,5)@(9,9) is 1.97 eV. This trend appears to be universally true from SWNTs to DWNTs of all types. The decrease in band gap from SWNT to DWNT is significant when the interlayer separation is small. As the interlayer separation increases the band gap of the DWNT tends to approach the band gap of the outer tube. For example, type 2 (3,3), (9,9), and (12,12) have band gaps 1.439 eV, 0.994 eV, and 0.980 eV respectively and that of type 2 (3,3)@(9,9), with an interlayer separation of 5.33Å is 0.772 eV but band gap of type 2 (3,3)@(12,12), with an interlayer separation of 8.02Å, is 0.978 eV. This indicates that the electronic structure of a DWNT is mainly dominated by that of the outer tube. This phenomenon has also been observed in double-walled boron nitride nanotubes [225]. We also note that the band gap increases as the size of the DWNT increases and tends to saturate, as has been observed before for SiC single-walled nanotubes. Figure 6.12 shows HOMO-LUMO plot of DWNTs (3,3)@(9,9) of types 1, 2 and 3.

After optimization, the nanotube surfaces were found to be slightly rippled. More electronegative C atoms moved outward and more electropositive Si moved inward, usually resulting in two concentric cylinders associated with each single walled nanotube. An absolute value of the difference between the average radii of the C atoms and the Si atoms is defined as the radial buckling *β:*

$$\beta = \left| \langle r_C \rangle - \langle r_{Si} \rangle \right| \qquad (6.3)$$

where $\langle r_C \rangle$ and $\langle r_{Si} \rangle$ are the average radii of C and Si atoms, respectively. Our previous studies on single-walled SiC nanotube have shown that the amount of buckling decreases as the tube diameter increases. Table 6.4 shows the variation of buckling of inner and outer walls with respect to the diameters of the inner and outer tubes. As we can see from Table 6.1, the

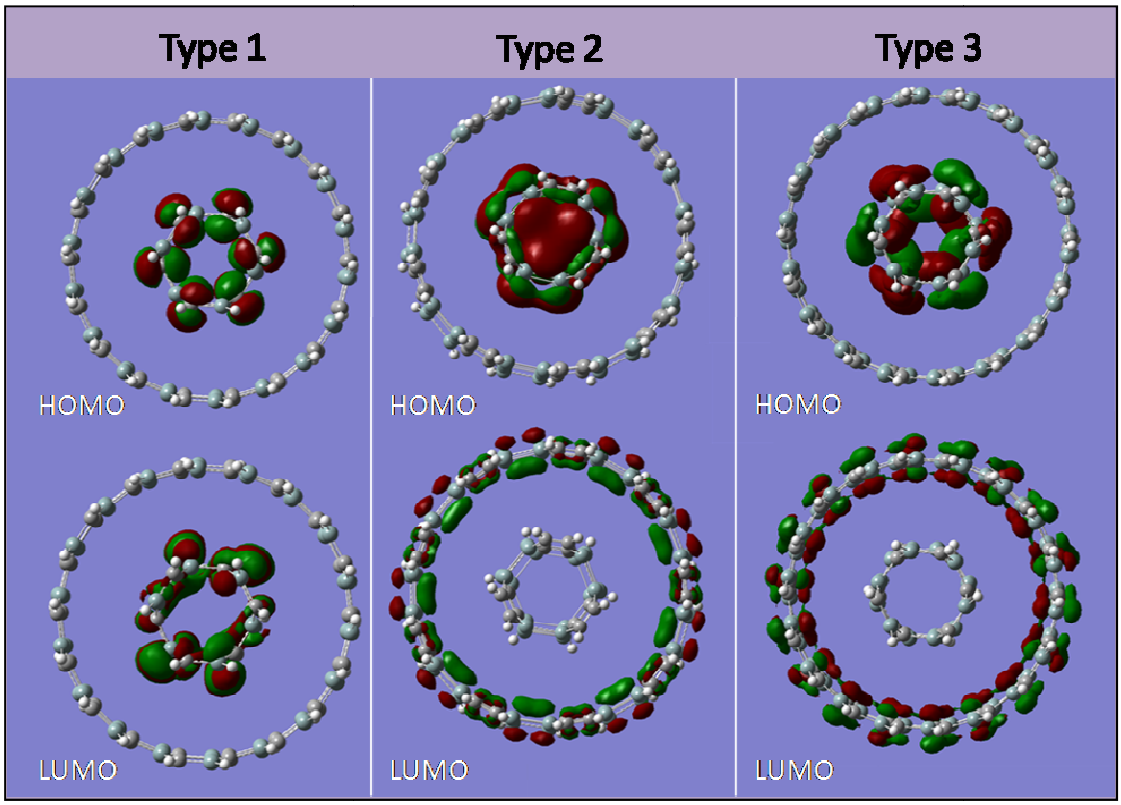

Figure 6.12 HOMO and LUMO plots of armchair SiCDWNT (3,3)@(9,9) in three configurations.

Table 6.4: Diameter ((in Å) and buckling (β) of inner and outer tubes (in Å) in SiC DWNTs.

	Type 1				Type 2				Type 3			
Nanotube	D(in)	D(out)	β(in)	β(out)	D(in)	D(out)	β(in)	β(out)	D(in)	D(out)	β(in)	β(out)
(3,3)@(6,6)	Collapsed				Collapsed				Collapsed			
(3,3)@(7,7)	5.231	11.982	0.078	0.047	Collapsed				Collapsed			
(3,3)@(8,8)	5.219	13.735	0.087	0.033	Collapsed				5.280	13.874	0.126	0.017
(3,3)@(9,9)	5.208	15.476	0.093	0.026	5.363	15.944	0.235	0.084	5.286	15.618	0.033	0.008
(3,3)@(10,10)	5.173	17.258	0.090	0.022	5.248	17.713	0.304	0.088	5.270	17.382	0.011	0.004
(3,3)@(11,11)	5.203	18.913	0.092	0.020	5.217	19.493	0.295	0.084	5.280	19.095	0.026	0.005
(3,3)@(12,12)	5.205	20.632	0.092	0.018	5.230	21.264	0.294	0.080	5.285	20.805	0.021	0.004
(4,4)@(7,7)	Collapsed				Collapsed				Collapsed			
(4,4)@(8,8)	6.884	13.789	0.052	0.041	Collapsed				Collapsed			
(4,4)@(9,9)	6.906	15.503	0.053	0.028	Collapsed				7.051	15.564	0.022	0.017
(4,4)@(10,10)	6.913	17.224	0.054	0.021	6.994	17.693	0.268	0.090	7.012	17.373	0.003	0.005
(4,4)@(11,11)	6.930	18.879	0.062	0.020	6.977	19.475	0.272	0.082	7.028	19.085	0.005	0.007
(4,4)@(12,12)	6.923	20.628	0.062	0.018	6.988	21.264	0.269	0.080	7.028	20.808	0.002	0.005
(5,5)@(10,10)	8.639	17.166	0.043	0.029	Collapsed				8.802	17.243	0.011	0.017
(5,5)@(11,11)	8.639	18.957	0.046	0.024	8.925	19.560	0.157	0.088	8.744	19.082	0.002	0.006
(5,5)@(12,12)	8.622	20.667	0.047	0.018	8.889	21.266	0.156	0.080	8.745	20.817	0.001	0.006
(6,6)@(9,9)	9.956	15.942	0.025	0.041	Collapsed				Collapsed			
(6,6)@(11,11)	10.411	18.779	0.033	0.026	Collapsed				10.531	18.954	0.010	0.018

buckling of single-walled type 2 nanotubes is greater than that of single-walled type 1 and type 3. Type 3 has the least buckling. As discussed before, type 2 DWNTs have a definite sequence of atoms i.e. Si (C) on top of Si (C); this causes even greater buckling since Si atoms in the two layers tend to come closer. Therefore, type 2 DWNTs do not preserve co-axial tubular structure even for relatively bigger interlayer separation. The buckling of the inner tubes is, in general, smaller than the buckling of the tubes in single walled geometry when the interlayer separation is small except in type 2 (4,4)@(n,n) and type 2 (5,5)@(n,n). Buckling of inner tube in type 2 (4,4)@(n,n) and (5,5)@(n,n) is about the same or slightly bigger than that in their single-walled geometry. For example, (4,4) type 2 nanotube has buckling of 0.267 Å in single-walled geometry and 0.272 Å when it is in type 2 DWNT (4,4)@(11,11). This is due to the definite stacking order of atoms in two layers of the type 2 DWNTs as described before. Inner tubes of type 1 DWNTs show a clear trend in variation of buckling. The buckling of the inner tube increases and approaches its corresponding value in single-walled configuration. For example, buckling of the SiC nanotube (3, 3) type 1 is calculated to be 0.09 Å in single-walled configuration. In double-walled configuration (3,3)@(7,7) type 1, the buckling of inner tube (3,3) is 0.08 Å, which increases to 0.09 Å in (3,3)@(12,12). The opposite trend is seen in the variation of buckling of outer wall of DWNTs with respect to interlayer separation. Buckling of the outer tubes in DWNTs is greater than the buckling of the tubes in single-walled configuration. As the interlayer separation increases, buckling of the outer tube decreases and approaches the corresponding value in single-walled configuration. For example, bucking of SiC nanotube (11,11) is 0.018 Å in single-walled configuration whereas in double-walled configuration, the buckling of outer wall (11,11) in (6,6)@(11,11) is 0.026 Å which decreases to 0.020 Å in (3,3)@(11,11).

We also performed Mulliken charge analysis [136] for the nanotubes studied here. Figure 6.13 shows Mulliken charge distributions for (4,4)@(10,10) nanotube of types 1, 2 and 3. The analysis shows significant electron transfer from Si to C atoms. Type 1 nanotubes are more

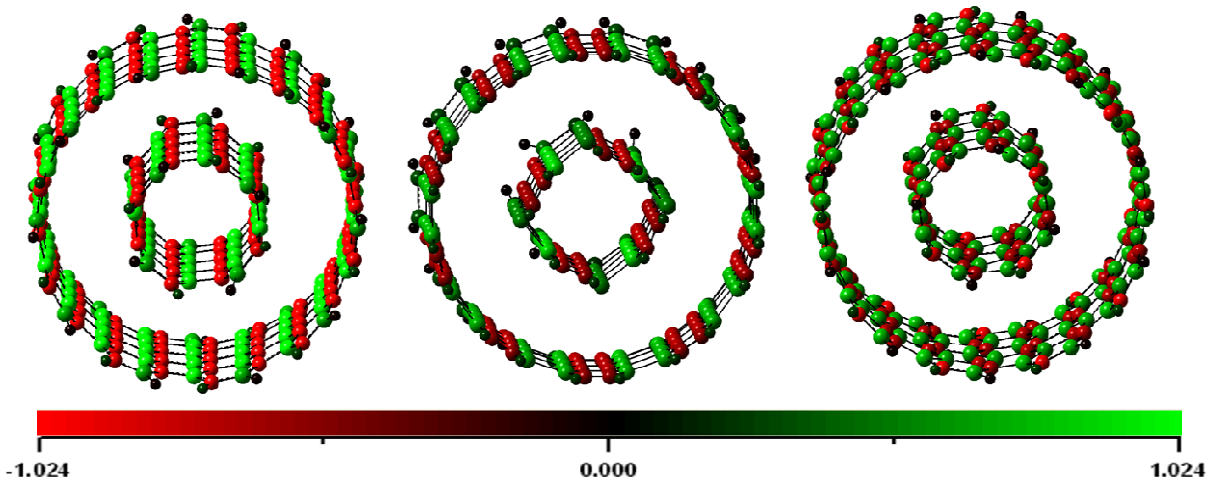

Figure 6.13: Mulliken charge distributions for (4,4)@(10,10) nanotube. Carbon gained and silicon atoms lost charge. Hydrogen atoms at dangling bonds remain almost neutral.

Table 6.5: Mulliken charges (in e) for inner tube (n_i) and outer tube (n_o)

Nanotube	Type 1		Type 2		Type 3	
	n_i	n_o	n_i	n_o	n_i	n_o
(3,3)@(6,6)	-0.9189	0.9189	2.0964	-2.0964	-0.4434	0.4434
(3,3)@(7,7)	-1.1684	1.1684	1.2991	-1.2991	0.2588	-0.2588
(3,3)@(8,8)	-0.0977	0.0977	1.0085	-1.0085	-0.0362	0.0362
(3,3)@(9,9)	-0.0065	0.0065	0.0891	-0.0891	0.0106	-0.0106
(3,3)@(10,10)	-0.0001	0.0001	0.0096	-0.0096	0.0013	-0.0013
(3,3)@(11,11)	-0.0001	0.0001	0.0008	-0.0008	0.0000	0.0000
(3,3)@(12,12)	0.0000	0.0000	0.0001	-0.0001	0.0000	0.0000
(4,4)@(7,7)	-0.9282	0.9282	1.5808	-1.5808	0.1489	-0.1489
(4,4)@(8,8)	-0.9548	0.9548	2.2359	-2.2359	-0.2611	0.2611
(4,4)@(9,9)	-0.2559	0.2559	1.6370	-1.6370	-0.0330	0.0330
(4,4)@(10,10)	-0.0057	0.0057	0.0321	-0.0321	0.0134	-0.0134
(4,4)@(11,11)	-0.0008	0.0008	0.0128	-0.0128	0.0017	-0.0017
(4,4)@(12,12)	-0.0007	0.0007	0.0013	-0.0013	0.0000	0.0000
(5,5)@(10,10)	-0.0891	0.0891	2.1772	-2.1772	-0.0252	0.0252
(5,5)@(11,11)	-0.0030	0.0030	0.0058	-0.0058	0.0128	-0.0128
(5,5)@(12,12)	-0.0010	0.0010	0.4495	-0.4495	0.0015	-0.0015
(6,6)@(9,9)	-0.9259	0.9259	2.2120	-2.2120	-0.6466	0.6466
(6,6)@(11,11)	−0.1046	0.1046	1.7257	-1.7257	-0.0505	0.0505

ionic than type 2 and type 3 nanotubes, as they have only Si-C bonds as compared to some C-C and Si-Si bonds in other two types. The Mulliken charge analysis also shows that there is electron transfer between the two walls of DWNTs. Table 6.5 shows the Mulliken charges in the inner and outer tubes of the DWNTs. It is evident that in type 1, inner tubes are negatively charged and outer tubes are positively charged, whereas in type 2, inner tubes are positively charged and outer tubes are negatively charged. The charge transfer is significant when the inter layer separation is small. The interlayer interaction is not only due to Van der Waals force but also due to Coulomb force. As the interlayer separation increases Van der Waals interaction dominates over the Coulomb interaction. In type 3 the charge transfer between the tubes is not very significant compared to types 1 and 2. Type 3 DWNTs do not seem to have definite pattern of charge transfer. The charge transfers between two walls of DWNTs can be exploited to achieve different electronic properties by exterior as well as interior decoration of the nanotube walls at different adsorption sites [226, 227].

6.4 Conclusions

In summary, we have studied double-walled armchair silicon carbide nanotube in types 1, 2 and 3 configurations. Evolution of electronic properties with the size of the nanotubes is also studied. The study showed that the stabilities of the double-walled SiC nanotubes are of the same order as those of single-walled SiC nanotube suggesting that it should be possible to synthesize both single-walled and double-walled SiC nanotubes. The B.E./atom or the cohesive energy of the double-walled nanotubes depends not only on the number of atoms but also on the coupling of its constituent single walled nanotubes. The favorable interlayer separation of double-walled SiC nanotube depends on the chirality of the constituent single-walled nanotubes and on the type of the tubes. Type 2 double-walled nanotubes have greater interlayer separation than type 1 and type 3. All double-walled SiC nanotubes are semiconductors.

However, the band gap is observed to decrease from single walled nanotube to double-walled nanotube.

CHAPTER 7

ARE MULTI-WALLED SILICON CARBIDE NANOTUBES METALLIC?

7.1 Introduction

All double-walled SiC nanotubes are found to be semiconducting like their single-walled constituent. However the comparison of band gaps of single walled nanotube and those of double walled nanotubes indicate that the band gap of a double walled nanotube is always smaller than that of its individual single-walled components. This decrement in band gap is shown by all first-principles studies of double-walled nanotubes. Irrespective of a finite cluster approximation [228, 229] or periodic boundary condition [41, 230] calculation, the result is consistent. This immediately poses a question whether SiC nanotube can be metallic with increased number of wall. In this chapter we will try to find answer to this question by studying the evolution of band gap of SiC nanotubes from single walled nanotube to multi-walled nanotube. We have already shown in previous chapter that that band gap of type 2 and type 3 SiC nanotubes are significantly lower than that of type 1 SiC nanotube in both single-walled and double-walled configuration. Therefore quest for looking for any metallic behavior in multi-walled SiC nanotube is incomplete without taking all three types into consideration. Therefore in this study we have considered all three types of armchair SiC nanotubes.

7.2 Discussions of Results

In the present work, we have used the B3LYP hybrid functional [110, 120, 122, 164] and the all electron 3-21G* basis set [136] as implemented in the *GAUSSIAN 03/09* suite of programs [168] for *full* geometry optimizations of individual single-walled nanotube and single

point calculations of multi-walled nanotubes. As before, we have used the finite cluster approximation where the dangling bonds at both ends of the tube were saturated with hydrogen atoms to simulate the effect of infinite nanotubes. Figure 7.1 shows top view of SiC nanotubes in type 1 configuration from single-walled to five-walled.

Stability of a multi-walled nanotube is calculated using two different approaches. The B.E./atom was calculated from

$$E_b=[aE(Si)+bE(C)+cE(H)-E(Si_aC_bH_c)]/(a+b+c) \quad (7.1)$$

where a, b and c are the numbers of Si, C, and H atoms respectively and $E(Si_aC_bH_c)$ is the total energy of the clusters representing the nanotubes. The formation energy for each MWNT is given by:

$$\Delta E = \Sigma E[SWNTs] - E[MWNT] \quad (7.2)$$

where E[SWNTs] and E[MWNT] are the ground state total energies of constituent SWNTs and MWNT with the energy convergence criterion being set to 10^{-6} a.u.

Table 7.1 shows B.E./atom and formation energies for all the single-walled and multi-walled nanotubes under consideration. As we can see from table and Figure 7.2, B.E./atom increases as the number of wall increases and saturates after few walls. This indicates that the multi-walled nanotubes are relatively more stable than the single walled nanotube. This is also confirmed by the formation energy of multi-walled nanotubes Figure 7.3. As in single-walled SiC nanotubes, the binding energies of all type1 multi-walled nanotubes are higher than those of type 2 and type 3. This is because of the presence of Si-Si homonuclear bonds in the type 2 and type 3 and also because of the overall symmetry of the nanotubes.

Table 7.2 and Figure 7.4 show the variation of the band gaps of the SiC nanotubes with respect to the number of walls. All the ground state structures we have studies here are in singlet state i.e. no magnetic structure have been found. It is evident that band gap of all type 1 nanotubes are greater than those of type 2 and type 3 nanotubes. This is because type 1 nanotubes have only Si-C bonds which are partially ionic as compared to type 2 and type 3

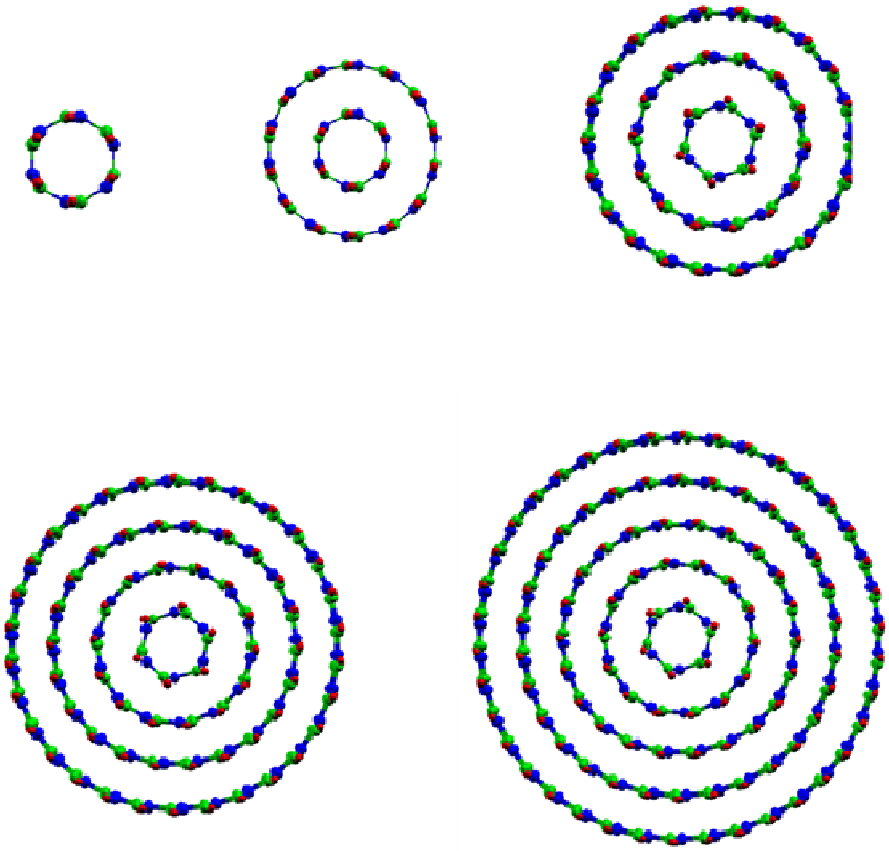

Figure 7.1 Top views of (3,3), (3,3)@(7,7), (3,3)@(7,7)@(11,11), (3,3)@(7,7)@(11,11)@(15,15), and (3,3)@(7,7)@(11,11)@(15,15)@(19,19) SiC nanotubes in type 1 configuration. Green atoms are carbon, blue atoms are silicon and red atoms are hydrogen atoms attached with dangling bond.

Table 7.1 B.E./atom (eV) and formation energies (eV) for single-walled and multi-walled nanotubes (m@n@.. represent (m,m)@(n,n)@... nanotube).

NANOTUBE	**Number of atoms**	**B.E./Atom(eV)**			**Formation energy (eV)**		
		Type 1	Type 2	Type 3	Type 1	Type 2	Type 3
(3,3)	72	4.849	4.686	4.588			
(7,7)	168	5.026	4.745	4.768			
(11,11)	264	5.052	4.769	4.795			
(15,15)	360	5.065	4.777	4.804			
(19,19)	456	5.069	4.781	4.808			
3@7	240	4.993	4.749	4.729	2.399	5.241	3.664
3@7@11	504	5.036	4.781	4.782	7.304	15.855	13.001
3@7@11@15	864	5.059	4.796	4.807	16.256	30.750	26.049
3@7@11@15@19	1320	5.071			28.712		

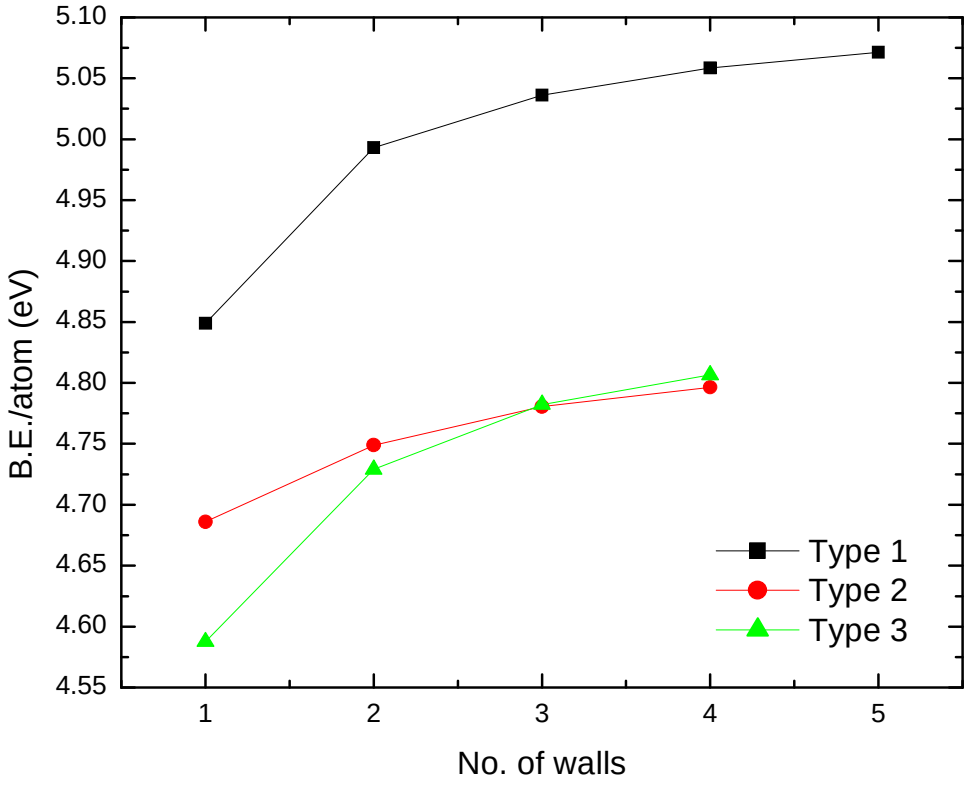

Figure 7.2: B.E./atom (eV) *versus* number of walls of SiC nanotubes.

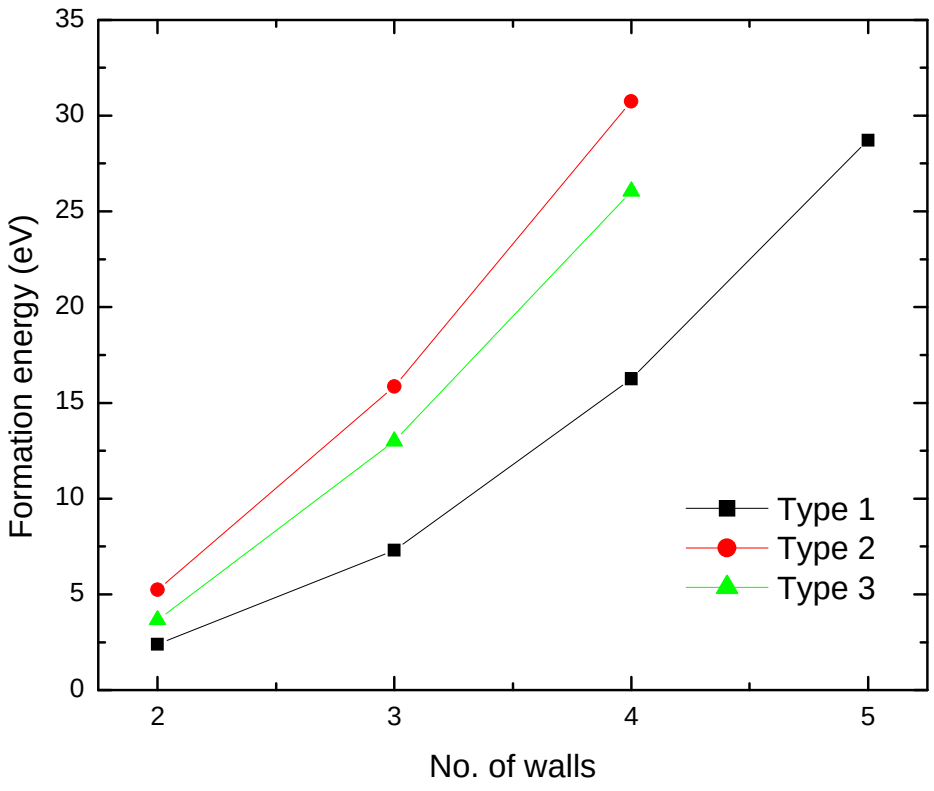

Figure 7.3: Formation energy (eV) *versus* number of walls of SiC nanotubes

Table 7.2 HOMO-LUMO gaps for single-walled and multi-walled nanotubes (m@n@.. represent (m,m)@(n,n)@... nanotube).

NANOTUBE	**Number of atoms**	**HOMO LUMO gap (eV)**		
		Type 1	Type 2	Type 3
(3,3)	72	3.335	1.446	1.281
(7,7)	168	3.493	0.961	1.008
(11,11)	264	3.441	0.982	1.003
(15,15)	360	3.430	0.973	1.005
(19,19)	456	3.430	0.971	1.007
3@7	240	2.571	0.623	0.568
3@7@11	504	2.262	0.308	0.333
3@7@11@15	864	1.994	0.243	0.222
3@7@11@15@19	1320	1.980		

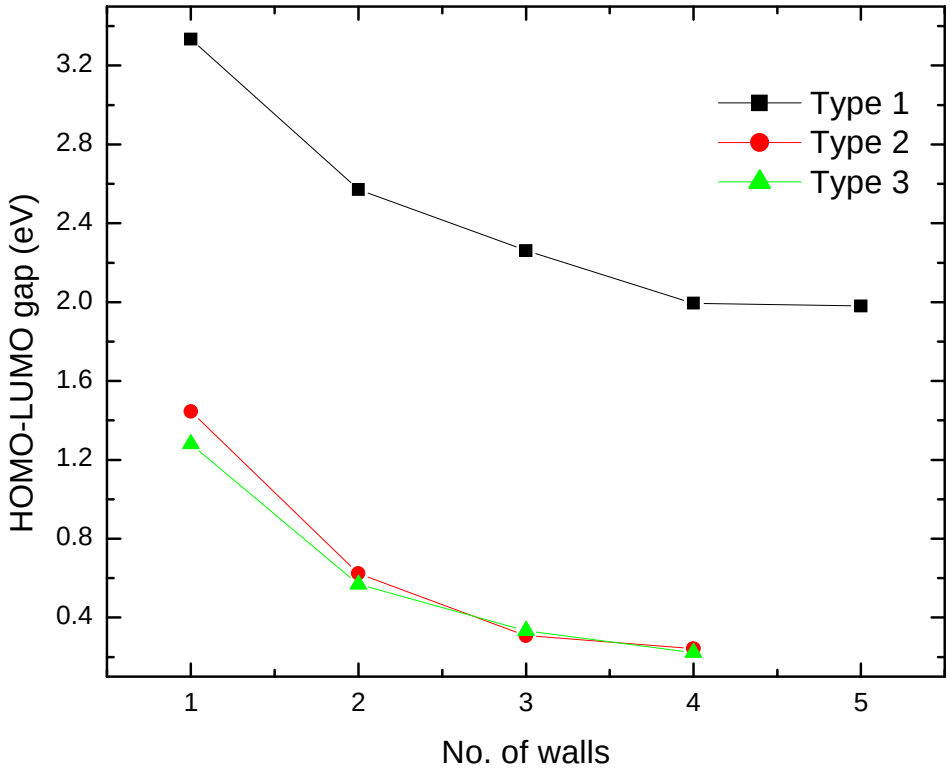

Figure 7.4: HOMO-LUMO gap (eV) of SiC nanotubes with respect to number of walls.

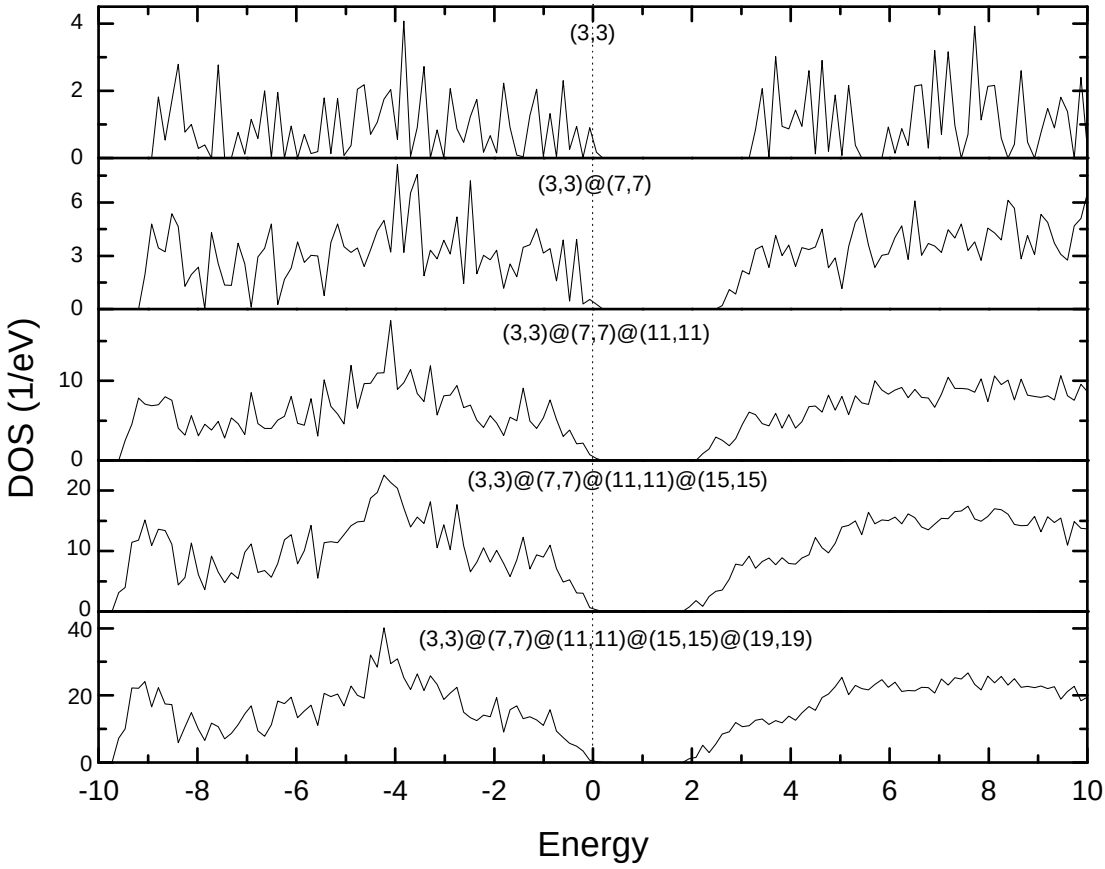

Figure 7.5: Density of states (DOS) of SiC nanotube from single walled to five-walled (Type 1)

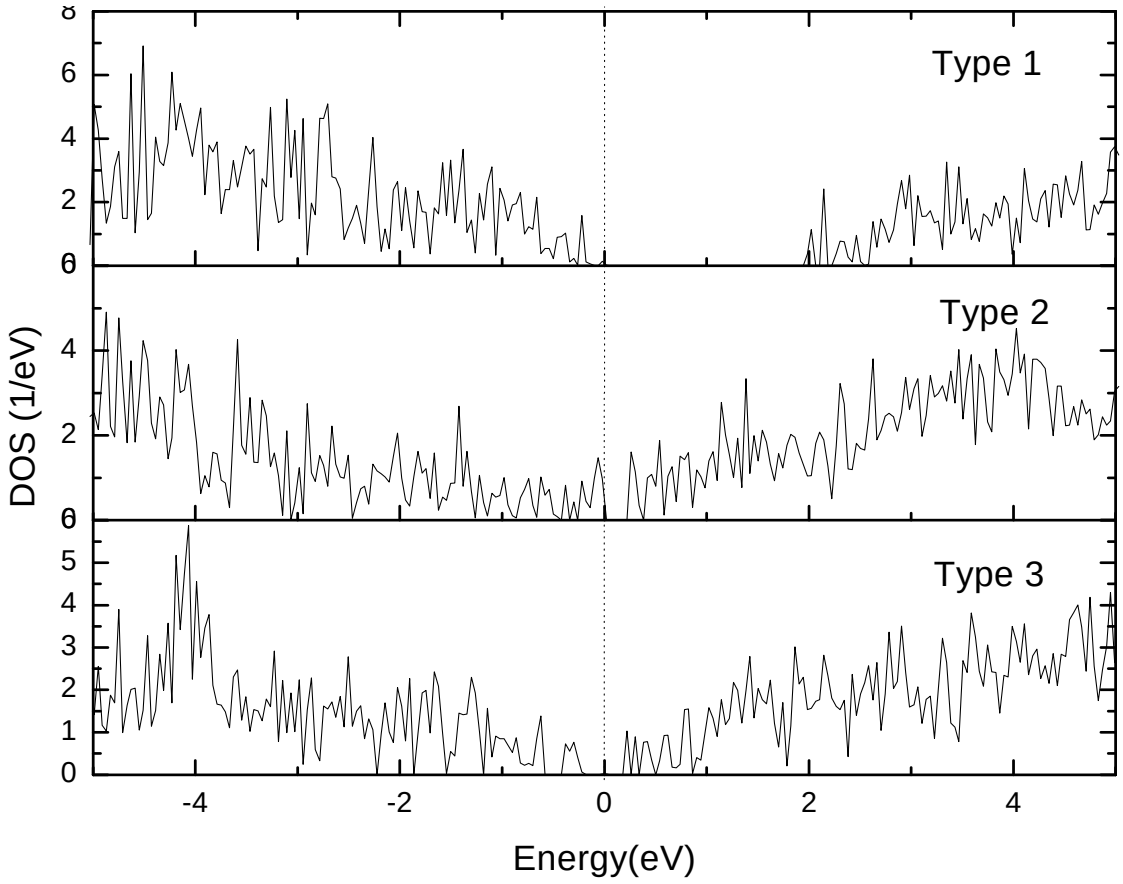

Figure 7.6: Density of states (DOS) of four-walled SiC nanotube 3@7@11@15 in type 1, type 2 and type 3 configurations.

which have some covalent C-C and Si-Si bonds in addition to Si-C bonds. HOMO-LUMO gap is the lowest for the nanotube with smallest diameter in each configuration. As the diameter increases the gap first increases swiftly and then decreases gradually for type 1 single-walled SiC nanotubes. But an opposite trend is observed in types 2 and 3 single-walled SiC nanotubes. This opposing trend can be understood in terms of ionicity of the bonds in the nanotube and the hybridization of orbitals in small-diameter nanotube. From Figure 7.4 it is clear that the band gap of SiC nanotubes decrease with increase in number of walls for all three types of configuration. However the band gap tends to saturate after four walls. For example type 1 SiC nanotubes has band gap ranging from 3.33 eV for (3,3) to 3.49 eV for (7,7) and this gap decreases to 2.57 eV (by almost 25 %) in double-walled nanotube (3,3)@(7,7). But going from four-walled to five-walled the gap decrement is insignificant (only by 0.5%). Type 2 and type 3 nanotubes also show similar trend. Figure 7.5 shows and density of states plots for type 1 SiC nanotubes from single-walled to five-walled geometry. Figure 7.6 shows the density of stated plots of four-walled SiC nanotubes of three types. All these results clearly indicate that the band gap of multi-walled SiC nanotubes is still in semiconducting regime.

7.3 Conclusions

The hybrid density functional calculation of band gap of silicon carbide nanotubes from single walled to five-walled structures have shown that the band gap of SiC nanotubes decrease with increase in number of walls. However the band gap tends saturate after four walls. Although we see a sharp decrement in band gap from single-walled to double-walled nanotubes, the present study clearly shows that the increment of number walls does not yield any metallic behavior in the silicon carbide nanotubes. However a detail study of a number of combinations of silicon carbide nanotubes accompanied by detailed analysis warrants further investigation.

CHAPTER 8

INTERACTION OF TRANSITION METALS WITH SILICON CARBIDE NANOTUBES

8.1 Introduction

As discussed in Chapter 4, nanotubes are fabricated by attaching carbon atoms to the initial cap structure formed on top transition metal catalyst. Transition metals are found to be very good catalysts for fabrication of the nanotubes. Therefore, understanding the nature of interaction of nanotubes with transition metals is very important to understand the process of nanotube synthesis. Also, interaction of transition metals with nanotube can alter the overall electronic and structural properties of a nanotube. The transition metal atom in a nanotube can act as an active center in chemical reaction. Since nanotubes have a large surface area, they can be used as sensors. Such sensors based on nanotubes can perform better if doped with transition metals. Recently, Shalabi *et al.* [231] have studied the interaction of Co with carbon nanotubes and reported the Co-doped nanotubes can be very useful in sensor technology. Nanotubes doped with transition metals can also find application in spintronic devices [232]. Single-walled nanotubes can be filled with transition metal like iron to fabricate quantum nanowires in bulk [233]. Nanowires of transition metals can be encapsulated into nanotubes to protect them from oxidation. Thus, transition metal-nanotube system might have various applications such as spintronics, high-density magnetic storage, and magnetically guided drug-delivery systems [234]. Silicon and germanium nanoclusters like nanotubes and nanocages can be stabilized by transition metals. It has been found that hexagonal metallic silicon nanotubes can be stabilized by doping with 3*d* transition metal atoms [235-237]. Significant amount of research has been done to understand the nature of interaction of transition metal nanowires and carbon

nanotubes [238-245]. As we have discussed in the first chapter, silicon carbide nanotube is a very promising and possible alternative to carbon nanotubes. High oxidation temperature makes it a suitable candidate for shielding a quantum nanowire. Zhang *et al.* [246] have studied the possibility of using silicon carbide nanotubes as the shield for Fe, Co and Ni nanowires. This study has shown that the stabilities of transition metal nanowires are enhanced by silicon carbide nanotube encapsulation. The authors have suggested that the nanowires encapsulated by silicon carbide nanotubes can be used to construct efficient spin transport devices. It has been predicted that the silicon carbide nanotube functionalized by transition metal Ti can be very useful for hydrogen storage [72]. Another study by Zhao and Ding [247] has shown that the chemical and physical properties of silicon carbide nanotubes can be changed and manipulated by doping them with transition metal atoms. However, since the study is focused on nanotubes (8,0) and (6,6) only, the effect of curvature on the nature of interaction is not very clear. In this chapter, we present a detailed and systematic study on the functionalization of silicon carbide nanotubes of different diameters with different transition metal atoms

. 8.2 Discussions of Results

In this work, we have used the PBE0 hybrid functional [134] and the all electron 3-21G* basis set [136] as implemented in the GAUSSIAN 09 suite of programs [168] for full geometry optimizations without any symmetry constraints of the nanotube structures. The optimized bare nanotubes are then doped with transition metals at different adsorption sites and the doped nanotube is again optimized by using basis set 3-21G* for the tube and 6-31G** for the transition metal. Then the single-point calculation is done for the optimized structure using basis set 6-31G** for the whole system. Since it has been reported that performance of the functional B3LYP is poor in metals [133] we chose the functional PBE0 for this study.

Five adsorption sites are chosen for both internal and external adsorption of transition metal atoms. The sites are named TC, TSi, NB, ZB, and H, where TC and TSi refer to the positions directly perpendicular to the tube wall along the C and Si atoms respectively; NB

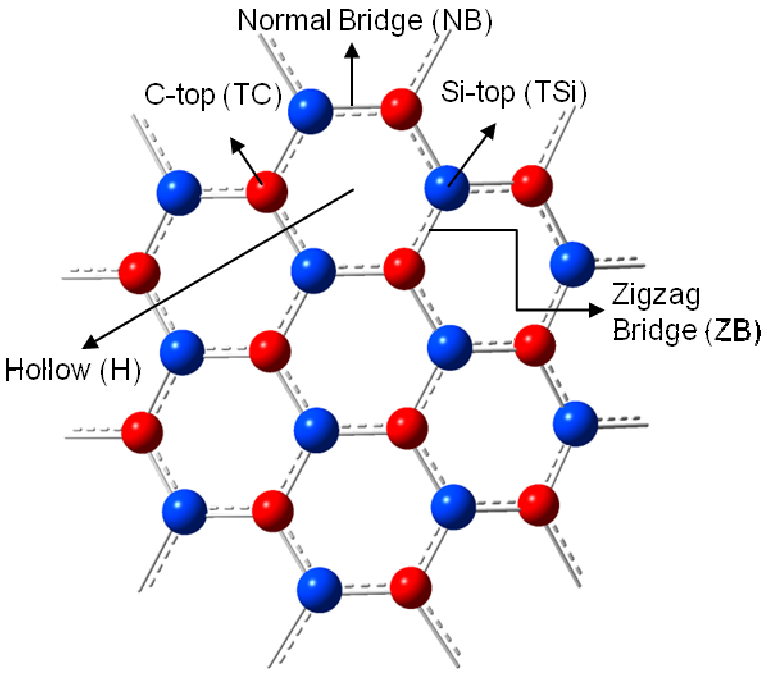

Figure 8.1 Different adsorption sites for transition metal atoms on silicon carbide nanotubes.

refers to the bridge site which is perpendicular to the tube axis; ZB refers to the bridge site at an angle with the axis; and H refers to the hollow site which is on top of the middle of the hexagon. There are in total ten adsorption sites including both inner and outer sites. Figure 8.1 shows the adsorption sites we have taken in this study. The nanotubes chosen for the adsorption are armchair silicon carbide nanotube- (3,3), (5,5), (7,7), and (9,9). Table 8.1 shows the B.E./atom (eV) and HOMO-LUMO gap, calculated by PBE0/6-31G**, of bare silicon carbide nanotubes we have chosen. The adsorption energy of transition metal with the silicon carbide nanotubes are calculated by,

$$E_b = E(TM) + E(SiCNT) - E(TM + SiCNT) \quad (8.1)$$

Where, $E(TM)$ is the ground state energy of transition metal atom, $E(SiCNT)$ is the ground state energy of bare silicon carbide nanotube, and $E(TM + SiCNT)$ is the ground state energy of the doped nanotube, all with the 6-31G** basis set. From this definition, the positive value of E_b is needed for a silicon carbide nanotube to adsorb a transition metal atom. The transition metal atoms put at the initial adsorption site migrate to more stable site after optimization. Tables 8.2-8.11 show the initial adsorption site and the final adsorption site after optimization for all the transition metals. As we can clearly see in the table, the most preferred sites are not the same for all the transition metals. For example, externally adsorbed Sc atom prefers the hollow sites more than any other sites. The binding energy of Sc atom with the (3,3) SiC nanotube is 2.67 eV for the H site whereas it is 1.03 eV and 2.22 eV for the adsorption sites TC and ZB. The most preferred external adsorption sites for Sc are H for all the nanotubes in this case. The most preferred adsorption sites for a transition metal is independent of the curvature of the nanotube, i.e. the most preferred adsorption site for a transition metal atom in the nanotube (3,3) is same as that in (5,5), (7,7) or (9,9). For example Fe atom prefers the NB site in (3,3), (5,5), (7,7), and (9,9) SiC nanotubes. For lighter transition metals Sc, Ti, and V the most preferred external adsorption site is the hollow site (H), for Cr, Mn, Fe, Co, Ni, and Cu the most preferred external adsorption sites are bridge sites (NB and ZB), and for Zn, the most

Table 8.1 B.E./atom and HOMO-LUMO gap of bare SiC nanotubes.

Nanotube	Stoichiometry	Number of atoms	B.E./Atom (eV)	HOMO-LUMO gap (eV)
(3,3)	$Si_{30}C_{30}H_{12}$	72	4.93	3.62
(5,5)	$Si_{50}C_{50}H_{20}$	120	5.04	3.79
(7,7)	$Si_{70}C_{70}H_{28}$	168	5.07	3.80
(9,9)	$Si_{90}C_{90}H_{36}$	216	5.09	3.76

Table 8.2 Initial site, the final site of adsorption after optimization, and the binding energy (B.E.) between SiC nanotubes and Sc atom at respective adsorption sites.

Nanotube	External			Internal		
	Initial site	Final site	B.E.(eV)	Initial site	Final site	B.E.(eV)
(3,3)	TC	TC	1.03	TC	TC	3.79
	TSi	~H	2.67	TSi	TSi	3.87
	NB	~H	2.67	NB	TSi	3.99
	ZB	ZB	2.22	ZB	~H	3.52
	H	~H	2.67	H	~H	3.55
(5,5)	TC	ZB	1.73	TC	TSi	3.01
	TSi	NB	1.75	TSi	~H	2.86
	NB	NB	1.75	NB	~H	3.01
	ZB	ZB	1.73	ZB	~H	2.48
	H	H	1.84	H	TSi	3.02
(7,7)	TC	ZB	1.52	TC	~H	1.81
	TSi	NB	1.52	TSi	TSi	2.67
	NB	NB	1.52	NB	TSi	2.67
	ZB	ZB	1.52	ZB	TSi	2.67
	H	H	1.61	H	TSi	2.67
(9,9)	TC	ZB	1.40	TC	TSi	2.55
	TSi	NB	1.42	TSi	TSi	2.55
	NB	NB	1.42	NB	TSi	2.55
	ZB	ZB	1.40	ZB	TSi	2.56
	H	H	1.49	H	TSi	2.55

Table 8.3 Initial site, the final site of adsorption after optimization, and the binding energy (B.E.) between SiC nanotubes and Ti atom at respective adsorption sites.

Nanotube	External			Internal		
	Initial Site	final site	B.E.(eV)	Initial Site	final site	B.E.(eV)
(3,3)	TC	H	2.62	TC	TSi	3.79
	TSi	NB	2.33	TSi	~Axis	3.73
	NB	NB	2.33	NB	TSi	3.79
	ZB	ZB	2.13	ZB	~Axis	3.21
	H	H	2.60	H	TSi	3.79
(5,5)	TC	NB	1.73	TC	~H	3.03
	TSi	~ZB	1.71	TSi	~H	3.03
	NB	NB	1.64	NB	~H	3.03
	ZB	ZB	1.68	ZB	~ZB	2.43
	H	H	1.93	H	~H	3.03
(7,7)	TC	NB	1.53	TC	~H	1.54
	TSi	ZB	1.51	TSi	~H	2.49
	NB	NB	1.37	NB	~H	1.54
	ZB	ZB	1.50	ZB	~H	2.80
	H	H	1.72	H	~H	2.80
(9,9)	TC	NB	1.44	TC	TC	1.48
	TSi	ZB	1.41	TSi	~H	2.34
	NB	NB	1.52	NB	TC	1.49
	ZB	ZB	1.52	ZB	TC	1.48
	H	H	1.63	H	~H	2.34

Table 8.4 Initial site, the final site of adsorption after optimization, and the binding energy (B.E.) between SiC nanotubes and V atom at respective adsorption sites.

Nanotube	External			Internal		
	Initial site	Final site	B.E.(eV)	Initial site	Final site	B.E.(eV)
(3,3)	TC	H	2.99	TC	~Axis	3.81
	TSi	NB	2.75	TSi	~Axis	3.81
	NB	~H	2.99	NB	~Axis	3.81
	ZB	ZB	2.42	ZB	~Axis	3.31
	H	~H	2.56	H	~Axis	3.81
(5,5)	TC	NB	2.20	TC	H	2.86
	TSi	~H	2.16	TSi	H	3.32
	NB	NB	2.20	NB	H	3.30
	ZB	ZB	2.06	ZB	H	2.87
	H	H	2.39	H	H	3.32
(7,7)	TC	NB	1.99	TC	H	3.05
	TSi	~H	1.98	TSi	H	3.06
	NB	NB	1.99	NB	NB	1.65
	ZB	ZB	1.91	ZB	H	2.85
	H	H	2.17	H	H	3.06
(9,9)	TC	ZB	1.82	TC	~H	1.72
	TSi	ZB	1.83	TSi	~H	1.72
	NB	NB	1.88	NB	~H	1.72
	ZB	ZB	1.82	ZB	~H	2.00
	H	~H	2.07	H	H	2.91

Table 8.5 Initial site, the final site of adsorption after optimization, and the binding energy (B.E.) between SiC nanotubes and Cr atom at respective adsorption sites.

Nanotube	External			Internal		
	Initial Site	final site	B.E.(eV)	Initial Site	final site	B.E.(eV)
(3,3)	TC	NB	2.77	TC	~Axis	2.65
	TSi	NB	2.77	TSi	~Axis	2.67
	NB	NB	2.77	NB	~Axis	2.67
	ZB	ZB	2.43	ZB	~Axis	2.67
	H	NB	2.77	H	~Axis	2.67
(5,5)	TC	NB	2.24	TC	H	1.98
	TSi	NB	2.24	TSi	H	1.97
	NB	NB	2.24	NB	H	1.96
	ZB	ZB	2.11	ZB	H	1.99
	H	NB	2.24	H	H	1.99
(7,7)	TC	NB	2.04	TC	H	1.86
	TSi	NB	2.04	TSi	H	1.86
	NB	NB	2.04	NB	H	1.86
	ZB	ZB	1.98	ZB	H	1.86
	H	NB	2.04	H	H	1.80
(9,9)	TC	NB	1.95	TC	H	1.83
	TSi	ZB	1.90	TSi	H	1.82
	NB	NB	1.95	NB	H	1.83
	ZB	ZB	1.89	ZB	H	1.83
	H	NB	1.95	H	H	1.83

Table 8.6 Initial site, the final site of adsorption after optimization, and the binding energy (B.E.) between SiC nanotubes and Mn atom at respective adsorption sites.

Nanotube	External			Internal		
	Initial Site	final site	B.E.(eV)	Initial Site	final site	B.E.(eV)
(3,3)	TC	NB	1.33	TC	~Axis	1.27
	TSi	NB	1.33	TSi	~Axis	1.27
	NB	NB	1.33	NB	~Axis	1.27
	ZB	ZB	1.02	ZB	~Axis	0.97
	H	NB	1.33	H	~Axis	1.27
(5,5)	TC	NB	0.92	TC	H	0.39
	TSi	TSi	0.48	TSi	TSi	1.10
	NB	NB	0.92	NB	H	0.58
	ZB	ZB	0.77	ZB	ZB	0.43
	H	NB	0.92	H	H	0.37
(7,7)	TC	NB	0.76	TC	H	0.36
	TSi	NB	0.76	TSi	TSi	1.02
	NB	NB	0.76	NB	H	0.28
	ZB	ZB	0.67	ZB	H	0.38
	H	NB	0.76	H	H	0.38
(9,9)	TC	NB	0.69	TC	TC	0.27
	TSi	NB	0.69	TSi	H	0.31
	NB	NB	0.69	NB	NB	0.27
	ZB	ZB	0.60	ZB	H	0.37
	H	NB	0.69	H	H	0.37

Table 8.7 Initial site, the final site of adsorption after optimization, and the binding energy (B.E.) between SiC nanotubes and Fe atom at respective adsorption sites.

Nanotube	External			Internal		
	Initial site	Final site	B.E.(eV)	Initial site	Final site	B.E.(eV)
(3,3)	TC	NB	1.88	TC	NB(~axis)	2.08
	TSi	NB	1.88	TSi	NB(~axis)	2.09
	NB	NB	1.88	NB	NB(~axis)	2.08
	ZB	ZB	1.61	ZB	NB(~axis)	2.06
	H	NB	1.88	H	NB(~axis)	2.08
(5,5)	TC	NB	1.47	TC	TC	1.09
	TSi	TC	1.36	TSi	H	1.11
	NB	NB	1.47	NB	H	1.10
	ZB	TC	1.36	ZB	H	1.08
	H	NB	1.47	H	H	1.10
(7,7)	TC	NB	1.26	TC	TC	0.93
	TSi	NB	1.24	TSi	H	0.92
	NB	NB	1.24	NB	H	0.93
	ZB	ZB	1.18	ZB	H	0.93
	H	H	0.98	H	H	0.94
(9,9)	TC	NB	1.23	TC	TC	0.84
	TSi	TC	1.20	TSi	H	0.90
	NB	NB	1.23	NB	NB	0.85
	ZB	TC	1.18	ZB	NB	0.63
	H	H	0.92	H	H	0.90

Table 8.8 Initial site, the final site of adsorption after optimization, and the binding energy (B.E.) between SiC nanotubes and Co atom at respective adsorption sites.

Nanotube	External			Internal		
	Initial site	Final site	B.E.(eV)	Initial site	Final site	B.E.(eV)
(3,3)	TC	NB	2.20	TC	NB(~axis)	3.00
	TSi	NB	2.14	TSi	NB(~axis)	3.00
	NB	NB	1.88	NB	NB(~axis)	2.99
	ZB	ZB	1.97	ZB	NB(~axis)	2.99
	H	NB	2.24	H	NB(~axis)	3.01
(5,5)	TC	NB	1.90	TC	TC	1.56
	TSi	ZB	1.81	TSi	H	2.18
	NB	NB	1.90	NB	NB	1.57
	ZB	ZB	1.77	ZB	H	1.83
	H	NB	1.72	H	H	1.81
(7,7)	TC	NB	1.78	TC	TC	1.46
	TSi	ZB	1.72	TSi	H	1.67
	NB	NB	1.78	NB	NB	1.46
	ZB	ZB	1.69	ZB	H	1.67
	H	~H	1.61	H	H	1.67
(9,9)	TC	NB	1.55	TC	TC	1.44
	TSi	NB	1.54	TSi	H	1.64
	NB	NB	1.62	NB	NB	1.45
	ZB	ZB	1.13	ZB	H	1.64
	H	~H	1.57	H	H	1.64

Table 8.9 Initial site, the final site of adsorption after optimization, and the binding energy (B.E.) between SiC nanotubes and Ni atom at respective adsorption sites.

Nanotube	External			Internal		
	Initial site	Final site	B.E.(eV)	Initial site	Final site	B.E.(eV)
(3,3)	TC	NB	2.70	TC	axis	3.82
	TSi	NB	2.70	TSi	axis	3.82
	NB	NB	2.70	NB	axis	3.84
	ZB	ZB	2.70	ZB	ZB	3.57
	H	H	2.42	H	axis	3.84
(5,5)	TC	ZB	2.43	TC	H	2.56
	TSi	H	2.33	TSi	H	2.57
	NB	NB	2.27	NB	H	2.56
	ZB	ZB	2.43	ZB	H	2.56
	H	H	2.34	H	H	2.53
(7,7)	TC	ZB	2.32	TC	H	2.48
	TSi	NB	2.10	TSi	H	2.48
	NB	NB	2.11	NB	H	2.48
	ZB	ZB	2.32	ZB	H	2.47
	H	H	2.37	H	H	2.47
(9,9)	TC	ZB	2.24	TC	TC	2.07
	TSi	H	2.39	TSi	TC	2.07
	NB	NB	2.03	NB	TC	2.07
	ZB	ZB	2.24	ZB	TC	2.07
	H	H	2.39	H	H	2.46

Table 8.10 Initial site, the final site of adsorption after optimization, and the binding energy (B.E.) between SiC nanotubes and Cu atom at respective adsorption sites.

Nanotube	External			Internal		
	Initial site	Final site	B.E.(eV)	Initial site	Final site	B.E.(eV)
(3,3)	TC	NB	3.15	TC	axis	3.21
	TSi	ZB	2.88	TSi	axis	3.21
	NB	NB	3.15	NB	axis	3.21
	ZB	ZB	2.88	ZB	H	3.77
	H	~H	2.98	H	H	3.75
(5,5)	TC	NB	2.79	TC	ZB	2.84
	TSi	NB	2.79	TSi	H	2.61
	NB	NB	2.79	NB	~H	2.56
	ZB	ZB	2.68	ZB	ZB	2.84
	H	~H	2.62	H	H	2.84
(7,7)	TC	ZB	2.60	TC	NB	2.35
	TSi	ZB	2.61	TSi	~H	2.49
	NB	NB	2.67	NB	NB	2.35
	ZB	ZB	2.60	ZB	NB	2.35
	H	~H	2.52	H	H	2.68
(9,9)	TC	NB	2.61	TC	NB	2.30
	TSi	NB	2.61	TSi	~H	2.46
	NB	NB	2.61	NB	NB	2.30
	ZB	ZB	2.55	ZB	NB	2.30
	H	~H	2.45	H	H	2.48

Table 8.11 Initial site, the final site of adsorption after optimization, and the binding energy (B.E.) between SiC nanotubes and Zn atom at respective adsorption sites.

Nanotube	External			Internal		
	Initial site	Final site	B.E.(eV)	Initial Site	Final site	B.E.(eV)
(3,3)	TC	TSi	0.80	TC	~Axis	-0.02
	TSi	TSi	0.80	TSi	~Axis	-0.02
	NB	TSi	0.80	NB	~Axis	-0.02
	ZB	TSi	0.80	ZB	NB	0.42
	H	H	0.64	H	~Axis	-0.02
(5,5)	TC	TSi	0.73	TC	H	0.86
	TSi	TSi	0.73	TSi	H	0.87
	NB	TSi	0.73	NB	H	0.86
	ZB	TSi	0.73	ZB	H	0.86
	H	H	0.62	H	H	0.86
(7,7)	TC	TSi	0.66	TC	H	0.66
	TSi	TSi	0.66	TSi	H	0.66
	NB	TSi	0.66	NB	H	0.66
	ZB	TSi	0.66	ZB	H	0.66
	H	H	0.59	H	H	0.66
(9,9)	TC	TSi	0.64	TC	H	0.59
	TSi	TSi	0.64	TSi	H	0.58
	NB	TSi	0.64	NB	H	0.59
	ZB	TSi	0.64	ZB	H	0.57
	H	H	0.57	H	H	0.59

Table 8.12 Most stable external adsorption site and the binding energy at those sites of adsorption for all the transition metal atoms with the silicon carbide nanotubes.

Transition Metal	(3,3)		(5,5)	
	Most stable site	Binding energy	Most stable site	Binding energy
Sc	H	2.67	H	1.84
Ti	H	2.62	H	1.93
V	H	2.99	H	2.39
Cr	NB	2.77	NB	2.24
Mn	NB	1.33	NB	0.92
Fe	NB	1.88	NB	1.47
Co	NB	2.24	NB	1.90
Ni	ZB	2.70	ZB	2.43
Cu	NB	3.15	NB	2.79
Zn	TSi	0.80	TSi	0.73
Transition Metal	(7,7)		(9,9)	
	Most stable site	Binding energy	Most stable site	Binding energy
Sc	H	1.61	H	1.49
Ti	H	1.72	H	1.63
V	H	2.17	H	2.07
Cr	NB	2.04	NB	1.95
Mn	NB	0.76	NB	0.69
Fe	NB	1.26	NB	1.23
Co	NB	1.78	NB	1.62
Ni	ZB	2.37	ZB	2.39
Cu	NB	2.67	NB	2.61
Zn	TSi	0.66	TSi	0.64

preferred external adsorption site is on-top-of-silicon (TSi). Table 8.12 shows the most stable sites and the corresponding binding energies of the transition metals externally adsorbed to silicon carbide nanotubes. As we can see in Table 8.12 and Figure 8.2, different transition metal atoms adsorb with silicon carbide nanotubes with different adsorption energies. Transition metals with smaller number of d-electrons have, in general, relatively higher adsorption energies, except in the case of Cu which has 10 d-electron and has the highest adsorption energy. The adsorption energy is the lowest for Zn.

It is evident from the data that there is a strong curvature effect in the adsorption energy of the transition metal on the silicon carbide nanotubes. The binding energy of transition metal with smaller nanotubes is greater than that with bigger nanotubes. For example the Sc is adsorbed on silicon carbide nanotube (3,3) with binding energy 2.67 eV. This adsorption energy decreases to 1.49 eV for the nanotube (9,9). This indicates that the smaller nanotubes are more reactive to transition metals than bigger nanotube. As we already discussed in Chapters 3 and 7, buckling of silicon carbide nanotube decreases with increase in diameter. Also the B.E./atom increases with diameter for bare nanotubes. Because of higher buckling and smaller B.E./atom in smaller bare nanotubes, the adsorption energy is higher in nanotubes with smaller diameter. The effect of curvature on the adsorption energy is clearer when we compare the external adsorption energy with the internal adsorption energy. If we compare the adsorption energy of externally adsorbed transition metals with that of internally adsorbed, in all cases the internal adsorption energy is greater. Curvature of nanotubes causes this difference. Transition metal atoms adsorbed internally interact with more atoms on the nanotube wall than those adsorbed externally. In other words, transition metal atom inside a nanotube “sees” more atoms of the wall of nanotube whereas the transition metal atom outside the nanotube “sees” less number of atoms. This causes greater adsorption energy for internal adsorption. Table 8.13 shows the most stable sites and the respective binding energy of the transition metal internally adsorbed to

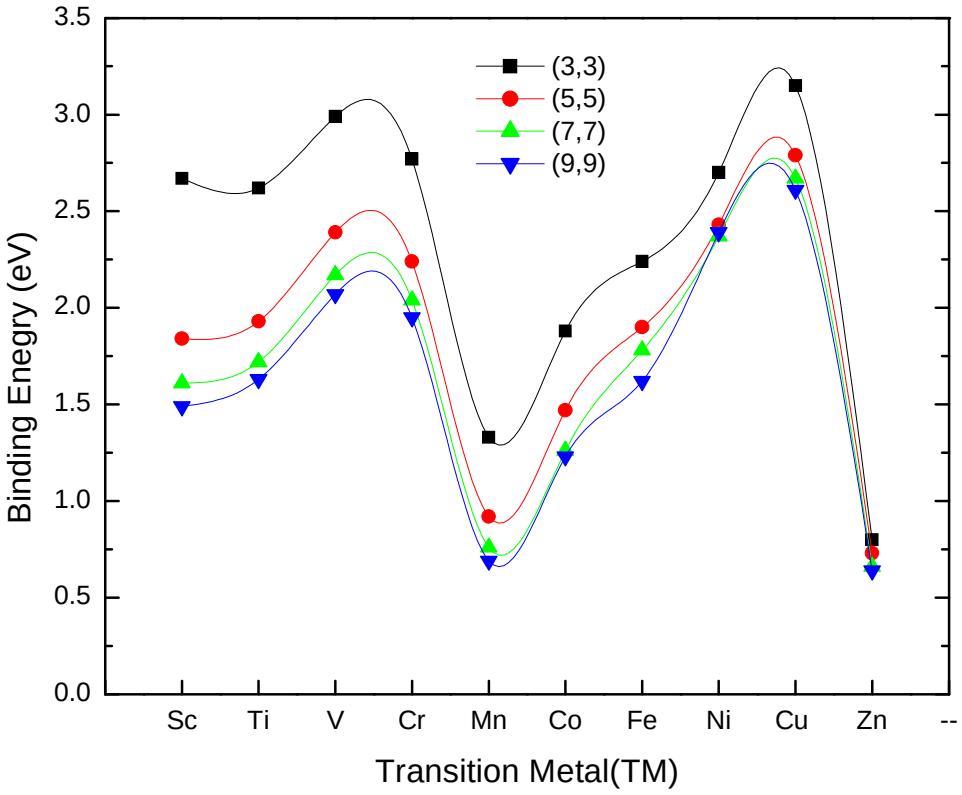

Figure 8.2 Binding energy of transition metals adsorbed externally with silicon carbide nanotubes.

Table 8.13 Most stable internal adsorption site and the binding energy at those sites of adsorption for all the transition metal atoms with the silicon carbide nanotubes.

Transition Metal	(3,3)		(5,5)	
	Most stable site	Binding energy	Most stable site	Binding energy
Sc	TSi	3.99	TSi	3.02
Ti	TSi	3.79	H	3.03
V	Axis	3.81	H	3.32
Cr	Axis	2.67	H	1.99
Mn	Axis	1.27	TSi	1.10
Fe	NB	2.09	H	1.11
Co	NB	3.01	H	2.18
Ni	Axis	3.84	H	2.57
Cu	H	3.77	H	2.84
Zn	NB	0.42	H	0.87
Transition Metal	(7,7)		(9,9)	
	Most stable site	Binding energy	Most stable site	Binding energy
Sc	TSi	2.67	TSi	2.56
Ti	H	2.80	H	2.34
V	H	3.06	H	2.91
Cr	H	1.86	H	1.83
Mn	TSi	1.02	H	0.37
Fe	H	0.94	H	0.90
Co	H	1.67	H	1.64
Ni	H	2.48	H	2.46
Cu	H	2.68	H	2.48
Zn	H	0.66	H	0.59

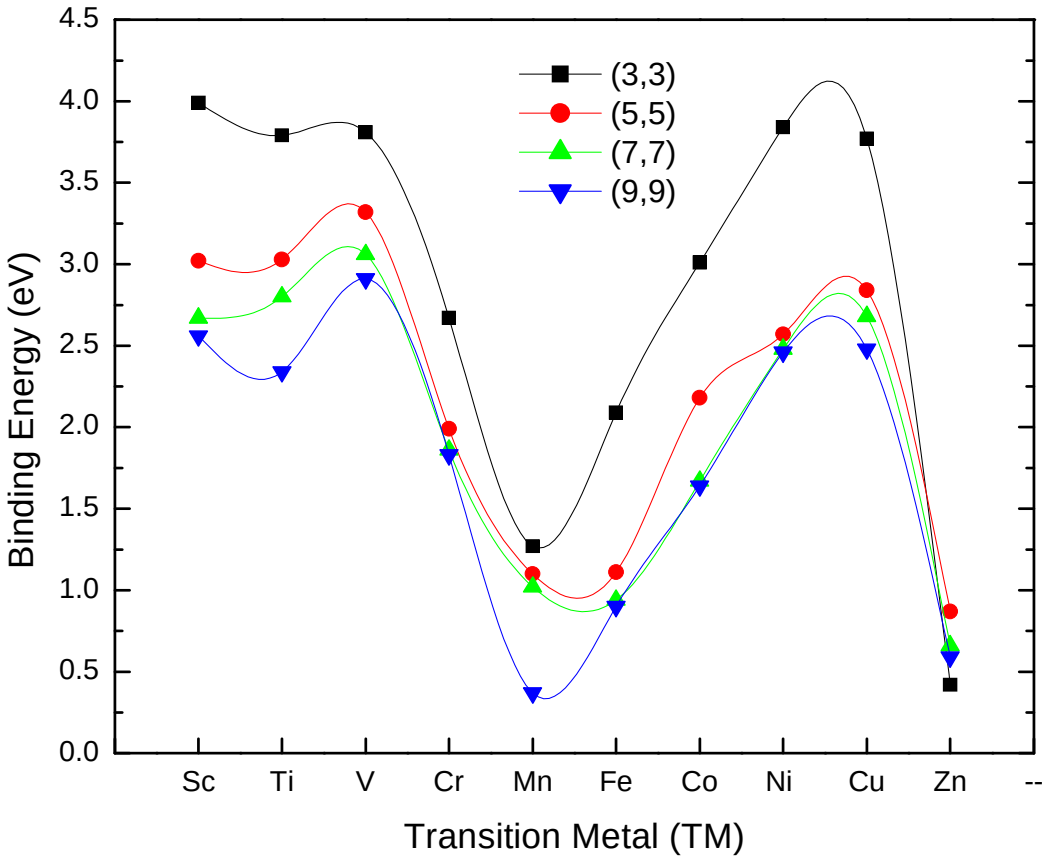

Figure 8.3 Binding energy of transition metals adsorbed internally with silicon carbide nanotubes.

silicon carbide nanotube. The most preferred adsorption sites in most of the cases of internal adsorption are the hollow sites.

In nanoelectronics, nanostructures with a wide variety of chemical and physical properties are required. The modification or tuning of band gap of such nanostructures is very important for their optimal applications. It is well known that the electronic structures of nanotubes can be altered by doping them with transition metal. It is very important to determine a suitable dopant for a nanotube to tailor its band gap as required. Tables 8.14, and 8.15 and Figures 8.4 and 8.5 show the change in the HOMO-LUMO gap of the nanotubes doped with transition metals as compared to the gap of bare nanotubes. As we have discussed in much detail in previous chapters, the HOMO-LUMO gaps of bare silicon carbide nanotubes increase with diameter. We have explained this phenomenon in detail in Chapter 3. The silicon carbide nanotubes doped with transition metals have significantly lower band gap in general than the bare nanotubes. The maximum decrement in HOMO-LUMO gap is observed for the internal adsorption of Cr on the silicon carbide nanotube (7,7). The bare nanotube (7,7) has a gap of 3.80 eV, this gap decreases to 1.91 eV when doped by Cr internally. The transition metals Ti and Zn have the least effect on the HOMO-LUMO gap. The least decrement observed is for the Zn doped (9,9) where we see the change of 0.21 eV. The ground state spin multiplicities of all functionalized nanotubes are greater than 1 except for those functionalized by Ni and Zn. This is the reason why Ni and Zn have the least effect in the HOMO-LUMO gap of the nanotubes. The change in gap is greater in case of internal adsorption than in case of external adsorption for the bigger nanotubes (7,7) and (9,9) whereas in case of (3,3) and (5,5) the change is gap is greater for internal adsorption than for external adsorption only for lighter transition metals Sc, Ti, V, Cr, and Mn. Figures 8.6 and 8.7 shows the localization of HOMO around most preferred external and internal adsorption sites of transition metal doped silicon carbide nanotube (5,5).

Mulliken charge analysis shows that the amount and direction of charge transfer depends on the curvature and the species of transition metal atoms. Tables 8.16 and 8.17 show

Table 8.14 The HOMO-LUMO gap of the nanotubes functionalized by transition metal atoms from outside and the change in gap of the nanotubes due to functionalization.

Transition Metal	(3,3)		(5,5)	
	HOMO-LUMO gap (E_g)	Change in HOMO-LUMO gap	HOMO-LUMO gap (E_g)	Change in HOMO-LUMO gap
Sc	2.44	1.18	2.26	1.53
Ti	2.72	0.90	2.70	1.09
V	2.87	0.76	2.74	1.04
Cr	2.95	0.67	2.97	0.81
Mn	2.43	1.19	2.65	1.14
Fe	2.52	1.11	2.59	1.19
Co	2.52	1.10	2.50	1.29
Ni	3.04	0.58	3.25	0.53
Cu	2.66	0.96	2.54	1.25
Zn	3.09	0.53	3.36	0.42
Transition Metal	(7,7)		(9,9)	
	HOMO-LUMO gap (E_g)	Change in HOMO-LUMO gap	HOMO-LUMO gap (E_g)	Change in HOMO-LUMO gap
Sc	2.13	1.67	2.09	1.66
Ti	2.40	1.40	2.41	1.35
V	2.68	1.12	2.60	1.16
Cr	2.93	0.87	2.84	0.92
Mn	2.73	1.07	2.76	1.00
Fe	2.52	1.28	2.64	1.12
Co	2.51	1.29	2.49	1.27
Ni	3.69	0.11	3.65	0.11
Cu	2.51	1.29	2.47	1.28
Zn	3.49	0.31	3.55	0.21

Table 8.15 The HOMO-LUMO gap of the nanotubes functionalized by transition metal atoms from inside and the change in gap of the nanotubes due to functionalization.

Transition Metal	(3,3)		(5,5)	
	HOMO-LUMO gap (E_g)	Change in HOMO-LUMO gap	HOMO-LUMO gap (E_g)	Change in HOMO-LUMO gap
Sc	1.91	1.71	2.26	1.52
Ti	2.39	1.24	2.69	1.09
V	2.22	1.40	2.28	1.50
Cr	2.60	1.03	1.95	1.83
Mn	2.36	1.27	2.23	1.55
Fe	2.85	0.78	2.28	1.50
Co	2.90	0.72	2.89	0.90
Ni	3.50	0.12	3.30	0.49
Cu	2.83	0.79	2.62	1.17
Zn	3.34	0.28	3.58	0.21
Transition Metal	(7,7)		(9,9)	
	HOMO-LUMO gap (E_g)	Change in HOMO-LUMO gap	HOMO-LUMO gap (E_g)	Change in HOMO-LUMO gap
Sc	1.95	1.85	1.98	1.78
Ti	2.82	0.98	2.30	1.46
V	2.39	1.41	2.37	1.38
Cr	1.91	1.89	1.86	1.90
Mn	2.37	1.43	2.42	1.34
Fe	2.32	1.48	2.27	1.49
Co	2.04	1.76	2.00	1.76
Ni	3.50	0.30	3.48	0.28
Cu	2.64	1.16	2.20	1.56
Zn	3.54	0.26	3.54	0.22

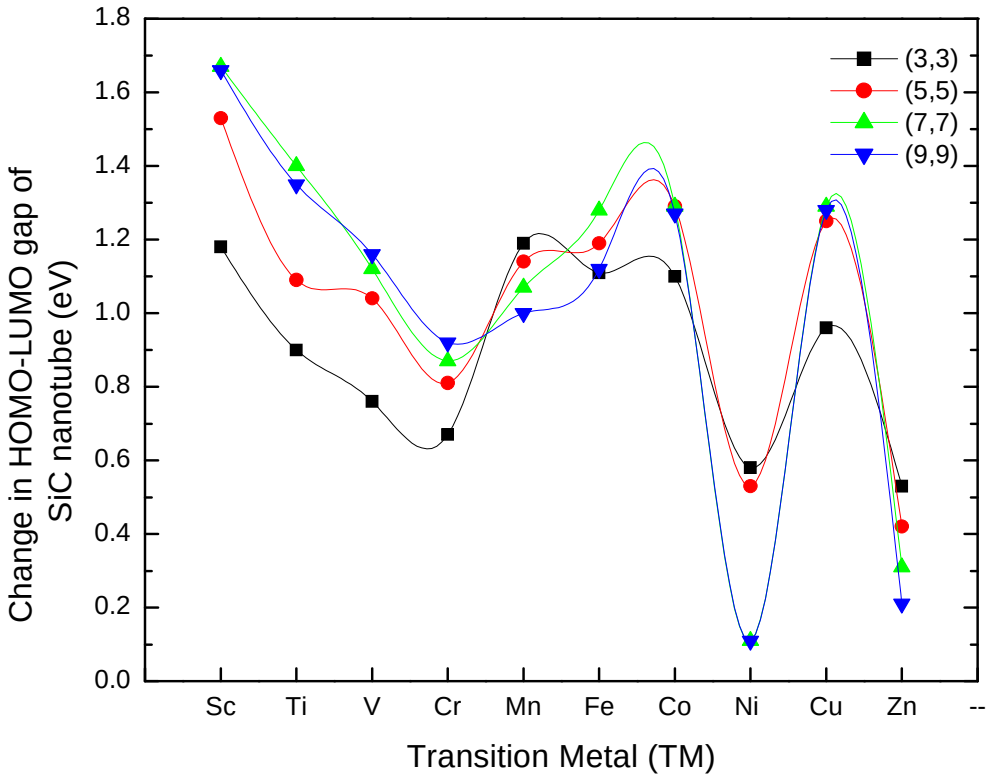

Figure 8.4 Change in HOMO-LUMO gaps (in eV) of the silicon carbide nanotubes due to functionalization by transition metals from outside.

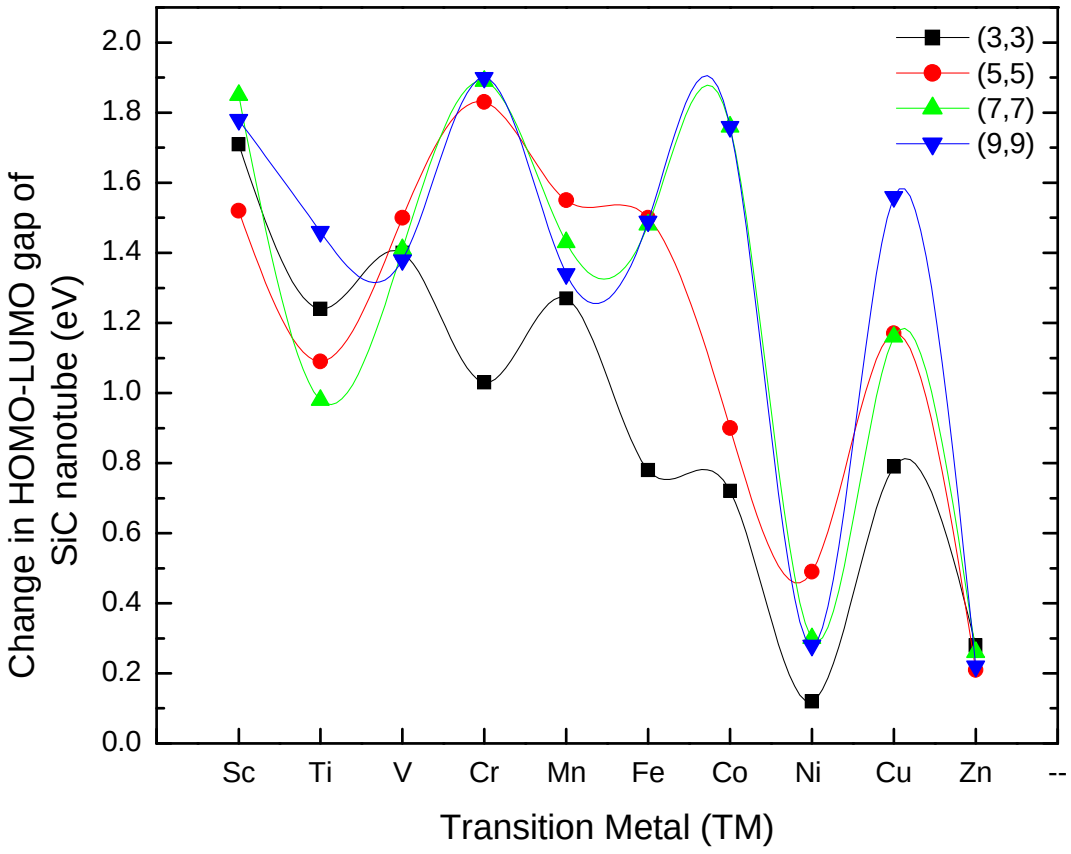

Figure 8.5 Change in HOMO-LUMO gaps (in eV) of the silicon carbide nanotubes due to functionalization by transition metals from inside.

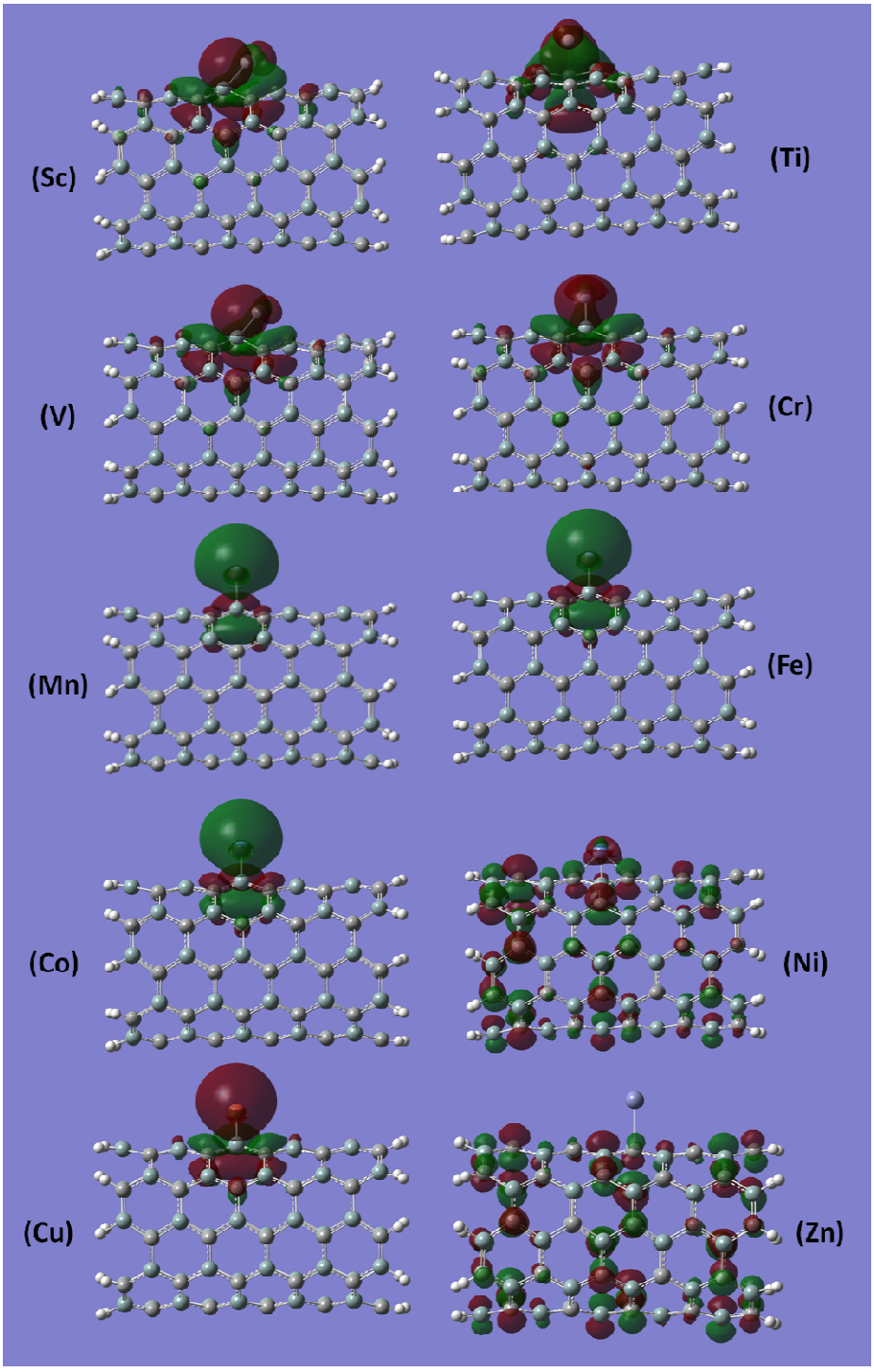

Figure 8.6 Localization of HOMO on the nanotubes functionalized by transition metals from outside.

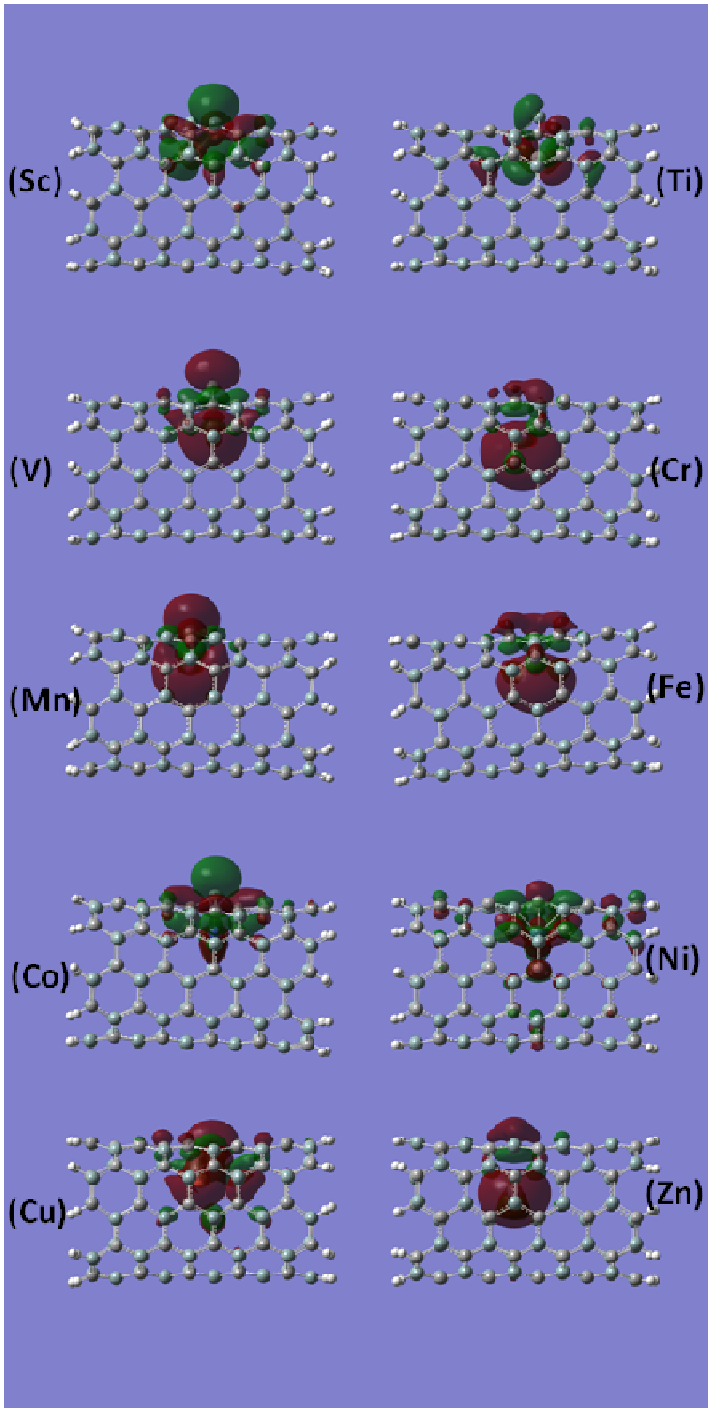

Figure 8.7 Localization of HOMO on the nanotubes functionalized by transition metals from inside.

Table 8.16 Mulliken charges and the spin magnetic moments (in Bohr magneton) of the transition metal atoms adsorbed on the external most stable sites of the nanotubes.

Transition Metal	(3,3)		(5,5)	
	Charge of TM atom (e)	Spin magnetic moment of TM atom(μ_B)	Charge of TM atom (e)	Spin magnetic moment of TM atom(μ_B)
Sc	0.72	0.39	0.56	0.73
Ti	0.67	1.92	0.58	2.12
V	0.66	3.26	0.56	3.34
Cr	0.61	4.50	0.52	4.51
Mn	0.54	5.49	0.47	5.51
Fe	0.54	4.18	0.42	4.25
Co	0.38	2.90	0.24	3.00
Ni	0.41	0.00	0.33	0.00
Cu	0.32	0.58	0.19	0.68
Zn	0.29	0.00	0.24	0.00
Transition Metal	(7,7)		(9,9)	
	Charge of TM atom (e)	Spin magnetic moment of TM atom(μ_B)	Charge of TM atom (e)	Spin magnetic moment of TM atom(μ_B)
Sc	0.49	0.81	0.45	0.88
Ti	0.58	2.09	0.57	2.09
V	0.52	3.35	0.51	3.35
Cr	0.47	4.51	0.45	4.51
Mn	0.44	5.50	0.42	5.50
Fe	0.29	4.17	0.37	4.26
Co	0.19	3.02	0.26	3.04
Ni	0.03	0.00	0.02	0.00
Cu	0.14	0.72	0.12	0.73
Zn	0.21	0.00	0.20	0.00

Table 8.17 Mulliken charges and the spin magnetic moments (in Bohr magneton) of the transition metal atoms adsorbed on the internal most stable sites of the nanotubes.

Transition Metal	(3,3)		(5,5)	
	Charge of TM atom (e)	Spin magnetic moment of TM atom(μ_B)	Charge of TM atom (e)	Spin magnetic moment of TM atom(μ_B)
Sc	-0.02	0.11	0.43	0.20
Ti	-0.17	1.75	0.26	1.95
V	-0.22	2.83	0.18	3.14
Cr	-0.13	4.61	-0.16	5.65
Mn	0.05	4.65	0.38	5.22
Fe	-0.12	3.17	0.01	4.22
Co	-0.32	2.02	0.14	2.16
Ni	-0.60	0.00	-0.04	0.00
Cu	-0.41	0.04	0.06	0.21
Zn	-0.05	0.00	-0.09	0.00
Transition Metal	(7,7)		(9,9)	
	Charge of TM atom (e)	Spin magnetic moment of TM atom(μ_B)	Charge of TM atom (e)	Spin magnetic moment of TM atom(μ_B)
Sc	0.43	0.66	0.45	0.66
Ti	0.33	1.96	0.27	2.01
V	0.27	3.14	0.31	3.14
Cr	-0.12	5.63	-0.10	5.62
Mn	0.45	5.19	0.33	5.46
Fe	0.07	4.22	0.09	4.21
Co	-0.18	3.04	-0.15	3.02
Ni	0.00	0.00	0.01	0.00
Cu	0.09	0.24	-0.11	0.69
Zn	-0.07	0.00	-0.04	0.00

the charge of the transition metal adsorbed externally and internally to the silicon carbide nanotubes. No specific trends were observed between the adsorption energies and the charge transfer. This suggests that the local structure of the adsorption site on a particular nanotube determines the amount and direction of the charge transfer. The direction of charge transfer is very much dependent on the curvature of the nanotube. If we compare the charge transfer in case of internal adsorption on (3,3) with that of external adsorption on the same nanotube we can clearly see this difference. In all cases of external adsorption, electron transfer occur from transition metal atom to the nanotubes, whereas the direction of electron transfer is reversed in all transition metals internally adsorbed in the nanotube (3,3) and also some transition metals in other nanotubes.

All silicon carbide nanotubes functionalized by transition metals have magnetic ground state except for those functionalized by Ni and Zn. Since the bare silicon carbide nanotubes have nonmagnetic ground states, the net spin in the functionalized nanotubes originates from the magnetic moment of the transition metal adsorbed in the nanotube. Tables 8.16 and 8.17 show the spin magnetic moment of the transition metal atoms adsorbed outside and inside of the nanotubes. The spin magnetic moment is the highest which is 5.65 μ_B for the transition metal Cr adsorbed inside the silicon carbide nanotubes. Net magnetic moment of the Ni and Zn atoms are zero. We can notice the curvature effect on the magnetic properties of the transition metal adsorbed on the nanotube. The magnetic moment of the transition metal increases with the diameter of the tube. For the smaller nanotubes, the magnetic moment of the transition metals are smaller indicating that the transfer of magnetism is more in smaller nanotube than in the bigger ones. All the values for magnetic moment of the transition metals adsorbed on the silicon carbide nanotubes are bigger than the respective values reported earlier for the transition metals on the carbon nanotubes [249]. This indicates that the transition metals retain their magnetic moment when adsorbed to silicon carbide nanotube more than they do when adsorbed to carbon nanotubes. The result is consistent with the previous results on Fe

functionalized silicon carbide nanotubes [250]. High magnetic moments of the functionalized nanotubes should have an important application in magnetic storage and spintronics.

8.3 Conclusions

In summary, we have done a systematic study of functionalization of silicon carbide nanotubes by transition metal atoms. Both internal and external adsorption sites have been considered. Comparison between internal and external adsorption sites shows that the interaction of transition metal with the nanotubes is more pronounced when adsorbed internally. The nature of interaction between transition metal atoms and silicon carbide nanotubes depends greatly on the curvature of the nanotubes. Greater the curvature more pronounced is the change in the electronic properties of the nanotubes. Nonmagnetic nanotubes become magnetic after functionalization and the quenching of magnetism is significantly higher in the nanotubes with higher curvature.

CHAPTER 9

CONCLUSIONS AND FUTURE DIRECTIONS

Nanotubes consisting of binary elements, such as silicon carbide (SiC), are important due to their fascinating chemical and physical properties and huge potential applications in the electronics and opto-electronics industries. Silicon carbide is one of the most promising candidates for nanotubes due to its high oxidation temperature and other fascinating properties. Our study focuses on the electronic and structural properties of silicon carbide nanotubes from single-walled to multi-walled.

Silicon carbide nanotubes are one of those nanotubes which show anomalous dependence of band gap on the diameter. All the binary nanotubes like group-III-nitride, GeC, SiC, etc. which have partially ionic bonds show this kind of anomaly. From density functional calculations we have shown that this anomalous dependence can be explained in terms of the effect of curvature on the ionicity of the Si-C bond [251]. The curvature of the nanotube reduces the ionicity of the bond due to extra sp^3 hybridization. Therefore the nanotubes with very high curvature have low band gaps. These findings can lead us to the designing of the nanotubes having some partially ionic bonds and some perfectly covalent bonds in such a way that the quantum confinement effect and the curvature effects are just balanced. The band gap of such nanotubes would be independent of the diameter. This can reduce the post production cost required for sorting out nanotubes with certain chirality and diameter in the nanotube fabrication process.

Our study on capped silicon carbide nanotubes [252] has shown that capping of a SiC nanotube changes cohesive energy, HOMO-LUMO gap and other geometrical and electronic properties of SiC nanotube. Also, the carbon-capped SiC nanotubes are energetically more

preferred than silicon-capped. Capping a silicon carbide nanotube significantly increases the binding energy of the nanotube. This might provide possible synthesis pathways to single-walled silicon carbide nanotubes. However, study of only two categories of nanotube (nanotubes that can be capped by fullerene hemispheres of C_{60} and C_{20}) has to be further expanded looking into possibility of capping various nanotubes of different chirality. Also, study of interaction of a capped silicon carbide nanotubes with another capped silicon carbide nanotube might lead us to the possibilities of liquid-crystal phases of the capped nanotubes. To further explore the possible applications of capped silicon carbide nanotubes, study of a wide range of chemicals encapsulated inside capped silicon carbide nanotubes should be pursued.

Nanocones are other possible structures observed at the tip of nanotubes during its fabrication. In our study [253] we have presented a detailed *ab initio* study of the evolution of electronic properties with the size of SiC nanocones of all possible disclination angles. Results have shown that the B.E./atom or the cohesive energy of the nanocones depends not only on the size of the nanocones but also on the disclination angle of the nanocones. The study also shows that the electronic properties of nanocones depend on disclination angles, size of the nanocone clusters and the structure of edge of the nanocones. Our study, however, was only for the free standing silicon carbide nanocones. Further investigation of silicon carbide nanocones as tip of the nanotubes rather than free standing structures can elucidate not only its practical application in field emission, atomic force microscopy and much more but also the possible synthesis pathways for silicon carbide nanotube itself. Also, study of interaction of various gases like NO_2, H_2S, HCN etc with silicon carbide nanocone tip might help to develop a detection and removal techniques for these toxic gases up to the precision of single molecule. Such gases can also be detected by studying the variation in electronic properties of nanotubes when the molecule is absorbed in the tube surface.

Our studies on double-walled silicon carbide nanotubes [228, 229] have confirmed the experimental observations that the interlayer separation of multi-walled silicon carbide

nanotubes is greater than that of multi-walled carbon nanotubes. From our study, all double-walled SiC nanotubes are found to be semiconducting like their single-walled constituents. However comparison of band gaps of single walled nanotube and those of double walled nanotubes indicates that the band gap of a double walled nanotube is always smaller than that of its individual single-walled components. This immediately poses a question whether SiC nanotube can be metallic with increased number of walls. Our study at this stage indicates that the multi-walled nanotubes cannot be metallic. We have performed single point hybrid density functional calculation of band gap of silicon carbide nanotubes from single walled to five-walled structures. The results have shown that the band gap of SiC nanotubes decrease with increase in number of walls. However the band gap tends saturate after four walls. Although we see a sharp decrement in band gap from single-walled to double-walled nanotubes our present study clearly shows that the increment of number walls does not yield any metallic behavior in the silicon carbide nanotubes.

The functionalization of silicon carbide nanotubes by transition metal atoms is an interesting area of research. Understanding nature of interaction between transition metal and the nanotubes might help us understand the process of fabrication of nanotube and also to design novel hybrid nanostructures applicable in nanoelectronics. Our study shows that the interaction of transition metal with nanotubes is more pronounced when adsorbed internally. The curvature and the adsorption side (inside/outside) plays a very important role in determining the nature of the interaction. Greater curvature and the inner adsorption alter the electronic structure of nanotube in a great extent. As an extension of the work reported here, functionalization of double-walled nanotube and associated electronic and magnetic structure properties need to be investigated in detail. The charge transfer between transition metal and walls of the nanotubes might create nanocapacitors to be used in nanocircuits.

Study of electron transport properties of nanotubes is important to understand the behavior of the nanotubes used in nano-electronic circuits. The combination of non equilibrium

Green's function (NEGF) with density functional theory (DFT) has been proved to be a successful method to study transport properties of carbon nanotubes and molecular wire junctions in nano-scale electronic circuits. Silicon carbide nanotubes are very promising material for nanoelectronics especially in very high temperature and high frequencies. To understand and control the electronic properties of the nanotubes for implementation in such applications, a detail study of transport properties of these nanotubes is required. An accurate and comprehensive analysis of such electronic transport properties of silicon carbide has not got enough attention and would be an interesting area of research. The computational methods which are already being used successfully to investigate transport properties of other nano-scale systems can be used in case of silicon carbide nanotubes also.

To conclude, despite great challenges and difficulties in fabricating silicon carbide nanotubes in experiments, much can be learned from computer experiments of these structures which would not only find possible future applications of silicon carbide nanotubes in various fields but also encourage experimental research by providing possible synthesis pathways. Hopefully, our study so far on silicon carbide nanotubes raises more questions than answers and further detailed experimental and theoretical studies will continue to provide answers to a relatively unexplored field in nanoscience and nanotechnology.

APPENDIX A

SOFTWARE FOR THE COORDINATES OF SINGLE-WALLED SILICON CARBIDE NANOTUBES

```
C       CODE TO AN ARMCHAIR CARBON NANOTUBE
C       RAYMOND ATTA-FYNN AND KAPIL ADHIKARI
C       UT ARLINGTON, TX, 2009
        IMPLICIT NONE
        DOUBLE PRECISION R,PHI,PI,A,X,Y,Z
        INTEGER S,U,T,N,NC
        CHARACTER*2 PP

        OPEN(14,FILE='NANO.XYZ',STATUS='UNKNOWN')
        PP='C'

        WRITE(*,*)'ENTER DIMENSION, THAT IS N'
        READ(*,*)N
        WRITE(*,*)'ENTER THE NUMBER OF UNIT CELLS'
        READ(*,*)NC

        PI = 2.*ASIN(1.)
        A=1.40*SQRT(3.)
        R=A*FLOAT(N)*SQRT(3.)/(2.*PI)
        WRITE(*,*)'RADIUS=',R
        WRITE(14,*)4*N*NC
        WRITE(14,*)
        DO T=0,2*NC-1
                DO U=0,1
                        DO S=0,N-1
                        Z=A*T/2
```

```
                PHI=(PI/FLOAT(3*N))*(2*(-1)**U + 3.*T +6*S)
                X=R*COS(PHI)
                Y=R*SIN(PHI)
                WRITE(14,132)PP,X,Y,Z
                END DO
            END DO
        END DO
        CLOSE(14)
132     FORMAT(A,3(F14.7))
        STOP
        END

c       Program builds an SiC armchair nanotube from an armchair carbon nanotube
c       such that ratio of Si to C is 1:1 and terminates the dangling bonds
c       with H at the lattice sites.
c       RAYMOND ATTA-FYNN AND KAPIL ADHIKARI, 2009
c       UT ARLINGTON, TX
        IMPLICIT NONE
        INTEGER NMAX1
        PARAMETER (NMAX1=2000)
        DOUBLE PRECISION XX (NMAX1),YY(NMAX1),ZZ(NMAX1),RCUT,ZMIN,ZMAX
        INTEGER NAT, II, JJ, KK, ICOUNT, SICOUNT, CCOUNT, LL, MM
        CHARACTER*6 PP (NMAX1), FNAME
        INTEGER NNMAP (NMAX1, 10), ILIST (NMAX1)
        DOUBLE PRECISION DSIH, DCH, X, Y, Z, RR1
```

```
      RCUT = 1.6
      DSIH = 1.066
      DCH = 1.2646

      ZMIN=10000.
      ZMAX=-ZMIN

      WRITE(*,*)'ENTER TYPE 1 OUTPUT FILE NAME'
      READ(*,*)FNAME

      OPEN(14,FILE='NANO.XYZ',STATUS='UNKNOWN')
      OPEN(15,FILE=FNAME,STATUS='UNKNOWN')

      READ(14,*)NAT
      DO II=1,NAT
        READ(14,132)PP(II),XX(II),YY(II),ZZ(II)
      END DO

132   FORMAT(A,3(F14.7))
      CLOSE(14)

      II=1
      PP(1)='SI'
```

```
100   CONTINUE

      ICOUNT =0
      CCOUNT=0
      SICOUNT=0

      DO II=1,NAT
      CALL MAP(XX,YY,ZZ,NAT,RCUT,II,NNMAP,ILIST)
        IF(PP(II)=='SI')THEN
          DO JJ=1,ILIST(II)
            KK=NNMAP(II,JJ)
            IF(PP(KK).NE.'C')PP(KK)='C'
            CALL MAP(XX,YY,ZZ,NAT,RCUT,KK,NNMAP,ILIST)
               DO LL=1,ILIST(KK)
                 MM=NNMAP(KK,LL)
                 IF(PP(MM).NE.'SI')PP(MM)='SI'
               END DO
          END DO
        END IF
      END DO

      DO II=1,NAT
        IF(PP(II)=='SI')SICOUNT=SICOUNT+1
        IF(PP(II)=='C')CCOUNT=CCOUNT+1
      END DO
```

```
      WRITE(*,*)SICOUNT,CCOUNT
      IF(SICOUNT .NE. CCOUNT)GOTO 100

      DO II=1,NAT
        ZMIN=MIN(ZMIN,ZZ(II))
        ZMAX=MAX(ZMAX,ZZ(II))
      END DO

      DO II=1,NAT
        IF((ZZ(II)==ZMIN).OR. (ZZ(II)==ZMAX))PP(II)='H'
      END DO

      DO II=1,NAT
        CALL MAP(XX,YY,ZZ,NAT,RCUT,II,NNMAP,ILIST)
      END DO

      DO II=1,NAT-1
        DO JJ=II+1,NAT
          IF(((PP(II)=='C').AND.(PP(JJ)=='H')) .OR.
     >       ((PP(II)=='H').AND.(PP(JJ)=='C')))THEN
            X = XX(II)-XX(JJ)
            Y = YY(II)-YY(JJ)
            Z = ZZ(II)-ZZ(JJ)
            RR1= X*X + Y*Y + Z*Z
            RR1 = SQRT(RR1)
```

```
            IF(RR1 < RCUT)THEN
                IF(PP(II)=='H')THEN
                    XX(II)=XX(JJ)+DCH*X/RR1
                    YY(II)=YY(JJ)+DCH*Y/RR1
                    ZZ(II)=ZZ(JJ)+DCH*Z/RR1
                END IF
                IF(PP(JJ)=='H')THEN
                  XX(JJ)=XX(II)-DCH*X/RR1
                  YY(JJ)=YY(II)-DCH*Y/RR1
                  ZZ(JJ)=ZZ(II)-DCH*Z/RR1
                END IF
            END IF

        ELSEIF(((PP(II)=='SI').AND.(PP(JJ)=='H')) .OR.
     >         ((PP(II)=='H').AND.(PP(JJ)=='SI')))THEN
            X = XX(II)-XX(JJ)
            Y = YY(II)-YY(JJ)
            Z = ZZ(II)-ZZ(JJ)
            RR1= X*X + Y*Y + Z*Z
            RR1 = SQRT(RR1)

            IF(RR1 < RCUT)THEN
                IF(PP(II)=='H')THEN
                    XX(II)=XX(JJ)+DSIH*X/RR1
                    YY(II)=YY(JJ)+DSIH*Y/RR1
                    ZZ(II)=ZZ(JJ)+DSIH*Z/RR1
```

```
            END IF
            IF(PP(JJ)=='H')THEN
              XX(JJ)=XX(II)-DSIH*X/RR1
              YY(JJ)=YY(II)-DSIH*Y/RR1
              ZZ(JJ)=ZZ(II)-DSIH*Z/RR1
            END IF
          END IF
        END IF
      END DO
    END DO

    WRITE(15,*)NAT
    WRITE(15,*)
    DO II=1,NAT
      WRITE(15,132)PP(II),XX(II),YY(II),ZZ(II)
    END DO
    CLOSE(15)

    STOP
    END

    SUBROUTINE MAP(XX,YY,ZZ,NAT,RCUT,II,NNMAP,ILIST)
    IMPLICIT NONE
    INTEGER NMAX1
    PARAMETER(NMAX1=2000)
    INTEGER II,JJ,NNMAP(NMAX1,10),ILIST(NMAX1),NAT
```

```
DOUBLE PRECISION X1,Y1,Z1,XX(NMAX1),YY(NMAX1),ZZ(NMAX1),RCUT,R
DOUBLE PRECISION RR

 ILIST(II)=0
 DO JJ=1,10
   NNMAP(II,JJ)=0
 END DO

 DO JJ=1,NAT
   IF(II.NE.JJ)THEN
     X1=XX(II)-XX(JJ)
     Y1=YY(II)-YY(JJ)
     Z1=ZZ(II)-ZZ(JJ)

     RR=SQRT(X1*X1+Y1*Y1+Z1*Z1)

     IF(RR<RCUT)THEN
       ILIST(II)=ILIST(II)+1
       NNMAP(II,ILIST(II))=JJ
     END IF
   END IF
 END DO

 RETURN
 END
```

Coordinates of type 1 SiC nanotube (3,3) generated from the codes above.

H	2.1259771	1.4524044	0.4489075
H	-2.3208077	1.1149478	0.4489075
H	0.1948308	-2.5673523	0.4489074
H	2.2006915	-1.3229952	0.7090442
H	0.0454018	2.5673524	0.7090441
H	-2.2460932	-1.2443572	0.7090441
C	-0.4526936	2.5673523	1.5761663
C	-1.9970454	-1.6757205	1.5761663
C	2.4497393	-0.8916317	1.5761663
Si	2.4497391	0.8916321	1.5761663
Si	-1.9970457	1.6757201	1.5761663
Si	-0.4526932	-2.5673524	1.5761663
C	-2.4497392	0.8916319	3.1523325
C	0.4526938	-2.5673523	3.1523325
C	1.9970453	1.6757206	3.1523325
Si	0.4526934	2.5673524	3.1523325
Si	-2.4497390	-0.8916324	3.1523325
Si	1.9970459	-1.6757199	3.1523325
C	-1.9970454	-1.6757205	4.7284988
C	2.4497393	-0.8916317	4.7284988
C	-0.4526941	2.5673523	4.7284988
Si	-1.9970457	1.6757201	4.7284988
Si	-0.4526932	-2.5673524	4.7284988
Si	2.4497389	0.8916326	4.7284988
C	0.4526938	-2.5673523	6.3046651

C	1.9970453	1.6757206	6.3046651
C	-2.4497393	0.8916315	6.3046651
Si	-2.4497390	-0.8916324	6.3046651
Si	1.9970459	-1.6757199	6.3046651
Si	0.4526929	2.5673525	6.3046651
C	2.4497393	-0.8916317	7.8808314
C	-0.4526941	2.5673523	7.8808314
C	-1.9970451	-1.6757208	7.8808314
Si	-0.4526932	-2.5673524	7.8808314
Si	2.4497389	0.8916326	7.8808314
Si	-1.9970460	1.6757198	7.8808314
C	1.9970453	1.6757206	9.4569976
C	-2.4497393	0.8916315	9.4569976
C	0.4526943	-2.5673522	9.4569976
Si	1.9970459	-1.6757199	9.4569976
Si	0.4526929	2.5673525	9.4569976
Si	-2.4497389	-0.8916328	9.4569976
C	-0.4526941	2.5673523	11.0331639
C	-1.9970451	-1.6757208	11.0331639
C	2.4497394	-0.8916313	11.0331639
Si	2.4497389	0.8916326	11.0331639
Si	-1.9970460	1.6757198	11.0331639
Si	-0.4526927	-2.5673525	11.0331639
C	-2.4497393	0.8916315	12.6093302
C	0.4526943	-2.5673522	12.6093302
C	1.9970450	1.6757210	12.6093302

Si	0.4526929	2.5673525	12.6093302
Si	-2.4497389	-0.8916328	12.6093302
Si	1.9970462	-1.6757196	12.6093302
C	-1.9970451	-1.6757208	14.1854964
C	2.4497394	-0.8916313	14.1854964
C	-0.4526945	2.5673522	14.1854964
Si	-1.9970460	1.6757198	14.1854964
Si	-0.4526927	-2.5673525	14.1854964
Si	2.4497388	0.8916330	14.1854964
C	0.4526943	-2.5673522	15.7616627
C	1.9970450	1.6757210	15.7616627
C	-2.4497395	0.8916311	15.7616627
Si	-2.4497389	-0.8916328	15.7616627
Si	1.9970462	-1.6757196	15.7616627
Si	0.4526925	2.5673525	15.7616627
H	2.3208080	-1.1149472	16.8889216
H	-0.1948315	2.5673523	16.8889216
H	-2.1259766	-1.4524052	16.8889214
H	-0.0454011	-2.5673524	16.6287849
H	2.2460929	1.2443578	16.6287849
H	-2.2006920	1.3229945	16.6287849

APPENDIX B

SOFTWARE FOR CALCULATIONS OF THE DIAMETER AND BUCKLING OF A SILICON CARBIDE NANOTUBE

```
C      MODIFIED ON BY R. ATTA-FYNN & KAPIL 06/09/2009
       IMPLICIT NONE
       INTEGER II,NAT,NSI,NC, I1, I2, I3
       DOUBLE PRECISION XX(1000),YY(1000),ZZ(1000),RR1,RR2,TEMP1
       DOUBLE PRECISION DIA,DIA1,DR
       CHARACTER*2 PP(1000)
       CHARACTER*25 FNAME

       WRITE(*,*)'ENTER INPUT FILE NAME'
       READ(*,*)FNAME
       OPEN(12,FILE=FNAME,STATUS='UNKNOWN')

       NSI=0
       NC=0

       READ(12,*)NAT
       DO II=1,NAT
         READ(12,*)PP(II),XX(II),YY(II),ZZ(II)
            IF(PP(II).EQ.'C')NC=NC + 1
            IF(PP(II).EQ.'SI')NSI=NSI + 1
       END DO
       CLOSE(12)
       RR1=0
       RR2=0

            DO II=1,NAT
```

```
          TEMP1=(YY(II)*YY(II))+(ZZ(II)*ZZ(II))

          IF(PP(II).EQ.'C')RR1=RR1+SQRT(TEMP1)
          IF(PP(II).EQ.'SI')RR2=RR2+SQRT(TEMP1)
        END DO

RR1=RR1/(FLOAT(NC))
RR2=RR2/(FLOAT(NSI))
DIA=2.D0*(FLOAT(NC)*RR1+FLOAT(NSI)*RR2)/FLOAT(NC+NSI)
DR = RR1 - RR2

WRITE(*,*)'AVE RADIUS CARBON=', RR1
WRITE(*,*)'AVE RADIUS SILICON=',RR2
WRITE(*,*)'AVE DIAMETER=',DIA
IF(DR > 0.)THEN
  WRITE(*,*)'BUCKLING =', ABS(DR)
  WRITE(*,*)'CARBON OUTWARDS SI INWARDS'
ELSE
  WRITE(*,*)'BUCKLING =', ABS(DR)
  WRITE(*,*)'SI OUTWARDS C INWARDS'
END IF
STOP
END
```

APPENDIX C

SOFTWARE FOR DENSITY OF STATES PLOTS

```
C       Simple f77 code to compute EDOS using data from Gaussian log file
C       R. Atta-Fynn, Sept. 30 2006, Modified on May 30, 2007 to cater for
C       Alpha/beta eigienvalues (mixed or single).
C       modified reads HOMO and LUMO and sets HOMO to zero
C       Further modification to read HOMO and LUMO and set HOMO to zero
C       by Kapil Adhikari and R. Atta-Fynn March 15, 2009.

      implicit none
      real*8 energy(20000),edos(20000),ehomo,elumo
      real*8 emin, emax,  de, xx, yy, sigma, norm, pi
      integer NEIGEN,ii, jj, np, ncount,iset
      character*25 ppc, ppc2, fname1, fname2
      call rwfiles

      pi = 2.*asin(1.)
      ncount = 0

      open(14,file='dos_parameters.dat',status='unknown')
      read(14,*)ppc,np
      if(np .le. 1)then
        write(*,*)'Energy points must be greater than 1'
        stop
      end if
      read(14,*)ppc,emin
      read(14,*)ppc,emax
      read(14,*)ppc,sigma
```

```
      read(14,*)fname1
      read(14,*)ppc,ehomo
      read(14,*)ppc2,elumo
      close(14)
      open(12,file=fname1,status='unknown')
      read(12,*)NEIGEN
      do ii=1,NEIGEN
         read(12,*)energy(ii)
      end do
      close(12)

      de = (emax - emin)/float(np-1)
      do ii = 1,np
        edos(ii)=0.
      end do
      do ii = 1, np
        xx = emin + float(ii-1)*de
         do jj = 1,NEIGEN
           yy = xx - energy(jj)
           edos(ii) = edos(ii) + exp( -yy*yy/(sigma*sigma))
         end do
      end do

c      norm = sqrt(pi) * sigma * float(np)
      norm = 1.
```

```
 open(15,file='EDOS.dat',status='unknown')
 do ii = 1,np
    yy = edos(ii)/norm
    xx = emin + float(ii-1)*de
    write(15,'(f12.6,2x,f12.6)')xx-ehomo, yy
 end do
 close(15)
 write(*,*)
 write(*,*)
 write(*,*)'E_HOMO has been shifted to zero energy in DOS'
 write(*,*)
 write(*,*)'Gaussian broadening factor in eV =', sigma
 write(*,*)
 write(*,*)'DOS data is in the file EDOS.dat'
 write(*,*)
 stop
 end

C       This subroutine rearranges EIGENVALUES from
C       Gaussian'03 log file
C       Raymond Atta-Fynn, Dept. of Physics
C       The University of Texas at Arlington
C       Date: 09-30-2007
C       Use at your own risk

      subroutine rwfiles
```

```
implicit none
real xx(1,1500),EMIN,EMAX,sigma
real yy(1,4500),alpha_gap,beta_gap,gap
real fac,xx2(1,1500),yy2(1,4500),ehomo, elumo
integer occupied, unoccupied,ii,np,jj,iset
integer occupied2, unoccupied2
character*20 fname1, fname2, contcheck

write(*,*)
write(*,*)'*******************************************'
write(*,*)'*                                         *'
write(*,*)'*  Program Gaussian_dos                   *'
write(*,*)'*  Computes DOS from Gaussian log file    *'
write(*,*)'*                                         *'
write(*,*)'*******************************************'
write(*,*)'DO YOU WANT TO CONTINUE?'
write(*,*)
write(*,*)'ENTER yes or no'
read(*,*)contcheck
write(*,*)
write(*,*)
if(contcheck=='yes')goto 156
if(contcheck=='no')then
  write(*,*)'ABORTING .....'
  write(*,*)'GOODBYE          '
```

```
      write(*,*)
      write(*,*)
    if(contcheck=='yes')goto 156
      stop
    end if

156    continue

    write(*,*)'Enter 0 for only ALPHA or 1 for ALPHA-BETA'
    read(*,*)iset
    write(*,*)'Enter total number of points'
    read(*,*)np
    write(*,*)'Enter broadening factor sigma'
    read(*,*)sigma

    fac=2.*13.605698
    if(iset.eq.0)then

    open(11,file='ALPHA_EIG.DAT',status='unknown')

    read(11,*)occupied
    read(11,*)(xx(1,jj),jj=1,occupied)
    read(11,*)unoccupied
    read(11,*)(yy(1,jj),jj=1,unoccupied)
    close(11)
    elumo = yy(1,1)*fac
```

```
ehomo = xx(1,occupied)*fac
alpha_gap = yy(1,1) - xx(1,occupied)
alpha_gap = alpha_gap*fac
gap = alpha_gap
ii=occupied+unoccupied
open(14,file='alpha_data.out',status='unknown')
fname1 = 'alpha_data.out'
write(14,*)ii
do jj=1,occupied
  write(14,'(f13.6)')xx(1,jj)*fac
end do
do jj=1,unoccupied
  write(14,'(f13.6)')yy(1,jj)*fac
end do
close(14)
open(15,file='dos_parameters.dat',status='unknown')
write(15,*)'np',np
write(15,*)'EMIN',  ehomo - 10.
write(15,*)'EMAX',  ehomo + 10.
write(15,*)'sigma',sigma
write(15,*)fname1
write(15,*)'HOMO',xx(1,occupied)*fac
write(15,*)'LUMO',yy(1,1)*fac
close(15)
goto 125
end if
```

```
open(11,file='ALPHA_EIG.DAT',status='unknown')
open(12,file='BETA_EIG.DAT',status='unknown')

read(11,*)occupied
read(11,*)(xx(1,jj),jj=1,occupied)
read(11,*)unoccupied
read(11,*)(yy(1,jj),jj=1,unoccupied)
read(12,*)occupied2
read(12,*)(xx2(1,jj),jj=1,occupied2)
read(12,*)unoccupied2
read(12,*)(yy2(1,jj),jj=1,unoccupied2)
close(11)
close(12)
alpha_gap = yy(1,1) - xx(1,occupied)
alpha_gap = alpha_gap*fac
beta_gap = yy2(1,1) - xx2(1,occupied2)
beta_gap = beta_gap*fac
gap = min(alpha_gap,beta_gap)
ii=occupied+unoccupied+occupied2+unoccupied2
open(14,file='alpha_data.out',status='unknown')
fname1 = 'alpha_data.out'

write(14,*)ii
do jj=1,occupied
   write(14,'(f13.6)')xx(1,jj)*fac
```

```
end do
do jj=1,unoccupied
  write(14,'(f13.6)')yy(1,jj)*fac
end do
do jj=1,occupied2
  write(14,'(f13.6)')xx2(1,jj)*fac
end do
do jj=1,unoccupied2
  write(14,'(f13.6)')yy2(1,jj)*fac
end do
close(14)

open(15,file='dos_parameters.dat',status='unknown')
write(15,*)'np',np
write(15,*)'EMIN',  ehomo - 10.
write(15,*)'EMAX',  ehomo + 10.
write(15,*)'sigma',sigma
write(15,*)fname1
IF(gap.eq.alpha_gap)THEN
  elumo = yy(1,1)*fac
  ehomo = xx(1,occupied)*fac
  write(15,*)'HOMO',xx(1,occupied)*fac
  write(15,*)'LUMO',yy(1,1)*fac
END IF
IF(gap.eq.beta_gap)THEN
  elumo = yy2(1,1)*fac
```

```
      ehomo = xx2(1,occupied2)*fac
      write(15,*)'HOMO',xx2(1,occupied2)*fac
      write(15,*)'LUMO',yy2(1,1)*fac
    END IF
    close(15)

125   continue

    write(*,*)
    write(*,*)
    write(*,*)' E_LUMO=', elumo
    write(*,*)
    write(*,*)' E_HOMO=', ehomo
    write(*,*)
    if(iset.eq.0)then
      write(*,*)' HOMO-LUMO GAP in eV =', gap
    else

      write(*,*)' ALPHA HOMO-LUMO GAP in eV =', alpha_gap
      write(*,*)' BETA HOMO-LUMO GAP in eV =', beta_gap
    end if
    write(*,*)
    return
    end
```

REFERENCES

[1] S. Iijima, Helical microtubules of graphitic carbon, Nature 354 (1991) 56-58. doi: 10.1038/354056a0.

[2] S. Iijima and T. Ichihashi, Single-shell carbon nanotubes of 1-nm diameter, Nature 363 (1993) 603-605. doi: 10.1038/363603a0

[3] M. S. Dresselhaus, G. Dresselhaus, and Ph. Avouris, Carbon Nanotubes-Synthesis, Structure, Properties and Applications, Topics in Applied Physics, Vol. 80, Springer, Berlin, (2001).

[4] N. Hamada, S. I. Sawada, and A. Oshiyama, New one-dimensional conductors: Graphitic microtubules, Physical Review Letters 68 (1992) 1579-1581. doi:10.1103/PhysRevLett.68.1579.

[5] R. Saito, M. Fujiata, G. Dresselhaus, and M. S. Dresselhaus, Electronic structure of chiral graphene tubules, Applied Physics Letters 60(1992) 2204-2206. doi:10.1063/1.107080.

[6] T. W. Odom, J. L. Huang, P. Kim, and C. M. Lieber, Atomic structure and electronic properties of single-walled carbon nanotubes, Nature 391 (1998) 62-64. doi:10.1038/34145.

[7] R. A. Jishi, J. Bragin, and L. Lou, Electronic structure of short and long carbon nanotubes from first principles, Physical Review B 59 (1999) 9862-9865. doi:10.1103/PhysRevB.59.9862.

[8] O. Gulseren, T. Yildirim, and S. Ciraci, Systematic ab initio study of curvature effects in carbon nanotubes, Physical Review B, 65 (2002), 153405-1-4. doi:10.1103/PhysRevB.65.153405.

[9] R. X. Ding, Y. T. Yang, and L. Liu, Working mechanism of a SiC nanotube NO2 gas sensor, Journal of Semiconductors 30, 114010-1-4 (2009). doi:10.1088/1674-4926/30/11/114010.

[10] R. Krupke, F. Hennrich, H. V. Löhneysen, and M. M. Kappes, Separation of metallic from semiconducting single-walled carbon nanotubes, Science 301, 344-347 (2003). doi: 10.1126/science.1086534.

[11] Y. Maeda, S. Kimura, M. Kanda, Y. Hirashima, T. Hasegawa, T. Wakahara, Y. Lian, T. Nakahodo, T. Tsuchiya, T. Akasaka, J. Lu, X. Zhang, Z. Gao, Y. Yu, S. Nagase, S. Kazaoui, N. Minami, T. Shimizu, H. Tokumoto, and R. Saito, Large-scale separation of metallic and semiconducting single-walled carbon nanotubes, Journal of the American Chemical Society 127 10287-10290 (2005). doi: 10.1021/ja051774o.

[12] Y. Maeda, S. Kimura, M. Kanda, M. Hashimoto, T. Hasegawa, S. Kimura, Y. Lian, T. Wakahara, T. Akasaka, S. Kazaoui, N. Minami, T. Okazaki, Y. Hayamizu, K. Hata, J. Lu, and S. Nagase, Dispersion and separation of small-diameter single-walled carbon nanotubes, Journal of the American Chemical Society 128, 12239-12242 (2006). doi:10.1021/ja063776u.

[13] J. Cumings, and A. Zettl, Mass-production of boron nitride double-wall nanotubes and nanococoons, Chemical Physics Letters 316 (2000) 211-216. doi:10.1016/S0009-2614(99)01277-4.

[14] Q. Wu, Z. Hu, X. Wang, Y. Lu, X. Chen, H. Xu, and Y. Chen, Synthesis and characterization of faceted hexagonal aluminum nitride nanotubes, Journal of the American Chemical Society 125 (2003) 10176-7. doi: 10.1021/ja0359963.

[15] J. Goldberger, R. He, Y. Zhang, S. Lee, H. Yan, H. J. Choi, and P. Yang, Single-crystal gallium nitride nanotubes, Nature 422, 599-602 (2003). doi: 10.1038/nature01551

[16] Y. R. Hacohen, E. Grunbaum, R. Tenne, J. Sloand, and J. L. Hutchinson, Cage structures and nanotubes of $NiCl_2$, Nature 395, 336-337 (1998). doi: 10.1038/26380

[17] Y. R. Hacohen, R. Popovitz-Biro, E. Grunbaum, Y. Prior, R. Tenne, Vapor–Liquid–Solid (VLS) growth of NiCl2 nanotubes via reactive gas laser ablation, Advanced Materials 14, 1075-1078 (2002). doi: 10.1002/1521-4095(20020805)14:15<1075::AID-ADMA1075>3.0.CO;2-H.

[18] Q. Chen, W. Zhou, G. H. Du, and L. M. Peng, Trititanate nanotubes made via a single alkali treatment, Advanced Materials 14, 1208-1211 (2002). doi:10.1002/1521-4095(20020903)14:17<1208::AID-ADMA1208>3.0.CO;2-0.

[19] G. R. Patzke, F. Krumeich, and R. Nesper, Oxidic nanotubes and nanorods--anisotropic modules for a future nanotechnology, Angewandte Chemie (International ed. in English) 41, 2446-2461(2002). doi: 10.1002/1521-3773(20020715)41:14<2446::AID-ANIE2446>3.0.CO;2-K.

[20] J. Sha, J. Niu, X. Ma, J. Xu, X. Zhang, Q. Yang, and D. Yang, Silicon Nanotubes, Advanced Materials 14, 1219-1221 (2002). doi: 10.1002/1521-4095(20020903)14:17<1219::AID-ADMA1219>3.0.CO;2-T.

[21] H. Dai, E. W. Wong, Y. Z. Lu, S. Fan, and C. M. Lieber, Synthesis and characterization of carbide nanorods, Nature 375, 769-772 (1995). doi:10.1038/375769a0.

[22] J. Luning, S. Eisebitt, J. E. Rubensson, C. Ellemers, and W. Eberhardt, Electronic structure of silicon carbide polytypes studied by soft x-ray spectroscopy, Physical Review B 59, 10573-10582 (1999). doi:10.1103/PhysRevB.59.10573.

[23] J. Li, L. Porter, and S. Yip, Atomistic modeling of finite-temperature properties of crystalline β-SiC: II. Thermal conductivity and effects of point defects, Journal of Nuclear Materials 255, 139-152 (1998). doi: 10.1016/S0022-3115(98)00034-8.

[24] L. Porter, J. Li, and S. Yip, Atomistic modeling of finite-temperature properties of β-SiC. I. Lattice vibrations, heat capacity, and thermal expansion, Journal of Nuclear Materials 246, 53-59. doi: 10.1016/S0022-3115(97)00035-4.

[25] R.W. Olesinski and G.J. Abbaschian, The C−Si (Carbon-Silicon) system, Bulletin of Alloy Phase Diagrams 5, 486-489 (1984). doi:10.1007/BF02872902.

[26] W.R.L. Lambrecht, B. Segall, M. Methfessel, and M. V. Schilfgaarde, Calculated elastic constants and deformation potentials of cubic SiC, Physical Review B 44, 3685-3694 (1991). doi:10.1103/PhysRevB.44.3685

[27] E. W. Wong, P. E. Sheehan, and C. M. Lieber, Nanobeam mechanics: elasticity, strength, and toughness of nanorods and nanotubes, Science 277, 1971-1975 (1997). doi:10.1126/science.277.5334.1971.

[28] W. Han, S. Fan, Q. Li, W. Liang, B. Gu, and D. Yu, Continuous synthesis and characterization of silicon carbide nanorods, Chemical Physics Letters 265, 374-378 (1996). doi:10.1016/S0009-2614(96)01441-8.

[29] Y. Miyamoto and B. D. Yu, Computational designing of graphitic silicon carbide and its tubular forms, Applied Physics Letters 80, 586-588 (2002). doi:10.1063/1.1445474.

[30] C. Pham-Huu, N. Keller, and G. Ehet, The first preparation of silicon carbide nanotubes by shape memory synthesis and their catalytic potential, Journal of Catalysis 200, 400-410 (2001). doi:10.1006/jcat.2001.3216.

[31] E. Borowiak-Palen, M. H. Ruemmeli, T. Gemming, M. Knupfer, K. Biedermann, A. Leonhardt, T. Pichler, and R. J. Kalenczuk, Bulk synthesis of carbon-filled silicon carbide

nanotubes with a narrow diameter distribution, Journal of Applied Physics 97, 056102-1-3 (2005). doi:10.1063/1.1853493.

[32] J. Q. Hu, Y. Bando, J. H. Zhan, and D. Golberg, Fabrication of ZnS/SiC nanocables, SiC-shelled ZnS nanoribbons (and sheets), and SiC nanotubes (and tubes), Applied Physics Letters 85, 2932-2934 (2004). doi:10.1063/1.1801168.

[33] N. Keller, C. Pham-Huu, G. Ehret, V. Keller, and M. J. Ledoux, Synthesis and characterisation of medium surface area silicon carbide nanotubes, Carbon 41, 2131-2139 (2003). doi:10.1016/S0008-6223(03)00239-2.

[34] T. Taguchi, N. Igawa, H. Yamamoto, S. Shamoto, and S. Jitsukawa, Preparation and characterization of single-phase SiC nanotubes and C-SiC coaxial nanotubes, Physica E 28, 431-438 (2005). doi:10.1016/j.physe.2005.05.048.

[35] J. M. Nhut, R. Vieira, L. Pesant, J.P. Tessonnier, N. Keller, G. Ehet, C. Pham-Huu, and M. J. Ledoux, Synthesis and catalytic uses of carbon and silicon carbide nanostructures, Catalysis Today 76, 11-32 (2002). doi:10.1016/S0920-5861(02)00206-7.

[36] T. Taguchi, N. Igawa, H. Yamamoto, and S. Jitsukawa, Synthesis of Silicon Carbide Nanotubes, Journal of the American Ceramic Society 88, 459-461 (2005). doi:10.1111/j.1551-2916.2005.00066.x.

[37] A. Huczko, M. Bystrzejewski, H. Lange, A. Fabianowska, S. Cudzilo, A. Panas, and M. Szala, Combustion synthesis as a novel method for production of 1-D SiC, The journal of physical chemistry B, 109, 16244-16251 (2005). doi:10.1021/jp050837m.

[38] X. H. Sun, C. P. Li, W. K. Wong, N. B. Wong, C. S. Lee, S. T. Lee, and B. K. Teo, Formation of silicon carbide nanotubes and nanowires via reaction of silicon (from

disproportionation of silicon monoxide) with carbon nanotubes, Journal of the American Chemical Society 124, 14464-14471 (2002). doi:10.1021/ja0273997.

[39] V.V. Pokropivnyi and P.M. Silenko, Silicon carbide nanotubes and nanotubular fibers: Synthesis, stability, structure, and classification, Theoretical and Experimental Chemistry 42, 3-15 (2006). doi:10.1007/s11237-006-0010-y.

[40] M. N. Huda, Y. Yan, and M. M. Al-Jassim, On the existence of Si–C double bonded graphene-like layers, Chemical Physics Letters 479, 255-258 (2009). doi:10.1016/j.cplett.2009.08.028.

[41] M. Yu, C. S. Jayanthi, and S. Y. Wu, Geometric and electronic structures of graphitic-like and tubular silicon carbides: Ab-initio studies, Physical Review B 82, 075407-1-8 (2010). doi:10.1103/PhysRevB.82.075407.

[42] S. M. Lee, Y. H. Lee, Y. G. Hwang, J. Elsner, D. Porezag, and T. Frauenheim, Stability and electronic structure of GaN nanotubes from density-functional calculations, Physical Review B 60, 7788-7791 (1999). doi:10.1103/PhysRevB.60.7788.

[43] M. Zhao, Y. Xia, D. Zhang, and L. Mei, Stability and electronic structure of AlN nanotubes, Physical Review B 68, 235415-1-4 (2003). doi:10.1103/PhysRevB.68.235415.

[44] A. Mavrandonakis, G. E. Froudakis, M. Schnell, and M. Mühlhäuser, From pure carbon to silicon−carbon nanotubes: an ab-initio study, Nano Letters 3, 1481-1484 (2003). doi:10.1021/nl0343250.

[45] M. W. Zhao, Y. Y. Xia, F. Li, R. Q. Zhang, and S. -T. Lee, Strain energy and electronic structures of silicon carbide nanotubes: Density functional calculations, Physical Review B 71, 085312-1-6 (2005). doi:10.1103/PhysRevB.71.085312.

[46] M. Menon, E. Richter, A. Mavrandonakis, G. Froudakis, and A. N. Andriotis, Structure and stability of SiC nanotubes, Physical Review B 69, 45-48 (2004). doi:10.1103/PhysRevB.69.115322.

[47] K. Alam and A.K. Ray, Hybrid density functional study of armchair SiC nanotubes, Physical Review B 77, 035436-1-10 (2008). doi:10.1103/PhysRevB.77.035436.

[48] K. Alam and A. K. Ray, A hybrid density functional study of zigzag SiC nanotubes, Nanotechnology 18, 495706-1-10 (2007). doi:10.1088/0957-4484/18/49/495706.

[49] R.J. Baierle, P. Piquini, L.P. Neves, and R.H. Miwa, Ab initio study of native defects in SiC nanotubes, Physical Review B 74, 155425-1-8 (2006). doi:10.1103/PhysRevB.74.155425.

[50] W. H. Moon, J. K. Ham, and H. J. Hwang, Mechanical properties of SiC nanotubes Nanotech 3, 158-161 (2003). http://nrc.org/publications/Nanotech/2003/pdf/T5404.pdf.

[51] E. Hernández, C. Goze, P. Bernier, and A. Rubio, Elastic properties of C and BxCyNz composite nanotubes, Physical Review Letters 80, 4502-4505 (1998). doi:10.1103/PhysRevLett.80.4502.

[52] J.J. Petrovic, J. V. Milewski, D. L. Rohr, and F. D. Gac, Tensile mechanical properties of SiC whiskers, Journal of Materials Science 20, 1167-1177 (1985). doi:10.1007/BF01026310.

[53] B. Baumeier, P. Kruger, and J. Pollmann, Structural, elastic, and electronic properties of SiC, BN, and BeO nanotubes, Physical Review B 76, 085407-1-10 (2007). doi:10.1103/PhysRevB.76.085407.

[54] Y. Zhang and H. Huang, Stability of single-wall silicon carbide nanotubes – molecular dynamics simulations, Computational Materials Science 43, 664-669 (2008). doi:10.1016/j.commatsci.2008.01.038.

[55] A.R. Setoodeh, M. Jahanshahi, and H. Attariani, Atomistic simulations of the buckling behavior of perfect and defective silicon carbide nanotubes, Computational Materials Science 47, 388-397 (2009). doi:10.1016/j.commatsci.2009.08.017.

[56] X. Wang, B. Wang, J. Zhao, and G. Wang, Structural transitions and electronic properties of the ultrathin SiC nanotubes under uniaxial compression, Chemical Physics Letters 461, 280-284 (2008). doi:10.1016/j.cplett.2008.07.040.

[57] Z. Wang, X. Zu, H. Xiao, F. Gao, and W. J. Weber, Tuning the band structures of single walled silicon carbide nanotubes with uniaxial strain: A first principles study, Applied Physics Letters 92, 183116-1-3 (2008). doi:10.1063/1.2924307.

[58] H. J. Shen, MD simulations on the melting and compression of C, SiC and Si nanotubes, Journal of Materials Science 42, 6382-6387 (2007). doi:10.1007/s10853-006-1205-2.

[59] S.-J. Wang, C.-L. Zhang, Z.-G. Wang, Melting of single-walled silicon carbide nanotubes: density functional molecular dynamics simulation, Chinese Physics Letters 27, 106101-1-3 (2010). doi:10.1088/0256-307X/27/10/106101.

[60] I.J. Wu and G.Y. Guo, Optical properties of SiC nanotubes: An ab initio study, Physical Review B 76, 035343-1-9 (2007). doi:10.1103/PhysRevB.76.035343.

[61] A. C. Dillon, T. Gennett, J. L. Alleman, K. M. Jones, P.A. Parilla, and M. J. Heben, Carbon nanotube materials for hydrogen storage, Proceedings of the 2000 DOE/NREL hydrogen program review (2000). http://www.eere.energy.gov/hydrogenandfuelcells/pdfs/28890kkk.pdf.

[62] C. Dillon, K. M. Jones, T. A. Bekkedahl, C. H. Kiang, D. S. Bethune, and M. J. Heben, Storage of hydrogen in single-walled carbon nanotubes, Nature 386, 377-379 (1997). doi:10.1038/386377a0.

[63] A. Züttel, Materials for hydrogen storage, Materials Today 6, 24-33 (2003). doi:10.1016/S1369-7021(03)00922-2.

[64] G.G. Tibbetts, G. P. Meisner, and C. H. Olk, Hydrogen storage capacity of carbon nanotubes, filaments, and vapor-grown fibers, Carbon 39, 2291-2301 (2001). doi:10.1016/S0008-6223(01)00051-3.

[65] L. Chen, Y. Zhang, N. Koratkar, P. Jena, and S. K. Nayak, First-principles study of interaction of molecular hydrogen with Li-doped carbon nanotube peapod structures, Physical Review B 77, 033405-1-4 (2008). doi:10.1103/PhysRevB.77.033405.

[66] G. Mpourmpakis, G.E. Froudakis, G. P. Lithoxoos, and J. Samios, SiC nanotubes: A novel material for hydrogen storage, Nano letters 6, 1581-1583 (2006). doi:10.1021/nl0603911.

[67] R.J. Baierle, and R.H. Miwa, Hydrogen interaction with native defects in SiC nanotubes, Physical Review B 76, 205410-1-7 (2007). doi:10.1103/PhysRevB.76.205410.

[68] S. Mukherjee and A.K. Ray, An ab initio study of molecular hydrogen interaction with SiC nanotube—a precursor to hydrogen storage, Journal of Computational and Theoretical Nanoscience 5, 1210-1219 (2008).doi: 10.1166/jctn.2008.003.

[69] S. Mukherjee and A.K. Ray, A computational study of endohedral and exohedral complexes of molecular hydrogen with single wall (3, 3) to (6, 6) armchair silicon carbide nanotubes**,** Journal of Computational and Theoretical Nanoscience 7, 1518-1530 (2010). doi:10.1166/jctn.2010.1515.

[70] S. Mukherjee and A.K. Ray, Co-adsorptions of hydrogen molecules with single wall silicon carbide nanotubes: an ab initio study**,** Journal of Computational and Theoretical Nanoscience 8, 1798-1810 (2011). doi: 10.1166/jctn.2011.1886.

[71] K. Malek and M. Sahimi, Molecular dynamics simulations of adsorption and diffusion of gases in silicon-carbide nanotubes, The Journal of chemical physics 132, 014310-1-10 (2010). doi:10.1063/1.3284542.

[72] T. Meng, C. -Y. Wang, and S. -Y. Wang, First-principles study of a single Ti atom adsorbed on silicon carbide nanotubes and the corresponding adsorption of hydrogen molecules to the Ti atom, Chemical Physics Letters 437, 224-228 (2007). doi:10.1016/j.cplett.2007.02.024.

[73] S. Banerjee, S. Nigam, C. G. S. Pillai, C. Majumder, Hydrogen storage on Ti decorated SiC nanostructures: A first principles study, International Journal of Hydrogen Energy 37, 3733-3740 (2011). doi:10.1016/j.ijhydene.2011.05.078.

[74] X. Wang and K. M. Liew, Hydrogen storage in silicon carbide nanotubes by lithium doping, The Journal of Physical Chemistry C 115, 3491-3496 (2011). doi:10.1021/jp106509g.

[75] X. -F. Li, K. -Q. Chen, L. Wang, M. -Q. Long, B. S. Zou, and Z. Shuai, Effect of length and size of heterojunction on the transport properties of carbon-nanotube devices, Applied Physics Letters 91, 133511-1-3 (2007). doi:10.1063/1.2790839.

[76] W.Y. Kim, S. K. Kwon, and K. S. Kim, Negative differential resistance of carbon nanotube electrodes with asymmetric coupling phenomena, Physical Review B 76, 033415-1-4 (2007). doi:10.1103/PhysRevB.76.033415.

[77] P. Bai, E. Li, K. T. Lam, O. Kurniawan, and W. S. Koh, Carbon nanotube Schottky diode: an atomic perspective, Nanotechnology 19, 115203-1-6 (2008). doi:10.1088/0957-4484/19/11/115203.

[78] Z. Li and D. S. Kosov, Dithiocarbamate anchoring in molecular wire junctions: a first principles study, The journal of physical chemistry B 110, 9893-9898 (2006). doi:10.1021/jp0610665.

[79] Y.T. Yang, J.X. Song, H.X. Liu, and C.C. Chai, Negative differential resistance in single-walled SiC nanotubes, Chinese Science Bulletin 53, 3770-3772 (2008). doi:10.1007/s11434-008-0529-5.

[80] H.X. Liu, H. Zhang, and Z. Zhang, Electronic transport properties of an (8, 0) carbon/silicon-carbide nanotube heterojunction, Journal of Semiconductors 30, 052002-1-4 (2009). doi:10.1088/1674-4926/30/5/052002.

[81] J.X. Song, Y.T. Yang, H.X. Liu, L. Guo, and Z. Zhang, Electronic transport properties of the armchair silicon carbide nanotube, Journal of Semiconductors 31, 114003-1-3 (2010). doi:10.1088/1674-4926/31/11/114003.

[82] Y.T. Yang, R.X. Ding, and J.X. Song, Transport properties of boron-doped single-walled silicon carbide nanotubes, Physica B 406, 216-219 (2011). doi:10.1016/j.physb.2010.10.046.

[83] J. Jia, S.-P. Ju, D. Shi, and K.-F. Lin, Electromechanical Response of a SiC Nanotube under Local Torsional Deformation, The Journal of Physical Chemistry C 115, 24347-24352 (2011). doi:10.1021/jp207857e.

[84] S. Choudhary, and S. Qureshi, Theoretical study on transport properties of a BN co-doped SiC nanotube, Physics Letters A 375, 3382-3385 (2011). doi:10.1016/j.physleta.2011.08.001.

[85] M. N. Huda and A. K. Ray, Evolution of SiC nanocluster from carbon fullerene: A density functional theoretic study, Chemical Physics Letters 457, 124-129 (2008). doi:10.1016/j.cplett.2008.03.057.

[86] M. Matsubara and C. Massobrio, Stable highly doped $C_{60-m}Si_m$ heterofullerenes: a first principles study of $C_{40}Si_{20}$, $C_{36}Si_{24}$, and $C_{30}Si_{30}$, The journal of physical chemistry A 109, 4415-4418 (2005). doi:10.1021/jp058094s.

[87] L. H. Thomas, The calculation of atomic fields, Proceedings of the Cambridge Philosophical Society 23, 542-548 (1927). doi: 10.1017/S0305004100011683.

[88] E. Fermi, Eine statistische Methode zur Bestimmung einiger Eigenschaften des Atoms und ihre Anwendung auf die Theorie des periodischen Systems der Elemente (A statistical method for the determination of some properties of the atom and its application to the theory of the periodic table of elements), Zeitschrift für Physik 48, 73-79 (1928). doi:10.1007/BF01351576.

[89] E. Teller, On the Stability of Molecules in the Thomas-Fermi Theory, Reviews of Modern Physics 34, 627-631 (1962). doi:10.1103/RevModPhys.34.627.

[90] P.A.M. Dirac, Note on Exchange Phenomena in the Thomas Atom. Mathematical Proceedings of the Cambridge Philosophical Society 26, 376-385 (1930). doi:10.1017/S0305004100016108.

[91] P. Hohenberg and W. Kohn, Inhomogeneous Electron Gas, Physical Review 136, B864-B871 (1964). doi:10.1103/PhysRev.136.B864.

[92] W. Kohn and L. J. Sham, Self-Consistent Equations Including Exchange and Correlation Effects, Physical Review 140, A1133-A1138 (1965). doi:10.1103/PhysRev.140.A1133.

[93] R. G. Parr and W. Yang, Density Functional Theory of Atoms and Molecules, Oxford University Press, New York (1989).

[94] R. M. Dreizler, E. K. U. Gross, Density Functional Theory: An Approach to the Quantum Many-body Problem, Springer-Verlag Berlin Heidelberg (1990).

[95] J. P. Perdew, Electronic Structure of Solids ’91, edited by P. Ziesche and H. Eschig (Akademie Verlag, Berlin (1991).

[96] E. Helmut, The Fundamental of Density Functional Theory, B. G. Teubner Verlagsgesellschaft, Stuttgart- Leipzig (1996).

[97] J. F. Dobson, G. Vignale and M. P. Das (Eds.), Electronic Density Functional Theory: Recent Progress and New Directions, Plenum Press, New York and London (1998).

[98] W. Koch, M. C. Holthausen, A Chemist’s Guide to Density Functional Theory, Second Edition, WILEY-VCH Verlag GmbH, D-69469 Weinheim (Federal Republic of Germany) (2001).

[99] C. Fiolhais, F. Nogueira, M. Marques (Eds.) A Primer in Density Functional Theory, Springer-Verlag Berlin Heidelberg (2003).

[100] E. Engel, R. M. Dreizler, Density Functinal Theory: An Advanced Course, Springer-Verlag Berlin Heidelberg (2011).

[101] D. R. Hartree, The Wave Mechanics of an Atom with a Non-Coulomb Central Field. Part I. Theory and Methods, Mathematical Proceedings of the Cambridge Philosophical Society 24, 89-110 (1928). doi:10.1017/S0305004100011919.

[102] V. Fock, Näherungsmethode zur Lösung des quantenmechanischen Mehrkörperproblems, Zeitschrift für Physik 61, 126-148 (1930). doi:10.1007/BF01340294.

[103] C. Coulson, Present State of Molecular Structure Calculations, Reviews of Modern Physics 32, 170-177 (1960). doi:10.1103/RevModPhys.32.170.

[104] W. J. Carr and A. A. Maradudin, Ground-state energy of a high-density electron gas, Physical Review 133, A371-A374 (1964). doi: 10.1103/PhysRev.133.A371.

[105] M. Gell-Mann and K. A. Brueckner, Correlation energy of an electron gas at high density, Physical Review 106, 364-368 (1957). doi: 10.1103/PhysRev.106.364.

[106] W. J. Carr, Energy, specific heat, and magnetic properties of the low-density electron gas, Physical Review 122, 1437-1446 (1961). doi: 10.1103/PhysRev.122.1437.

[107] P. Nozieres and D. Pines, The Theory of Quantum Liquids, Cambridge, MA (1999).

[108] U. von Barth and L. Hedin, A local exchange-correlation potential for the spin polarized case. I Journal of Physics C: Solid State Physics 5, 1629-1642 (1972).doi:10.1088/0022-3719/5/13/012

[109] O. Gunnarsson and B. I. Lundqvist, Exchange and correlation in atoms, molecules, and solids by the spin-density-functional formalism, Physical Review B 13, 4274-4298 (1976).

doi: 10.1103/PhysRevB.13.4274.

[110] S. H. Vosko, L. Wilk and M. Nusair, Accurate spin-dependent electron liquid correlation energies for local spin density calculations: a critical analysis, Canadian Journal of Physics 58, 1200-1211 (1980). doi: 10.1139/p80-159.

[111] L. A. Cole and J. P. Perdew, Calculated electron affinities of the elements, Physical Review A 25, 1265-1271 (1982).doi:10.1103/PhysRevA.25.1265.

[112] J. P. Perdew and A. Zunger, Self-interaction correction to density-functional approximations for many-electron systems, Physical Review B 23, 5048-5079(1981). doi:10.1103/PhysRevB.23.5048.

[113] J. P. Perdew and Y. Wang, Accurate and simple analytic representation of the electron-gas correlation energy, Physical Review B 45, 13244–13249 (1992).doi:10.1103/PhysRevB.45.13244.

[114] O. Gunnarsson, M. Jonson, and B. I. Lundqvist,Exchange and correlation in inhomogeneous electron systems, Solid State Communications 24, 765–768 (1977). doi:10.1016/0038-1098(77)91185-1.

[115] T. Ziegler, A. Rauk, and E. J. Baerends, On the calculation of multiplet energies by the hartree-fock-slater method, Theoretical Chemistry Accounts: Theory, Computation, and Modeling (Theoretica Chimica Acta)43, 261-271 (1977). doi:10.1007/BF00551551.

[116] K. Burke, J. P. Perdew, and M. Ernzerhof, Why semilocal functionals work: Accuracy of the on-top pair density and importance of system averaging, Journal of Chemical Physics 109, 3760-3771 (1998). doi: 10.1063/1.476976.

[117] D. C. Langreth and J. P. Perdew, Theory of nonuniform electronic systems. I. Analysis of the gradient approximation and a generalization that works, Physical Review B 21, 5469–5493 (1980). doi: 10.1103/PhysRevB.21.5469.

[118] J. P. Perdew, Accurate Density Functional for the Energy: Real-Space Cutoff of the Gradient Expansion for the Exchange Hole, Physical Review Letters 55, 1665–1668 (1985). doi: 10.1103/PhysRevLett.55.1665.

[119] J. P. Perdew, Density-functional approximation for the correlation energy of the inhomogeneous electron gas, Physical Review B 33, 8822–8824 (1986). doi: 10.1103/PhysRevB.33.8822.

[120] A.D. Becke, Density-functional thermochemistry. III. The role of exact exchange, The Journal of Chemical Physics 98, 5648-5652 (1993). doi:10.1063/1.464913.

[121] A. D. Becke, A new mixing of Hartree-Fock and local density-functional theories, The Journal of Chemical Physics 98, 1372-1377 (1993). doi: 10.1063/1.464304.

[122] C. Lee, W. Yang, R.G. Parr, Development of the Colle-Salvetti correlation-energy formula into a functional of the electron density, Physical Review B 37, 785-789 (1988). doi:10.1103/PhysRevB.37.785.

[123] J. P. Perdew, J. A. Chevary, S. H. Vosko, K. A. Jackson, M. R. Pederson, D. J. Singh, and C. Fiolhais, Atoms, molecules, solids, and surfaces: Applications of the generalized gradient approximation for exchange and correlation, Physical Review B 48, 6671–6687 (1992). doi: 10.1103/PhysRevB.46.6671.

[124] K. Burke, J. P. Perdew, and Y. Wang, in Electronic Density Functional Theory: Recent Progress and New Directions, Ed. J. F. Dobson, G. Vignale, and M. P. Das (Plenum, New York, 1998).

[125] J. P. Perdew, K. Burke and M. Ernzerhof, Generalized Gradient Approximation Made Simple, Physical Review Letters 77, 3865–3868 (1996). doi: 10.1103/PhysRevLett.77.3865.

[126] J. Muscat, A. Wander, N. M. Harrison, On the prediction of band gaps from hybrid functional theory, Chemical Physics Letters 342, 397-401 (2001). doi:10.1016/S0009-2614(01)00616-9.

[127] J. Heyd, G. Scuseria, Efficient hybrid density functional calculations in solids: assessment of the Heyd-Scuseria-Ernzerhof screened Coulomb hybrid functional, The Journal of chemical physics 121, 1187-1192 (2004). doi:10.1063/1.1760074.

[128] C.W. Bauschlicher, A comparison of the accuracy of different functional, Chemical Physics Letters 246, 40-44 (1995). doi:10.1016/0009-2614(95)01089-R.

[129] S. Tomic, B. Montanari, N.M. Harrison, The group III–V's semiconductor energy gaps predicted using the B3LYP hybrid functional, Physica E 40, 2125-2127 (2008). doi:10.1016/j.physe.2007.10.022.

[130] S. Tomic, N.M. Harrison, Electronic structure of III–V's semiconductors from B3LYP and PBE0 functionals, AIP Conference Proceedings 65, 65-66 (2010). doi:10.1063/1.3295556.

[131] F.D. Proft, P. Geerlings, Calculation of ionization energies, electron affinities, electronegativities, and hardnesses using density functional methods, The Journal of Chemical Physics 106, 3270-3279 (1997). doi:10.1063/1.473796.

[132] M.W. Wong, Vibrational frequency prediction using density functional theory, Chemical Physics Letters, 256, 391-399 (1996). doi:10.1016/0009-2614(96)00483-6.

[133] J. Paier, M. Marsman, and G. Kresse, Why does the B3LYP hybrid functional fails for metals?, The Journal of Chemical Physics 127, 024103-1-10(2007). doi: 10.1063/1.2747249.

[134] C. Adamo and V. Barone, Toward reliable density functional methods without adjustable parameters: The PBE0 model, Journal of Chemical Physics 110, 6158-6170 (1999). doi: 10.1063/1.478522.

[135] S. F. Boys, Electronic Wave Functions. I. A General Method of Calculation for the Stationary States of Any Molecular System, Proceedings of the Royal Society of London. Series A, Mathematical and Physical Sciences 200, 542-554(1950). DOI: 10.1098/rspa.1950.0036.

[136] W.J. Hehre, L. Radom, P.R. Schleyer, and J.A. Pople, Ab initio Molecular Orbital Theory, first ed., Wiley, New York, 1986.

[137] E. G. Lewars, Computational Chemistry: Introduction to the Theory and Applications of Molecular and Quantum Mechanics, second ed., Springer, 2011.

[138] K. I. Ramachandran, Gopakumar Deepa, and Krishnan Namboori, Computational Chemistry and Molecular Modeling: Principles and Applications, Springer-Verlag Berling Heidelberg, 2008.

[139] J.W. Mintmire, C.T. White, Electronic and structural properties of carbon nanotubes, Carbon 33, 893-902 (1995). doi: 10.1016/0008-6223(95)00018-9.

[140] M. N. Huda, A. K. Ray, Electronic structures and magic numbers of small silver clusters: A many-body perturbation-theoretic study, Physical Review A 67, 013201-1-15 (2003). doi: 10.1103/PhysRevA.67.013201.

[141]. E. Bekaroglu, M. Topsakal, S. Cahangirov, and S. Ciraci, First-principles study of defects and adatoms in silicon carbide honeycomb structures, Physical Review B 81, 075433-1-10 (2010). doi:10.1103/PhysRevB.81.075433.

[142] A. Garcia and M.L. Cohen, First-principles ionicity scales. I. Charge asymmetry in the solid state, Physical Review B 47, 4215-4220 (1993). doi:10.1103/PhysRevB.47.4215.

[143] S. Ismail-Beigi,Electronic excitations in single-walled GaN nanotubes from first principles: Dark excitons and unconventional diameter dependences, Physical Review B 77, 035306-1-10 (2008). doi:10.1103/PhysRevB.77.035306.

[144] E. A. Pentaleri, V. A. Gubanov, C. Boekema, and C. Y. Fong, First-Principles Band-Structure Calculations of p- and n-Type Substitutional Impurities in Zinc-Blende Aluminum Nitride, Physica Status Solidi (b) 203, 149-168 (1997). doi:10.1002/1521-3951(199709)203:1<149::AID-PSSB149>3.0.CO;2-J.

[145] A. Rubio, J.L. Corkill, and M.L. Cohen, Theory of graphitic boron nitride nanotubes, Physical Review B 49, 5081-5084 (1994). doi:10.1103/PhysRevB.49.5081.

[146] M. Côté, M. L. Cohen, D. J. Chadi, Theoretical study of the structural and electronic properties of GaSe nanotubes, Physical Review B 58, R4277-R4280 (1998). doi:10.1103/PhysRevB.58.R4277.

[147] J.W. Kang, H. J. Hwang, Atomistic study of III-nitride nanotubes, Computational Materials Science 31, 237–246 (2004). doi: 10.1016/j.commatsci.2004.03.004.

[148] R. R. Zope, B. I. Dunlap, Electronic structure of fullerenelike cages and finite nanotubes of aluminum nitride, Physical Review B 72, 045439-1-6 (2005). doi: 10.1103/PhysRevB.72.045439.

[149] M. Zhao, Y. Xia, Z. Tan, X. Liu, F. Li, B. Huang, Y. Ji, and L. Mei, Strain energy and thermal stability of single-walled aluminum nitride nanotubes from first-principles calculations, Chemical Physics Letters 389, 160–164 (2004). doi: 10.1016/j.cplett.2004.03.082.

[150] D. Zhang, R.Q. Zhang, Theoretical prediction on aluminum nitride nanotubes, Chemical Physics Letters 371, 426–432 (2003). doi: 10.1016/S0009-2614(03)00289-6.

[151] K. Rezouali, M. A. Belkhir, A. Houari, J. Bai, Ab initio study of confinement and surface effects in hexagonal AlN nanotubes, Computational Materials Science 45, 305–309 (2009). doi: 10.1016/j.commatsci.2008.10.004.

[152] S. Hou, J. Zhang, Z. Shen, X. Zhao, Z. Xue, First-principles calculations on the open end of single-walled AlN nanotubes, Physica E 27, 45-50 (2005). doi: 10.1016/j.physe.2004.10.006.

[153] M. Menon, D. Srivastava, Structure of boron nitride nanotubes: tube closing *versus* chirality, Chemical Physics Letters 307, 407–412 (1999). doi: 10.1016/S0009-2614(99)00552-7.

[154] M. Zhang, Z. Su, L. Yan, Y. Qiu, G. Chen, R. Wang, Theoretical interpretation of different nanotube morphologies among Group III (B, Al, Ga) nitrides, Chemical Physics Letters 408, 145–149 (2005). doi: 10.1016/j.cplett.2005.04.025.

[155] H.J. Xiang, J. Yang, J.G. Hou, Q. Zhu, First-principles study of small-radius single-walled BN nanotubes, Physical Review B 68, 035427-1-5 (2003). doi: 10.1103/PhysRevB.68.035427.

[156] S. Hou, Z. Shen, J. Zhang, X. Zhao, Z. Xue, Ab initio calculations on the open end of single-walled BN nanotubes, Chemical Physics Letters 393, 179–183 (2004). doi: 10.1016/j.cplett.2004.06.014.

[157] X. Blase, A. Rubio, S. G. Louie, M. L. Cohen, Stability and Band Gap Constancy of Boron Nitride Nanotubes, Europhysics Letters 28, 335-340 (1994). doi: 10.1209/0295-5075/28/5/007.

[158] Z. Qian, S. Hou, J. Zhang, R. Li, Z. Shen, X. Zhao, Z. Xue, Stability and electronic structure of single-walled InN nanotubes, Physica E 30, 81-85 (2005). doi: 10.1016/j.physe.2005.07.002.

[159] O.G. Schmidt and K. Eberl, Nanotechnology: Thin solid films roll up into nanotubes, Nature 410, 168 (2001). doi:10.1038/35065525.

[160] O.G. Schmidt, C. Deneke, N. Schmarje, C. Müller, N.Y. Jin-Phillipp, Free-standing semiconductor micro- and nano-objects, Materials Science and Engineering C 19, 393-396 (2002). doi: 10.1016/S0928-4931(01)00428-3.

[161] M. N. Huda, L. Kleinman, A. K. Ray, Silicon-Carbide Nanostructures to Nanotubes, Journal of Computational and Theoretical Nanoscience 4, 739-744 (2007). doi: 10.1166/jctn.2007.003.

[162] R. Saito, G. Dresselhaus, M.S. Dresselhaus, Physical Properties of Carbon Nanotubes, first ed., Imperial College Press, London (1998).

[163] J.P. Perdew, R.G. Parr, M. Levy, J.L. Balduz, Density-Functional Theory for Fractional Particle Number: Derivative Discontinuities of the Energy, Physical Review Letters 49, 1691-1694 (1982). doi:10.1103/PhysRevLett.49.1691.

[164] P.J. Stephens, F.J. Devlin, C.F. Chabalowski, M.J. Frisch, Ab Initio Calculation of Vibrational Absorption and Circular Dichroism Spectra Using Density Functional Force Fields, The Journal of Physical Chemistry 98, 11623-11627 (1994). doi: 10.1021/j100096a001.

[165] P.J. Hay and W.R. Wadt, Ab initio effective core potentials for molecular calculations. Potentials for the transition metal atoms Sc to Hg, The Journal of Chemical Physics 82, 270-283 (1985). doi:10.1063/1.448799.

[166] W.R. Wadt and P.J. Hay, Ab initio effective core potentials for molecular calculations. Potentials for main group elements Na to Bi, The Journal of Chemical Physics 82, 284-298 (1985). doi:10.1063/1.448800.

[167] P.J. Hay and W.R. Wadt, Ab initio effective core potentials for molecular calculations. Potentials for K to Au including the outermost core orbitals, The Journal of Chemical Physics 82, 299-310 (1985). doi:10.1063/1.448975

[168] Gaussian 03, Revision D.02, M. J. Frisch, G. W. Trucks, H. B. Schlegel, G. E. Scuseria, M. A. Robb, J. R. Cheeseman, J. A. Montgomery, Jr., T. Vreven, K. N. Kudin, J. C. Burant, J. M. Millam, S. S. Iyengar, J. Tomasi, V. Barone, B. Mennucci, M. Cossi, G. Scalmani, N. Rega, G. A. Petersson, H. Nakatsuji, M. Hada, M. Ehara, K. Toyota, R. Fukuda, J. Hasegawa, M. Ishida, T. Nakajima, Y. Honda, O. Kitao, H. Nakai, M. Klene, X. Li, J. E. Knox, H. P. Hratchian, J. B. Cross, V. Bakken, C. Adamo, J. Jaramillo, R. Gomperts, R. E. Stratmann, O. Yazyev, A. J. Austin, R. Cammi, C. Pomelli, J. W. Ochterski, P. Y. Ayala, K. Morokuma, G. A. Voth, P. Salvador, J. J. Dannenberg, V. G. Zakrzewski, S. Dapprich, A. D. Daniels, M. C. Strain, O. Farkas, D. K. Malick, A. D. Rabuck, K. Raghavachari, J. B. Foresman, J. V. Ortiz, Q. Cui, A. G. Baboul, S. Clifford, J. Cioslowski, B. B. Stefanov, G. Liu, A. Liashenko, P. Piskorz, I. Komaromi, R. L. Martin, D. J. Fox, T. Keith, M. A. Al-Laham, C. Y. Peng, A. Nanayakkara, M. Challacombe, P. M. W. Gill, B. Johnson, W. Chen, M. W. Wong, C. Gonzalez, and J. A. Pople, Gaussian, Inc., Wallingford CT, 2004.

[169] S.J. Rathi, A.K. Ray, On the electronic and geometric structures of armchair GeC nanotubes: a hybrid density functional study, Nanotechnology 19, 335706 (2008). doi:10.1088/0957-4484/19/33/335706.

[170] Y. Shibutaa and S. Maruyama, Molecular dynamics simulation of formation process of single-walled carbon nanotubes by CCVD method, Chemical Physics Letters 382, 381-386 (2003). doi: 10.1016/j.cplett.2003.10.080.

[171] Y. Saito, M. Okuda, N. Fujimoto, T. Yoshikawa, M. Tomita, and T. Hayashi, Single-Wall Carbon Nanotubes Growing Radially from Ni Fine Particles Formed by Arc Evaporation, Japanese Journal of Applied Physics 33, L526-L529 (1994). doi: 10.1143/JJAP.33.L526.

[172] X. Fan, R. Buczko, A. A. Puretzky, D. B. Geohegan, J. Y. Howe, S. T. Pantelides, and S. J. Pennycook, Nucleation of Single-Walled Carbon Nanotubes, Physical Review Letters 90, 145501-1-4 (2003). doi: 10.1103/PhysRevLett.90.145501.

[173] J. Gavillet, A. Loiseau, C. Journet, F. Willaime, F. Ducastelle, and J.-C. Charlier, Root-Growth Mechanism for Single-Wall Carbon Nanotubes, Physical Review Letters 87, 275504-1-4 (2001). doi: 10.1103/PhysRevLett.87.275504

[174] X. Yu, J. Zhang, W. M. Choi, J.-Y. Choi, J. M. Kim, L. Gan, and Z. Liu, Cap Formation Engineering: From Opened C_{60} to Single-Walled Carbon Nanotubes, *Nano Letters* 10, 3343–3349 (2010). doi: 10.1021/nl1010178.

[175] S. Reich, L. Li, and J. Robertson, Structure and formation energy of carbon nanotube caps, Physical Review B 72, 165423-1-8 (2005). doi: 10.1103/PhysRevB.72.165423.

[176] S. Reich, L. Li, and J. Robertson, Epitaxial growth of carbon caps on Ni for chiral selectivity, physica status solidi (b) 243, 3494–3499(2006). doi: 10.1002/pssb.200669224

[177] G. Brinkmann, U.V. Nathusius, A.H.R. Palser, Aconstructive enumeration of nanotube caps, Discrete Applied Mathematics 116, 55-71 (2002). doi: 10.1016/S0166-218X(00)00328-0.

[178] G. Brinkmann, P. W. Fowler, D. E. Manolopoulos, A. H. R. Palser, A census of nanotube caps, Chemical Physics Letters 315, 335-347 (1999). doi: 10.1016/S0009-2614(99)01111-2.

[179] T. Yu. Astakhova, G. A. Vinogradov, E. Osawa, Numerical Generation of Nanotube Caps II. Exact Results Up to (10, 10), Fullerene Science and Technology 7 (1999) 769-779. doi: 10.1080/10641229909351377.

[180] Y. Miyauchi, S. Chiashi, Y. Murakami, Y. Hayashida, S. Maruyama, Fluorescence spectroscopy of single-walled carbon nanotubes synthesized from alcohol, Chemical Physics Letters 387, 198-203 (2004). doi: 10.1016/j.cplett.2004.01.116.

[181] L. Guan, K. Suenaga, S. Iijima, Smallest Carbon Nanotube Assigned with Atomic Resolution Accuracy, Nano Letters 8, 459-462 (2008). doi: 10.1021/nl072396j.

[182] A. V. Bazilevsky, K. Sun, A. L. Yarin, and C. M. Megaridis, Room-temperature, open-air, wet intercalation of liquids, surfactants, polymers and nanoparticles within nanotubes and microchannels, Journal of Materials Chemistry 18, 696-702 (2008). doi: 10.1039/B714541C.

[183] A. M. Somoza, C. Sagui, and C. Roland, Liquid-crystal phases of capped carbon nanotubes, Physical Review B 63, 081403-1-4(R) (2001). doi: 10.1103/PhysRevB.63.081403.

[184] N.S. Lee, D.S. Chung, I.T. Han, J.H. Kang, Y.S. Choi, H.Y. Kim, S.H. Park, Y.W. Jin, W.K. Yi, M.J. Yun, J.E. Jung, C.J. Lee, J.H. You, S.H. Jo, C.G. Lee, and J.M. Kim, Application of carbon nanotubes to field emission displays, Diamond Related Materials 10, 265-270 (2001). doi: 10.1016/S0925-9635(00)00478-7.

[185] T. Yumura, K. Hirahara, S. Bandow, K. Yoshizawa, and S. Iijima, A theoretical study on the geometrical features of finite-length carbon nanotubes capped with fullerene hemisphere, Chemical Physics Letters 386, 38-43 (2006). doi: 10.1016/j.cplett.2003.12.123.

[186] T. Yamabe, M. Imade, M. Tanaka, and T. Sato, Electronic structures and transport properties of carbon nanotube, Synthetic Metals 117, 61-65 (2001). doi: 10.1016/S0379-6779(00)00539-7.

[187] Y. Li, D. Lu, K. Schulten, U. Ravaioli, and S. V. Rotkin, Screening of Water Dipoles Inside Finite-Length Armchair Carbon Nanotubes, Journal of Computational Electronics 4, 161-165 (2005). doi: 10.1007/s10825-005-7130-9.

[188] A. Rochefort, D. R. Salahub, and P. Avouris, Effects of Finite Length on the Electronic Structure of Carbon Nanotubes, The Journal of Physical Chemistry B 103, 641-646 (1999). doi: 10.1021/jp983725m.

[189] D. L. Carroll, P. Redlich, P. M. Ajayan , J. C. Charlier, X. Blase, A. De Vita, and R. Car, Electronic Structure and Localized States at Carbon Nanotube Tips, Physical Review Letters 78, 2811–2814 (1997). doi: 10.1103/PhysRevLett.78.2811.

[190] R. Tamura and M. Tsukada, Electronic states of the cap structure in the carbon nanotube, Physical Review B 52, 6015–6026 (1995). doi:10.1103/PhysRevB.52.6015.

[191] M. Ge, and K. Sattler, Observation of fullerene cones, Chemical Physics Letters 220, 192-196 (1994). doi:10.1016/0009-2614(94)00167-7.

[192] J. C. Charlier, and G. M. Rignanese, Electronic Structure of Carbon Nanocones. Physical Review Letters 86, 5970–5973 (2001). doi: 10.1103/PhysRevLett.86.5970.

[193] J. Zhu, Z. Yu , G. F. Burkhard, C. M. Hsu, S. T. Connor, Y. Xu, Q. Wang, M. McGehee, S. Fan, and Y. Cui, Optical Absorption Enhancement in Amorphous Silicon Nanowire and Nanocone Arrays. Nano Letters 9, 279-282(2009). doi: 10.1021/nl802886y.

[194] H. C. Lo, D. Das, J. S. Hwang, K. H. Chen, C. H. Hsu, C. F. Chen, and L. C. Chen, SiC-capped nanotip arrays for field emission with ultralow turn-on field, Applied Physics Letters 83, 1420-1422 (2003). doi: 10.1063/1.1599967.

[195] A. Mavrandonakis, G. E. Froudakis, A. Andriotis, and M. Menon, Silicon carbide nanotube tips: Promising materials for atomic force microscopy and/or scanning tunneling microscopy, Applied Physics Letters 89, 123126-1-3 (2006). doi: 10.1063/1.2221418.

[196] G. Alfieri, and T. Kimoto, Structural stability and electronic properties of SiC nanocones: First-principles calculations and symmetry considerations, Applied Physics Letters 98, 123102-1-3 (2011). doi: 10.1063/1.3567535

[197] M. Machado, P. Piquini, and R. Mota, Electronic properties of selected BN nanocones, Materials Characterization 50, 179-182 (2003). doi:10.1016/S1044-5803(03)00085-8.

[198] M. Machado, P. Piquini, and R. Mota, Energetic and electronic properties of BN nanocones with pentagonal rings at their apexes, The European Physical Journal D 23, 91–93 (2003). doi: 10.1140/epjd/e2003-00040-x.

[199] M. Machado, P. Piquini, and R. Mota, Charge distributions in BN nanocones: electric field and tip termination effects, Chemical Physics Letters 392: 428-432 (2004). doi:10.1016/j.cplett.2004.05.088.

[200] D. Pedreira, S. Azevedo, M. Machado, Electronic properties of boron nitride nanocones under the influence of parallel and perpendicular external electric fields, Physical Review B 78, 085427-1-6(2008). doi: 10.1103/PhysRevB.78.085427.

[201] E. D. Glendening, A. E. Reed, J. E. Carpenter, and F. Weinhold, NBO Version 3.1, Gaussian Inc, Pittsburgh, PA (2009).

[202] J. L. Hutchison, N. A. Kiselev, E. P. Krinichnaya, A. V. Krestinin, R. O. Loutfy, A. P. Morawsky, V. E. Muradyan, E. D. Obraztsova, J. Sloan, S. V. Terekhov and D. N. Zakharov, Double-walled carbon nanotubes fabricated by a hydrogen arc discharge method, Carbon 39, 761-770 (2001). doi: 10.1016/S0008-6223(00)00187-1.

[203] R. Saito, R. Matsuo, T. Kimura, G. Dresselhaus, and M.S. Dresselhaus, Anomalous potential barrier of double-wall carbon nanotube, Chemical Physics Letters 348, 187-193 (2001). doi: 10.1016/S0009-2614(01)01127-7.

[204] A. Hashimoto, K. Suenaga, K. Urita, T. Shimada, T. Sugai, S. Bandow, H. Shinohara, and S. Ijima, Atomic Correlation Between Adjacent Graphene Layers in Double-Wall Carbon Nanotubes, Physical Review Letters 94, 045504-1-4 (2005). doi:10.1103/PhysRevLett.94.045504

[205] G. Rinzler, J. H. Hafner, P. Nikolaev, L. Lou, S. G. Kim, D. Tomanek, D. Colbert, and R. E. Smalley, Unraveling Nanotubes: Field Emission from an Atomic Wire, Science 269, 1550-1553 (1995). doi: 10.1126/science.269.5230.1550.

[206] W. A. De Heer, A. Chatelain, and D. Ugarte, A Carbon Nanotube Field-Emission Electron Source, Science 270, 1179 -1180 (1995). doi: 10.1126/science.270.5239.1179.

[207] J. -M.Bonard, J. -P.Salvetat, T. Stöckli, W. A. De Heer, L. Forró, and A. Châtelain, Field emission from single-wall carbon nanotube films, Applied Physics Letters 73, 918-920 (1998). doi: 10.1063/1.122037.

[208] Z. F. Ren, Z. P.Huang, J. W. Xu, J. H. Wang, P. Bush, M. P. Siegal, and P. N. Provencio, Synthesis of Large Arrays of Well-Aligned Carbon Nanotubes on Glass, Science 282, 1105-1107 (1998). doi: 10.1126/science.282.5391.1105.

[209] Y. A. Kim, H. Muramatsu, T. Hayashi, M. Endo, M. Terrones and M. S. Dresselhaus, Thermal stability and structural changes of double-walled carbon nanotubes by heat treatment, Chemical Physics Letters 398, 87–92 (2004). doi: 10.1016/j.cplett.2004.09.024.

[210] Q. Liu, W. Ren, F. Li, H. Cong and H. Cheng, Synthesis and High Thermal Stability of Double-Walled Carbon Nanotubes Using Nickel Formate Dihydrate as Catalyst Precursor, The Journal of Physical Chemistry C 111, 5006-5013 (2007). doi: 10.1021/jp068672k.

[211] X. Wei, Q. Chen, L. -M. Peng, R. Cui and Y. Li, Tensile Loading of Double-Walled and Triple-Walled Carbon Nanotubes and their Mechanical Properties, The Journal of Physical Chemistry C 113, 17002-17005 (2009). doi: 10.1021/jp902471q.

[212] K. Metenier, S. Bonnamy, F. Beguin, C. Journet, P. Bernier, M. L. de La Chapelle, O. Chauvet and S. Lefrant, Coalescence of single-walled carbon nanotubes and formation of multi-walled carbon nanotubes under high-temperature treatments, Carbon 40, 1765-1773 (2002). doi: 10.1016/S0008-6223(02)00044-1.

[213] T. Thostenson, C. Li, and T. W. Chou, Nanocomposites in context, Composites Science and Technology 65, 491-516 (2005). doi: 10.1016/j.compscitech.2004.11.003.

[214] B. Ha, D. H. Shin, J. Park, and C. J. Lee, Electronic Structure and Field Emission Properties of Double-Walled Carbon Nanotubes Synthesized by Hydrogen Arc Discharge, The Journal of Physical Chemistry C 112, 430-435 (2008). doi: 10.1021/jp0768468.

[215] T. Shimada, T. Sugai, Y. Ohno, S. Kishimoto, T. Mizutani, H. Yoshida, T. Okazaki, and H. Shinohara, Double-wall carbon nanotube field-effect transistors: Ambipolar transport characteristics, Applied Physics Letters 84, 2412-2414 (2004). doi:10.1063/1.1689404.

[216] Y. F. Li, R. Hatakeyama, T. Kaneko, T. Izumida, T. Okada, and T. Kato, Electronic transport properties of Cs-encapsulated double-walled carbon nanotubes, Applied Physics Letters 89, 093110-1-3 (2006). doi: 10.1063/1.2339931.

[217] S. Kuwahara, S. Akita, M. Shirakihara, T. Sugai, Y. Nakayama, and H. Shinohara, Fabrication and characterization of high-resolution AFM tips with high-quality double-wall carbon nanotubes, Chemical Physics Letters 429, 581-585 (2006). doi: 10.1016/j.cplett.2006.08.045.

[218] J. Cumings, W. Mickelson, and A. Zettl, Simplified synthesis of double-wall carbon nanotubes, Solid State Communications 126, 359-362 (2003). doi: 10.1016/S0038-1098(02)00881-5.

[219] T. Hayashi, D. Shimamoto, Y. A. Kim, H. Muramatsu, F. Okino, H. Touhara, T. Shimada, Y. Miyauchi, S. Maruyama, M. Terrones, M. S. Dresselhaus and M. Endo, Selective Optical Property Modification of Double-Walled Carbon Nanotubes by Fluorination, ACS Nano 2, 485 – 488 (2008). doi: 10.1021/nn700391w

[220] Y. C. Jung, D. Shimamoto, H. Muramatsu, Y. A. Kim, T. Hayashi, M. Terrones, and M. Endo, Robust, Conducting, and Transparent Polymer Composites Using Surface-Modified and Individualized Double-Walled Carbon Nanotubes, Advanced Materials 20, 4509-4512(2008). doi: 10.1002/adma.200801659.

[221] Y. A. Kim, H. Muramatsu, K. C. Park, D. Shimamoto, Y. C. Jung, J. H. Kim, T. Hayashi, Y. Saito, M. Endo, M. Terrones, and M. S. Dresselhaus, CdSe quantum dot-decorated double walled carbon nanotubes: The effect of chemical moieties, Applied Physics Letters 93, 051901-1-3 (2008). doi: 10.1063/1.2966341.

[222] C. Shen , A. H. Brozena, and Y. H. Wang, Double-walled carbon nanotubes: Challenges and opportunities, Nanoscale 3, 503-518 (2011). doi: 10.1039/C0NR00620C.

[223] H. Rafii-Tabar, Computational Physics of Carbon Nanotubes, First ed., Cambridge Univerisity Press, (2008).

[224] Ph. Lambin, V. Meunier, and A. Rubio, Electronic structure of polychiral carbon nanotubes, Physical Review B 62, 5129-5135 (2000). doi: 10.1103/PhysRevB.62.5129.

[225] S.H. Jhi, D. J. Roundy, S. G. Louie, and M. L. Cohen, Formation and electronic properties of double-walled boron nitride nanotubes, Solid State Communication 134, 397-402 (2005). doi: 10.1016/j.ssc.2005.02.007.

[226] M. W. Zhao, Y. Y. Xia, R. Q. Zhang, S.-T. Lee, Manipulating the electronic structures of silicon carbide nanotubes by selected hydrogenation, The Journal of Chemical Physics 122, 214707-1-5 (2005). doi: 10.1063/1.1927520 .

[227] F. Li, Y. Y. Xia, M. W. Zhao, X. D. Liu, B. D. Huang, Z. H. Yang, Y. J. Ji, C. Song, Density-functional theory calculations of XH3-decorated SiC nanotubes (X = {C, Si}): Structures, energetics, and electronic structures, Journal of Applied Physics 97, 104311-1-4 (2005). doi: 10.1063/1.1891281.

[228] K. Adhikari and A. K. Ray, On the existence and stability of double-walled armchair siliconcarbide nanotubes, Solid State Communication 151, 430-435 (2011). doi: 10.1016/j.ssc.2011.01.004.

[229] K. Adhikari and A. K. Ray, Cluster modeling of three types of double-walled armchair silicon carbide nanotubes, The European Physical Journal D 64, 353-363 (2011). doi: 10.1140/epjd/e2011-20280-3.

[230] R. Moradian, S. Behzad, and R. Chegel, Ab initio density functional theory investigation of structural and electronic properties of double-walled silicon carbide nanotubes, Physica E 42, 172-175 (2009). doi: 10.1016/j.physe.2009.10.005.

[231] A. S. Shalabi, M. M. Assem, S. Abdel Aal, and K. A. Soliman, Magnetic and binding properties of Co-doped single-walled carbon nanotubes: a first principles study, Journal of Nanoparticle Research 14, 892 (1-15) (2012) doi: 10.1007/s11051-012-0892-7.

[232] B.W. Alphennar, K. Tsukagoshi, and M. Wagner, Spin transport in nanotubes, Journal of Applied Physics 89, 6863–6867(2001). doi: 10.1063/1.1359220.

[233] E. Borowiak-Palen, E. Mendoza, A. Bachmatiuk, M. H. Rummeli, T. Gemming, J. Nogues, V. Skumryev, R. J. Kalenczuk, T. Pichler, and S. R. P. Silva, Iron filled single-wall carbon nanotubes – A novel ferromagnetic medium, Chemical Physics Letters 421, 129-133 (2006). doi: 10.1016/j.cplett.2006.01.072.

[234] S.-F. Wang, Y. Zhang, L.-Y. Chen, J.-M. Zhang, and K.-W. Xu, First-principles study on structural, electronic and magnetic properties of iron nanowire encapsulated in carbon nanotube, physica status solidi (a) 208, 97-103(2011). doi: 10.1002/pssa.201026157.

[235] A. K. Singh, V. Kumar, and Y. Kawazoe, Metal encapsulated nanotubes of silicon and germanium, Journal of Materials Chemistry 14, 555-563 (2004). doi: 10.1039/B311850A.

[236] A. K. Singh, V. Kumar, and Y. Kawazoe, Ferromagnetism and piezomagnetic behavior in Mn-doped germanium nanotubes, Physical Review B 69, 233406-1-4 (2004). doi: 10.1103/PhysRevB.69.233406.

[237] A. K. Singh, T. M. Briere, V. Kumar, and Y. Kawazoe, Magnetism in Transition-Metal-Doped Silicon Nanotubes, Physical Review Letters 91, 146802-1-4 (2003). doi: 10.1103/PhysRevLett.91.146802.

[238] Y. Zhang and H. Dai, Formation of metal nanowires on suspended single-walled carbon nanotubes, Applied Physics Letters 77, 3015-3017(2000). doi:10.1063/1.1324731.

[239] I. Ovsienko, T. Len, L. Matzui, Yu. Prylutskyy, P. Eklund, F. Normand, U. Ritter, and P. Scharff, Transport properties of carbon nanotube–metal nanocomposites, Physica E 37,78-80 (2007). doi:10.1016/j.physe.2006.06.007.

[240] N. Grobert, W.K. Hsu, Y.Q. Zhu, J.P. Hare, H.W. Kroto, R.M.D. Walton, M. Terrones, H. Terrones, Ph. Redlich, M. Rühle, R. Escudero, and F. Morales, Enhanced magnetic coercivities in Fe nanowires, Applied Physics Letters 75, 3363-3365 (1999). doi: 10.1063/1.125352.

[241]B.C. Satishkumar, A. Govindaraj, P.V. Vanitha, A.K. Raychaudhuri, and C.N.R. Rao, Barkhausen jumps and related magnetic properties of iron nanowires encapsulated in aligned carbon nanotube bundles, Chemical Physics Letters 362, 301–306 (2002). doi: 10.1016/S0009-2614(02)01082-5.

[242] D. Seifu, Y. Hijji, G. Hirsch, and S.P. Karna, Chemical method of filling carbon nanotubes with magnetic material, Journal of Magnetism and Magnetic Materials 320, 312-315 (2008). doi:10.1016/j.jmmm.2007.06.015.

[243] Y.J. Kang, J. Choi, C.Y. Moon, and K.J. Chang, Electronic and magnetic properties of single-wall carbon nanotubes filled with iron atoms, Physical Review B 71, 115441-1-7 (2005). doi:10.1103/PhysRevB.71.115441

[244] C. Yang, J.J. Zhao, and J.P. Lu, Magnetism of Transition-Metal/Carbon-Nanotube Hybrid Structures, Physical Review Letters 90, 257203-1-4 (2003). doi: 10.1103/PhysRevLett.90.257203.

[245] Y. Yagi, T.M. Briere, M.H.F. Sluiter, V. Kumar, A.A. Farajian, and Y. Kawazoe, Stable geometries and magnetic properties of single-walled carbon nanotubes doped with 3d transition metals: A first-principles study, Physical Review B 69, 075414-1-9 (2004). doi: 10.1103/PhysRevB.69.075414.

[246] J.-M. Zhang, L.-Y. Chen, S.-F. Wang, and K.-W. Xu, Comparision of the structural, electronic and magnetic properties of Fe , Co and Ni nanowires encapsulated into silicon carbide nanotube, The European Physical Journal B 73, 555-561 (2010). doi: 10.1140/epjb/e2010-00020-y.

[247] J. -X. Zhao and Y. –H Ding, Silicon carbide nanotubes functionalized by transition metal atoms: A density-functional study, The Journal of Physical Chemistry C 112, 2558-2564 (2008). doi: 10.1021/jp073722m.

[249] E. Durgun, S. Dag, V. M. K. Bagci, O. Gulseren, T. Yildirim, and S. Ciraci, Systematic study of adsorption of single atoms on a carbon nanotube, Physical Review B 67, 20140(R)1-4 (2003). doi: 10.1103/PhysRevB.67.201401.

[250] K. Alam and A. K. Ray, Interactions of Fe atom with single wall armchair SiC nanotubes: an ab initio study, Journal of Nanoparticle Research 11, 1405-1420 (2009). doi: 10.1007/s11051-008-9529-2.

[251] K. Adhikari, M. N. Huda and A. K. Ray, Anomalous Dependence of Band Gaps of Binary Nanotubes on Diameters, Journal of Computational and Theoretical Nanoscience 8, 1502-1508 (2011). doi:10.1166/jctn.2011.1842.

[252] K. Adhikari and A. K. Ray, Carbon- and silicon-capped silicon carbide nanotubes: An *ab initio* study, Physics Letters A 375, 1817–1823 (2011). doi: 10.1016/j.physleta.2011.03.016.

[253] K. Adhikari and A. K. Ray, Stabilities of silicon carbide nanocones: a nanocluster-based study, Journal of Nanoparticle Research 14, 816 (2012). doi: 10.1007/s11051-012-0816-6.

BIOGRAPHICAL INFORMATION

Kapil Adhikari received his master's degree in physics with specialization in solid state physics from Tribhuvan University, Nepal. His research during his master's studies was on the experimental investigation of surface modification of polycarbonate by *dc* glow discharge plasma. After receiving his master's degree he was involved in teaching physics at undergraduate level. He joined the University of Texas at Arlington (UTA) in the fall of 2008. His current research interest is in theoretical and computational condensed matter physics. In the department of physics at UTA, he worked under the supervision of Prof. Dr. Asok K Ray. He intends to continue his research in academia after completion of his Ph. D.